COMPUTER SIMULATIONS OF GLYCOLIPID BILAYERS UNDER ANHYDROUS AND HYDRATED CONDITIONS

M.VIJAYAN A/L MANICKAM ACHARI

FACULTY OF SCIENCE
UNIVERSITY OF MALAYA
KUALA LUMPUR

2016

COMPUTER SIMULATIONS OF GLYCOLIPID BILAYERS UNDER ANHYDROUS AND HYDRATED CONDITIONS

M.VIJAYAN A/L MANICKAM ACHARI

THESIS SUBMITTED IN FULFILMENT
OF THE REQUIREMENTS
FOR THE DEGREE OF DOCTOR OF PHILOSOPHY

DEPARTMENT OF CHEMISTRY
FACULTY OF SCIENCE
UNIVERSITY OF MALAYA
KUALA LUMPUR

2016

UNIVERSITI MALAYA

ORIGINAL LITERARY WORK DECLARATION

Name of Candidate: **M. VIJAYAN A/L MANICKAM ACHARI**

Registration/Matrix No.: **SHC 070047**

Name of Degree: **DOCTOR OF PHILOSOPHY**

Title of Project Paper/Research Report/Dissertation/Thesis ("this Work"):

COMPUTER SIMULATIONS OF GLYCOLIPID BILAYERS UNDER ANHYDROUS AND HYDRATED CONDITIONS

Field of Study: **COMPUTATIONAL CHEMISTRY**

I do solemnly and sincerely declare that:

(1) I am the sole author/writer of this Work;
(2) This work is original;
(3) Any use of any work in which copyright exists was done by way of fair dealing and for permitted purposes and any excerpt or extract from, or reference to or reproduction of any copyright work has been disclosed expressly and sufficiently and the title of the Work and its authorship have been acknowledged in this Work;
(4) I do not have any actual knowledge nor do I ought reasonably to know that the making of this work constitutes an infringement of any copyright work;
(5) I hereby assign all and every rights in the copyright to this Work to the University of Malaya ("UM"), who henceforth shall be owner of the copyright in this Work and that any reproduction or use in any form or by any means whatsoever is prohibited without the written consent of UM having been first had and obtained;
(6) I am fully aware that if in the course of making this Work I have infringed any copyright whether intentionally or otherwise, I may be subject to legal action or any other action as may be determined by UM.

Candidate's Signature Date

Subscribed and solemnly declared before,

Witness's Signature Date

Name:
Designation:

ABSTRACT

Glycolipids are ubiquitous membrane components and amphiphilic in character. They can be found in a variety of living cells and are involved in cell activities like markers for cellular recognition, cell adhesions, also in signal-receiving and transmitting. Understanding the interplay between the complex cell function to their structural and dynamical properties is important to help design new glycolipid-based materials for many applications in medicine, pharmacy and cosmetics. Molecular dynamics simulation is a useful method to explore the bilayer properties. Using this method we simulated glycolipid bilayers in an anhydrous (dry) and lyotropic (hydrated) conditions. The anhydrous monoalkylated glycolipids (such as βMal-C_{12}, βCel-C_{12}, and βIsoMal-C_{12}) bilayers were compared with a $C_{12}C_{10}$ branched β-maltoside. It was found that the chain branching in the glycolipid leads to a measurable difference in the dimensions and interactions of the lamellar assembly, as well as more fluid-like behavior in the hydrophobic chain region. Substitution of the maltosyl headgroup of βMal-C_{12} by an isomaltosyl moiety leads to a significant decrease in the bilayer spacing as well as a markedly altered pattern of inter-headgroup hydrogen bonding. Additionally, the monoalkylated glycosides possess a small amount of *gauche* conformers ($\sim$20%) in the hydrophobic region of the lamellar crystal (L_C) phase. In contrast, the branched chain glycolipid in the fluid L_α phase has a high *gauche* population of up to $\sim$40%. Meanwhile, the rotational diffusion analysis reveals that the carbons closest to the headgroup have the highest correlation times where the rotational dynamics of an isomaltose was found to be 11–15% higher and more restrained near the sugar compared to the other monoalkylated lipids, possibly due to the chain disorder and partial inter-digitation. We have also simulated hydrated bilayers of single and Guerbet branched chain maltosides namely βMal-C_{12}(12%wat), βMal-C_{12}(23%wat), βMal-$C_{12}C_8$(*R*)(25%wat), βMal-$C_{12}C_8$(*S*)(25%wat), and βMal-$C_{12}C_8$(*RS*)(25%wat), in a liquid crystalline L_α phase. In the hydrated condition, these showed that the increase in hydration level correspondingly increases the area per lipid. The bimodal distribution of angle between the chains and the sugar headgroup with *z*-axis for βMal-C_{12}(23%wat) showed that the chain and the non-reducing sugar ring may flip and protrude into the headgroup region where these observations suggest the βMal-C_{12}(23%wat) system may begin to shift into a

metastable phase where, the lipids may try to reorient themselves into different assembly structure such as the hexagonal phase. We have also found that the intermolecular hydrogen bonding of the sugar rings in maltose headgroup shows no significant change although the bilayers are under the effect of water concentration and temperature difference. We also noticed that the non-reducing sugars from all bilayer systems rotate faster than the reducing sugar. Meanwhile, the exocyclic groups rotate much quicker than the sugar ring itself and there is no chirality effect to the rotational diffusion. The order parameter of chain segments shows that they are quite sensitive to the temperature and water concentration and there is a subtle effect of chirality, especially in the racemic mixture of bilayer. These insights into structure-property relationships from simulation provide an important molecular basis for future design of synthetic glycolipid materials.

ABSTRAK

Molekul glikolipid sentiasa hadir sebagai komponen membran dan bersifat amfifilik. Ianya boleh dijumpai dalam pelbagai jenis sel hidupan dan terlibat dalam aktiviti sel seperti penanda untuk pengesanan sel, penyatuan-sel, serta sebagai penerima dan pemancar isyarat. Pemahaman di antara fungsi-fungsi sel yang kompleks dengan sifat struktur dan dinamik sel adalah penting untuk merekabentuk bahan glikolipid yang baru untuk diaplikasi ke bidang perubatan, farmasi dan kosmetik. Kaedah simulasi dinamik molekul sangat berguna untuk meneroka sifat-sifat dwilapisan. Dengan menggunakan kaedah ini kami melakukan simulasi pada dwilapisan glikolipid dalam keadaan kering (kering) dan dalam keadaan liotropik (dihidrasikan). Dwilapisan glikolipid rantai tunggal dalam keadaan kering (seperti βMal-C_{12}, βCel-C_{12}, dan βIsoMal-C_{12}) dibandingkan dengan maltosida rantai bercabang (βMal-$C_{12}C_{10}$). Kami mendapati kehadiran rantai bercabang di dalam glikolipid menunjukkan perubahan yang jelas pada dimensi dan interaksi swa-susunan lamela, di samping bahagian hidrofobik yang lebih bersifat seperti cecair. Penggantian kumpulan kepala maltosil (βMal-C_{12}) dengan isomaltosil menyebabkan pengurangan yang ketara pada jarak dwilapisan dan juga mengubah corak ikatan hidrogen di antara kumpulan kepala. Seterusnya, semua glikosida rantai tunggal mempunyai peratusan konformer *gauche* ($\sim$20%) yang rendah di bahagian hidrofobik bagi fasa kristal lamela (L_C). Sebaliknya, glikolipid rantai bercabang di dalam fasa cecair lamela L_α menunjukkan populasi *gauche* yang tinggi sehingga $\sim$40%. Sementara itu, analisis resapan putaran menunjukkan karbon yang berdekatan dengan kumpulan kepala mempunyai masa korelasi yang paling tinggi, di mana putaran dinamik bagi isomaltosa didapati tinggi sebanyak 11–15% dan lebih terhindar berhampiran kumpulan kepala berbanding dengan lipid rantai tunggal yang lain dan ini kemungkinan besar disebabkan oleh rantai karbon yang tidak teratur dan interdigitasi separa. Kami juga menjalankan simulasi bagi beberapa dwilapisan maltosida rantai tunggal dan rantai bercabang dalam keadaan terhidrat seperti βMal-C_{12}(12%wat), βMal-C_{12}(23%wat), βMal-$C_{12}C_8$(*R*)(25%wat), βMal-$C_{12}C_8$(*S*)(25%wat), dan βMal-$C_{12}C_8$(*RS*)(25%wat), di dalam fasa hablur cecair L_α. Dalam keadaan terhidrat, kesemuanya menunjukkan peningkatan dalam darjah penghidratan yang sepadan dengan pembesaran luas setiap lipid. Manakala pengedaran dwimodal sudut di antara rantai karbon dan kumpulan kepala gula dengan paksi-*z* bagi βMal-C_{12}(23%wat) menunjukkan bahawa

rantai karbon dan cincin gula bukan-penurun berkemungkinan terpusing dan menonjol ke dalam bahagian kumpulan kepala di mana permerhatian ini mencadangkan bahawa sistem βMal-C_{12}(23%wat) mungkin beralih ke fasa metastabil di mana lipid-lipid tersebut cuba menyusun semula kepada struktur swa-susunan yang berlainan seperti fasa hexagonal. Kami juga mendapati ikatan hidrogen di antara molekul cincin gula di dalam kumpulan kepala maltosa tidak menunjukkan sebarang perubahan yang jelas walaupun dwilapisannya di bawah pengaruh kepekatan air dan suhu yang berlainan. Turut diperhatikan gula bukan-penurun dari semua sistem dwilapisan berputar laju berbanding gula penurun, manakala kumpulan eksosiklik berputar lebih laju berbanding cincin gula itu sendiri dan tiada kesan sifat kiral terhadap diffusi putaran. Parameter susunan pada segmen rantai karbon menunjukkan ianya agak sensitif terhadap suhu dan kepekatan air serta ianya sedikit dipengaruhi oleh sifat kekiralan, khususnya dalam campuran racemic dwilapisan. Simulasi ini memberi pemahaman yang penting mengenai hubungkait di antara struktur dan sifat asas molekul untuk mereka bentuk bahan glikolipid sintetik.

ACKNOWLEDGEMENTS

I would like to express my utmost gratitude to my supervisor Professor Dr. Rauzah Hashim for providing a professional, yet, informal environment rich in nourishing scientific curiosity. She introduced me to the field of liquid crystal and simulation during my MS'c program. One point in teachings was "crystal does flow", and that information really stirred my mind. I started to wonder how crystal, a hardened material could flow. That was the way how she inculcated the interest for science in me. Nevertheless, she also offered unfading encouragement, financial support and guidance with patience throughout my studies and research trainings. I am also truly thankful to Professor Dr. Rauzah Hashim for granting me the opportunity to visit a computational lab at Manchester Pharmacy School, The University of Manchester, UK, under the supervision of Dr. Richard Bryce. During my six months there, I had a wonderful time with Richard in discussing many aspects on modelling and simulation. Many thanks also to all the people in Richard's lab for welcoming me and being helpful.

Besides that, often we had visitors to our lab (FSSA–Fundamental Science of Self-Assembly) and they too offered valuable discussions relating science in general, and glycolipids specifically. Amongst them are Professor Dr. John M. Seddon, Associate Professor Dr. Osama K. Abou-Zied, Professor Dr. Claudio Zannanoni and Dr. Timimi. I wish to thank them for their willingness in sharing their expertise.

In addition, I also would like to express my heart felt thanks to all my lab members Dr. Nguan Hock Seng, Dr. Sara Ahmadi, Dr. Noraini Ahmad, Dr. Idayu, Dr. Zahrabatoul Mosapour, Dr. Karem Sabah, Associate Professor Dr. Thorsten Heidelberg, Dr. Rusnah Syahila, Dr. Malinda, Seyed Mirzadeh Hosseini, Meloney, Liew and Hairul Amani for their help and support at all times. I also wish to thank Mr. Mohamad Safwan from ITC (Information Technology Center) for offering help in handling Academic Computing (High Performance Computers (HPC) & Clusters) and GPGPU machines.

I am also deeply grateful to my late parents, Manickam Achari and Rajamani Ammal. Without their unconditional love, care and sacrifice, I would not have been able to step into higher learning institutions. Both my elder brother (Nagaretnam) and sister (Saroja Devi) supported me morally and financially throughout my studies. I also wish to thank uncle

Tharumalingam and Mr Kanthan who seeded the interest and the value for pursuing higher learning after my high school. I also wish to thank and bow down in gratitude to all my school teachers right from primary until my postgraduate level for their invaluable help in my academic path. Additionally, I wish to extend my humble obligation to my spiritual masters Sri Ramana Maharishi, Vethathiri Maharishi, T.K.Subramaniam, and Sadguru-Jaggi Vasudev, who taught me about the reality of existence from another dimension. Last but not least, I wish to thank my beloved friends whose support was always there when I needed it.

Finally, I extend my thanks to the University of Malaya's Pasca Siswazah financial scheme, Postgraduate Research Grant (PPP), and High Impact Research Grant (UM.C/HIR/MOHE/SC/11) for their financial support to attend conferences locally and abroad.

TABLE OF CONTENTS

LIST OF FIGURES

LIST OF TABLES

LIST OF ABBREVIATIONS

A	Hamaker constant.
A_b	Area of bilayer.
C_V	Heat capacity.
E	Interaction energy / Total energy.
H	Mean curvature.
K	Gaussian curvature.
M	Number of hydrocarbon chain / Number of time steps.
N	Number of particles.
N_A	Avogadro number, 6.23×10^{23}.
N_d	Number density.
P	Pressure.
P_2	Legendre polynomial.
R	Particle radius / packing parameter (shape factor) / Radius of curvature.
T	Temperature.
V	Hydrocarbon chain volume / Volume of box.
V_b	Volume of bilayer.
Z_1, Z_2	Number of charges.
α	Average tilt angle.
α_1, α_2	Polarizability.
γ	Constant related to surface potential.
$\hat{n}$	Director.
κ^{-1}	Double layer thickness.
$\langle\rangle$	Statistical average.
μ	Dipole moment / Chemical potential.
ν	Characteristic vibration frequency.
ψ	Angle between the line of centers and the axis of the dipole.
τ	Simulation time.
ε	Permitivity.
ε_0	Dielectric constant.
φ	Electrical potential.
φ_0	Surface potential.
ζ, β	Pre-exponent constant.
a_0	Area per molecule at interface.
c	Molar concentration.
c_0	Spontaneous curvature.
c_1, c_2	Principal curvatures.
d-spacing	Bilayer thickness.
e	Electronic charge.
h	Planck constant, $6.626\,075\,5 \times 10^{-34}$ Js.
l_0	Critical hydrocarbon chain length.
$n_\parallel$	Parallel to the director.
$n_\perp$	Perpendicular to the director.
n_i	Concentration of the charged species.
p	Momenta.

r	Cut-off distance / Atomic positions.
x	Separation distance of two ions.
z	Number of charges on the counter ion.
z_i	Number of charges on the charged species.
S	Order parameter.
ρ^*	Volume charge density.
∇^2	Laplacian operator.
Å	Angstrom.
Q_{II}	Inverse bicontinues cubic.
I_{II}	Inverse micellar cubic.
H_2O	Chemical formula for water molecule.
Q	Cubic phase.
S_o	Solid ordered phase.
T_g	Glass transition.
H	Hexagonal phase.
H_I	Normal hexagonal phase.
H_{II}	Reverse hexagonal phase.
T_C	Critical temperature, clearing temperature.
T_m	Melting temperature or main phase transition.
L_I	Normal micellar phase.
L_{II}	Inverse micellar liquid phase.
P_β	Ripple phase.
P	Pitch, distance needed to rotate the director $\hat{n}$ by 2π along the helix axis.
e.g.	exempli gratia; for example.
et al.	et alii; and others.
k_B	Boltzmann's constant, 1.3807×10^{-23} JK^{-1}.
Q_I,I_I	Discontinues cubic phase.
L_α,L_d	Lamellar phase.
L_β,S_o	Gel phase, lamellar gel phase.
AMBER	Assisted Model Building with Energy Refinement.
BD	Brownian dynamics.
C_D	Lateral diffusion coefficient.
CHARMM	Chemistry at HARvard, Macromolecular mechanics.
CPU	Central Processing Unit.
DPPC	Dipalmitoylphosphatidylcholine.
FEP	Free Energy Perturbation.
ffTK	Force Field Toolkit.
GAFF	General Amber Force Field.
GL	Glycolipid.
GLYCAM	Glycoprotein and Carbohydrate Parameters for AMBER.
GROMACS	GROningen MAchine for Chemical Simulations.
GROMOS	GROningen MOlecular Simulation.
HB	Hydrogen bonding.
L	Simulation box side length.
LAMMPS	Large-scale Atomic/Molecular Massively Parallel Simulator.

LC	Liquid crystal.
LDP	Local density profile.
LINCS	linear constraint solver.
MC	Monte-Carlo.
MD	Molecular dynamics.
MM	Molecular mechanics.
NAMD	NAnoscale Molecular Dynamics.
NMR	Nuclear Magnetic Resonance.
P1, P2	Peaks at distribution function.
PBC	Periodic boundary condition.
PC	Phosphatidylcholine.
PDB	protein data bank.
PE	Phosphatidylethanolamine.
PME	Particle Mesh Ewald.
PMF	Potential of Mean Force.
QM	Quantum mechanics.
RACF	Rotational autocorrelation function.
RDF	Radial distribution function.
SD	Steepest descent.
SPC	Simple point charge.
XRD	X-Ray diffraction.

LIST OF APPENDICES

CHAPTER 1

INTRODUCTION

Imagination is more important than knowledge.
Albert Einstein (1879-1955)

This chapter briefly highlights the content of the thesis and begins with the definition for the term 'glycolipid' (a material commonly found in nature) which is described and its classifications are given. Following this, various possible self-assembled structures of glycolipids are explained. One of these structures is the 'lipid bilayer' which is commonly used as a model for cell membrane and of interest in this thesis. Subsequently, the objectives of this research work are outlined. These objectives are related to some fundamental questions that help us to understand the physicochemical properties of glycolipid bilayer systems. The experimentation by computational approach is illustrated next because this technique has been used successfully as a tool to explore the structural and dynamical behavior of bilayer self-assembly. Finally, the thesis frame work is summarized to ease the readability of this report.

1.1 Brief overview of glycolipids

Lipid is a class of biomolecule (other than proteins and nucleic acids) that facilitates multiple biochemical and biophysical functions to regulate living organisms (Dowhan, Bogdanov, & Mileykovskaya, 2008). In general, a lipid is divided into several categories like fatty acyls, sterol lipids, glycerolipids, glycerophospholipids, waxes, and sphingolipids (see Figure 1.1). This classification scheme is based on chemical features where each lipid type contains distinct classes and subclasses of molecules as its functional groups (Fahy et al., 2005).

Among these lipids, the term 'glycolipid' refers to any compound, containing one or more saccharide (sugar) residues bound by a glycosidic linkage to a chain moiety such as an acylglycerol, a sphingoid or a ceramide (see Figure 1.2a). This falls under the class of sphingolipids (Merrill et al., 1997). For example, a ceramide is a sphingolipid containing an amino group of the sphingosine linked to the acyl group of a fatty acid (see Figure 1.2b). While most sphingolipids contain a ceramide unit, it is the different

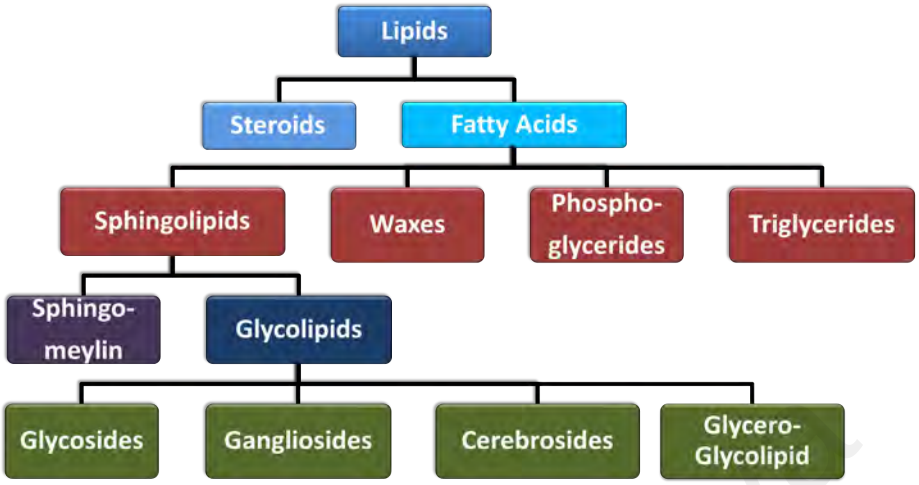

Figure 1.1: Lipid classification. Redrawn and extended from Ball et al. (2011).

headgroup that are attached to these sphingosine that gives rise to a variety of lipids. For instance, if the primary hydroxyl (−OH) on a sphingosine is bonded to a phosphocholine or phosphoethanolamine via an ester linkage, it then becomes a sphingomyelin. On the other hand, if the primary −OH group of the sphingosine bonds with a sugar residue by a glycosidic linkage, then it becomes a glycosphingolipid. Since the sphingomyelin contains a phosphate group, it is not classified as glycosphingolipid but as a phospholipid. Several examples of these lipids are shown in Figure 1.3.

The glycolipid is also collectively regarded as a part of a larger family of substances known as glycoconjugates (see Figure 1.2c) including glycoproteins, glycopeptides, peptidoglycans, and proteoglycans to name a few, where each glycoconjugate sugar moiety binds to the specific biomolecule via covalent chemical bond (Chester, 1997).

Glycolipids are structurally very heterogeneous moieties (Dembitsky, 2004a) and they are membrane-bound compounds found in all living organisms — from prokaryotic to eukaryotic cells, from bacteria to humans. For instance, cerebrosides, globosides, and gangliosides are the main classes of glycolipids found in higher concentrations in the membranes of nerve cells (Goodby et al., 2007; Posse de Chaves & Sipione, 2010). These are an important class of cell membrane components since they facilitate many biological functions. In particular, they are found in the exterior of cell walls and involved in the intercellular recognition processes while acting as receptors and providing specific contacts.

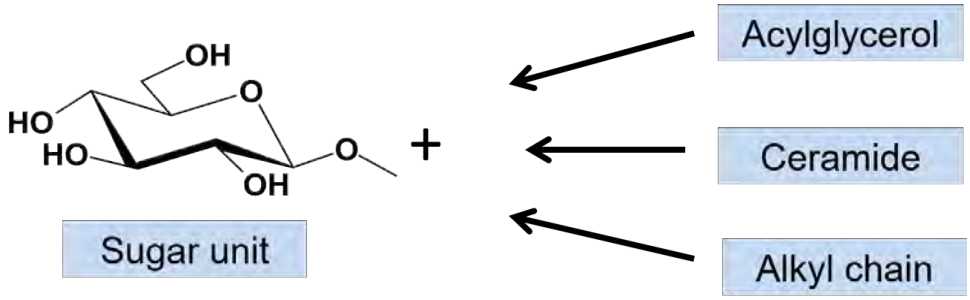

(a) Sugar moiety attach with different type of chains.

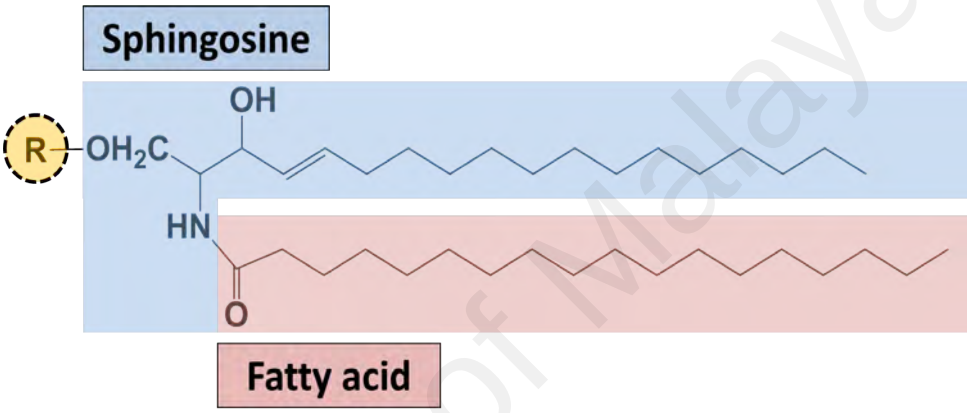

(b) Composition of a sphingolipid.

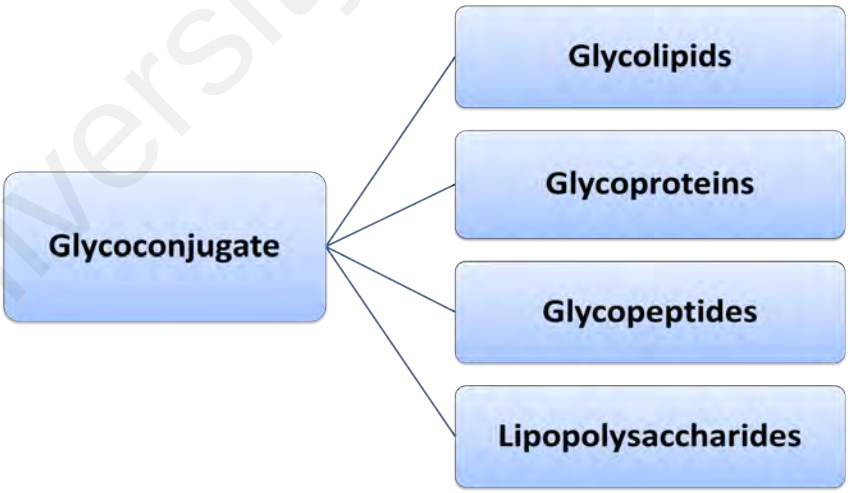

(c) Classes of glycoconjugates

Figure 1.2: (a) Sugar moiety attached to different types of chains possibly forms different glycolipid compounds. (b) Composition of a sphingolipid which forms the basic structure of ceramide unit. (c) Classes of glycoconjugates based on saccharides.

(a) Sphingomeylin

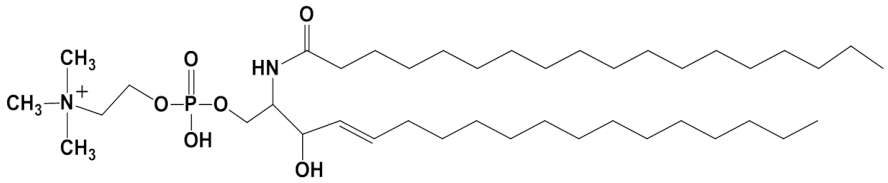

(b) Glucosylceramide

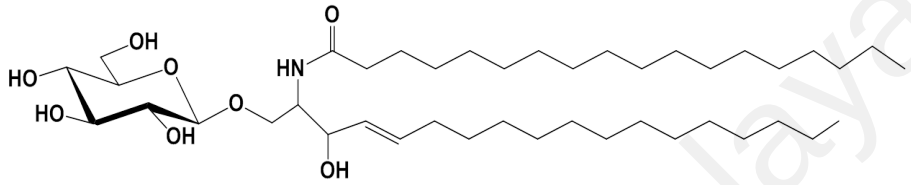

(c) Galactosylceramide

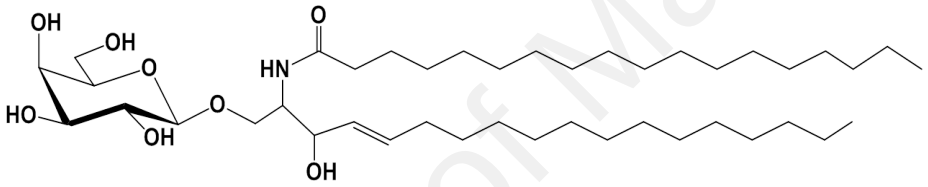

(d) Ganglioside

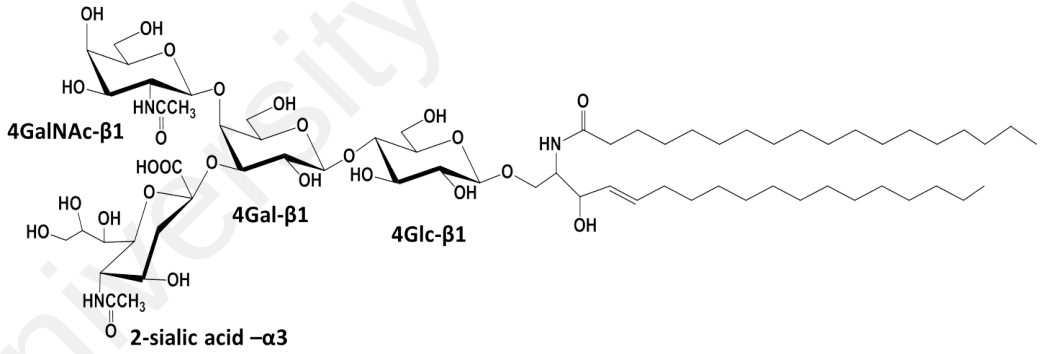

(e) Guerbet glycoside-C18C14

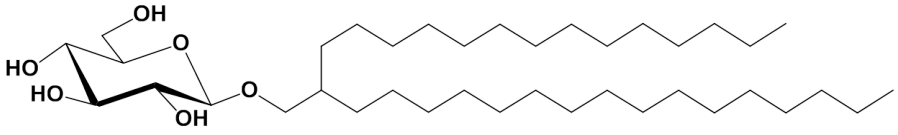

Figure 1.3: Various types of lipid including (a) sphingomeylin which is a phospholipid and glycolipids (b) glucosylceramide, (c) galactosylceramide, (d) ganglioside and (e) a synthetic Guerbet glycoside. Structures (a) to (d) are redrawn from King (2014b) and (e) from Hashim et al. (2006).

Moreover, the antigen receptors of the T cells (known as invariant natural killer T (iNKT) cells), specifically recognize certain glycolipids, most notably glycosphingolipids with α-anomeric monosaccharides. Upon activation, the iNKT cells can secrete a very diverse array of pro- and anti-inflammatory cytokines to modulate innate and adaptive immune responses. Therefore, the glycolipid-mediated activation of iNKT cells has been explored for immunotherapy in a variety of disease states, including cancer and a range of infections (Carreño, Saavedra-Ávila, & Porcelli, 2016).

Beside their biological importance, glycolipids have many industrial applications due to their surface-active property – their tendency to segregate to an air-water interface and consequently to lower the surface tension compared to pure water. For example, surfactant alkyl polyglucosides (APG) is a nonionic surfactant with a carbohydrate-derived headgroup. These glycolipids possess features such as readily biodegradable, non-toxic, mild to the skin, and have synergistic effects in combinations with anionic surfactants (John & Vemula, 2006; Kitamoto, Isoda, & Nakahara, 2002). Due to their versatile qualities and environmentally friendly nature, they are applicable in the areas of foods, pharmaceuticals, cosmetics, and detergents (Balzer, 2000; John & Vemula, 2006).

Like synthetic lipids, many naturally produced lipids (biosurfactants – structurally diverse group of surface-active substances produced by microorganisms) have also given rise to many commercial applications in numerous industries as indicated in Table 1.1. These days, microorganisms are used as renewable resources to produce natural glycolipids as alternatives to synthetic surfactants in several industrial processes, such as lubrication, wetting, softening, making emulsions, stabilizing dispersions, foaming, preventing foaming, as well as bioremediation of organic- or inorganic-contaminated sites (Reis et al., 2013). For example, glycolipid rhamnolipids which are produced by the bacteria *Pseudomonas aeruginosa*, are used in several applications such as in bioremediation, food industry, cosmetics and as antimicrobial agents. Several studies had shown rhamnolipids to be efficient in chelating and removing washing heavy metals. Further, their interaction with organic compounds increases their bioavailability or aids their mobilization and removing wastes from washing treatments. Interestingly, rhamnolipids combined with a pool of enzymes produced by *Penicillium simplicissimum* enhanced the biodegradation of effluents with high fat content from poultry processing plants, suggesting a synergistic interaction between biosurfactants and enzymes in waste

Table 1.1: Types of glycolipid biosurfactants and microorganism producing them followed by their applications. Taken from (Reis et al., 2013).

Biosurfactant	**Microorganism**	**Application**
Rhamnolipids	*Pseudomonas aeruginosa (P. aeruginosa)* and *Pseudomonas putida (P. putida)*	Bioremediation
	Pseudomonas chlororaphis (P. chlororaphis)	Biocontrol agent
	Bacillus subtilis (B. subtilis)	Antifungal agent
	Renibacterium salmoninarum (R. salmoninarum)	Bioremediation
Sophorolipids	*Candida bombicola (C. bombicola)* and *Candida apicola (C. apicola)*	Emulsifier, MEOR, alkane dissimilation
Trehalose lipids	*Rhodococcus* spp.	Bioremediation
	Tsukamurella sp. and *Arthrobacter* sp.	Antimicrobial agent
Mannosylerythritol lipids	*Candida antartica (C. antarctica)*	Neuroreceptor antagonist, antimicrobial agent
	Kurtzmanomyces sp.	Biomedical application

treatment (Damasceno, Cammarota, & Freire, 2012; Nitschke & Costa, 2007; Reis et al., 2013).

From a chemical point of view, the many uses of glycolipids are related to the amphiphilic nature of the lipid. That is the lipid has two regions — headgroup and tail as shown in Figure 1.4, where both the regions have different affinities toward solvents like organic or non-organic. The headgroup (hydrophilic) usually has a high affinity toward non-organic solvent like water and the tail region (hydrophobic) shows a very low affinity towards non-organic solvents but high affinity towards organic solvents. This unique amphiphilic character of lipids enables them to self-assemble when they are being in the close proximity in the presence of a solvent. For instance, when amphiphilic molecules are added into water, they self-assemble at the air-water interface with the hydrophilic headgroup submerged into water and the hydrophobic tail pointing at air forming a mono-layer assembly. This layer formation physically reduces the surface tension of the water-surface and the increase in the surfactant concentration induces the formation of other self-assembly structures such as lamellar (L_α), hexagonal (H) and cubic (Q), rippled (P_β) and gel (L_β) phases, depending on the degree of amphiphilicity in the molecule.

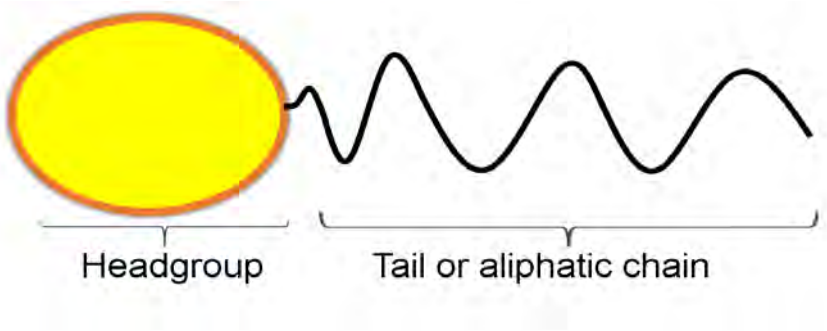

Figure 1.4: Model of a amphiphilic molecule

Additionally, the amphiphilic nature of a lipid molecule is related to the type of headgroup, linkage, and hydrocarbon chain. For example, surfactants with a negatively charged headgroup are referred to as anionic, whereas cationic surfactants contain a positively charged headgroup. Uncharged surfactants are generally referred to as non-ionic, while zwitterionic surfactants contain both negatively and positively charged groups. Naturally occurring phospholipids such as Phosphatidylcholine (PC) and Phosphatidylethanolamine (PE) are zwitterionic lipids (Holmberg, Jönsson, Kronberg, & Lindman, 2003) while surfactant with carbohydrate moieties is non-ionic (dos Santos, Medronho, dos Santos, & Antunes, 2013). The latter is interesting since it forms a multitude self-assembled structures (mesophases) in the anhydrous (dry condition) and in the presence of polar solvent (Hashim et al., 2010; Kitamoto, Morita, Fukuoka, Konishi, & Imura, 2009). Nonetheless, the hydrophobic group with long carbon chain, $n(CH_2)CH_3$, with $4 < n < 16$, also influences the mesophase formation with the tail part being mono- or asymmetric branched hydrocarbon chains with the terminal group being methyl. The detailed discussion on the formation of mesophases with regard to carbohydrate-surfactants is given in Chapter 2 (Background and Literature review).

1.2 Lipid bilayer

Among various mesophases that a glycolipid can form, the lipid bilayer structure (see Figure 1.5) is considered as an interesting phase since it mimics the structure of a biological membrane. Although the major component of a biological membrane is phospholipid, the basic matrix of the membrane is the lipid bilayer structure. It is interesting to have a brief view on the historical development of the biomembrane concepts since they gave us profound understanding of their structure and dynamics properties through extensive

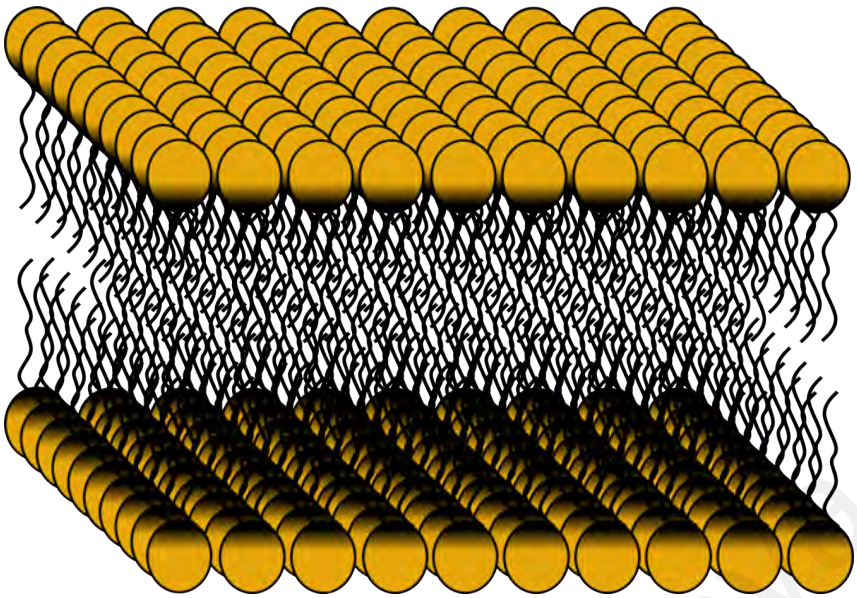

Figure 1.5: Lipid bilayer model structure composed of two layers arranged with the hydrophobic core pointing in the middle and the hydrophilic region pointing oppositely.

experiments and theoretical investigations. Historically, the concept of the biological membrane being composed of two layers of lipids was first proposed by Gorter and Grendel (1925) (see Figure 1.5). They observed red blood cells using Langmuir method and concluded that the molecular area of lipids extracted from red blood cells was two times the area of the red blood cells measured by microscopy. Following the above observation, Danielli and Davson (1935) coined another model which includes protein in the membrane. Their study postulated that a protein layer is tightly associated to the polar heads of lipids composing the cell membranes. After about thirty years, another observation saying that the protein may also span through membranes was postulated and a model representing this idea was proposed by Singer and Nicolson (1972) which was known as a fluid mosaic model of membrane (see Figure 1.6). According to this model, each leaflet of the bilayer is formed by a homogeneous environment of lipids (surrounds with a sea of lipids) in a fluid state incorporating globular assembling of proteins and glycoproteins. It was also assumed that the lipid composition within the bilayers is most likely asymmetric (Epand, 2015).

Ever since this conception was formulated in 1972, some developments and refinements were brought to the fluid mosaic model especially in terms of composition and molecular organization by D. A. Brown and London (1997); Simons and Ikonen (1997) showed that biological membranes do not form a homogeneous fluid lipid phase as predicted by Singer and Nicolson (1972). But, they suggested that membrane lipids are

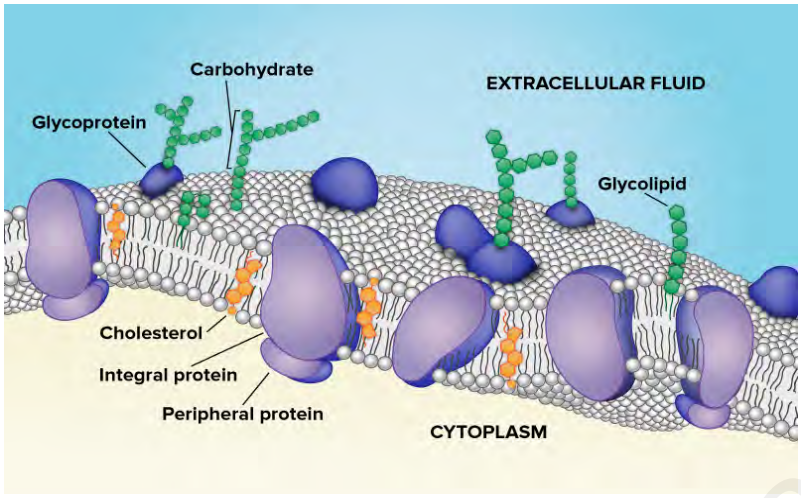

Figure 1.6: Fluid mosaic model for biomembrane. Adopted from King (2014a) and image: reproduced with permission of themedicalbiochemistrypage, LLC.

organized into phase-separated microdomains, known as lipid rafts, where the membrane has specific composition types and dynamic modes of the molecules compared to the ones surrounded by liquid crystalline phase. Nowadays, while there is no doubt about the presence of phase separation in the plane of the membrane, the existence of lipid rafts, which is believed to be accompanied by sphingolipids and cholesterol, possess high mobility in the plane of the membrane and enhance many biological processes such as signal transduction, membrane transport and protein sorting (Cambi & Lidke, 2015; Simons & Ikonen, 1997).

Despite the above findings are based from biological membranes, they give valuable impression about lipid bilayer systems in general and that can be extended to the bilayers formed by single type lipids (e.g. glycolipids or phospholipids). Additionally, the structures of the bilayers are influenced by factors like solvent type, concentration, and temperature. These factors allow the formation of many different kinds of bilayer structures. For example, a hydrated bilayer is classified as a liquid crystalline (L_α) phase in which the alkyl chains are disordered above the main transition temperature, T_C, while below that, the system assumes a gel phase (L_β), where the extended lipid chains tilt to the normal of the bilayer. At a much lower temperature, the bilayer forms a lamellar crystalline phase (L_C) where the extended lipid chains now have much lower tilting angles relative to those in the gel phase (Lewis & McElhaney, 1992). At zero or a very low hydration, most of the lipids form a lamellar crystalline (L_C) phase (Cullis & De Kruijff, 1979; Goodby et al., 2007; Kulkarni, 2012). Usually, these lamellar phases show both long and short range order similar to a

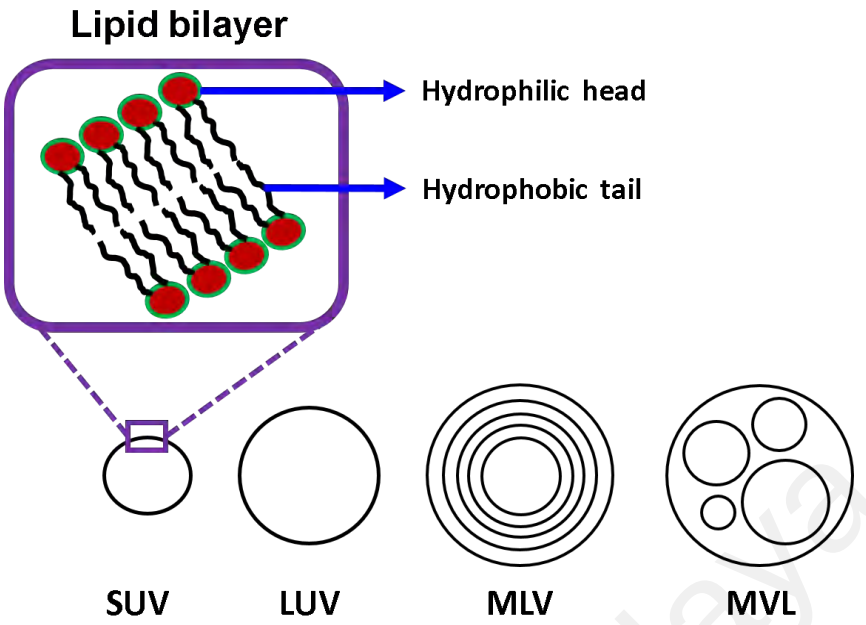

Figure 1.7: Schematic diagram of different types of vesicle structures. SUV (small unilamellar vesicles), LUV (large unilamellar vesicles), MLV (multilamellar vesicles), and MVL (multivesicular liposomes). Each circle represents a lipid bilayer structure (adapted from Salim et al. (2014)).

true crystal (Kulkarni, 2012). Additionally, other factors such as the molecular geometry (stereochemistry), chain design, and headgroup size also influence the occurrence of these phases (Lewis & McElhaney, 1992).

By the way, surfactants with a suitable hydrophobic and hydrophilic ratio preferably form a bilayer structure with a curved surface[1]. The edge-closed curved bilayer forms a structure called vesicle (from the Latin *vesicula* which means a small bubble as shown in Figure 1.7). Vesicle carriers can be in different structures as shown in Figure 1.7; such as multilamellar vesicles/MLV, small unilamellar vesicles/SUV, large unilamellar vesicles/LUV and multi-vesicular liposomes/MVL. Their sizes range from *nm* to *mm* in diameters. These vesicle carriers are able to entrap multiple bioactive molecules and cargo, both hydrophobic and hydrophilic nature elements (Salim et al., 2014).

Conventionally the vesicle is also called as a liposome (from Greek *some* means body) which is typically constructed by phospholipids (Antonietti & Förster, 2003). But a vesicle formed from carbohydrate-derived surfactants (like APG – alkylpolyglycosides) is called a *niosomes* due to its non-ionic characteristic. Niosomes are easy to prepare in large amounts and a multitude industrial applications are believed to be promising (John & Vemula, 2006;

[1]Detailed explanations are given in the next chapter

Kitamoto et al., 2002, 2009). Thus, the understanding of the physicochemical properties of glycolipids is important for designing lipid moieties with controllable features, especially for the self-assembling structure like lamellar. Lamentably, their fundamental studies on liquid crystals are scarce (Goodby, Pfannemüller, Welte, Chin, & Goodby, 2006; Vill & Hashim, 2002). Therefore, we have made an attempt to study the structure-property relationship of glycolipids, especially in the lamellar phase, by computational methods (the details are given in chapter three).

1.3 Motivation and research objectives

The natural glycosides (see Figure 1.8) are difficult to extract in high yields and purity, but the synthetic glycolipids are highly sought after, especially those with promising properties that mimic the natural ones (Balzer & Lüders, 2000; Hashim, Sugimura, Minamikawa, & Heidelberg, 2012; Vill, Bocker, Thiem, & Fischer, 1989). Since the synthetic glycolipids are non-ionic, biodegradable (Garelli-Calvet, Brisset, Rico, & Lattes, 1993) and possess other features like low toxicity and low immunogenicity (Curatolo, 1987; Ellens, Bentz, & Szoka, 1985; Kasahara & Sanai, 1999), they draw attention of many researchers from various fields and promote a broad scope of interest including many fundamental studies.

For instance, industrially produced dodecyl β-maltoside (βMal-C_{12}) has been used in the purification and stabilization of proteins, like RNA polymerase, and the detection of protein-lipid interactions (Bujarski, Hardy, Miller, & Hall, 1982; Lambert, Levy, Ranck, Leblanc, & Rigaud, 1998; Sasaki, Demura, Kato, & Mukai, 2011). But the α-maltoside, which is anomerically different to βMal-C_{12}, is not used for the purification of membrane

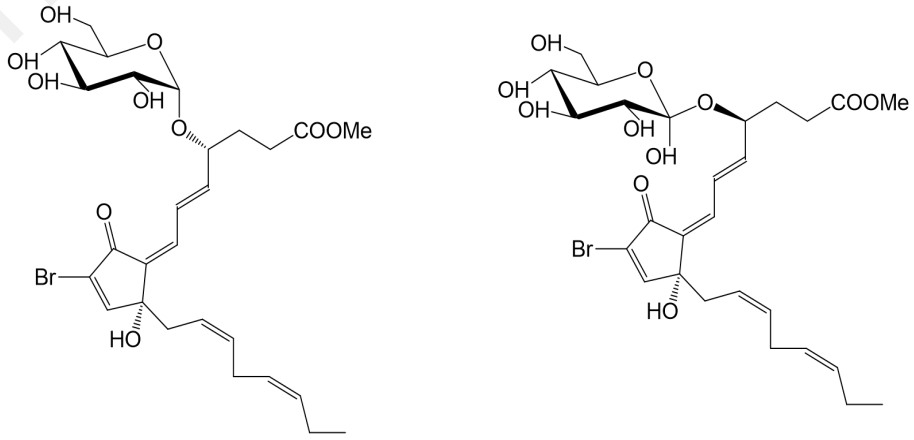

Figure 1.8: Examples of natural glycosides. These compounds are brominated oxylipins, which were isolated from the Red Sea invertebrates. Redrawn from Dembitsky (2004b).

protein. Additionally, the phase diagrams of anomers α-dodecyl maltoside and β-dodecyl maltoside shows very different (Auvray et al., 2001) behavior of those two molecules in self-assembled environment, as in C4 epimers in alkyl β-glucoside and β-galactoside (Ahmadi, Manickam Achari, Nguan, & Hashim, 2014).

Therefore, the ability of a glycolipid molecule to form various self-assembled structures is unambiguously related to its unique amphiphilic nature and the molecular structural conformations (N. Ahmad et al., 2012; Goodby et al., 2007; Hashim et al., 2012; Jayaraman, Singh, Rao, & Prasad, 2007; Sakya, Seddon, & Vill, 1997; Vill & Hashim, 2002). Of all possible self-assembly structures, the lamellar or a lipid bilayer structure, which acts as the basic matrix for the biomembrane (Singer & Nicolson, 1972) and also for the vesicle (M. U. Ahmad et al., 2015; Imura et al., 2005; Inès & Dhouha, 2015; Uchegbu & Vyas, 1998) has been studied both experimentally (Kučerka et al., 2005; Nagle & Tristram-Nagle, 2000b; Pabst, Kučerka, Nieh, Rheinstädter, & Katsaras, 2010) and theoretically (Muckom, Stanzione, Gandour, & Sum, 2013; P. Niemelä, Hyvönen, & Vattulainen, 2004; Venable, Brooks, & Pastor, 2000) to understand the relationship from the molecular structure to the behavior in various environments. Additionally, reports on the structure to property relationship of synthetic branched chain glycolipids, especially the newly discovered Guerbet glycosides, are gaining more attention in recent years (Hashim et al., 2012). For the Guerbet glycoside, apart from the sugar complexity in disaccharides, there is also the presence of a chiral center at the chain branching which has been rarely addressed in the literature (Hashim et al., 2012). In general, chiral isomers affect the physicochemical behavior of chemical substances. For instance, the chirality in the glycolipid molecules may be expected to affect the physical properties of their self-assembled structures (Seddon, Ces, Templer, Mannock, & McElhaney, 2003). Likewise, the large difference between thermotropic and lyotropic phase behavior may be related to the molecular shape resulting from the very subtle differences in chemical structures like chiral isomers and conformations which in turn affect the stability of the liquid crystalline phases of glycosides (Boyd, Krodkiewska, Drummond, & Grieser, 2002).

Although, investigations on glycolipids are receiving appreciable attention, but studies on the lamellar structures of glycosides with disaccharides as the hydrophilic moiety have received less focus. Considering the versatile applicability of glycolipids and their

interesting self-assembling behavior (especially in lamellar), together with their unique stereochemical properties, there is a need to unravel the structure-property relationship with regards to the molecular level of understanding in a systematic way. This may help to rationalize the designing of new glycolipid materials to be applicable in multitude uses, like in vesicle formulations. Investigation of these systems in the anhydrous state is also necessary to understand the detailed behavior of individual lipids uncomplicated by the presence of a solvent. Previously, some synthetic glycolipid bilayers have been studied experimentally in dry as well as hydrated forms (Auvray et al., 2001; Ericsson, Ericsson, Kocherbitov, et al., 2005), including dodecyl β-maltoside (βMal-C_{12}) which exists in an L_C phase over a temperature range of 20 −80 °C (Auvray et al., 2001).

With these ideas in mind, we conduct "computational experiments" on several glycolipid bilayer structures, not only in the normal hydrated form but also in a completely anhydrous (dry) condition, which is difficult to achieve in reality since glycolipids are highly hygroscopic. The lipids we choose in the bilayer construction are differ in sugar types (maltose, cellobiose, isomaltose) at the hydrophilic region and chain (single or branching – including Guerbet branch chain) in the hydrophobic region. They comprise dodecyl β-D-maltoside (βMal-C_{12}), dodecyl β-D-cellobioside (βCel-C_{12}), dodecyl β-D-isomaltoside (βIsoMal-C_{12}), as well as branched chain maltoside (βMal-$C_{12}C_{10}$) together with asymmetric branched chain Guerbet maltosides, βMal-$C_{12}C_8$(R) and βMal-$C_{12}C_8$(S), in the R & S isomeric forms respectively.

Our first objective is to observe the conformational behavior of the sugars and chain moieties in the anhydrous condition. Secondly, we hope to rationalize the stability of the bilayer structures with respect to the hydrogen bonding within sugars in the hydrophilic region. Our third objective is to understand the effects of temperature, water concentration, chain branching and chirality on the behavior of bilayer structures. As a fourth objective, we would like to understand the dynamics of sugar moieties at the headgroup and the chain segment with regards to the dry and hydrated conditions.

In our study, we have used computational methods, especially molecular dynamics simulation, which is considered as one of the powerful tools for characterizing the structure and dynamic properties of self-assembled structures like lamellar at the molecular-level and at atomic resolution (Dickson et al., 2014; Kapla, Stevensson, Dahlberg, & Maliniak, 2011; Róg, Vattulainen, Bunker, & Karttunen, 2007; Tessier, DeMarco, Yongye, & Woods,

2008). Below, we have given a brief overview of the computational experimentation that have made an notable impact on the scientific field.

1.4 *In silico* experimentation

In the year 2013, the Royal Swedish Academy of Sciences awarded the 'Noble Prize' to Martin Karplus, Michael Levitt and Arieh Warshel for 'the development of multiscale models for complex chemical systems' (Schlick, 2013). This award is for honoring their work on the development and application of methods to simulate the behavior of molecules at various scales – from single molecules to complex proteins – in order to understand diverse phenomena like protein folding, catalysis, electron transfer and drug design. This marks the accreditation given to the field of computational chemistry indicating that the field has matured and is on par with other traditional experimental sciences.

Although computational sciences have received much attention in recent times, their importance has only been realized in recent decades. As a reflection, at the end of the 1980's a term "*in silico*" was coined to refer to an experiment that was carried out virtually. This "new" term was used to distinguish scientific results produced from "computers" or virtual experiments from those which were obtained by the conventional way in a laboratory. An interesting discussion regarding the term "*in silico* experimentation" is given by Moretti (2011). The author gives two view points – the first view emphasizes "computer programs" that realize some specific operations under particular experimental conditions which allow one to investigate biological phenomena by complementing those results from *in vivo* and *in vitro* experiments. Meanwhile, in the second view, he highlights the meaning of "simulation" where its identity is mostly linked to that of a "model" used to construct such simulation.

Later, the second view has received much appreciation and is widely accepted, especially in bio-molecular simulation, ever since the first simulation work by Alder and Wainwright (1957). As time evolved, simulation of biological systems, such as nucleic acid, proteins and lipids have become virtual disciplines which take more definitive forms and play central roles between experiment and theory (Haile, 1992). This includes modelling of a biological system and virtually makes it "alive". Subsequently, interesting properties are evaluated using well-defined methodologies.

The extent of investigation carried out for a biological system via "computer experiment" mostly depends on hardware and software (algorithm) besides simulation methodologies such as molecular dynamics (MD) and Monte Carlo (MC). High processing power, sufficient memory, and adequate power supplies are the basic requirements for designing a preferred bio-molecular system. In addition, a well-defined numerical algorithm is crucial for efficient simulation and reproduction of experimental results. In recent years, software has been made available (commercially and freely for academic use) for performing a simulation. Software packages like AMBER (Assisted Model Building with Energy Refinement) by D. Case et al. (2006) and GROMACS (Groningen Machine for Chemical Simulations) by Lindahl, Hess, and Van Der Spoel (2001) are widely used due to their simplicity and usability.

In brief, *in silico* experiment effectively provides a number of significant advantages such as higher precision and better quality, more accurate simulation via a reliable model and a higher work productivity. Hence, simulation provides a promising solutions for investigating system properties beyond experimental limitations, especially in bio-molecular systems. There are some interesting texts available to improve our understanding of a simulation methodology and development (Allen & Tildesley, 1989; Haile, 1992; Leach, 2001; Van Der Spoel et al., 2010).

1.5 Thesis framework

Chapter one introduces the definition of the term 'glycolipid' and its classifications. Then various possible self-assembled structures of glycolipids are explained briefly and of these the 'lipid bilayer' is depicted as a model assembly of liquid crystal phase. This chapter also gives the motivation and objectives of this thesis and outlines the related fundamental study to understand the physicochemical properties of glycolipid bilayer systems. It as well addresses the computational approach which is used as a tool to explore the structural and dynamical behavior of biological systems in general before giving the thesis framework.

Chapter two briefly accounts for some fundamental physical principles relating to the self-assembly phenomena of surfactants. In particular, an introduction to the liquid crystal properties of materials forming liquid crystalline phases (including glycolipids) is given, covering the history and fundamental theories related to liquid crystals in general, for both thermotropic and lyotropic systems in particular. We also give a brief overview

of the experimental and computational research works related to glycolipid bilayers and other related assembly systems like hexagonal and micellar phases.

The third chapter elaborates on the computational techniques and methodology, particularly the molecular dynamics (MD) simulation method. With regards to this, a short list of force fields and software, which are routinely used to simulate biomolecules among simulators, is given. Additionally, the methods of analysis of structures and dynamical properties of bilayer that are calculated in this study are provided.

Chapter four presents the modelling and simulation of glycolipid bilayers in an anhydrous condition. The glycolipids' systems of interest are dodecyl β-maltoside (βMal-C_{12}), dodecyl β-cellobioside (βCel-C_{12}), dodecyl β-isomaltoside (βIsoMal-C_{12}) and a $C_{12}C_{10}$ branched β-maltoside (βMal-$C_{12}C_{10}$). Specifically, we examined the consequences of chain branching and headgroup types on their structural and dynamical properties.

The fifth chapter focuses on the same glycolipid types as described in chapter four in an anhydrous condition. However, the simulation methodology had been changed slightly and the production time was extended to 200 ns. This extension helped to determine the dynamical behavior of the lipids, especially segments like reducing, non-reducing sugars and hydrocarbon chain in the bilayers. We also made an attempt to understand the dynamics between the branched alkyl chains and the sugar groups at the hydrophilic region.

Meanwhile, the sixth chapter describes the properties of bilayer in the presence of water. We explained the behavior of bilayers with single and branched chain in the varying water concentrations, temperatures, and presence of chiral center at chain branching. Finally, concluding remarks and perspectives are given in the seventh chapter followed by references, appendixes and a list of scientific contributions.

CHAPTER 2

BACKGROUND AND LITERATURE REVIEW

Research is what I'm doing when I don't know what I'm doing.
Wernher von Braun (1912-1977)

This chapter gives a general perspective about liquid crystal state of matter – its history, classification, and properties. The thermotropic and lyotropic terms are explained by giving examples with various liquid crystal mesophases like the smectic, nematic, discotic nematic, lamellar, cubic and many others. This is followed by a general explanation of the associated interaction forces among lipid moieties which are crucial for the self-assembly phenomena. Additionally, theories on molecular packing and interfacial curvature are also discussed since these two ideas are routinely used to address the interesting behavior of self-assembly related to the headgroup and chain designs. The importance of the structure-property relationship of glycolipid liquid crystal is highlighted with regards to the lamellar structure which is the basis matrix for the plasma membrane of a biological cell.

2.1 Liquid crystals: a general perspective

2.1.1 Brief history

The discovery of Liquid crystal (LC) is thought to have occurred nearly 300 years ago although its usage and significance was not fully realized until over a hundred years later. The documented history of LCs can be traced back to George-Luis LeClerc (Compte de Buffon, 1707-1788) who observed myelin figures consisting of concentric cylindrical phospholipids in bilayers (Palffy-Muhoray, 2007). Following that, in 1850, Rudolf Virchow identified that myelin's line nerve fibers formed a fluid substance when left in water and exhibited a strange behavior when viewed using polarized light. They could not truly understand these strange behaviors. Later, in the year 1888, an Austrian botanist, Friederich Reinitzer, who was working in the Institute of Plant Physiology at the University of Prague, reported the observation of "double melting points" in cholesterol benzoate which he extracted from plants (Collings & Patel, 1997). The crystals of this material melted at 145.5 °C, forming a turbid fluid and upon further heating to 178.5 °C, it became completely

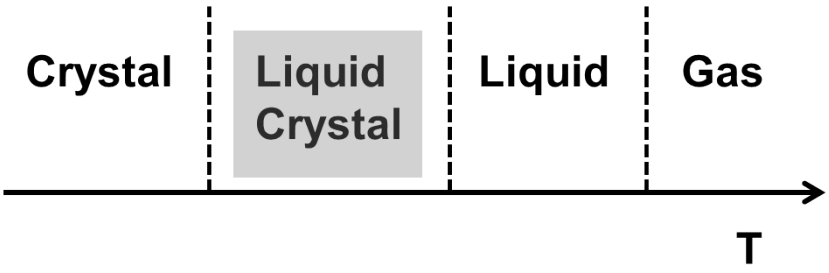

Figure 2.1: Phase diagram depicts the changing states of substance as the temperature is raised; from crystalline solid → liquid crystal → isotorpic liquid → gas. Adopted from Dierking (2003).

clear and he suggested that this cloudy fluid was a new phase of the said matter. Therefore, Reinitzer was officially credited for the discovery of this new phase of matter.

Puzzled by his discovery, Reinitzer turned to German physicist, Otto Lehmann in Karlsruhe for help, as he was an expert in crystal optics. Lehmann then verified the discovery and was convinced that the cloudy liquid had a unique type of order. Subsequently, he noticed the transparent liquid at higher temperatures had the characteristic of common disordered liquids but the cloudy liquid was a new state of matter. At first he named the cloudy liquid as *fileβende Kristalle* – in German (crystals showing fluidity) and later in 1890, he coined the name *flussige Kristalle* – in German (liquid crystals) (Kelker, 1973; Sluckin, Dunmur, & Stegemeyer, 2004), illustrating the fact that it was a state of matter in between liquid and solid and sharing important properties of both (see the illustration in Figure 2.1).

Investigations into some other substances in the turbid fluid state were carried out with much debate on whether they were homogeneous liquid crystals, incompletely melted crystals or substances with impurities. While these doubts surfaced in the minds of many scientists at that time, in the year 1916, Max Born proposed a dipolar theory for the fluids in liquid crystal phase but it proved to be unsuccessful. Following that, in 1922, Georges Friedel, a French crystallographer, convincingly argued that “liquid crystals” represent a new state of matter – between solid crystals and ordinary liquids, where the intermediate phases exhibit mesomorphic structures like nematic (from the Greek word *nematos* meaning "thread"), smectic (from the Greek word *smectos* meaning "soap") and cholesteric (better defined as chiral nematic) (Sackmann, 1989).

Another major contribution was done, in 1935, Vsevolod Freedericksz ii from St. Petersburg pointed out that the electric fields can orient the liquid crystal forming molecules

– mesogens (D. Dunmur, 2011). This set the stage for optical applications, where the birefringent properties of liquid crystals could be controlled via electric fields. But, during World War II, much of liquid crystal research came to an abrupt halt. After the end of the war in 1948, George Gray, a British chemist from the University of Hull, began to synthesize mesogens and published a full-length book on liquid crystals (Collings & Hird, 1997). His work stimulated enthusiastic interest among those in this field. By the mid-1950s, an American chemist, Glenn Brown, published a lengthy review article on liquid crystals and founded the Liquid Crystal Institute at Kent State University (Collings & Hird, 1997). Consequently, the liquid crystal research became active again towards a new paradigm.

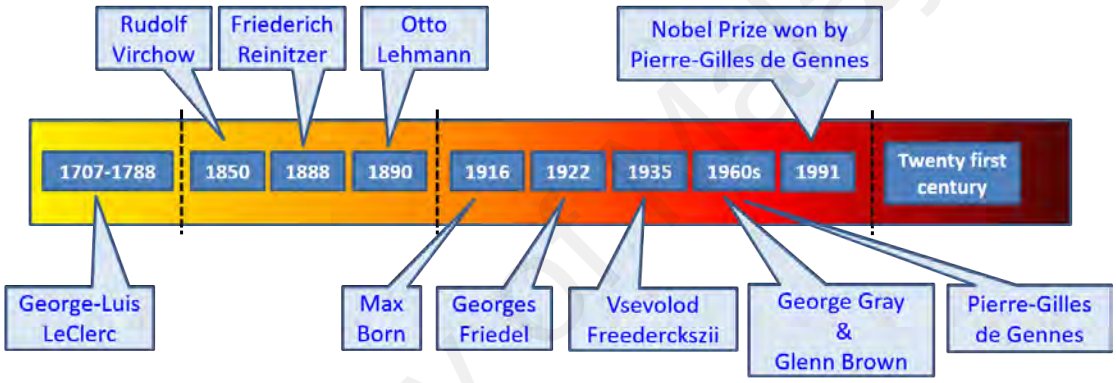

Figure 2.2: Timeline of liquid crystal field development in three centuries.

In the 1960s, a French theoretical physicist, Pierre-Gilles de Gennes, who had been working with magnetism and superconductivity, found fascinating characteristics between liquid crystals and superconductors as well as magnetic materials. In 1991, he was rewarded with the Nobel Prize for discovering the methods developed for studying order phenomena in simple systems which can be generalized to more complex forms of matter, in particular liquid crystals and polymers. This achievement was collectively proclaimed by LC scientists as an acknowledgment of the contribution of LC science to humanity (de Gennes & Prost, 1993). The timeline on the development of liquid crystal field is given above in Figure 2.2

2.1.2 Properties of liquid crystal

When we heat water in the state of a pure crystalline solid (ice) beyond its melting temperature, it undergoes a single transition state from a solid crystal (ice) to an isotropic

liquid. However, many organic compounds do not immediately transform to an isotropic liquid phase when heated beyond their melting temperature but exhibit more than a single transition from solid to liquid, showing the existence of one or more intermediate phases and exhibit the properties of both solids and liquids. For instance, the material may possess some typical properties of a liquid (e.g. fluidity, inability to support shear, formation and coalescence of droplets) as well as some crystalline (anisotropy in optical, electrical, magnetic properties, and periodic arrangement of molecules in one spatial direction, etc.) (Andrienko, 2006). These materials are called liquid crystal materials (or mesogens) and the term liquid crystal itself implies a physical state of matter (phase) possessing properties in between the solid crystal and the liquid phase. For example, when p-azoxy anisole (shown in Figure 2.3) is heated, it does not transform into the liquid state but adopts a molecular arrangement, that is both birefringence (a property of crystalline solid) and fluid (a property of liquid). The combination of these solid- and liquid-like properties gives the turbid appearance of a liquid crystal phase to the naked eyes. The fluid nature of this condition varies consistently with different types of compounds, that is of a paste like to that of a freely flowing liquid. The transitions between the solid crystalline and isotropic liquid states are definite and precisely reversible and the phases in between these two limits are generally called as mesophases ("meso" means "in-between" or "intermediate") (G. Brown & Wolken, 1979; S. Singh & Dunmur, 2002).

Sometimes it is important to know how close a liquid crystal state is from the solid or liquid phases to facilitate the understanding of their phase properties (Collings, 2002). But determining whether a material is in a crystal or liquid crystal state is difficult. Often the *latent heat* of phase transition is used as a measuring tool for the degree of liquid crystallinity. For example, in the case of cholesteryl myristate, the *latent heat* of solid to liquid crystal is 65 calories/gram, while that for liquid crystal to liquid transition is only 7 calories/gram. These numbers allow us to answer the question posed earlier. The degree of smallness of the *latent heat* for the liquid crystal to liquid phase transition provides evidence that the liquid crystal is more similar to the liquid than it is to the solid. When a solid melts to a liquid crystal, it become less oriented. This remaining degree of ordering is then lost at the liquid crystal to the liquid phase transition. The fact that liquid crystals are similar to the liquid phase with only a small amount of additional order, is the key

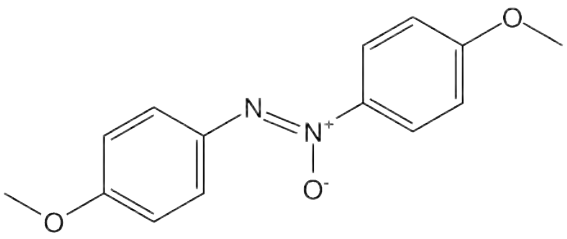

Figure 2.3: Molecular structure of para-Azoxy anisole.

to understanding many of the unique physical properties that make them nature's most delicate state of matter (Collings, 2002).

Another intriguing feature of the LC phase compared to the normal states of matter (solid and isotropic liquid) is in the ordering that the constituent molecules possess – the presence of high orientational order but low positional order in three dimensions (Collings, 2002). The above mentioned "ordering" concept can be understood by considering a normal liquid state of matter (e.g. water). The two most common states of water are the isotropic liquid phase and the crystalline solid phase (ice). For instance, in an isotropic liquid, the molecules have neither positional nor orientational order. Consequently, they are distributed randomly. There is no degree of ordering in the molecules; there is no preferred direction in the molecular arrangement either. Additionally, measurement of any physical property does not depend on the direction of the measurement is made. For example, the values of the measurements are same in all directions, implying the phase is isotropic in nature. Further, the liquid state possesses only short-range and not a long-range ordering. On the contrary, in a solid crystal, the molecules or atoms have both orientational and three-dimensional positional orders over a long-range. Nevertheless, many solid crystals show anisotropic nature – the measurement of properties depend on the orientation of the constituent molecules although there are few solids that show isotropic behavior (glassy phase) (Collings, 2002).

In liquid crystal realm, the anisotropic properties are strongly related to the ordering of the constituent molecules. Since the molecules lose their positional order fully or partially in the LC phase, they move freely as much in the same fashion as in a liquid state, but as they do so they tend to be oriented in a certain direction. This orientational order is not nearly as perfect as in a solid phase. This means, the molecules in the liquid crystal phase orient themselves more along a specific direction (director) than some other directions.

Therefore, the degree of orientational ordering is called the *order parameter*, (S) and always measured from a fixed reference vector ($\hat{n}$) called *director* as shown in Figure 2.4.

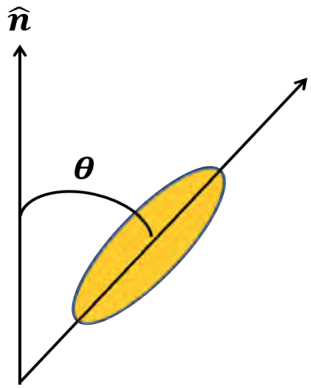

Figure 2.4: Geometry used for defining the *order parameter* (S). Redrawn from (Collings & Hird, 1997)

The *order parameter*, (S) is defined as the average of the second Legendre polynomial:

$$S = P_2(cos\theta) = \frac{3}{2}\langle cos^2\theta\rangle - \frac{1}{2}, \tag{2.1}$$

where θ is the angle between the director ($\hat{n}$) and the long molecular axis of each molecule (see Figure 2.4) and the angular brackets ($\langle\rangle$) denote a statistical average of $cos^2\theta$. A director is a vector to represent the direction of preferred molecular orientation within a domain (see Figure 2.5).

In any order-disorder problem, the *order parameter* is conveniently taken as unity for implying a perfectly ordered phase and vanishes for the completely disordered phase (Luckhurst, 1993). For instance when $\theta = 0°$ or $180°$ (parallel alignment with director), the *order parameter* value, $S = 1$. If $\theta = 90°$ (perpendicular alignment to the director), the $S = -\frac{1}{2}$. Finally, if the molecular orientations are random i.e. θ takes all values, $\langle cos^2\theta\rangle = \frac{1}{3}$ thus $S = 0$ (de Gennes & Prost, 1993). The *order parameter* can be measured experimentally by several types of experiments, such as NMR or XRD and diamagnetic susceptibilities (Meier, Sackmann, & Grabmaier, 1975; Wojtowicz, Sheng, & Priestley, 1975).

The *order parameter* is temperature sensitive. The increase of temperature increases the thermal energy of the phase and consequently the randomness of the director increases too. Below the critical temperature T_C (before LC become completely isotropic), the *order parameter* values reduce as temperature gets higher. The typical plot as for *order*

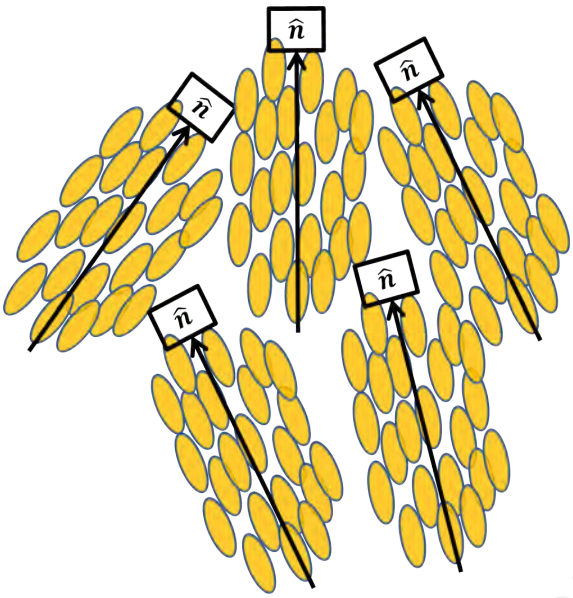

Figure 2.5: Preferred molecule orientation, $\hat{n}$ within a domain (represented by a loosely–defined boundary).

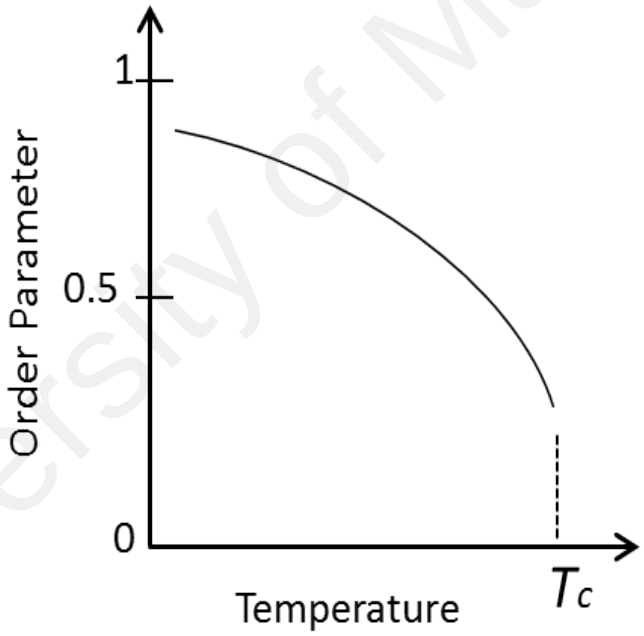

Figure 2.6: Typical *order parameter* plot. Redrawn from (Collings, 2002)

parameter vs temperature is given in Figure 2.6. Typical value for the *order parameter* lies between 0.3 and 0.9 (Collings, 2002).

In general, the shape of liquid crystal forming molecules (mesogens) contributes to the many interesting anisotropic properties like optical, mechanical, magnetic, electrical and thermal conductivity, and flow properties (Dierking, 2003). These molecules have an elongated or ellipsoid shape with a *uniaxial* symmetry; having one axis that is longer and preferred – like cylinder or rod shapes and this allows the magnitude of measured

physical property along the average molecular orientation, i.e. along the director vector $\hat{n}$, is different from that of measured orthogonal to the director.

For instance, the birefringent effect is related to the shape of the molecule, like elongated, which has two axises (long and short as shown in Figure 2.7) called *indicatrix* – an ellipsoid of revolution whose major and minor axes correspond to parallel ($n_{\|}$) and perpendicular ($n_{\perp}$) to the director respectively. The differences between these axises manifest distinct values of the refractive indices along the optical axis (director): $n_{\|}$, and perpendicular to it: $n_{\perp}$. Relating to this, a molecule is said to be optically positive when the refractive index $n_{\|} > n_{\perp}$ and optically negative for $n_{\|} < n_{\perp}$, as shown in Figure 2.7, (Dierking, 2003; Sengupta, 2013).

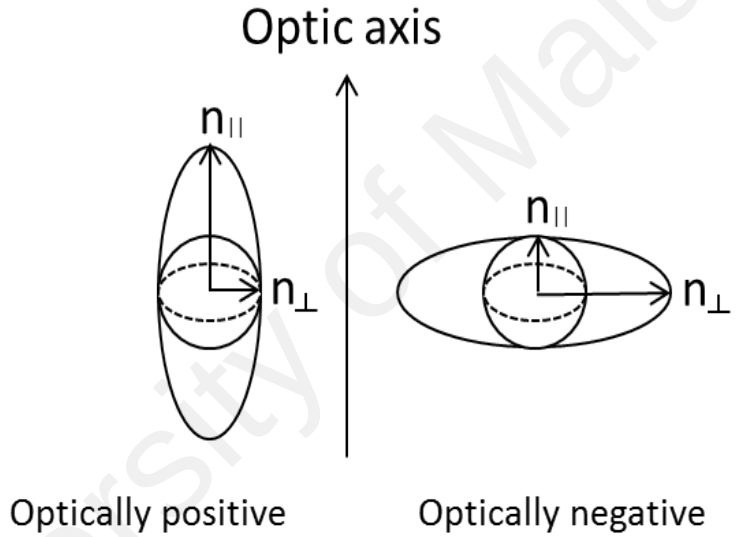

Figure 2.7: Adopted from Dierking (2003)

Meanwhile, when an electric or magnetic field interacts with a dielectrically anisotropic medium, it can shift away the phase transition points, change the *order parameter*s, or induce a new symmetry and in turn, influence the structure and thermodynamic properties of the medium (D. A. Dunmur & Palffy-Muhoray, 1988).

The effects of electric and magnetic fields on LC substances made a huge impact on the liquid crystal industry and developed much faster due to its potential applicability in TV panels. This is due to the quintessential property of an LC – its anisotropy. The optical, mechanical, electrical and magnetic properties of LC medium are defined by the orientation order of the constituent molecules. Due to the anisotropy of the electrical and magnetic properties, the orientation of the LC molecules is effectively controlled by weak

electric or magnetic fields. As a result, by changing the LC molecules orientation, it is possible to change the optical and mechanical properties of the medium. All of these are important to the functioning of devices based on LCs: digital watches, calculators, flat TV-displays, thermometers and LC displays are all examples of what LC technology can achieve.

2.1.3 Liquid crystal classification

In a broad sense, liquid crystals can be divided into two categories, the thermotropic and the lyotropic mesophases. A liquid crystal phase is sometimes referred to as "mesophase" means "in between" and mesogens are compounds forming mesophases. Certain mesogens may exhibit both thermotropic and lyotropic phases and they are called amphitropic (Barón, 2001; Tschierske, 2002). A thermotropic group of materials exhibit LC phases subject to the thermal energy supplied or extracted from the system, whereas lyotropic LCs are dependent on the nature of solvent and concentration and on the temperature. Most of the biological molecules (specifically amphiphilic molecules from cell membranes) exhibit lyotropic phase behavior. The glycolipids (GLs) used in the present thesis are classified as amphitropic liquid crystals since they can form both lyotropic liquid crystals in a suitable solvent and a thermotropic liquid crystal phases in dry form at a suitable temperature range.

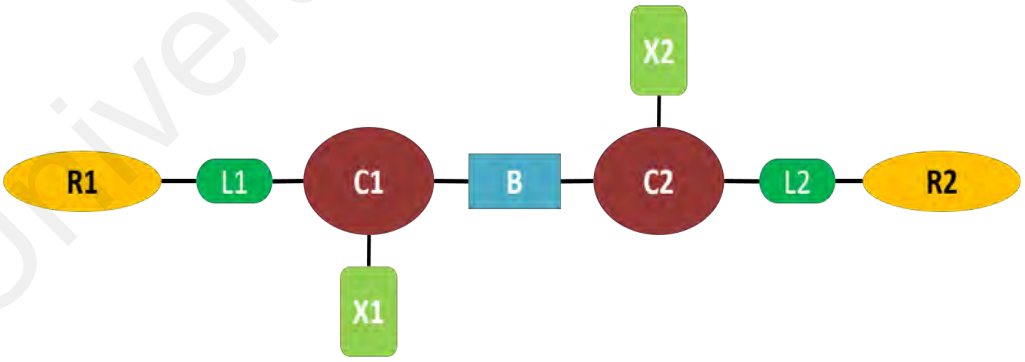

Figure 2.8: Molecular structure of a rod-like liquid crystal. Redrawn from Collings and Hird (1997).

The geometrical structure of a mesogenic molecule is considered important in understanding the classification and behavior of liquid crystal phases (S. Singh & Dunmur, 2002). To simplify the understanding of this, a general molecular structure of a typical liquid crystal molecule is depicted in Figure 2.8. There are two core groups (C1 and C2),

a bridging group (B), two terminal units (R1 and R2), two groups linking the terminal units to the cores (L1 and L2), and two lateral substituents on the cores (X1 and X2). The combination of those units is the key factor for the type of liquid crystal and physical properties exhibited by a compound (Collings & Hird, 1997). The core units (C1 and C2) are usually linearly-linked aromatic systems (e.g. 1,4-phenyl, 2,5-pyrimidinyl) or alicyclic (e.g. trans-1,4-cyclohexyl). These units contribute to the rigidity which is required to provide the anisotropic molecular structure. They are joined by the bridging group (B) which maintains the linearity of the core (e.g. $-CO_2$, $-CH_2CH_2-$). The flexibility which is needed to obtain low melting points and molecular alignment for stabilization within the mesophase structure is provided by the terminal substituents (R1 and R2). They are normally straight alkyl or alkoxy chains with one terminal unit, often a small polar substituent (e.g. CN, F, NO_2). Chiral molecules can be obtained when the terminal chains are branched, and the branching unit can be non-polar (e.g. CH_3) or polar (e.g. CN, F). As for the lateral substituents (X1 and X2), F is the most useful due to its small size and high electronegativity apart from Cl, CN, and CH_3 (Collings & Hird, 1997).

2.1.3 (a) Thermotropic phases

When a liquid crystal phase appears upon heating or cooling, it is classified as a thermotropic phase (Barón, 2001). This phase is sensitive to temperature variation. Solid LC material is able to form a thermotropic LC phase if it is heated above its melting point, T_m. Continuous heating of this substance causes its phase to change from liquid crystalline phase to isotropic liquid phase. This temperature is called the clearing point (T_C). The molecular organization of thermotropic liquid crystal is strongly influenced by its chemical architecture and will be described in the following section.

Monophilic mesogen

Many thermotropic liquid crystal forming materials (mesogens) have a monophilic shape with a rigid core in the middle and short chains at both the ends. Molecules of this shape can be derived from a simple geometrical form and they are classified such as *calamitic* (rod-like), *discotic* (disk-like) (Chandrasekhar, 1992; Collings, 2002; Collings & Hird, 1997) and the recently-described *sanidic* (lath-like) liquid crystal (Dierking, 2003) (see Figure 2.9). A common characteristic of calamitic mesogens is a relatively rigid core as

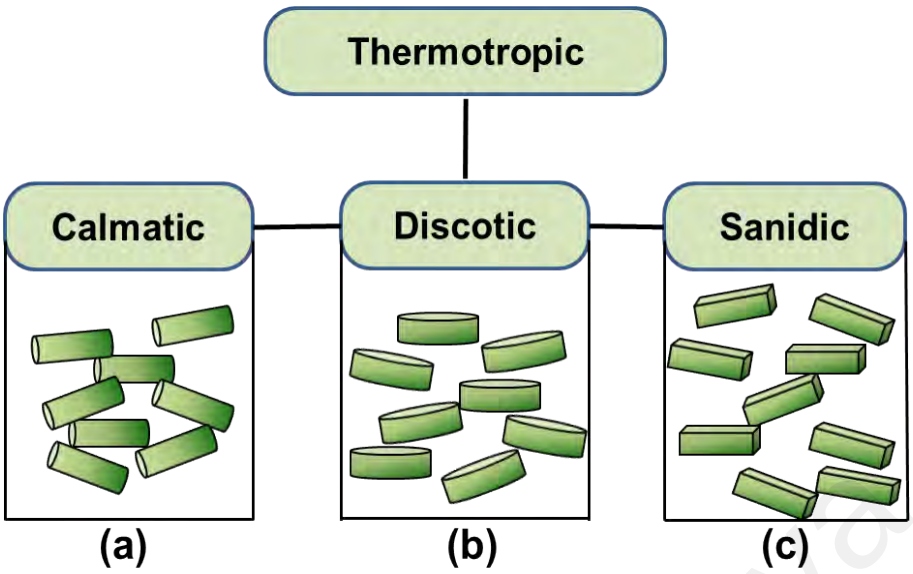

Figure 2.9: Molecular shapes of monophilic liquid crystals. Redrawn from Dierking (2003).

found in phenyl and biphenyl groups, and with two flexible endgroups (either alkyl or alkoxy chains) (Dierking, 2003). As proposed by Georges Friedel (Friedel, 1922), there are three basic types of liquid crystals namely, nematic, cholesteric (chiral nematic) and smectic. These phases are depicted in Figure 2.10.

Nematic phase

The word "nematic" comes from $\upsilon\eta\mu\alpha$ (nema), the Greek word "nematos" which means "thread" (Collings, 2002; Dierking, 2003). The nematic phase is the most liquid-like structure (low viscosity) similar to isotropic liquid. However, it exhibits anisotropy characteristic due to the molecular long axes arranging themselves almost parallel to the director, $\hat{n}$ (Chandrasekhar, 1992; Dierking, 2003). The nematic state possesses long-range orientational order and short-range positional order. The molecules are mobile in three directions because there is no periodic arrangement and they can rotate freely about one axis (long axis). Under a polarizing microscope, they display mainly thread-like disclination line textures which are related to structural discontinuities in the material. Common examples are 4,4'-dimethoxyazoxy benzene (p-azoxyanisole), and the first moderately stable room temperature liquid crystal, 4-methoxybenzylidene-4'- n-butylaniline (MBBA). Their chemical structures are shown in Figure 2.11. This liquid crystal exhibits nematic phase at room temperature with a weakly aligned director which can be manipulated easily

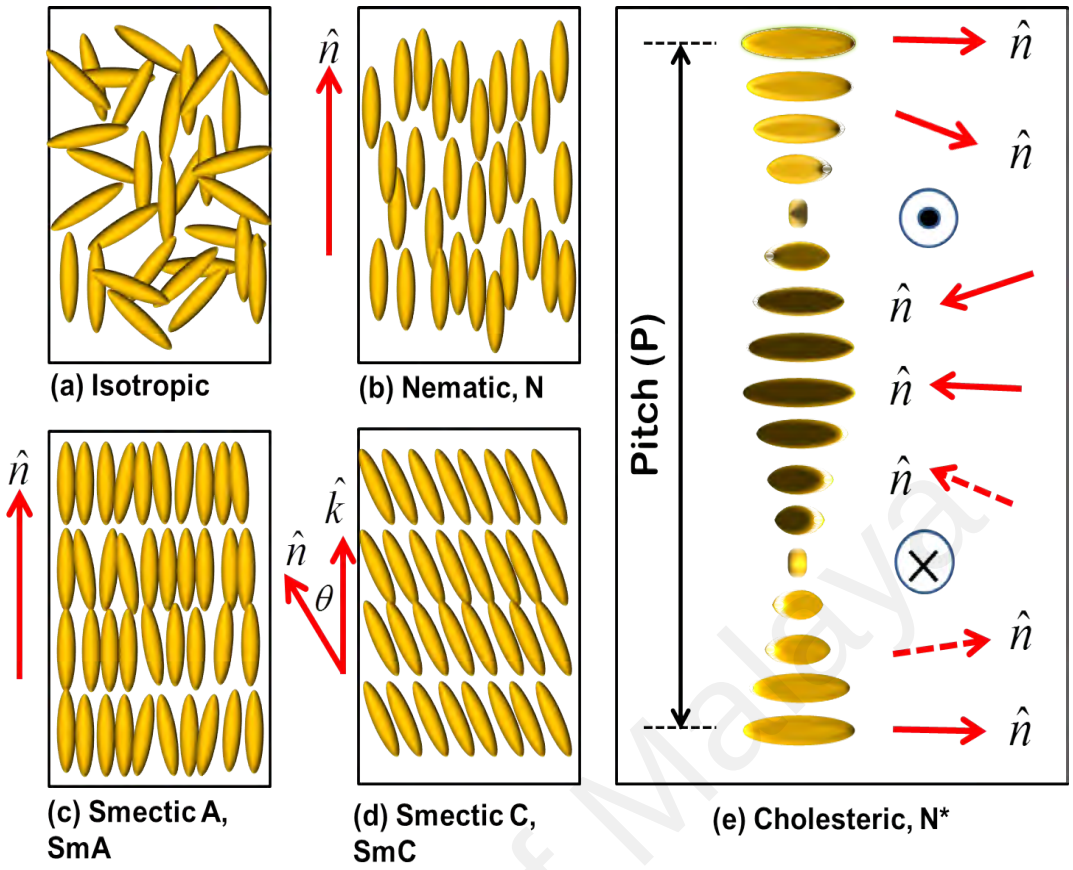

Figure 2.10: The molecular organization of calamatic liquid crystals. The vector, $\hat{n}$ represents the director and $\hat{k}$ is the layer normal. Redrawn from Dierking (2003).

enabling the development of liquid crystal display (Hoogboom, Rasing, Rowan, & Nolte, 2006; Kirsch & Bremer, 2000).

Cholesteric phase

Cholesteric liquid crystal, also known as a chiral nematic, is produced when the director in a nematic mesophase has a helical superstructure with a twist axis perpendicular to the local director, $\hat{n}$. The nematic and cholesteric structures are similar, except on a large scale when the cholesteric director follows a helical form (Meier et al., 1975). The pitch, **P** of the structure refers to the distance needed to rotate the director by 2π along the helix axis. **P** usually ranges between 2000 Å which is within the wavelength of the visible light spectrum. Whereas, the infinite **P** corresponds to the normal nematic (Meier et al., 1975). Cholesterols of low **P** (below 5000 Å), exhibit what are known as blue phases which exist over a small temperature range ($\sim 1^{\circ}$C) between the cholesteric liquid crystal phase and the isotropic liquid. Cholesteryl benzoate shows a cholesteric liquid crystal phase, and the first observation of a blue phase was recognized by Friedrich Reinitzer in 1888

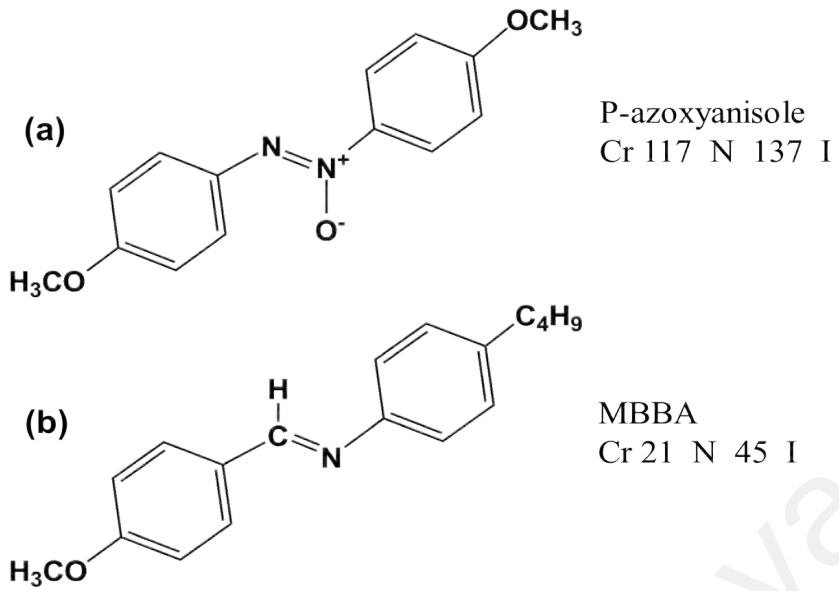

Figure 2.11: Some examples of compounds that exhibit nematic phase together with their liquid crystals phase behaviors (Cr means crystal, I stands for isotropic and N denotes nematic phase) (Jákli & Saupe, 2006).

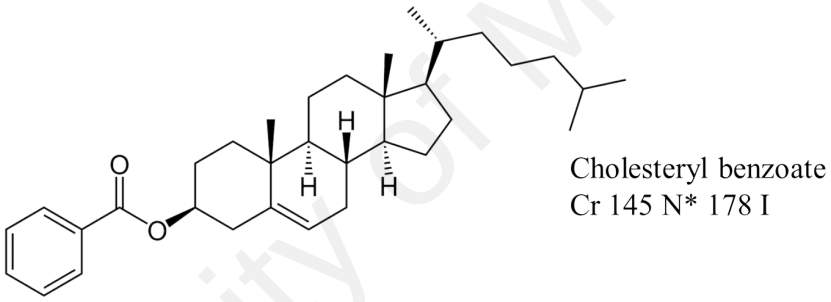

Figure 2.12: Cholesteryl benzoate that exhibits cholesteric phase together with its liquid crystals phase behaviors. (Cr means crystal, I stands for isotropic and N* denotes chiral nematic phase) (S. Singh & Dunmur, 2002).

(Chandrasekhar, 1992), where the blue phase appeared within a temperature range between the helical and isotropic phases. Figure 2.12 shows the chemical structure of cholesteryl benzoate. Cholesteric liquid crystal materials have the ability to change colour (due to the high sensitivity of the pitch) as a function of temperature, mechanical stress, electric fields or non-chiralic solute molecules (Meier et al., 1975). These characteristics make these materials useful as a thermal sensor in thermometers and other thermometry technical applications (Domanski, Wolinski, & Borys, 1990).

Smectic phase

The third category of liquid crystal phase is the “smectic” phase, from the Greek word $\sigma\mu\eta\gamma\mu\alpha$ meaning “soap” (owing to the fact that smectic liquid crystals have mechanical

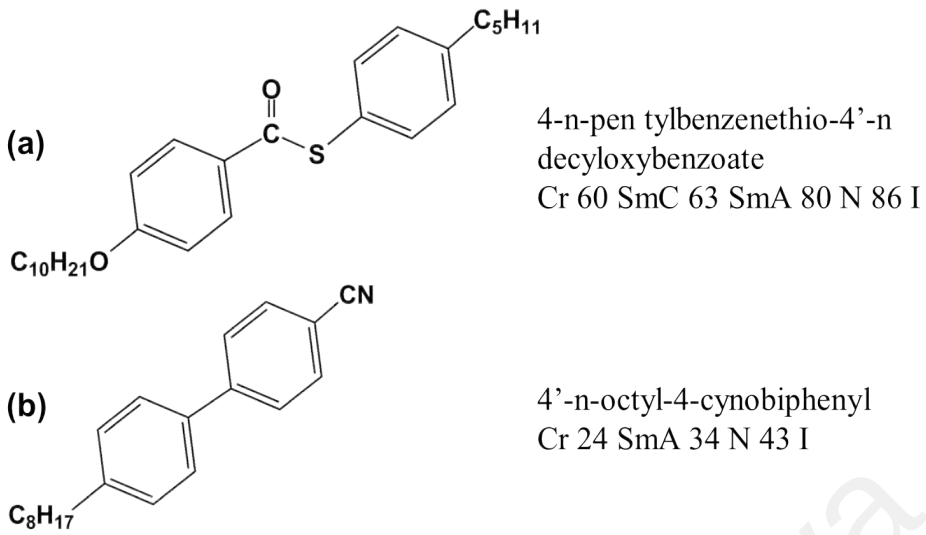

Figure 2.13: Some examples of compounds that exhibit smectic phase together with their liquid crystal phase behaviors (Cr means crystal, I stands for isotropic, N denotes to nematic, SmA denotes smectic A and SmC refers to smectic C phase) (Chandrasekhar, 1992).

properties similar to those of concentrated aqueous soap solutions). (Collings, 2002). The molecules in this phase are parallel to one another and are arranged in layers with the mean direction of the long axes of the molecules normal to the layers. Smectic liquid crystals are fluid but are far more viscous than nematic liquid crystals. Their fluidity is due to the flexibility of the layers and weak interlayer attractions compared to that of lateral intermolecular forces which enable the layers to slide over one another easily while still remaining essentially parallel. Thus, when observed under a polarizing microscope, they exhibit different characteristic textures such as homeotropic, focal conic, batonnets, and fan-like textures (Muñoz & Alfaro, 2000). There are many different types of smectic phases (A, B, C, F, I...). The two most commons are smectic A (SmA) and smectic C (SmC). The molecules in SmA are on average normal to the layers, while the molecules in SmC phase are on average tilted with respect to the layer normal (see Figure 2.10). Certain compounds possess more than one mesophase (polymorphism). For instance, 4'-n-octyl-4-cyanobiphenyl has two liquid crystal phases whereas 4-n-pentylbenzenethio-4'-n decyloxybenzoate shows three liquid crystal phases. Their molecular structures are depicted in Figure 2.13.

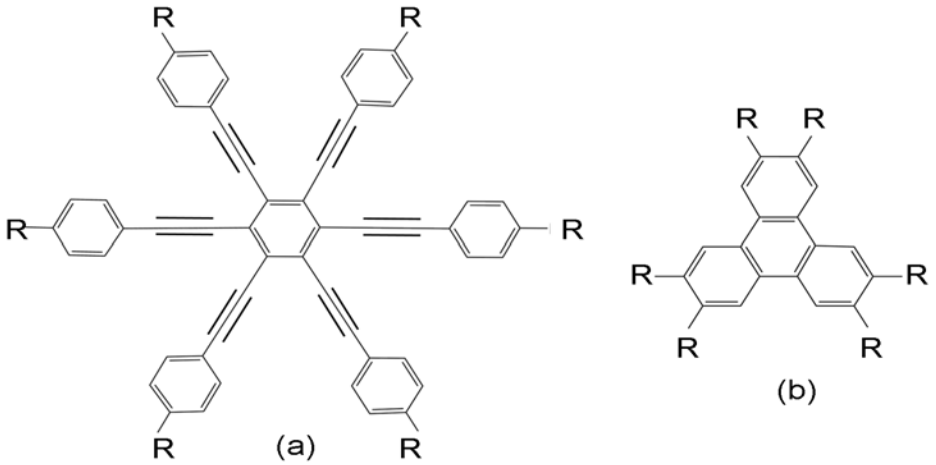

Figure 2.14: A typical chemical structure of discotic mesogens: (a) hexa-n-alkanoates of triphenylene and hexa-n-alkoxytriphenylene (b) hexakis ((4-octylphenyl)ethynyl) benzene (Chandrasekhar, 1992).

Discotic phase

Disc-like molecules which normally form discotic liquid crystals are molecules with one molecular axis shorter than the other two. The core of discotic liquid crystals is usually based on benzene, triphenylene, or truxene with six or eight flexible side chains (Collings & Hird, 1997) (see Figure 2.14). Due to their unique structural and electronic properties, they show potential for applications involving charge transport processes (Lemaur et al., 2004), such as in molecular electronics (Xiao et al., 2005) and high-efficiency organic photovoltaics (Schmidt-Mende et al., 2001). Generally, they can be categorized into two distinct phases: nematic and columnar (Chandrasekhar, 1992).

The most simple discotic phase is the nematic phase as shown in Figure 2.15(a). It possesses orientational order but no positional order. Unlike the typical nematic of rod-like molecules, this phase is optically negative (Chandrasekhar, 1992). The nematic phase of discotic mesogens is usually found in shorter chain compounds. Therefore, increasing the chain length in a homologous series of disc-like molecules will result in the disappearance of the nematic phase (Collings & Patel, 1997). The positional order of discotic liquid crystals causes a tendency for the molecules to arrange themselves in columns. Hence, in the plane perpendicular to the columns, the disc-like molecules tend to align in a two-dimensional lattice, either rectangular or hexagonal, as they diffuse throughout the sample. This is also known as the columnar phase (see Figure 2.15(b)).

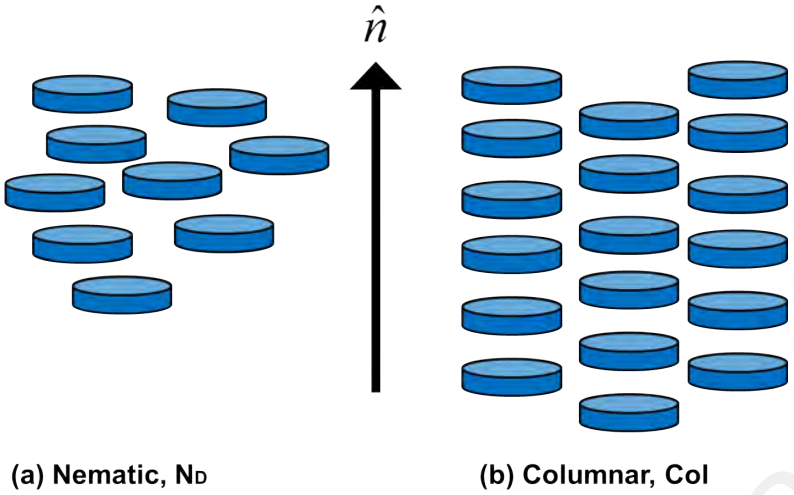

Figure 2.15: Schematic illustration of discotic liquid crystals. Redrawn from (Collings, 2002).

Additionally, two other discotic LC phases also found. Namely, *chiral nematic discotic*, and *Sanidic* liquid crystals. In the *chiral nematic discotic* phase, the director rotates in a helical fashion throughout the sample similar to the rotation of the chiral nematic calamitic liquid crystal (Collings, 2002; Dierking, 2003). Meanwhile, in the *sanidic*-liquid crystal phase, the disk-shape molecules assemble in stacks packed parallel to one another on a one- or two-dimensional lattice and the rotation of the molecules around their long axes is considerably hindered and they are expected to form the biaxial nematic mesophase (Barón, 2001).

Polymeric liquid crystal phase

Another type of liquid crystal is the *polymer liquid crystal*. The basic monomer units are low mass mesogens, rod-like or disc-like, and are attached to the polymer backbone in the main chain or as side groups (see Figure 2.16). As for the former, the rigid structural units are separated by flexible hydrocarbon chains whereas in the latter, the rigid parts are attached to a long flexible polymer chain by short flexible hydrocarbon chains (Chandrasekhar, 1992; Collings & Hird, 1997). Nematic, cholesteric and smectic phases have also been found in polymers.

2.1.3 (b) Amphiphilic liquid crystals

The possible molecular shapes of an amphiphilic molecule are given in Figure 2.17. It shows possible arrangements of the hydrophilic groups and hydrophobic alkyl chains.

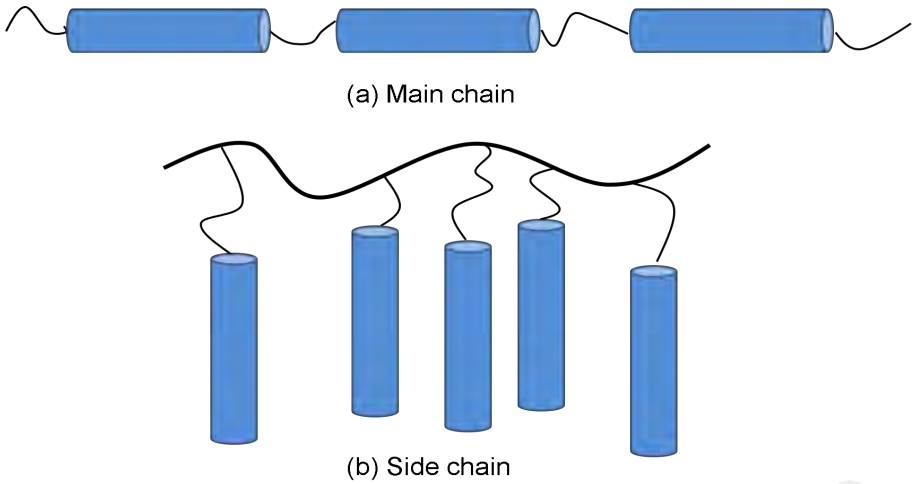

Figure 2.16: Rod-like polymeric liquid crystal. Redrawn from Chandrasekhar (1992).

In the case of glycolipid, the hydrophilic part is replaced with a sugar group and the hydrophobic part is represented by a hydrocarbon chain. The dual-character of this amphiphilic molecule results in the microseparation of the hydrophilic and hydrophobic moieties that give rise to mesomorphic properties. The relationship of these molecular shapes to the thermotropic phase behavior can be summarized as follows (Vill & Hashim, 2002). Elongated amphiphiles in the case of A, B and C will exhibit smectic phase. Forked or pie-shaped mesogens (D and E) usually prefer columnar phase. The non-linear dialkylated sugars like F will also give columnar phase. Banana-shaped amphiphiles (G) and elongated forks (H) are between smectic and columnar phases, or may even form bicontinuous cubic phase. The cone-shaped molecule, J, can give discontinuous cubic phase. Lastly, star-like substituted molecules prefer columnar phase. If this star is asymmetric like K, then rectangular and tetragonal columnar phases are possible. In this work, the structural models of the monosaccharide-branched compounds that we have prepared are represented by molecular shape D. Hence, they are predicted to give non-lamellar or curved mesophases like columnar and bicontinuous cubic phases.

Lytopropic phase

When amphiphilic materials such as ethylene oxide are mixed with suitable solvents, the mixtures can display different liquid crystal phases at appropriate conditions, with regards to concentration, temperature, and pressure. This class of liquid crystals is termed lyotropic (Barón, 2001). The word “lyo”- refers to the concentration of the solvent (Hamley, 2000). It may form a variety of structures above some critical concentration and temperature,

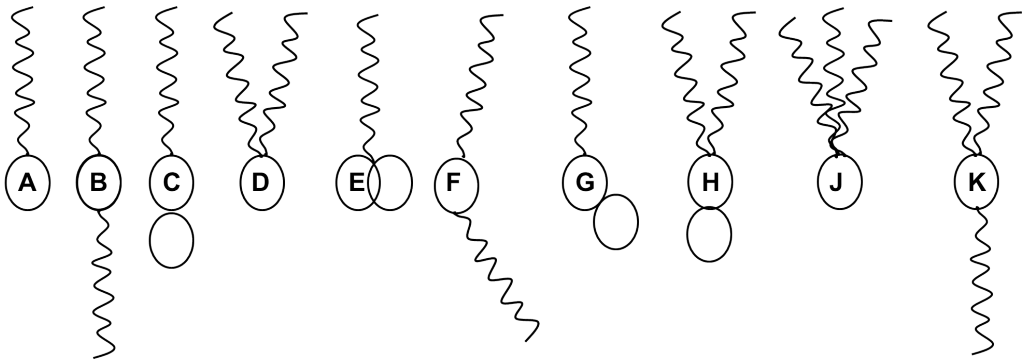

Figure 2.17: Structural models of GLs. Redrawn from Vill and Hashim (2002).

governed by the geometrical constraint of the molecule and the interfacial curvature which, in turn, is determined by intra-micellar forces occurring in different planes. As the composition increases, inter-micellar forces become more important and may cause either a change in the critical packing parameter (see Section 2.2.2) leading to further shape transition, or disorder/order transition to the liquid crystalline phase (Muñoz & Alfaro, 2000).

The lyotropic phases have a wide range of applications in different fields such as the cosmetics industry (Klein, 2002), in pharmacy as drug-delivery systems (Boyd, Whittaker, Khoo, & Davey, 2006; Drummond & Fong, 1999; Engström, Nordén, & Nyquist, 1999; Guo, Wang, Cao, Lee, & Zhai, 2010; Shah, Sadhale, & Chilukuri, 2001), in the food industry (Larsson & Dejmek, 1990), in situ templating (N. M. Huang, Shahidan, Khiew, Peter, & Kan, 2004) and in membrane protein crystallization (Borshchevskiy et al., 2010). A typical example of lyotropic liquid crystals is mixtures of alkali n-alkoates (soaps) and water. The various lyotropic mesophases are lamellar, cubic and hexagonal phases.

Lamellar phase

A one-dimensional translational order of lyotropic phase is called the lamellar phase L_α (see Figure 2.18(a)). The structural unit of a lamellar phase is simple, consisting of repetitive bilayers separated by a solvent. The bilayers are packed parallel to one another and are separated from one another by a water layer. The hydrophilic headgroup of the molecules is in contact with the aqueous solvent, whereas the lipophilic hydrocarbon chains are either interdigitated, tilted or fluid disorder to avoid water. The double layer is usually smaller than twice the amphiphilic molecule length. Both bilayer and water layer thickness values are very much dependent on temperature and concentration of the

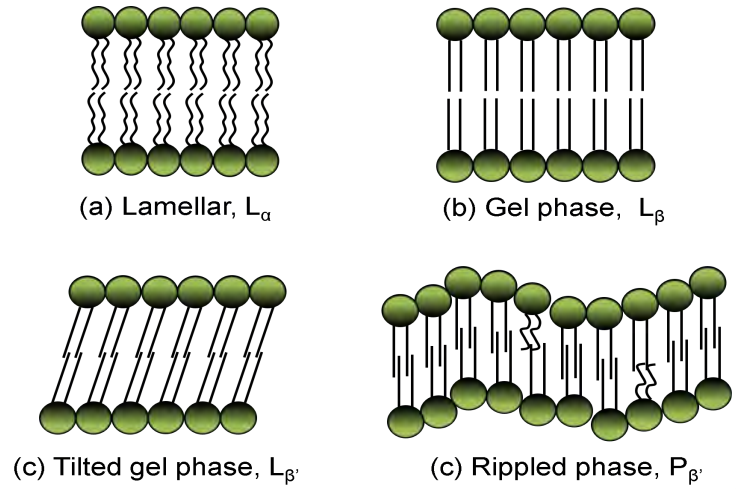

Figure 2.18: Schematic structures of lamellar phases. Redrawn from Corti et al. (2007).

lamellar phase. Additionally, there are variety of assembly structures of the lamellar phase like L_β (parallel) and L_β' (tilted) as shown in Figure 2.18(b)-(d). The lamellar in β' are distorted due to the distortion propagating from layer to layer (Burducea, 2004).

Cubic phase

In general, the highly-ordered cubic phase is more viscous than that of the isotropic micellar solutions and even the hexagonal phase. The high viscosity is due to the lack of shear planes within the structure that would allow for sliding movement. Therefore, under an optical polarizing microscope, the cubic phase exhibits no texture because it is optically isotropic, and yet a cubic phase can be distinguished from an isotropic micellar solution by its viscosity. The isotropic nature of the cubic phase often makes it difficult to observe them under the optical polarizing microscope and so they are sometimes undetected (Collings, 2002). However, the structural information of the cubic phases can be obtained from the x-ray scattering technique. The cubic phase can be categorized into two groups which are bicontinuous based on the triply periodic minimal surfaces (TPMS), and the other type is micellar or discontinuous cubic phase based on the complex packing of discrete micellar aggregates (Burducea, 2004; Seddon, Robins, Gulik-Krzywicki, & Delacroix, 2000; Tresset, 2009).

The bicontinuous cubic phase of an amphiphilic molecule can be divided into the direct (normal) and inverse (reverse) phases (Garstecki & Hołyst, 2001; Seddon & Templer, 1995). Figure 2.19(b) shows the normal phase, denoted as Q_I (Seddon & Templer, 1995), in which water film is centered on the TPMS while the surfactant molecules fill the two

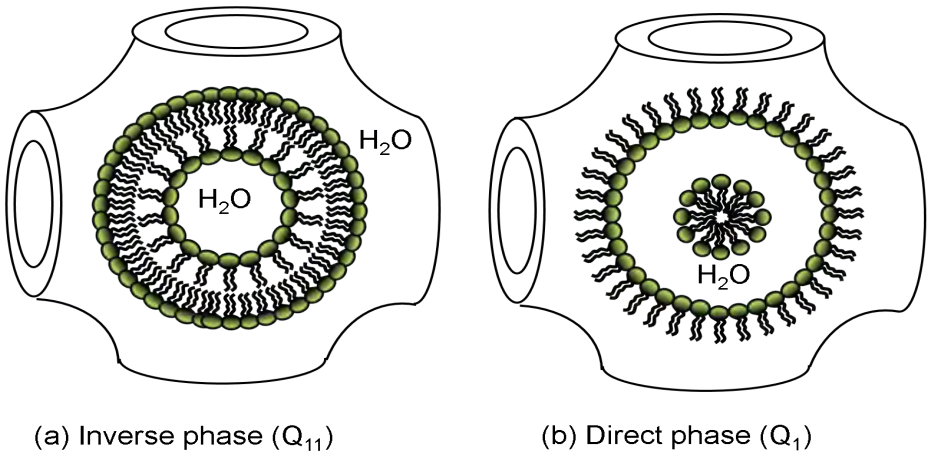

Figure 2.19: The bicontinuous cubic phase of an amphiphilic molecule. Redrawn from Garstecki and Holyst (2002).

disjoint subspaces. The second group is an inverse phase, denoted as Q_{II} (Seddon & Templer, 1995), where the TPMS is occupied by a surfactant bilayer and the two channels are filled with water (see Figure 2.19(a)) (Garstecki & Hołyst, 2001; Garstecki & Holyst, 2002). The TPMS can be further categorized into three structures: Schoen gyroid (G) minimal surfaces, Schwarz diamond (D), and primitive (P) with crystallographic space groups of *Ia3d* (230), *Pn3m* (224), and *Im3m* (229) respectively as shown in Figure 2.20. A detailed explanations are given in the following references (Garstecki & Hołyst, 2001; Garstecki & Holyst, 2002; Seddon & Templer, 1995; Tresset, 2009)

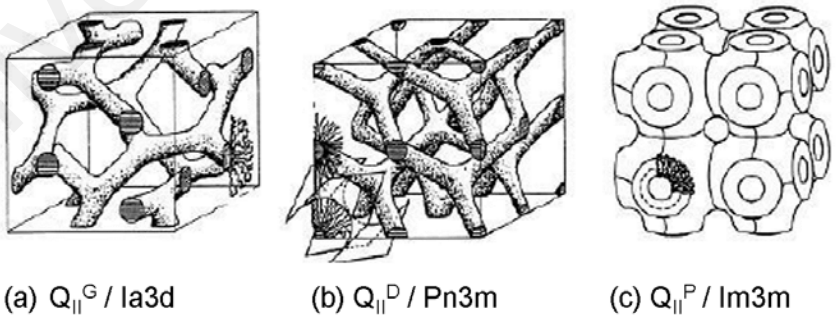

Figure 2.20: Structures of inverse bicontinuous cubic phases. Adopted from Tresset (2009).

Hexagonal phase

When a solvent concentration is increased further in the cubic phase, a two-dimensional hexagonal phase occurs and forms a normal hexagonal phase, H_I or inverse hexagonal,

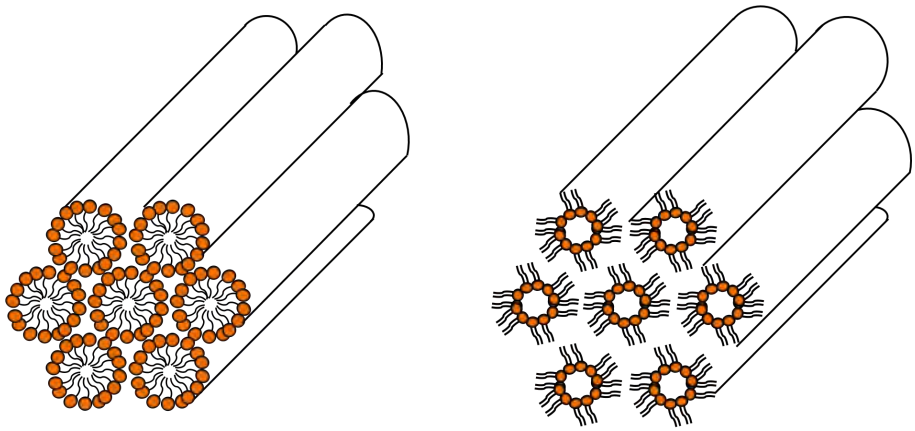

Figure 2.21: Schematic structures of hexagonal phases. Redrawn from Borshchevskiy et al. (2010).

H_{II}, depending on the solvent polarity. The hexagonal phase consists of micellar cylinders of indefinite length packed in hexagonal arrangement as in the Figure 2.21. The diameter of the micellar cylinders is usually 10–30% shorter than twice the length of an "all-*trans*" non-polar chain. The spacing between each cylinder varies between 10 and 50 Å depending on the relative amounts of water and surfactant. This phase exhibits a birefringent texture when examined under an optical polarizing microscope (Collings & Hird, 1997).

Hypothetical binary phase diagram

The thermodynamic properties of amphiphiles in solution are controlled by the tendency for the hydrophobic region to avoid water. This tendency is called the hydrophobic effect (Hamley, 2000). When an amphiphilic material is mixed with water, the amphiphiles begin to arrange themselves into spheres with the polar headgroups on the outside and the hydrocarbon tails toward the center. This structure is called a micelle (L_I) and is stable as long as the amount of amphiphilic material is above its critical micelle concentration (Collings, 2002). An intermediate phase between micellar and hexagonal phases is often a discontinuous cubic phase (I_I). At higher concentration of amphiphilic materials, the micelles combine to form larger structures called hexagonal phase (H_I) in which long cylindrical rods of amphiphilic molecules arrange the long axes of the rods in a hexagonal array. As we increase the concentration of the material, the lamellar phase (L_α) is formed whereby the amphiphilic molecules form flat normal bilayers and are separated by water. Sometimes the discontinuous cubic phase (Q_I) is formed at concentrations between the

hexagonal and lamellar phases. This viscous isotropic phase is made up of spheres of amphiphilic molecules that can arrange themselves into two networks of continuous cubic lattices called bicontinuous cubic or mesh structure (Hamley, 2000).

When the water becomes the minority phase, inverse structures are favourable i.e. inverse micellar liquid phase (L_{II}), inverse micellar cubic phase (I_{II}), inverse hexagonal (H_{II}), which is a rod-like water channel in an amphiphile matrix, and inverse bicontinuous cubic phase (Q_{II}). An increased tendency for curvature is associated with a more wedge-shape structure of the molecule which results in the formation of an inverse hexagonal phase (H_{II}). At an extremely high curvature, the inverse micelle phase (L_{II}) may be formed where hydrophilic headgroups are arranged towards water cores while hydrophobic chains point outwards (Sagnella, Conn, Krodkiewska, & Drummond, 2009).

The hypothetical sequence of phases formed by varying the concentration and temperature is illustrated in Figure 2.22. In reality, not all amphiphilic surfactants have the same phase sequences as presented here, but the hydration process always ends in the isotropic liquid state for all of them (Burducea, 2004). For instance, binary phase diagram of n-octyl-β-D-glucoside/water system measured by two different methods, namely small-angle x-ray scattering (Figure 2.23(a)) and fluorescence spectroscopy (Figure 2.23(b)), forms normal liquid crystalline mesophases of L_α, Q_I and H_I as predicted by the hypothetical binary phase diagram. The exception is the cubic, I_I phase.

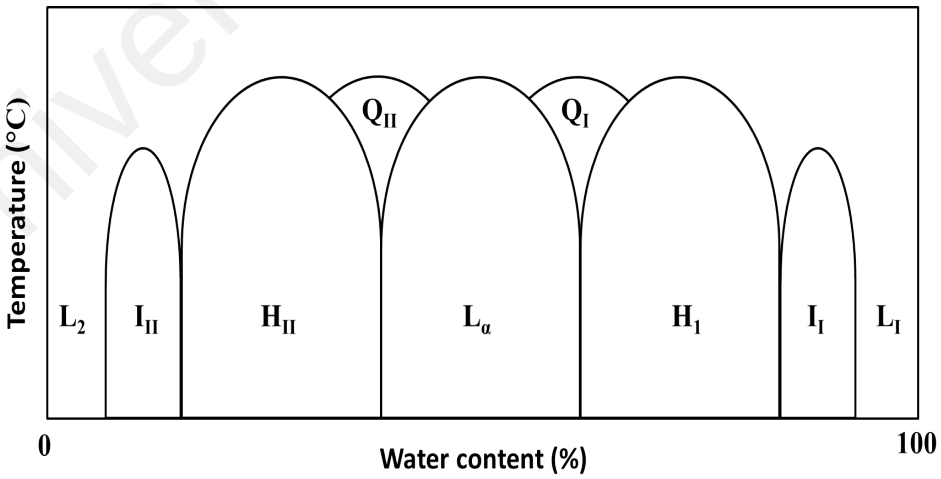

Figure 2.22: Hypothetical lipid/water binary phase diagram. Redrawn from von Minden et al. (2000).

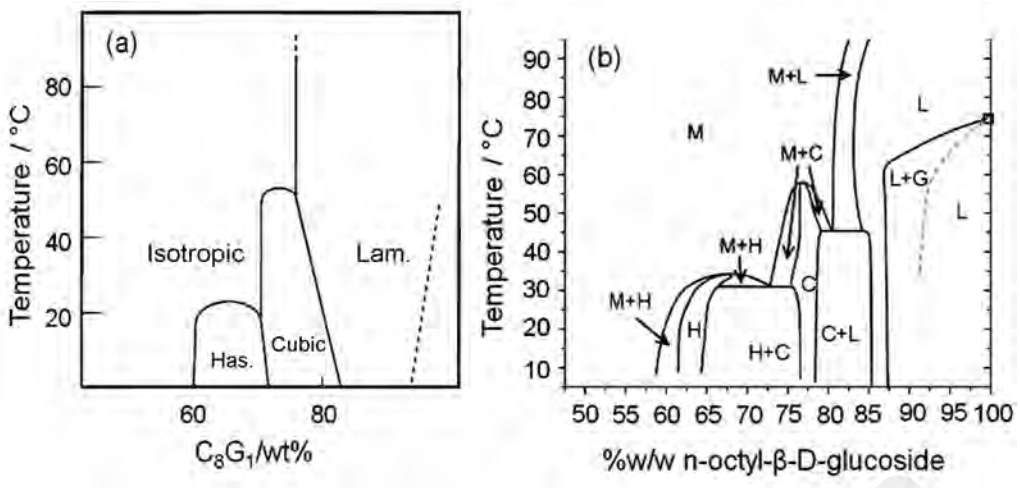

Figure 2.23: An example of binary phase diagram of n-octyl-β-D-glucoside in water by (a) small angle x-ray scattering (Nilsson et al., 1996) (b) fluorescence spectroscopy. (M) isotropic micellar solution, and (H), (C), (L), (G) and (S) representing liquid crystalline phases like hexagonal, cubic, lamellar, gel phase and a "solid surfactant" phase respectively. (Karukstis et al., 2012).

2.1.4 Theory of liquid crystal

Liquid crystals are now classified under the newly defined field of soft materials which encompasses colloids, surfactants and polymers, and can be induced to flow under certain conditions. This new field is at the interface between chemistry, physics and biology. Unlike a well-ordered crystalline solid, the weak ordering within the liquid crystal phase is due to the lack of long-range positional order, leading to its softness. The main intermolecular forces responsible for the formation of soft materials include the long-range electrostatic dispersion and short-range repulsion (Hamley, 2000). The phenomenological theory that best describes the nature of phase transition in liquid crystals is based on the Landau-de Gennes theory. It describes the overall consistency of the microscopic characteristics of the transitions and the results of the measurement of various macroscopic quantities such as thermal and optical properties (Tolédano, 1996). It is the characteristic of liquid crystals specifically and soft materials in general that phase transitions are often weak. This implies that the Landau-de Gennes theory is applicable to a system with continuous phase transitions or to weak first-order transitions where the enthalpy and entropy change is small (S. Singh, 2000).

In contrast to the phenomenological theory by de Gennes, a simple microscopic theory that describes the liquid crystal phase was formulated by the German physicist Alfred Saupe, in his 1958 thesis under the supervision of Wilhelm Maier (Cladis, Palffy-Muhoray,

& Saupe, 1998). The theory became known as the Maier-Saupe theory. It begins with the assumption that the most important force between liquid crystal molecules is the dispersion force (Collings, 2002; Jákli & Saupe, 2006). Accordingly, it is assumed that the interaction between permanent electrical dipole moments, as intermolecular interactions, are important, not for the orientational order, but only for the arrangements of the centers of gravity of the molecules and for the energy content of the isotropic distribution along the axes (Jákli & Saupe, 2006). The dominant force for the orientational order between molecules is an interaction between induced dipoles. A momentary dipole moment of one molecule induces a momentary moment on the neighbouring molecule, resulting in an attractive dispersion force keeping the two molecules aligned (Collings, 2002; Jákli & Saupe, 2006). Besides, it is assumed that the molecules are cylindrically symmetric in their long axes. As a result, the potential energy between two molecules can depend only on the angle between their long axes, with an angular dependence proportional to the second Legendre polynomial of this angle (Jákli & Saupe, 2006). Finally, it is assumed that the degree of orientational order of the molecules enters into the mean-field potential in a linear fashion, i.e. the larger the orientational order, the larger the effective potential is (Jákli & Saupe, 2006).

2.2 Self-assembly and associated interactions

Self-assembly phenomena has become a very intriguing subject in the nanoscale materials field (J. Z. Zhang et al., 2003). In the self-assembly processes, atoms, molecules, particles, and other building blocks organize themselves into functional structures as driven by the energetics of the system. The most important driving force for self-assembly is the interaction energies between the subunits, whether they are atoms, molecules, or particles. In this section, we briefly highlight the types of interaction forces and their related equations.

2.2.1 Interaction forces in self-assembly

The fundamental interactions among atoms, ions, and molecules are classified into three main categories, depending on whether the species are charged: (i) Coulomb interactions due to the electrostatic effects from the permanent charges, (ii) van der Waals interactions due to instantaneous polarizations induced by the neighboring molecules (or atoms, ions),

and (iii) short range strong repulsions (Hiemenz & Rajagopalan, 1997; Israelachvili, 2011). A detailed description for these interaction forces has been extensively discussed in Hiemenz and Rajagopalan (1997); Israelachvili (2011); Shaw (1992). Below a brief summary is provided based on those above references and from J. Z. Zhang et al. (2003) specifically:

Molecular interaction energies

Coulomb interactions

The interactions among the charged particles primarily governed by the Coulomb interactions.

(i) Ion-ion pair interaction: (can be positive and negative particles)

$$E_{(i-i)} = \frac{(Z_1 e)(Z_2 e)}{4\pi\varepsilon_0 x} \tag{2.2}$$

where $E_{(i-i)}$ is the interaction energy between two ions, Z_1 and Z_2 are the valence (or number of charges) of the ions, e is the electronic charge, ε_0 the dielectric constant in vacuum, and x is the separation distance between the two ions.

(ii) Ion-permanent dipole interaction (Israelachvili, 2011)

$$E_{(i-pd)} = \frac{(Ze)\mu cos(\psi)}{4\pi\varepsilon_0 x^2} \tag{2.3}$$

where $E_{(i-pd)}$ is the interaction energy between an ion and a permanent dipole, μ is the dipole moment, and ψ is the angle between the line of centers and the axis of the dipole.

(iii) Permanent dipole-permanent-dipole interaction (Israelachvili, 2011)

$$E_{(pd-pd)} = \frac{(constant)\mu_1\mu_2}{4\pi\varepsilon_0 x^3} \tag{2.4}$$

where the $E_{(pd-pd)}$ is the permanent dipole-permanent dipole interaction energy. The *constant* depends on the relative orientation between the two dipoles: The $constant = \sqrt{2}$ for average over all orientations; $constant = 2$ for parallel dipoles and $constant = -2$ for anti-parallel dipoles.

van der Waals interactions

The van der Waals interactions are due to instantaneous dipoles due to polarizations induced by the neighboring charged molecules (or atoms, ions) and are always negative (attraction). The van der Waals interactions possibly happen between (i) permanent dipole-induced dipole, (ii) permanent dipole-permanent dipole, and (iii) induced dipole-induced dipole. The potential function, representing these interaction forces, has a power law exponent of 6 with respect to the separation distance. Below are given the general equations of Debye (Permanent dipole(PD) - induced dipole(ID)), Keesom (Permanent dipole(PD) - permanent dipole(PD)), and London (Induced dipole(ID) - induced dipole(ID)) adapted from J. Z. Zhang et al. (2003).

(i) Permanent dipole(PD)-induced dipole(ID) interaction also known as (Debye interaction) (Israelachvili, 2011),

$$E_{(PD-ID)} = -\frac{(\alpha_1\mu_2^2 + \alpha_2\mu_1^2)}{(4\pi\varepsilon_0)^2 x^6} \tag{2.5}$$

where the $E_{(PD-ID)}$ is the permanent dipole-induced dipole interaction energy. The α_1 and α_2 are the polarizabilities of the two dipoles.

(ii) Permanent dipole(PD)-permanent dipole(PD) (Keesom interaction due to the average effect of the rotational contribution of the polarizability) (Israelachvili, 2011)

$$E_{(PD-PD)} = -\frac{(\frac{2}{3})\mu_2^2\mu_1^2)}{(4\pi\varepsilon_0)^2 kTx^6} \tag{2.6}$$

where the $E_{(PD-PD)}$ is the permanent dipole-permanent dipole interaction energy. The k is the Boltzmann constant and T is the temperature.

(iii) Instantaneously induced dipole(ID)-induced dipole(ID) interaction (London interaction) (Israelachvili, 2011)

$$E_{(ID-ID)} = -\frac{(\frac{3h}{3})[\frac{\nu_1\nu_2}{(\nu_1+\nu_2)}]\alpha_1\alpha_2}{(4\pi\varepsilon_0)^2 x^6} \tag{2.7}$$

where h is Plank constant, and ν is the characteristic vibration frequency of the electrons.

Short-range (or strong interaction)

At a very short distance between particles, a very strong repulsive force develops and rises sharply with respect to distance like two hard spheres approaching each other. The formation of this interaction is not well defined but is usually treated as a power law with an exponent of 12, where ζ is a pre-exponent constant

$$E = \zeta x^{-12} \tag{2.8}$$

Total interaction potential

At a long distance, other forms of intermolecular interactions come into play, but at a close distance the most important interactions are van der Waals forces and the short-range repulsion. For convenience, these interaction energies are usually summarized in a power law equation known as Lennard–Jones potential which includes the repulsive and attractive terms:

$$E = \zeta x^{-12} - \beta x^{-6} \tag{2.9}$$

The van der Waals 6^{th} power term reflects the summation of the contribution from the random dipole–dipole interactions from equations (2.5) to (2.7) related to the polarizability of the molecules, and is always attractive (negative). The β is the pre-exponent constant.

Macroscopic interaction energies

van der Waals attraction between two spherical particles

For macroscopic bodies, such as spherical particles, the van der Waals attraction energy can be assumed to be the addition of all the contributions from individual atoms (molecules) (Hiemenz & Rajagopalan, 1997). If the number of atoms per unit volume is ρ, using the $6th$ power expression for the van der Waals attraction in the Lennard–Jones equation, the pairwise interaction between the increment volumes (dV_1, dV_2) of the two objects is (Hiemenz & Rajagopalan, 1997)

$$dE_a = -(1/2)\rho^2\beta/x^6 dV_1 dV_2 \tag{2.10}$$

The total attraction energy is the integration over the volumes of the two objects:

$$E_a = -(1/2)\rho^2\beta \iint dV_1 dV_2 / x^6 \tag{2.11}$$

By assuming certain geometric consideration, it is not difficult to derive the van der Waals attraction energies between a wide range of macroscopic bodies. Some of these expressions, under the approximate conditions (Hiemenz & Rajagopalan, 1997), are shown below:

Two identical spheres ($R \gg x$)

$$E_a = \frac{-AR}{12x} \tag{2.12}$$

where, the R is the particle radius and A is the Hamaker constant, defined as $A = (\rho\pi)^2\beta$.

Two spheres of the same composition but of different size (R_1 and $R_2 \gg x$)

$$E_a = \frac{-AR_1R_2}{6x(R_1+R_2)} \tag{2.13}$$

Two surfaces with indefinite thickness:

$$E_a = \frac{-A}{12\pi x^2} \tag{2.14}$$

Electrostatic repulsive energy

The electrostatic interactions between macroscopic bodies are more difficult to treat quantitatively than the van der Waals interactions. Usually, a charged surface is assumed to be composed of two regions (the so-called double layer structure): an inner region consisting of the charged surface itself and a layer of adsorbed species, and an outer diffuse region in which the charged species are distributed according to the Boltzmann distribution functions as determined by the electric potential, φ:

$$n_i = n_{io} exp[-\frac{z_i e\varphi}{kT}] \tag{2.15}$$

where n_i is the concentration of the charged species (number of charges per unit volume) and z_i is the number of charges on the charged species.

The net volume charge density ρ^* at any position is

$$\rho^* = \sum n_i = \sum n_{io} exp[-\frac{z_i e \varphi}{kT}]$$

The variation of the surface potential as a function of distance from the surface and the charge distribution in space satisfies the Poisson equation:

$$\nabla^2 \varphi = -\frac{\rho^*}{\varepsilon} \tag{2.16}$$

where ∇^2 is the Laplacian operator, and ε is the permitivity.

These equations can be solved together with the proper boundary conditions ($\varphi = \varphi_0$) when $x = 0$; $\varphi = 0$ and $d\varphi/dx = 0$ when $x = \infty$) to give the electrical potential as a function of distance from the surface. Normally, the solution is complicated, but when the electric potential is low compared to the thermal effect, a simple solution can be derived (The Debye–Hückel approximation) for flat surfaces (J. Z. Zhang et al., 2003):

$$\varphi = \varphi_0 exp[-x/\kappa^{-1}] \tag{2.17}$$

where κ^{-1} is called the double layer thickness, and is defined by the electrolyte concentrations (ionic strength) (J. Z. Zhang et al., 2003):

$$\kappa^2 = [\frac{c^2 N_A}{\varepsilon kT}] \sum z_i^2 c_i \tag{2.18}$$

where N_A is the Avogadro's constant, and c is the molar concentration of the charged species (Shaw, 1992).

When the electric potential overlaps, a repulsive potential is produced between two surfaces. A variety of analytical and numerical solutions is obtained, depending on the approximations made, including whether a constant potential or constant charge is assumed. One of the widely used expressions for two identical spheres was derived by Verwey and Overbeek by considering the balance of the electrostatic repulsive force and the osmotic pressure developed between the surfaces at constant surface potential: (Overbeek, 1977;

Verwey, Overbeek, & Overbeek, 1999)

$$E_r = [\frac{32 \cdot \varepsilon R k^2 T^2 \gamma^2}{c^2 z^2}] e^{-\kappa x}, \qquad \gamma = \frac{e^{\frac{ze\varphi_0}{2kT}} - 1}{e^{\frac{ze\varphi_0}{2kT}} + 1}. \tag{2.19}$$

where z is the number of charges on the counter ion, and γ is a constant related to the surface potential φ_0. Although the above equation is only applicable under a strict restriction of low surface potential ($\kappa x > 1$), acceptable results have been obtained for both large surface potential and low surface potential (J. Z. Zhang et al., 2003).

In general, the total interaction energy is the summation of the electrostatic repulsion and the van der Waals attraction. With a high particle surface potential, the repulsion force is stronger, and the total interaction becomes positive. The particles will remain separated because an energy barrier needs to be overcome for the particles to approach each other. For a low surface potential, the repulsion is not strong and the total interaction energy is mostly attractive. Under these conditions, the particles will come together to form aggregated clusters and help the self-assembly of particles.

Hydrogen bonding and hydrophobic effect

Hydrogen Bond: Hydrogen bonding is probably the most important noncovalent interaction to think about in the self-assembly of biological or biomimetic membrane lipids (Israelachvili, 2011; Ohya, 2002). Together with the presence of water, the most ubiquitous medium in nature, both the lipid and solvent forms strong intermolecular hydrogen bonds. Nonetheless, the tetrahedral structure of water molecules also forms the solvent-solvent hydrogen bonds. Although this bonding is weaker in strength compared to covalent or ionic bonding, its highly selective and directional nature allows the bond to have dynamic characters around the thermodynamics equilibrium state (Ohya, 2002).

The hydrogen bond is an attractive interaction between a hydrogen atom from a molecule or a molecular fragment D−H in which D is more electronegative than H, and an atom or a group of atoms in the same or a different molecule, in which there is evidence of bond formation (Arunan et al., 2011). In other words, hydrogen bond is formed when a donor (D) from a highly electronegative segment is brought into intimate contact with an acceptor (A) which carries available nonbonding lone pair (see Figure 2.24). Generally

both the D and A are highly electronegative atoms (O,N,F,Cl,Br,S). Although the hydrogen bond is considered optimum when the angle (θ) between donor and acceptor is 180° (see angle for D−H···A in Figure 2.24), the most probable angle observed for various samples of hydrogen bonds is around 165° in solid state (Ohya, 2002). This is consistent with the theoretical calculation of hydrogen bond between OH···O in carbohydrates using the *ab initio* quantum mechanics on a model system (Newton, Jeffrey, & Takagi, 1979).

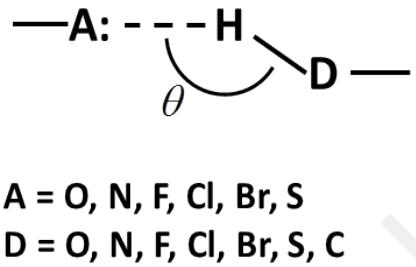

Figure 2.24: Hydrogen Bonding (linear type). The three dot lines represent the hydrogen bonding interaction. Redrawn from Ohya (2002).

Hydrophilic Effect: Amphiphilic molecules self-assemble in water and their self-organization factor is primarily due to the hydrophobic effect (Akiyoshi, 2002). In fact, the hydrophobic effect can be explained in terms of hydrophobic hydration and hydrophobic interaction (Tanford, 1980). The structures of water molecules around hydrophobic molecules become more crystalline compared to those of bulk water. Frank and Evans (1945) named this phenomenon as hydrophobic hydration. This is to say, when water molecules approach an inert surface that cannot form a hydrogen bond such as alkanes, hydrocarbons, and fluorocarbons, the molecules need to reorient themselves so that the four charges on the water molecules will point away from the surface. The tetrahedral water molecules rearrange themselves so that the polarized groups on the molecules are still available for hydrogen bonding with the rest of the molecules, while also minimizing contact with the inert surface. As a result, the water molecules near the surface become more ordered as compared to free water molecules, producing a hydrophobic hydration layer of interconnected water molecules with open cage structures. A consequence of the hydrophobic hydration is the so-called hydrophobic attractive interaction between nonpolar molecules and the surfaces (J. Z. Zhang et al., 2003).

Kauzmann (1959) proposed an idea called *hydrophobic bonding* (to distinguish it from van der Waals interaction) looking at the interactions among hydrophobic amino

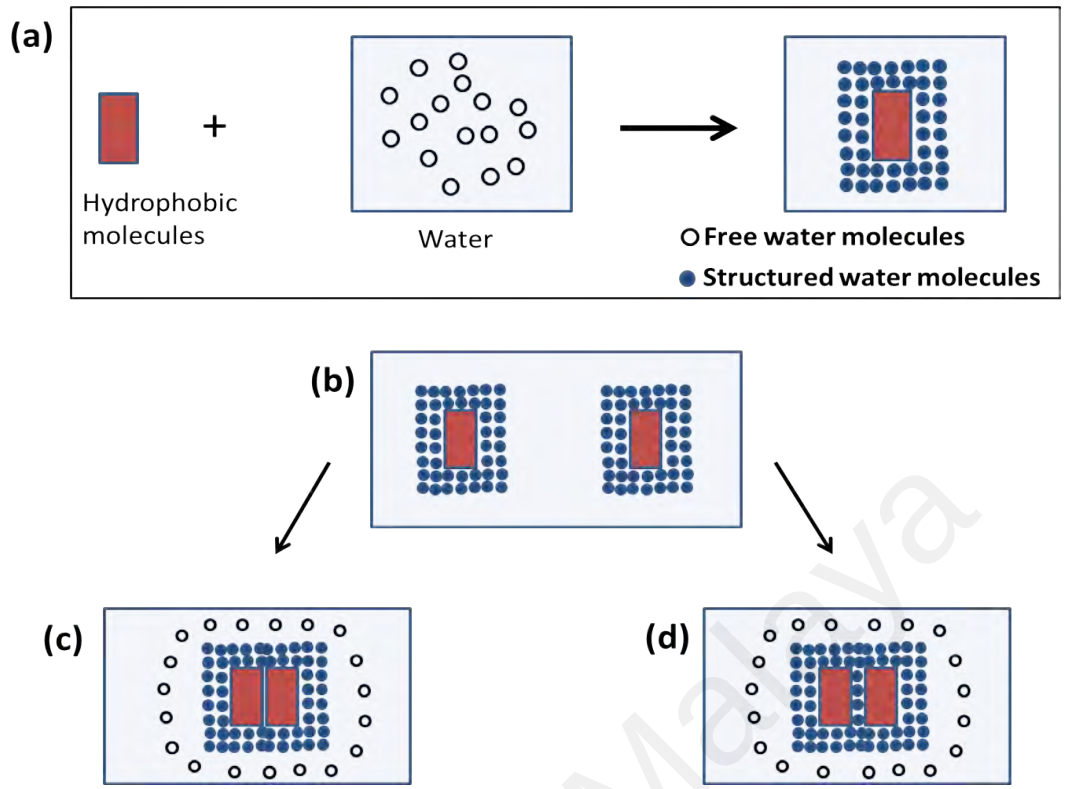

Figure 2.25: Schematic representations of hydrophobic hydration add hydrophobic interaction. (a) model for hydrophobic hydration (hydrophobic molecule is surrounded by structured water molecules), (b) to (c) is the model for hydrophobic interaction (self-assembly of hydrophobic molecules to avoid contact with water as much as possible), and (b) to (d) is another model for hydrophobic interaction (solvent-separated hydrophobic pair interaction). Redrawn from Akiyoshi (2002).

acid residues from polypeptides playing a decisive role in the formation of higher-order structures of proteins in an aqueous solution. This bonding is not like the chemical bonding between atoms, therefore, Ben-Naim (1980) address this *hydrophobic interaction* by giving statistical mechanics theories for describing this behavior.

The above concepts can be described via schematic representation as in Figure 2.25 which, (a) shows the hydrophobic hydration in which networks of water molecules surround a hydrophobic molecule and (b) represents a model for hydrophobic interaction in which molecules like those seen in (a) tend to self-assemble to avoid contact with water as much as possible. As a result of this kind of aggregation, the amount of structured water surrounding the solute decreases. However, recent studies show that (b) to (c) type interaction is less valid in the hydrophobic interaction model. It is generally accepted that interactions among hydrophobic molecules are due to solvent-separated hydrophobic like those in (b) to (d) pair interactions, but not direct contact.

2.2.2 Molecular packing and interfacial curvature

Amphiphilic molecules are able to form a wide range of ordered microstructures in the condensed states. These structures can transform from one to another when the solution conditions like pH, temperature, or electrolyte concentrations are changed. The equilibrium of the structures is determined by the thermodynamics of the self-assembly process and the inter- and intra-aggregate forces. The major driving forces for the amphiphiles to form well-defined aggregates are the hydrophobic attractions at the hydrocarbon-water interfaces and the hydrophilic ionic or steric repulsion between the headgroups as discussed in Section 2.2.1 . The phases attributed to these types of interactions in high concentration of amphiphilic molecules can be described by two types of models. The first is based on the shape of the surfactant molecules and the second is based on the curvature of a surfactant film at an interface.

Molecular packing geometry

The relationship of molecular structure to phase geometry is important because it establishes a design strategy of new materials. Israelachvili (2011) proposed a simple packing model which can predict the phase behavior from the knowledge of packing geometry parameter. The packing geometry of a molecule depends on its equilibrium area per molecule at the aggregate interface, a_0, the hydrocarbon chain volume, V and the critical hydrocarbon chain length, l_0. The value of the dimensionless packing parameter, also known as shape factor, is given as (Hamley, 2000)

$$R = \frac{V}{a_0 l_0} \tag{2.20}$$

where R determines whether they form spherical micelles, non-spherical or cylinder micelles, vesicles or bilayers, or inverted structures. The preferred phase formed corresponds to the minimum-sized aggregate in minimum free energy (J. Z. Zhang et al., 2003). In general, the molecular packing parameter concept emphasizes the importance of the surfactant headgroup and tail in predicting the shape and size of equilibrium aggregates although the former plays a more dominant in controlling the phase formation (Nagarajan, 2002).

Table 2.1: Preferred geometries for different values of critical packing parameter. Redrawn from Israelachvili (2011).

Lipid	**Critical Packing Parameter** ($R = \frac{V}{a_0 l_0}$)	**Critical Packing Shape**	**Preferred Phase Geometry**
Single-chained lipids with large headgroup areas	$< \frac{1}{3}$	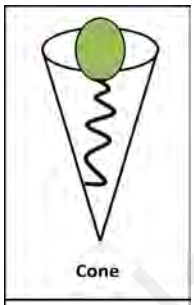	Spheres
Single-chained lipids with small headgroup areas	$\frac{1}{3} - \frac{1}{2}$	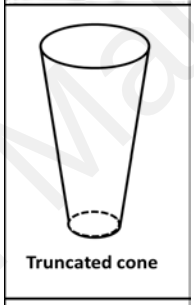	Cylinders
Double-chained lipids with large headgroup areas, fluid chains	$\frac{1}{2} - 1$	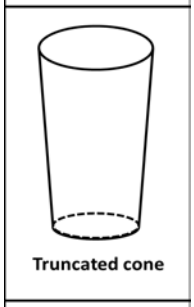	Flexible bilayers
Double-chained lipids with small headgroup areas, anionic lipids in high salt	~ 1	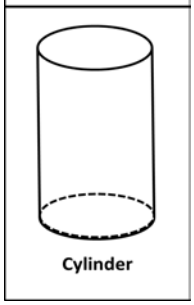	Planar bilayers
Double-chained lipids with small headgroup areas, non-ionic lipids, poly (*cis*) unsaturated chains, high temperature	> 1	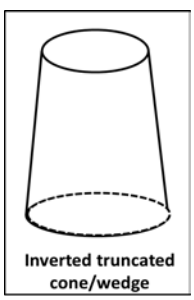	Inverse structures

Table 2.1 shows the packing parameter values and their associated probable aggregate structures. A small critical packing parameter ($< 1/2$) favors the formation of a highly curved interface (spherical micelles and rod-like micelles), and a larger critical packing parameter ($> 1/2$) favors the formation of flat interfaces (flexible bilayers and planar bilayers). A critical packing parameter greater than 1 will produce inverse structures.

Although many experimental parameters affect the changes from one phase to another, the change is not random. It follows a consistent pattern. For example, as the surfactant concentrations are increased, the phases go through spherical micelles, rod-like micelles, hexagonal, cubic, and lamellar phases (Tiddy, 1980) as shown in Figure 2.26. These changes are consistent with the change of packing geometry when the experimental conditions are changed. Below is a brief description on the relationship between external factors such as surfactant concentration, chain length, cosolvent, and salts and ionic moieties to the packing parameter values (Hamley, 2000; J. Z. Zhang et al., 2003).

Effect of Surfactant Concentration: The increase of surfactant concentration causes the amount of water available for association with the surfactant headgroup to decrease. Subsequently, the degree of hydration of the surfactant headgroup decreases. The reduction of hydration at the headgroups leads to a decrease in the effective headgroup area. Based on the critical packing parameters, for fixed surfactant tail length, a reduction in the headgroup area increases the critical packing parameters. A larger critical packing parameter indicates a less curved geometry. The transition from the more curved spherical micelles to flat

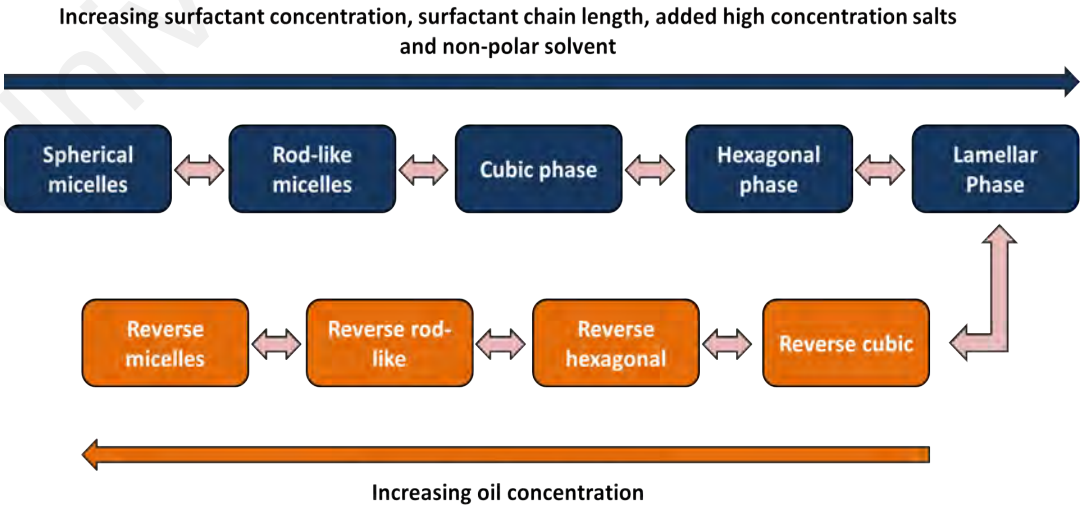

Figure 2.26: Phase changes as a function of external condition. Redrawn from J. Z. Zhang et al. (2003).

lamellar phase is observed. This is depicted in Figure 2.26 which agrees with the packing geometry illustrated in Table 2.1.

Effect of chain length: Increasing the surfactant chain length has a similar effect as increasing the surfactant concentrations. When the headgroup area is fixed, both the volume and the chain length increase, but their effects on the packing geometry does not cancel out. From Table 2.1, it can be seen that for a fixed number of surfactants within a fixed headgroup area in one spherical micelle, if the chain length is increased beyond a certain limit, the packing of the surfactants is no longer space filling and the spherical geometry will not be stable. This implies that when the chain length increases, the packing parameter is also increasing, and phase transition from spherical to less curved hexagonal and lamellar structures is favored.

Effect of cosolvents: Polar solvents, like alcohol or water, tend to associate with the headgroups and reduce the tendency for the surfactant molecules to associate. In some cases, it can make the tendency completely disappear, which means the surfactants will not aggregate at all. On the other hand, nonpolar solvent molecules tend to associate with the hydrophobic chains of the surfactants. The addition of the nonpolar groups will, therefore, increase the volume of the surfactant, and increase the packing parameter. For normal aggregates, there will be a tendency for the transition from a more curved structure to a less curved structure. If the packing parameter is further increased, reverse micellar structures will form with an increased tendency for reverse curved structure.

Effect of salts and ionic species: The effect of adding salts and ionic species to ionic surfactant systems is not difficult to understand. For ions that do not specifically bind to the charged headgroup, the increased ionic strength has a screening effect on the charged headgroup and this reduces the repulsive energy between the headgroups, therefore reducing the headgroup area. This leads to an increase in the packing parameter, and a similar phase transition from a more curved structure to less curved structure. On the other hand, for ionic species that strongly bind to the headgroup, a significant increase in the packing parameters can lead to the formation of larger vesicles, bilayer structures, and even reverse micelles. But for nonionic surfactants, the addition of salts will have less effect, where the inorganic species can interact with the micellar structures in a more complicated fashion and alter the phase diagrams (J. Z. Zhang et al., 2003).

Table 2.2: Mean and Gaussian interfacial curvature for common aggregate shapes. Here $R = R_1 = R_2$ denotes a radius of curvature. Adapted from Hamley (2000).

Structure / phase	**Mean curvature** $(H = (c_1 + c_2)/2)$	**Gaussian curvature** $(K = c_1 c_2)$
Spherical micelles or vesicles (outer layer)	$+\frac{1}{R}$	$+\frac{1}{R^2}$
Cylindrical micelles	$+\frac{1}{2R}$	0
Bicontinuous cubic phases	0 to $+\frac{1}{2R}$	$-\frac{1}{R^2}$ to 0
Lamellar (planar bilayers)	0	0
Inverse bicontinuous cubic phases	$-\frac{1}{2R}$ to 0	$-\frac{1}{R^2}$ to 0
Inverse cylindrical micelles	$-\frac{1}{2R}$	0
Inverse spherical micelles or inner layer of vesicles	$-\frac{1}{R}$	$-\frac{1}{R^2}$

Interfacial curvature

In addition to the structural parameters such as the packing parameter, the curvature of the interface can also possibly be used to explain the phase behavior. There are two fundamental types of curvatures which characterize each point on the curved surface, namely the mean curvature, H and the Gaussian curvature, K. They are related to the principal curvatures $c_1 = {}^1/_{R_1}$ and $c_2 = {}^1/_{R_2}$ at a point P on the surface by the following equation, respectively (Hamley, 2000) (see Figure 2.27):

$$H = \frac{c_1 + c_2}{2} \tag{2.21}$$

$$K = c_1 c_2 \tag{2.22}$$

where R_1 and R_2 are the principal radii of the curvatures H and K may or may not be uniform along the interface, and may be positive, zero or negative (see Table 2.2).

A positive value of H denotes the interface curves towards the hydrophobic chain region (type I) since R_1 and R_2 are positive (the surface curves upwards around P). The negative value of H denotes a curvature towards the polar aqueous region (inverse, type II). In this case, both R_1 and R_2 are negative (the surface curves downwards).

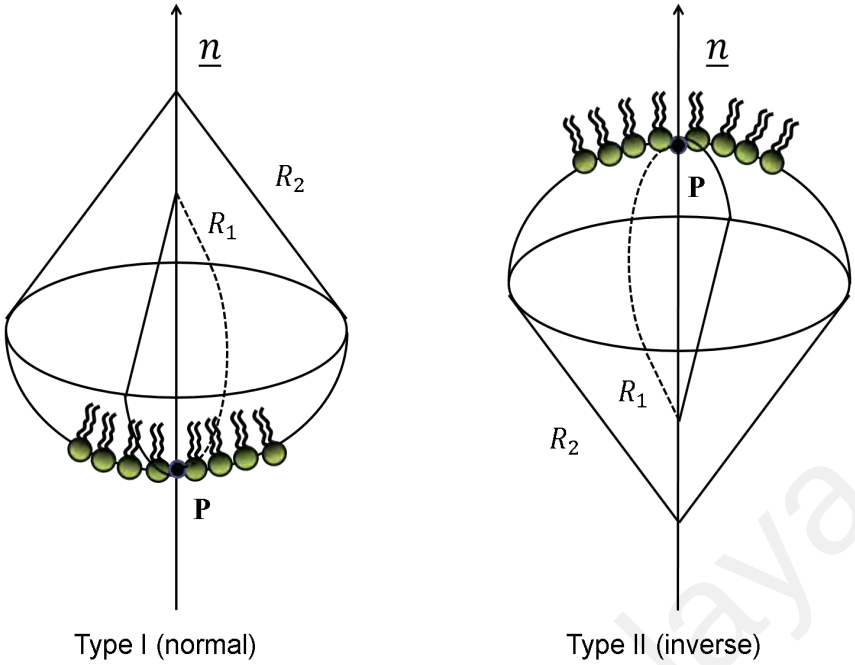

Figure 2.27: Sign convention adopted for mean curvature, H of a lipid monolayer. Redrawn from Seddon (1990).

The sign of K determines the form of the interface. The simplest example for the positive value of K is a sphere whereas the surface of the cylinder or plane has zero Gaussian curvature. The surface of negative K has two principal curvatures, c_1 and c_2 of opposite signs. An example is the saddle surface. The Gaussian curvature is most negative at the saddle point and the K value approaches zero when moving along the surface towards the apex point. The saddle surface is also known as the minimal surface since it has zero H value at all points and they appear to form the basis of a bicontinuous cubic phase (Seddon, 1990).

The elastic free energy density associated with the curvature of a surface contains, for small deformations, the sum of contributions from mean and Gaussian curvature (Hamley, 2000). It is given approximately by

$$F_{curv} = F_{mean} + F_{Gauss} = \frac{1}{2}\kappa(c_1 + c_2 - c_0)^2 + \bar{\kappa}(c_1 c_2) \tag{2.23}$$

where the c_0 is spontaneous curvature. For zero Gaussian curvature, the equilibrium mean curvature becomes twice the value as $c_0 = c_1 = 2H_{equilibrium}, c_2 = 0$. As the term suggests, the spontaneous curvature is that adopted by a surfactant membrane in the absence of constraints to reduce the curvature elastic free energy, which in eq. (2.23) is defined with

respect to the flat membrane. The quantities κ and $\bar{\kappa}$ are the elastic moduli for mean and Gaussian curvatures respectively and have units of energy. This interfacial curvature model is useful because it defines these elastic moduli, which can be measured e.g. light scattering, and characterize the flexibility of surfactant films. The uncharged surfactant films typically have elastic energies $F_{el} \leqq k_B T$ i.e. they are quite flexible (Hamley, 2000).

2.3 Glycolipid liquid crystal

The importance of glycolipid was realized following a work by Emil Fischer and Burckhardt Helferich who had observed a "double melting" phenomenon in one of the long-chain alkyl glucopyranoside, i.e. hexadecyl β-D-glucopyranoside (Fischer & Helferich, 1911). This finding was the first reported with observation of thermotropic liquid crystalline properties from this amphiphilic carbohydrate. As for lyotropic behavior, Robert Koch made the first observation in alkylated sugar where he observed an unusual optical texture of aqueous dispersions while analyzing the extracts from tuberculosis bacteria (Koch, 1884). Subsequently, in the past few decades, glycolipid research has received much attention for exploiting their unique properties as biosurfactants (Kitamoto et al., 2009).

One of its dominant property is to self-assemble into several liquid crystalline mesophases when being in contact with and without water (lyotropic and thermotropic respectively). The self-assembling feature of this molecule is due to its amphiphilic nature, that is, the hydrophilic region is primarily composed of sugars and the hydrophobic part filled with aliphatic hydrocarbon chain where both types of moieties are connected via glycosidic bond. The sugar part can be a simple monosaccharide, disaccharide or complex oligosaccharide while the tail part can be mono- or asymmetrically branched hydrocarbon chains with the terminal group being methyl. With the different combinations of sugar types and alkylated chains, various glycolipids can be prepared and studies of such glycolipids have shown that they are rich with liquid crystalline properties as well as surfactant property. Many of the self-aggregated structures are mostly in liquid crystalline domain, such as lamellar (L_α), hexagonal (H), cubic (Q), rippled (P), and gel (L_β) phases depending on the degree of amphiphilicity in the molecule. The general phase diagram was shown in Figure 2.22 and the specific assembled structures were shown in Figure 2.18

(lamellar phases), Figure 2.21 (normal and reverse hexagonal phases), and Figure 2.20 (cubic phases).

We know that the driving force for the mesophase formation of these amphiphilic molecules is the microphase separation of the hydrophilic and hydrophobic groups which lead to structural aggregation of oppositely-behaving moieties. Those self-assembling structures are maintained by both the hydrophobic force (short-range repulsion) dominant within the alkyl chain region and the hydrogen bonding network in the hydrophilic region, each stabilising the formed mesophase (Milkereit, Morr, Thiem, & Vill, 2004; M. K. Singh, Jayaraman, Rao, & Prasad, 2008). However, the fundamental difference between GLs and other amphiphiles resides in the complexity of interactions among hydroxyl groups within the sugar moieties. This adds a greater intricacy to the usual hydrophilic–hydrophobic balance governing the self-assembly, where the headgroup plays the attractive role and chain group the repulsive one. Unlike biological amphiphiles aggregating in lamellar-type assemblies (i.e. phospholipids) whose structural arrangement is controlled by the hydrophobic tails (Corti et al., 2007), studies on GLs showed that "small" differences in the sugar headgroup, like those between glucose, galactose and mannose, can give rise to new features in the liquid crystalline behavior (Hinz et al., 1991; Köberl, Schöppe, Hinz, & Rapp, 1998).

2.4 Structure-property relationship

This section is allocated for a brief description of the liquid crystalline properties of synthetic glycolipids as a function of modified molecular structure. The amphiphilic carbohydrate molecule is composed of three major parts; headgroup, hydrocarbon chain and linkage (connecting headgroup and chain). This composition gives an opportunity to study the behavior of the structure by varying the chemical constitution or configuration of one part of the amphiphile while retaining the other parts intact. Many authors have reported complete and informative reviews on carbohydrate-based liquid crystals (Goodby et al., 2007; Hashim et al., 2012; Hato, 2001; Jeffrey, 1986; M. K. Singh & Jayaraman, 2009; Stubenrauch, 2001; Vill & Hashim, 2002). Astonishingly, the infinite diversity of the chemical structures of GLs has opened a wide area of possible research on liquid crystal phase behaviors which is very much depend on the type and number of sugar units in the headgroups, type of linkages and variety of the hydrocarbon tails.

Hydrophilic group

For instance, Sakya, Seddon, and Vill (1997) investigated the thermotropic and lyotropic phase behavior of different headgroups of monoalkyl glycosides (i.e. glucose, galactose and mannose). These sugars contain a small modification in the chemical structure and this can lead to a large change in the phase behavior. This finding is consistent with the behavior of dialkyl glycolipids (Seddon et al., 2003), where it was found that both glucose and galactose headgroup adopt the L_α phase upon cooling from the H_{II} phase. However, below the chain-melting transition, the glucoside forms a metastable gel phase (L_β) whereas the galactoside forms only a crystalline lamellar phase (L_C).

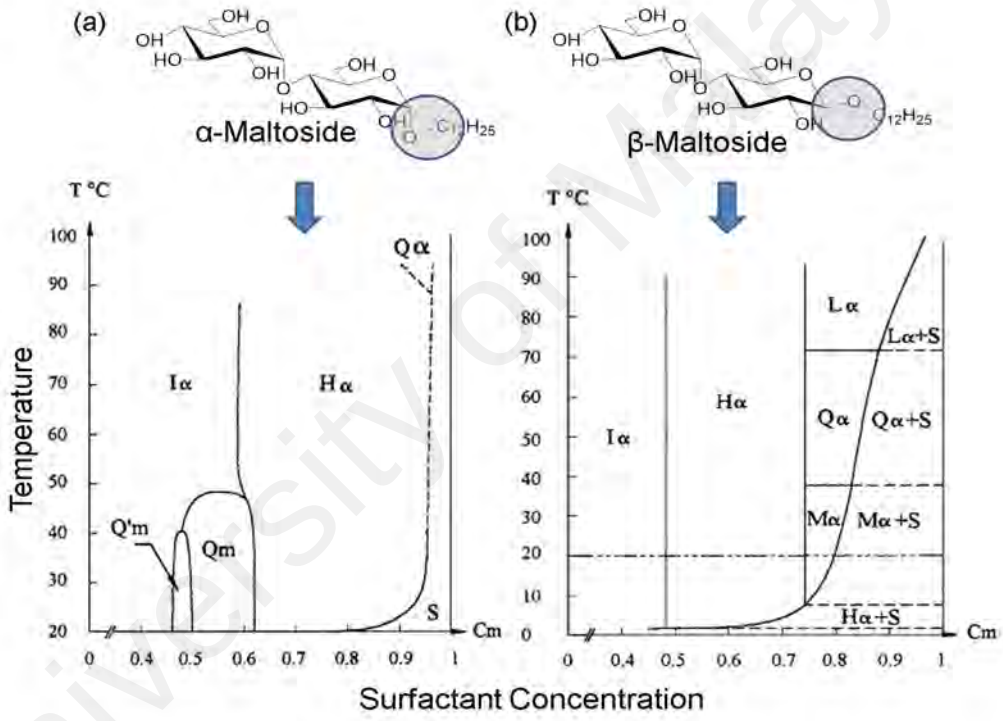

Figure 2.28: Molecular structures of lipid (a) α-Maltoside and (b) β-Maltoside are shown. The glycosidic linkage for each glycoside is circled. Below the structures corresponding phase diagrams of α-Maltoside and β-Maltoside are given where both show different phase formation. Q_m is Pm3m cubic phase, H_α is hexagonal phase, Q_α is Ia3d cubic phase, L_α is lamellar phase and I_α is micellar solution phase. Adopted from Auvray et al. (2001).

Similarly, a work by Auvray et al. (2001) on disaccharide lipids, like single chain dodecyl-maltosides (α-Maltoside and β-Maltoside) in lyotropic condition shows different mesophase patterns as given in Figure 2.28. The difference in the phase diagrams is attributed to the molecular structure of the respective lipids. The glycosidic linkage of α-Maltoside and β-Maltoside is orientated axial and equatorial respectively at anomeric

position (circled in the diagram Figure 2.28). The effect of anomeric configuration has also been investigated by Boyd, Drummond, Krodkiewska, and Grieser (2000); Nilsson, Söderman, and Johansson (1998); Sakya, Seddon, Templer, Mirkin, and Tiddy (1997). Boyd et al. (2000) showed that the phase transition temperatures are influenced significantly by the anomeric configuration in the shorter octyl derivatives, but less pronounced in the longer alkyl chain derivatives. A shorter chain (octyl) glycolipids with the α-anomers have a higher clearing point (T_C) than the β-anomers. This is due to α-anomers having greater space for the chain groups to vibrate, therefore, making the liquid crystalline phases more stable at higher temperatures.

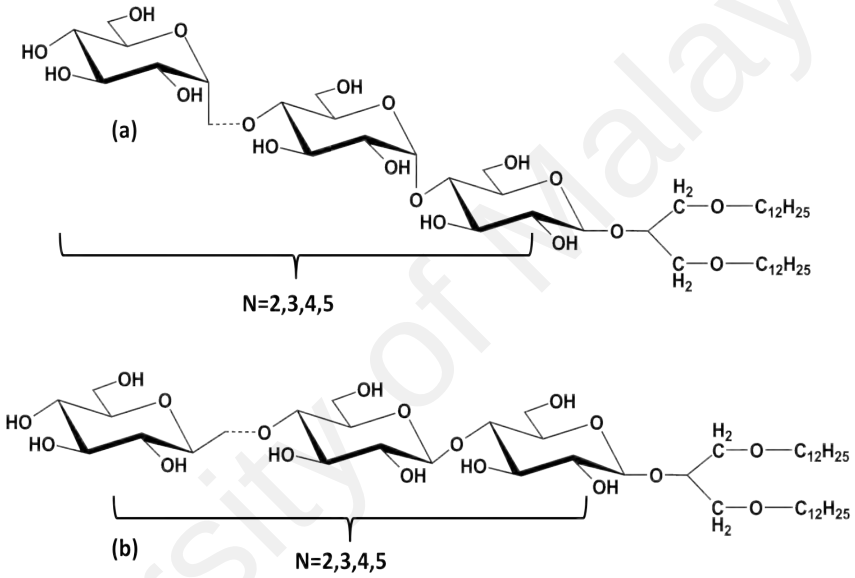

Figure 2.29: The chemical structures of the 1,3-di-O-dodecyl-2-O-(β-glycosyl) glycerols bearing a series of (a) maltose oligosaccharides and (b) cellobiose oligosaccharides as the headgroup (Hato & Minamikawa, 1996).

In the meantime, the effect of increasing the degree of headgroup polymerization has also been studied. For example, malto-oligosaccharides greatly increase the solubility of the surfactant in water when the number of glucose units, N is increased (Boyd et al., 2000; Minamikawa & Hato, 2005), and it also improves the stability of the thermotropic liquid crystalline state (Boyd et al., 2000). Nevertheless, the stereochemistry of oligosaccharide headgroups has a strong effect on the physical properties of aqueous synthetic GLs (Hato & Minamikawa, 1996). It has been found that an increase in N of the malto-oligosaccharide containing lipids decreases the melting point, (T_m) of hydrated solid/liquid crystalline phase, thus increasing the "hydrophilicity" of the lipid. Meanwhile the T_m of cello-oligosaccharide containing lipids increases with increasing N. The opposite phenomena is

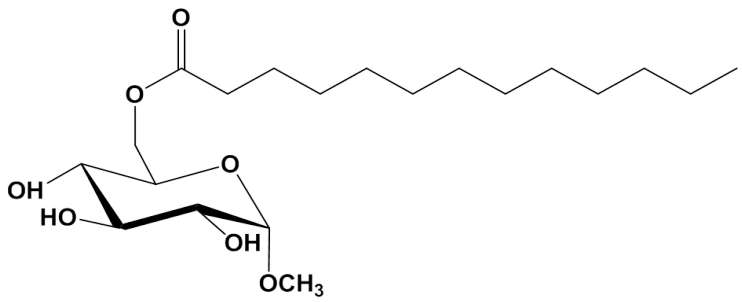

Figure 2.30: The chemical structures of methyl-6- O-dodecanoyl-α-D-glucoside. Redrawn from Cook et al. (2011).

related to the different conformations of the headgroups, that is, a "helical" conformation of the malto-oligosaccharides and an "extended" conformation of the cello-oligosaccharides (see Figure 2.29).

It was found that the exact configuration of the carbohydrate headgroup (e.g. glucose, galactose) has its main influence on the transition temperatures of the compounds, but not on the phase sequence (Vill, Von Minden, Koch, Seydel, & Brandenburg, 2000; von Minden et al., 2000; von Minden, Morr, Milkereit, Heinz, & Vill, 2002). Nevertheless, the carbon position where the linkage establishes to a hydrocarbon chain also influences the phase of assembly structures. Examples in Figure 2.29 and Figure 2.28 show the glycosidic linkage between the sugar and lipid parts occur at C1 position (the anomeric carbon). But in a few other cases, the C6 position may also be involved, as reported by Cook et al. (2011). The methyl-6-O-(n-acyl)-α-D-glucopyranosides with hydrocarbon chain lengths between 12 and 16 exhibit a monotropic *SmA* phase (see Figure 2.30 for example). Their T_m initially increases on increasing chain lengths but subsequently decreases on a further increase in chain length. This is attributed to the disruption of molecules packing due to back folding of the alkyl chain.

Linkage

Although oxygen is often regarded as the main linkage between the sugar and hydrophobic chain, other moieties take the role as connectors, e.g. sulphur and amide (Auvray et al., 2001; Gerber et al., 2009; Sakya et al., 1994). For instance, sulphur may be involved in linking the carbohydrate and hydrocarbon chain such as in n-octyl-1-S-β-D-glucopyranoside (Sakya et al., 1994) (see Figure 2.31). The presence of the sulphur linkage suppresses the formation of the hexagonal phase and stabilizes the

(a) N-octyl-1-S-β-D-glucopyranoside

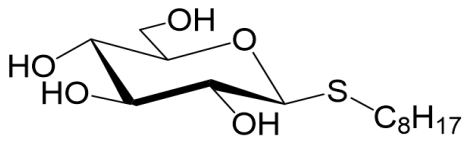

(b) N-(Hexadecanoyl)-4-O-(α-D-glucopyranosyl)-β-D-glucopyranosyl-amine

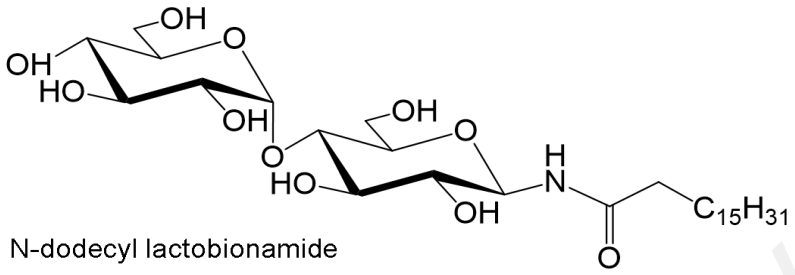

(c) N-dodecyl lactobionamide

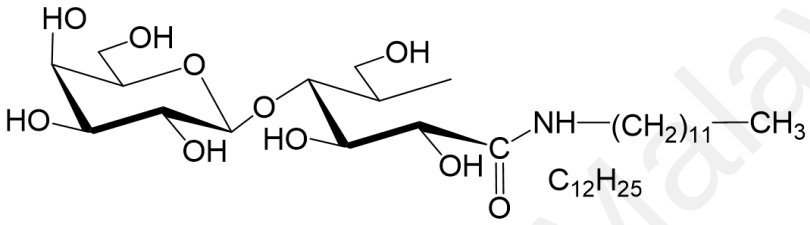

Figure 2.31: Examples of compounds with (a) sulphur linkage by Sakya et al. (1994), (b) amide linkage by Gerber et al. (2009), and (c) amino linkage by Auvray et al. (2001).

cubic phase, which is in contradiction to what has been observed in the case of n-octyl-1-O-β-D-glucopyranoside. Additionally, the thio linkage may differ from the oxygen linkage in three ways, i) the bond angle in oxygen linkage is higher (113°) compared to that of thio linkage (96°) and this affects the angle of the sugar headgroup to the hydrocarbon chain, ii) sulphur has a greater steric bulk than oxygen, and iii) sulphur has weaker hydrogen bond bonding capability because it is less ionic in character than oxygen (Sakya et al., 1994).

Besides, investigations into amide-linked monoacylated compounds like maltoside, mellibioside and lactosides show various structural polymorphism like uni- and multilamellar assemblies (Garidel et al., 2008; Howe et al., 2007; Vill et al., 2000; von Minden et al., 2000). There is no evidence for the existence of micelles – of spherical or of H_I type – or of interdigitated phases although the compounds has one acyl chain. This contradictory result of ether-linked monoacylated monosaccharides (Vill et al., 2000) suggests a reason for the preference for lamellar structures. It is related to the presence of the amide-linkage which causes the formation of a region with a high conformational order in the low hydration; e.g. as found in ceramides (Garidel, 2002, 2006).

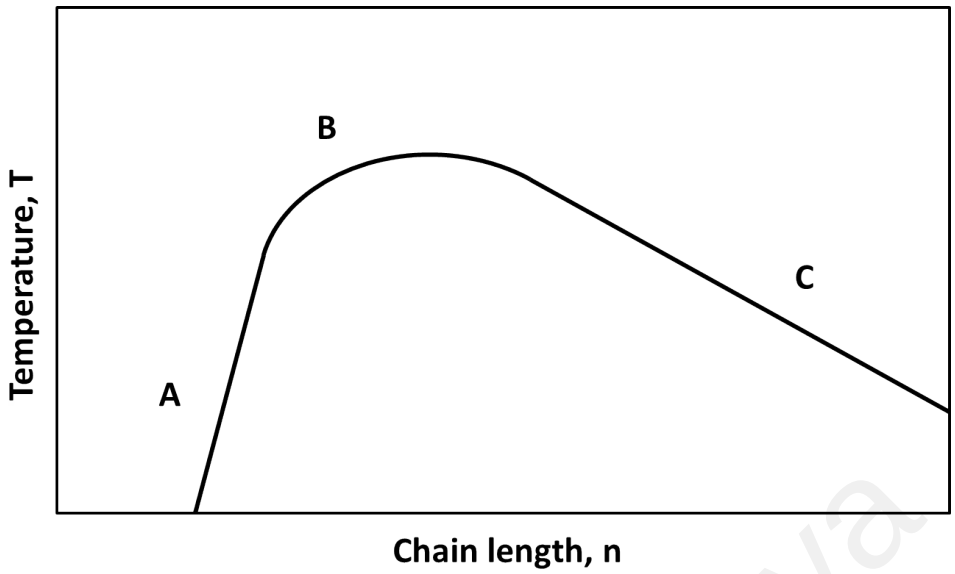

Figure 2.32: The general chain length dependency of homologous series. Redrawn from Vill and Hashim (2002).

Hydrophobic domain

The modification in hydrocarbon tail also plays an important role in determining liquid crystalline phase behavior. Increasing the straight alkyl chain length results in higher thermal stability in both thermotropic and lyotropic phases (Boyd et al., 2000; Sakya, Seddon, Templer, et al., 1997). This is because the longer the chain, the stronger the van der Waals interactions between them, and thus the greater the energy required to melt them.

In general, a homologous series has a dependency of the transition temperatures on the chain length as shown in Figure 2.32. The mesophase behavior starts with minimal chain lengths of 6, 7 or 8 (**A**). An elongation of the alkyl chain gives an increase in the *clearing temperature*. The plateau (**B**) is characterized by an optimal relationship between polar and non-polar molecular parts. Thus, higher OH group numbers would require higher numbers of CH_2 groups. After the plateau, a change of the chain length has only a minimal effect on the mesophase behavior. Finally, region **C** is characterized by a dominating paraffin chain. The *clearing temperature* decreases gradually with the chain length (Vill & Hashim, 2002).

Hashim et al. (2006) found a trend when they increased the chain length of branched glycolipids. The shorter chains seem to favour smectic phases while longer chains prefer a columnar arrangement due to the significantly increased bulkiness of the alkyl chain. This

behavior is not found for straight chains because they do not show an equivalent increase in bulkiness on increasing the chain length. The introduction of a double bond into the aliphatic chain has led to the formation of highly curved lyotropic phases (Hato, Yamashita, & Shiono, 2009; Mannock et al., 1992; Mannock & McElhaney, 2004; J. Yamashita, Shiono, & Hato, 2008). This is due to the molecules having a wedge shape structure since the hydrophilic headgroup is small compared to the volume occupied by the hydrophobic chain (see Figure 1.3(b)-(c) for example). Besides, in a thermotropic study, the branching effect leads to a decrease in the T_m of the GLs and the mesophase can be obtained at ambient temperature (Vill et al., 2000).

2.5 The lipid bilayer: an interesting phase

In Section 1.2 we have briefly discussed the structure of a lipid bilayer pertinent to biomembrane function and vesicle. Meanwhile, in this section we extend the discussion to some alluring characteristics possessed by the self-assembly of two monolayered lipid arrays. The function of lipid bilayer as a supporting matrix for biological membranes naturally exhibit highly dynamic structures as shown in Figure 2.33 (Eeman & Deleu, 2010). The position and orientation (i.e. lateral and rotational order respectively) of a lipid within a membrane continuously change with time and the time scales may vary from picoseconds to hours (Eeman & Deleu, 2010; Klaus, 2005). For instance, the hydrocarbon chain of a lipid may undergo conformational changes (such as *trans-gauche* isomerisation) over a time scale of a few picoseconds and affect the conformational order of the lipid

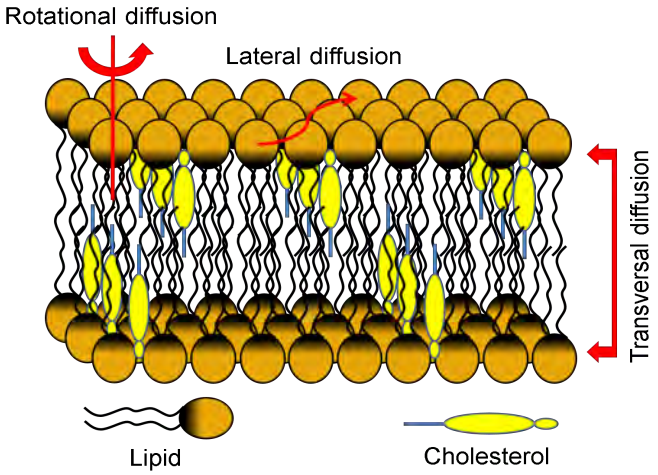

Figure 2.33: Graphical representation of types of motion undergo by lipids in a bilayer. The lipids involve in, rotational motion around lipid's long axis, translational diffusion and transversal diffusion from one layer to another. Redrawn from Eeman and Deleu (2010)

molecules. The time scale for the lateral diffusion coefficient (Lateral diffusion coefficient (C_D)) ranges typically from 10^{-7} to 10^{-10} cm^2 s^{-1}, and this shows the ability of a lipid molecule to laterally exchange with one of its neighbors within a layer. The time scale for this phenomenon is less than a minute. Meanwhile, the rotational diffusion coefficient defines the angular rotation of a lipid molecule around its long molecular axis perpendicular to the plane of the bilayer and this motion takes place over a time scale of nanoseconds. The translation of one lipid molecule from one leaflet to the other is a special case. This process is called transversal diffusion or flip-flop which involves rotation of the lipid molecule in the plane of the bilayer followed by its translation perpendicular to the plane of the bilayer. This type of diffusion is slow (of the order of hours to days) and is energetically unfavorable as it forces the passage of the polar lipid headgroup through the hydrophobic core at the center of the lipid bilayer (Jain, 1979; Klaus, 2005). However, some lipid molecules such as cholesterol are able to undergo a fast flip-flop ($< 1\ s^{-1}$) between the two leaflets of the lipid bilayer (Eeman & Deleu, 2010; Müller & Herrmann, 2002) . This behavior is most likely related to the small effective area of the polar headgroup of cholesterol which is limited to one hydroxyl group only.

Lipid bilayer in an aqueous medium can exist in various physical states (mesophases), which are characterized by the temperature, lateral organization, the molecular order as well as the mobility of the lipid molecules within the bilayer. In the solid-ordered phase, (S_o) (also known as gel phase), the lipids are arranged on a two-dimensional triangular lattice in the plane of the membrane (Heimburg, 2009; Janiak, Small, & Shipley, 1979).

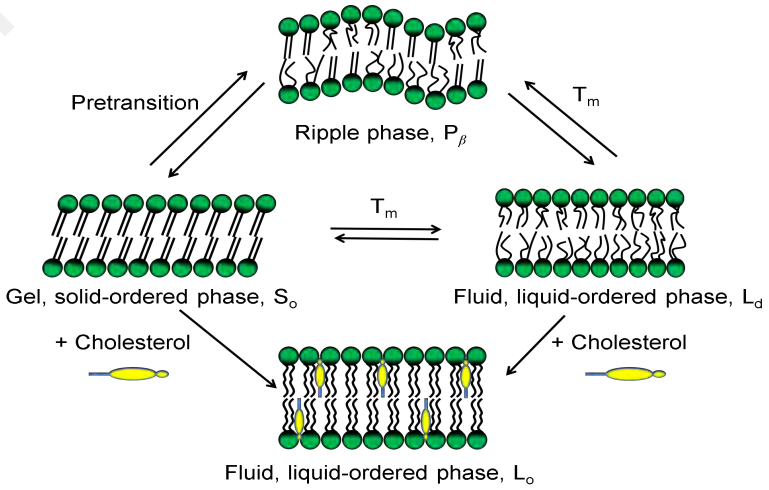

Figure 2.34: Representation of the different physical states achieved by lipid bilayer in aqueous meduim. T_m: main phase transition. Redrawn from Eeman and Deleu (2010).

The lipid's hydrocarbon chains display an all-trans configuration and are elongated to the maximum giving rise to an extremely compact lipid order. The gel phase can be further classified as (L_{β}' or L_{β}), where the former is due to the tilting of the lipid chain to the bilayer normal and the later is aligned without tilting (Eeman & Deleu, 2010). In the gel phase, the diffusion of lipids is greatly reduced to about $10^{-11}\,cm^2s^{-1}$ (Koynova & Tenchov, 2013). Additionally, the tilt of the chain is also influenced by the hydration level at the hydrophilic region of the bilayer. The tilt angle of the chain to the bilayer normal increases as the water content increases, that is the tilt can change from no tilt (L_{β}) to tilt (L_{β}') order (Tardieu, Luzzati, & Reman, 1973). As a result, the thickness of a lipid bilayer in the gel state decreases as the amount of water increases.

When the temperature of a bilayer is increased, the degree of *trans-gauche* isomerization in the hydrocarbon chains also increases (see Figure 2.34). This reduces the extended length of the lipid chain and the two-dimensional triangular lattice is completely lost. Since the chains possess more flexible configuration, this phase is known as fluid phase and also as a liquid-disordered (L_{α} or L_d) phase. In this phase, the lipid's lateral diffusion becomes higher than lipids in L_{β} phase: $\sim 10^{-8}\,cm^{-2}s^{-1}$ and the rotational diffusion of lipids are favored in fluid lipid bilayers (Eeman & Deleu, 2010). The specific temperature at which this phase transition occurs is named as thermotropic phase transition (T_m) and this temperature, which depends on the nature of the lipid experimentally, can be determined by using the differential scanning calorimetry technique (Demchenko, 2012).

In some membrane lipids, the lipid disordering occurs in two steps during their phase transition. The first transition is normally observed a few degrees below to the main transition T_m. This pretransition may be due to changes in the vicinity of the polar headgroup such as an increase in the interaction of the lipid headgroups with the solvent (McIntosh, 1980). Heimburg (2000) proposed that both the pretransition and main transition are part of the chain melting transition with the splitting into two transitions being the consequence of simultaneous changes in the lipid order and membrane curvature. Consequently, for the lipids that exhibit a pretransition temperature, an additional lamellar phase exists. This phase, called the ripple phase (P_{β}), is characterized by periodic one-dimensional undulations on the surface of the lipid bilayer (Janiak et al., 1979). Since this phase appears prior to the main chain melting, it must correspond to a partially disordered

lipid phase. For this reason, it has been proposed that the undulations observed on the top of the lipid bilayers arise from periodic arrangements of linear ordered and disordered lipid domains (de Vries, Yefimov, Mark, & Marrink, 2005; Heimburg, 2000).

Presence of other moieties like cholesterol which embed between lipids in membrane, can adopt an extra lamellar phase called the liquid-ordered (L_o) phase, which shares the characteristics of both gel and fluid phases (see 2.34) (Ipsen, Karlström, Mourtisen, Wennerström, & Zuckermann, 1987). This phase, especially, resembles a phase where the chains take less lateral packing order like in gel phase and at the same time resemble the fluid phase with more packing order. This is because the cholesterol into a solid-ordered lamellar phase disturbs the lateral triangular lattice and consequently reduces the ordering of the lipid chains. But in a liquid-disordered lamellar phase, the rigid hydrophobic moiety of cholesterol is intercalated between the lipid chains and favors a trans chain conformation (Demchenko, 2012; Sankaram & Thompson, 1990).

One of the recent concepts which is still debatable is the "raft"– partitioning of membrane lipids into a liquid-disordered or a liquid-ordered phase. This strongly depends on the chemical structure of the lipids involved (London, 2005). Most of the glycerophospholipids found in biological membranes are composed of an unsaturated fatty acid chain in position *sn*-2 of the glycerol backbone. The presence of double bonds in configuration *cis* induces a kink in the hydrocarbon chain and hampers a very compact assembling of the lipids. Consequently, this class of membrane lipids has very little affinity for highly ordered lipid domains. Therefore, sphingolipids have a high tendency to form ordered lipid phases (Wang, Leventis, & Silvius, 2000). Conversely, sphingolipids which display long saturated alkyl chains segregate together via van der Waals and hydrophobic interactions. Moreover, hydrogen bonds between the hydroxyl groups of sphingomyelin polar heads or between the oligosaccharidic headgroups of glycosphingolipids may also accentuate the auto-assembling of these lipids (Eeman & Deleu, 2010).

2.6 State of art - glycolipid bilayer

Traditionally the fields of thermotropic and lyotropic liquid crystal (the former induced by heating and the later induced by a solvent concentration), has always tended to evolve quite separately from each other, although, in fact, they are the two facets of the same underlying state of matter, intermediate in orientational and/or translational order between

the crystalline and the normal liquid states (Seddon, 2002). Thermotropic liquid crystals have been of particular interest to condensed matter physicists and display device scientists, whereas lyotropic liquid crystals have been studied intensively by physical chemists, engineers and biophysical chemists, interested in surfactant and colloid science, and lipid membranes (Imura et al., 2006). Synthetic chemists have played a crucial role in both fields, producing many thousands of pure new liquid-crystalline materials for detailed study (Abeyrathne, Perera, & Karunaratne, 2013; N. J. Brooks et al., 2011; Hato, Minamikawa, Tamada, Baba, & Tanabe, 1999; Seddon et al., 2003). In recent years, we have witnessed a convergence between the two fields, with many systems being found which exhibit both thermotropic and lyotropic properties and phase behavior. In the context of glycolipids which are often found in living cells, the liquid crystalline phase they exhibit give rise to a question on how the liquid crystalline properties affect or influence the living systems (Goodby et al., 2007). There is a growing consciousness that the observed lyotropic, and thermotropic liquid crystallinity of many biological materials possess key biological functionality which may be more than curious coincidence (Goodby, 1998; Goodby, Cowling, Davisa, & Queneaub, 2014). Borshchevskiy et al. (2010)

Though glycolipid materials possibly self-assemble into various aggregate structures like micelles, hexagonal, and cubic, which have curved surfaces (Auvray, Petipas, Lattes, & Rico-Lattes, 1997; Hashim et al., 2006; Hoffmann & Platz, 2001), the lamellar structure has attracted the attention of many due to its resemblance of biological cell membrane structure (Corti et al., 2007). Concerning this, many experimental works like synthesis and physical characterization (using optical polarizing microscopy (OPM), differential scanning calorimetry (DSC), x-ray diffraction (XRD), nuclear magnetic resonance (NMR)) relating to glycolipid materials on lamellar or smectic A phase have been carried out. For instance, early work in the 1980s on *n*-alkyl-1-*O*-β-glucopyranosides, *n*-alkylgluconamides, *N*-substituted aldonamides, 1-*O*-alkyl derivatives of 2,5-anhydrohexitols, a series of acyclic carbohydrates, 1-deoxy-1-(*N*-methylalkanamido)-D-glucitols, and their closely related derivatives, *N*-(2-(alkanamido) ethyl)-D-gluconamides and also on *N*-(2-(*N*-methylalkanamido) ethyl)-D-glucanamides established that these compounds exhibit smectic A or smectic A_d phases (see Figure 2.35) originating from monolayer or bilayer supramolecular structures (Paleos & Tsiourvas, 2001). This structure of bilayer was postulated in which the

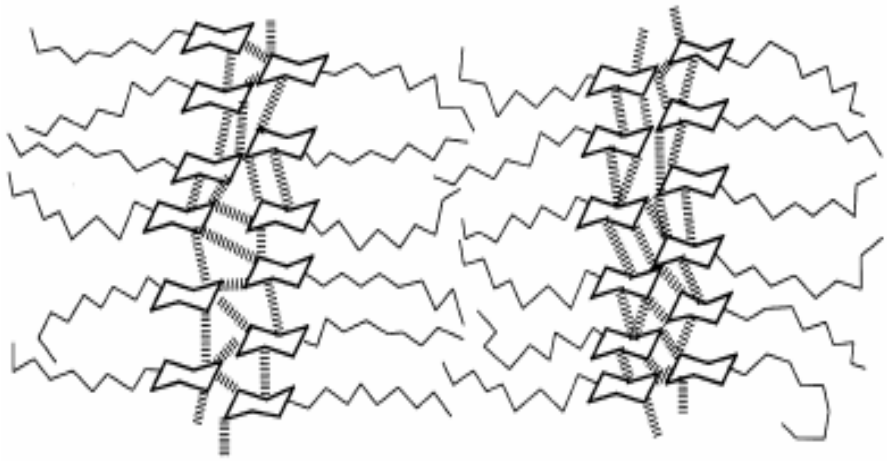

Figure 2.35: Structure of smectic A. Broken lines shows the hydrogen bonding interaction among hydrophilic sugar group. Adopted from Paleos and Tsiourvas (2001)

carbohydrate moieties overlap each other and help together through extensive hydrogen bonding while the alkyl chains are located in the exterior of the supramolecular structure. This structure is consistent with the experimental data that was originally proposed by Jeffrey (1990b). Meanwhile, Marcus and Finn (1985) performed miscibility experiments for identifying the phases of *n*-decyl-β-glucopyranoside and they found that its smectic phase is thermodynamically identical to the lyotropic lamellar phase. Besides, smectic phases were also reported for the amphiphilic derivatives of 1-*O*-alkyl derivatives of 2,5-anhydrohexitols, some of which are liquid crystals even at room temperature. It was concluded that smectic A phases are usually observed for single-tailed amphiphilic carbohydrates as shown in Figure 2.35.

Apart from experimental studies on glycolipid bilayer phase, several theoretical works such as computer simulations have also been reported. A molecular dynamics (MD) work by Kapla et al. (2011) on lipid bilayer composed with using 1,2-di-(9Z,12Z,15Z)-octadecatrienoyl-3-O-β-D-galactosyl-*sn*-glycerol or monogalactosyldiacylglycerol (MGDG) and 1,2-dimyristoyl-*sn*-glycero-3-phosphocholine (DMPC) were studied in three lipid compositions: 0%, 20%, and 45% of MGDG (by mole). They calculated the NMR dipolar interactions from dynamical and orientational distributions which are relevant for the averaging of dipolar interactions. They found only a minor change in DMPC properties upon the increased of MGDG/DMPC ratio and whereas properties related to MGDG undergo a more pronounced change. The area-per lipid of MGDG increases but the DMPC decreases. This difference is related to the large packing parameter and small headgroup of

MGDG to form lamellar phases and rather organized into (reversed) hexagonal structures. This effect was ascribed to the fact that DMPC is a bilayer (L_α) forming lipid, whereas MGDG prefers a reverse hexagonal (H_{II}) arrangement.

Unlike the extensive simulation works published in the literature on the phospholipid systems, the number of reported glycolipid simulations is scarce. Róg et al. (2007) simulated bilayers of glycolipids (glucose and galactose) and compared the results with bilayers of phospholipids (phosphatidylcholine (PC) or phosphatidylethanolamine (PE)) where the phospholipids that contain hydrocarbon chains are identical to the two glycolipids. They observed that the glycolipid systems are characterized by a substantial number of hydrogen bonds in the headgroup region, leading to membrane packing that is stronger than in a PC but less significant than that in a PE bilayer. Also, this simulation has become evident for the electrostatic membrane potential, where the potential is particularly large in the glycolipid membranes and this causes the interfacial forces near glycolipid bilayers to be significantly different from those found in PC and PE bilayers, affecting the ordering of water close to the membrane.

Recently, a full atomistic MD simulation studies of dry bilayers was performed by Ahmadi et al. (2014) using a set of glycosides namely *n*-octyl-β-D-glucopyranoside, *n*-octyl-α-D-glucopyranoside, *n*-octyl-β-D-galactopyranoside, and *n*-octyl-α-D-galactopyranoside to investigate the stereochemical relationship of the epimeric/anomeric quartet linear glycolipids with the same octyl chain group. They observed that the anomeric stereochemistry or the axial/equatorial orientation of C1-O1 (α/β) is an important factor controlling the area and *d*-spacing (bilayer repeat distance) of the glycolipid bilayer systems in the dry phase. Also, the headgroup tilt angle and the chain ordering properties are affected by the anomeric effect. Additionally, the β-galactoside in L_C phase tilt less when compared to those that are in the fluid L_α phase. Nonetheless, the stereochemistry of the C4-epimeric (axial/equatorial) and anomeric (α/β) centers simultaneously influence the intermolecular hydrogen bond. Consequently, β-galactoside has the highest hydrogen bonding strength while α-galactoside has the lowest hydrogen bonding interaction. Meanwhile, both the α/β glucosides have in between. It was apparent that the lateral diffusion of the lipids are in the reverse order of the hydrogen bonding strength which indicates high HB values which slows down the motion of the lipid in bilayer.

Besides the simulations on lamellar phases, a few other studies have been done on non-lamellar phases as well as those involving glycolipids – in both micellar and hexagonal phases. In both these studies, the mono-glucopyranoside is used with single and branched chains respectively. Bogusz, Venable, and Pastor (2000, 2001) explored the effect of aggregate size on the structural properties of octyl glycoside micelles constructed from α and β anomeric glucosides where each micelle structure contains from 1 to 75 surfactants in water. Micelles with small numbers are unstable and more than 10 had remained intact (except for rare single lipid escapes) during the simulations. However, the aggregate shape and internal properties like tail length, dihedral angle distributions, and isomerization rates change very little with size. But surface properties do vary with size due to the decrease of surface area-to-volume ratio in larger aggregates.

Furthermore, the dynamics of octyl glucoside (OG) micelles in term of NMR T1 relaxation times for the hydrophobic chain had a good overall agreement with the experiment especially for the micelles with a higher number of surfactants. These results are consistent with estimates of the micelle size based on translational diffusion. However, T1's for the headgroup carbons are large due to the strong solvent effect on the sugars which concurs to the TIP3P water model. Meanwhile, the shape of micelles change on the time scale of tens to hundreds of picoseconds, while rotation and lipid diffusion within the micelles occurs in nanoseconds range (Bogusz et al., 2001).

H. Nguan, Ahmadi, and Hashim (2014) conducted a study on the behavior of water channels formed in the lyotropic reverse hexagonal phase of H_{II}. The glycolipid Guerbet branched-chain β-D-glucoside is used to build the hexagonal struture. At low water concentration the sugar headgroup extensively overlapped and protruded into the water channel but in high water concentration a water column free from the sugar interdigitation ('free' water) was formed, where in both concentrations the water is diffused along the *xy*-plane (the two-dimensional space confined by the surface of the cylinder) anomalously. But along the *z* direction, the water diffusion obeyed the Einstein relation. It also reported that the *xy*-plane displacement of the 'bound' water is higher than that for the 'free' water.

The study by Róg et al. (2007) shows the glycolipid's behavior is different than the phospholipid in many ways. The different properties and behavior of glycolipids can be used in the application level by designing new materials in a controlled manner. Therefore, to support the designing phase of these materials, a simulation study is highly

recommended. Together with high-end computer hardware and software, simulations on systems bigger in size and timescale can be performed to complement the actual experimental setup. The next chapter is devoted to explain the concepts on simulation methodologies and analysis.

CHAPTER 3

RESEARCH METHODOLOGY

"...everything that is living can be understood in terms of the jiggling and wiggling of atoms."
Richard Feynman (1918-1988)

This chapter presents the basic concept of the molecular dynamics (MD) simulation technique. Since the molecular simulation is a well-established technique and has been extensively explained in many excellent classical references, only a few basic elements of its methodology will be treated here. Following the MD descriptions, a special consideration will be given to the modelling of anhydrous and hydrated glycolipid bilayer systems using atomistic models together with their GLYCAM force field parameters and their energy minimization protocols. Finally, the analysis tools to investigate the bilayer properties, like structure and dynamics, will be presented.

3.1 Brief ideas on molecular simulation methodologies

In general, computer simulations play a vital role in science and technology today. In the early days, the realm of physical sciences was often considered as the interplay between laboratory experiments and theories. In the context of an experiment, a system is subjected to some measurements and the quantitative results are obtained in the numeric form. Nonetheless, in theory, a model is constructed and it is then validated by its ability to describe the system's behavior in selected cases. Mostly, the model is simple enough to allow the solution to be computed. In many cases, under some special 'circumstances', this implies a considerable amount of simplification in order to eliminate all the complexities invariably associated with real world problems, for example the application of the mean field approximation/theory. The mean field theory (also known as self-consistent field theory) studies the behavior of a large and complex stochastic system by reducing it to a simpler model. Such a model with a huge amount of individual particles, interacting with each other, can be approximated to a single particle interacting with an averaged field which are formed from averaging all the neighbors interactions. This reduces a many-body problem to a one-body problem and the use of a single particle pseudo-potential. The

advantage of this theory is that some insights into the behavior of the system can be obtained at a relatively low cost. But, undeniably, many physical problems of interest fall outside the realm of these 'circumstances'. Among them, one could mention the physics and chemistry of defects, surfaces, biological macromolecules etc... which involve a large amount of degrees of freedom and require an accurate treatment of the thermodynamic properties like temperature effects and phase transitions. These complex equations may be solved numerically using computer simulation without applying drastic simplifications and approximations.

In recent times, computer simulation technique has extended its applicability as a principal tool in the theoretical studies of biological molecules and their assembly systems like micelle, lipid bilayer, and hexagonal phases to provide insight into issues in the life sciences. The broadness, diversity, and level of sophistication of this technique enable one to solve or study these unique/challenging scientific problems by numerical experiments (calculations). On the one hand, the primary aim of a computational simulation is to reproduce laboratory experimental results to elucidate the invisible microscopic details and further explain the underlying physiochemical relationships with detail – literally on the length and time scales where motion of individual atoms can be tracked. On the other hand, simulation can also be used as a useful predictive tool. The most widely used simulation methods for molecular systems are Monte-Carlo (MC), Brownian dynamics (BD), and Molecular dynamics (MD).

The Monte Carlo method is stochastic in nature where it relies on repeated random samplings of the configurational space and statistical analysis to compute the relevant averages (Raychaudhuri, 2008). Specifically, this method uses the random sampling technique which generates large numbers of configurations or microstates of an equilibrated system by stepping from one microstate to the next within a particular statistical ensemble. This is very closely related to a random experiment and is useful to study the equilibrium properties of a system which are derived as an average over these configurations (Allen & Tildesley, 1989).

Unlike the MC, the Brownian dynamics deals with a mathematical model for the diffusive motion of microscopic particles of various shapes in gaseous, liquids, or in solid environments (Satoh, 2011). Nevertheless, this simulation approach is efficient for large polymer molecules or colloidal particles in which explicit solvent molecules are replaced

by a stochastic force (Doyle & Underhill, 2005). In this approach, the solvent is treated as a viscous continuum which dissipates energy as macromolecules or particles move through it. The technique takes advantage of the fact that there is a large separation in time scales between the rapid motion of solvent molecules and the most sluggish motion of polymers or colloids. In fact, the ability to coarse-grain out these fast modes of the solvent allows one to simulate a much longer time scale compared with that of a molecular dynamics simulation. At the core of a BD simulation is a stochastic differential equation which is integrated forward in time to create trajectories of molecules. Time enters naturally into the scheme allowing for the study of the temporal evolution and dynamics of complex fluids (e.g. polymers, large proteins, DNA molecules and colloidal solutions) (Lipková, Zygalakis, Chapman, & Erban, 2011).

Between MC and BD, molecular dynamics method is the most applied and detailed method (Allen & Tildesley, 1989; Frenkel & Smit, 2002; Haile, 1992; Leach, 2001). This method computes the motions of individual molecules using the Newton's equations of motion, which generate trajectories of the evolution of particles containing information such as position and velocity for a large number of interacting particles in an isolated cluster (the central box) or in the bulk using periodic boundary conditions. With these trajectories, one can calculate physical properties as time averages, which are equivalent to ensemble averages according to the ergodic hypothesis in statistical mechanics. The equations of motion for these particles can be solved accurately using various numerical integration methods such as the common predictor-corrector or Verlet methods. The prominent advantage of MD method is its efficiency in evaluating different configurational properties and dynamic quantities which cannot generally be obtained by Monte Carlo (Haile, 1992).

Although both the MD and MC methods are suitable for simulation of amphiphiles (the subject of this thesis) each of them has different strengths and weaknesses. The MD method gives the time evolution of the simulated system and therefore, the time-dependent properties are calculated easily. On the other hand, the advantage of the Monte Carlo simulation method is the possibility of implementing the "non-physical" biased moves and sample system states that are important but have a very small probability of occurrence (Allen & Tildesley, 1989).

Besides above mentioned methods, the detailed quantum mechanical approach for calculating the energetics of a chemical system is considered as the most exact description of a molecule (Leach, 2001). This method explicitly considers the electronic configurations in the calculation and enables one to investigate chemical reactions involving bonds breaking and forming which are the properties that depend on the electronic distribution in a molecule. However, one major problem of implementing this method is the CPU time it consumes since it has to consider all the electrons present in the system. Thus, it takes a longer time to do calculation and limits the size of the system of interest. On the other hand, empirical force field methods (also known as molecular mechanics) ignore the electronic motions and calculate the energy of a system as a function of the nuclear positions only. Hence, molecular mechanics, which underlies the MD method, is capable of performing calculations on a very large system containing thousands of atoms. In some cases, molecular mechanics is able to provide accuracy as good as quantum mechanics but, of course, cannot provide properties that depend upon the electronic distribution in a molecule (Leach, 2001).

In addition to the application of empirical force field mentioned above, there are also hybrid force fields like the quantum mechanical/molecular mechanical (QM/MM) used in molecular dynamics (MD) methods. For instance, the QM/MM investigation on the acid hydrolysis of cellulose in water using two different models, cellobiose and a 40-unit cellulose chain, showed that the explicitly treated solvent molecules strongly influence the conformations, intra-molecular hydrogen bonds, and exo-anomeric effects in these models (Loerbroks, Heimermann, & Thiel, 2015). Also the conformation of model disaccharide (4-O-α-D-xylopyranosyl-α-D-xylopyranose,) in aqueous solution was investigated using a combined quantum mechanical (QM)/molecular mechanical (MM) potential (Muslim & Bryce, 2004) and many more QM/MM studies have been reported elsewhere.

3.1.1 Application of MD in lipid bilayer and biomolecular systems

The molecular dynamics simulation of lipid bilayer has been widely used to study the behavior and properties which correspond to the understanding of biological cell membrane (Berger, Edholm, & Jähnig, 1997; Feller, 2000; Hofsäß, Lindahl, & Edholm, 2003; Martinez-Seara & Rog, 2013; Merz, 1997). In reality, a cell membrane exhibits a much more complex behavior with the presence of various types of biomolecules like

phospholipids (PC, PE), proteins (peripheral and trans-membrane), and cholesterol. The single lipid model bilayer structure gives a good approximation for the many interesting properties of cell membrane (Srivastava, 2005). Since the phospholipids are the main constituents of the membrane, which give the basic structural matrix, an extensive set of experimental and theoretical studies are focused on pure lipid bilayers to reveal their intrinsic properties (Martinez-Seara & Rog, 2013). Eventually, these studies help to enhance the understanding of the interplay between the constituent lipids and intriguing physicochemical properties of self-assembly. For instance, a large membrane of hydrated dipalmitoylphosphatidylcholine (DPPC) bilayers containing different levels of cholesterol content had been simulated by Hofsäß et al. (2003) for about 10 ns to investigate the microscopic interactions between cholesterol and lipids in biological membranes. Their study showed some interesting results like a significant bond ordering of the DPPC chains which can be confirmed experimentally by using nuclear magnetic resonance (NMR), a reduced fraction of *gauche* bonds and a reduced surface area per lipid to name a few.

Furthermore, recent MD simulations of membrane proteins enable their structural analysis to the accuracy of atomic-detail (Gumbart, Wang, Aksimentiev, Tajkhorshid, & Schulten, 2005). For example, the x-ray crystallography study of mechanosensitive channel MscS, in the membrane protein, showed the channel is open. But the MD simulation of the same protein revealed that the protein channel closes spontaneously when lifted from the crystal environment to a lipid bilayer environment (Anishkin & Sukharev, 2004; Sotomayor & Schulten, 2004). In that study, the MD simulations become increasingly valuable for the understanding of membrane protein function, as they can unleash the complex dynamic behavior concealed in the static structures.

Although phospholipids and proteins were routinely studied using MD and other simulation methods, glycolipids have scarcely been investigated via computational approach. This may be due to the difficulty in developing accurate and appropriate force fields especially for carbohydrate moieties which usually assumed to be a complex hydrogen bonded system, where intricate stereochemistry play an important role. However, several fascinating works have been reported in literature like, interaction of glycolipids on the surface of phospholipid bilayers (Kapla et al., 2011; Ram, Kim, Thomson, Howard, & Prestegard, 1992), structure and dynamical properties of single-component glycolipid bilayer (Ahmadi et al., 2014; Róg et al., 2007) and two-component (phospholipid and

glycolipid) bilayer. Besides lipid bilayer structures, several other assembly systems have also been simulated like micelles (Bogusz et al., 2000, 2001), and hexagonal (H. Nguan et al., 2014) phases to study their bulk properties. Therefore, in this thesis we have undertaken the method of MD simulation to study glycolipid bilayers in anhydrous and hydrated conditions to evaluate their structural and dynamical behavior.

3.2 Molecular dynamics simulation

3.2.1 A brief history

The technique of molecular dynamics was originally developed by Alder & Wainwright in the late 1950's (Alder & Wainwright, 1957, 1959) to simulate a system of colliding hard spherical particles to study the interactions between them. Intriguingly, many important insights concerning the behavior of simple liquids emerged from their studies such as the revelation that the velocity autocorrelation function does not decay exponentially at long times but instead exhibits the much slower dependence to the spacial dimensionality of the system. The next major advancement was made in 1964 when Rahman carried out the first simulation using a more realistic potential (the Lennard-Jones potential) for liquid argon (Rahman, 1964). The first molecular dynamics simulation of a realistic liquid water system was done by Rahman and Stillinger (1971). Later in 1974, they improved the interaction potential of the simulated system and calculated some thermodynamic properties at room temperature where the results were better in agreement with x-ray scattering experiments (Stillinger & Rahman, 1974). Meanwhile, in the late 1970's, McCammon, Gelin, and Karplus (1977) simulated the first folding protein of the bovine pancreatic trypsin inhibitor (BPTI) system and in the following year they published the dynamical behavior of the activated rotations of a tyrosine ring inside the BPTI (McCammon & Karplus, 1980) which exhibited a great variety of internal motions.

Today in the literature, one routinely finds molecular dynamics simulations of solvated proteins, protein-DNA complexes as well as lipid systems addressing a variety of issues including the thermodynamics of ligand binding and the folding of small proteins (Abriata & Dal Peraro, 2015). The number of simulation techniques has greatly expanded; there exists now many specialized techniques for particular problems, including mixed quantum mechanical - classical simulations, that are being employed to study enzymatic reactions in the context of the full protein (Leach, 2001). Also, molecular dynamics simulation

techniques are widely used in experimental procedures such as x-ray crystallography and NMR structure determination.

3.2.2 The method of molecular dynamics

Basic concept

In practice, a simulation system contains many particles (atoms or molecules) from a few hundred to millions. Each atom in the system will be interacting with its surrounding atoms or molecules via interaction potential and this allows the constituent atoms to be in a state of motion. Classically, the motion of the atoms could be described by Newton's equation of motion where the positions and velocities of the atoms are calculated as a function of a time step. If a system contains a group of N atoms and the instantaneous force acting on each atom can be obtained by solving the equation of motion,

$$F_i = m_i \frac{d^2\mathbf{r}_i}{dt^2}, \qquad i = 1, \ldots, N \tag{3.1}$$

where m_i and $\mathbf{r}_i$ are the mass and position of atom i, t is the time, and F_i is the momentary force on the atom. This force is easily obtainable from the negative gradient of the potential energy, $U_{pot}(\mathbf{r}_1, \mathbf{r}_2, \ldots, \mathbf{r}_N)$ of the interactions occurring between the atoms in the system depend on the distance $\mathbf{r}_i$ defined for a given atom from a reference coordinate:

$$-\nabla_i U_{pot}(\mathbf{r}_1, \mathbf{r}_2, \ldots, \mathbf{r}_N) = F_i, \qquad i = 1, \ldots, N \tag{3.2}$$

The calculation of this potential function is a central part of the simulation because it defines the model of the system. In most cases, this potential function is approximated to the pairwise interaction between two particles. Subsequently, the differential equations of motion are integrated using some MD algorithms (for examples Verlet and leap-frog) during which both positions and velocities of the particles are updated. (The integration algorithm will be discussed in the subsequent sections.)

Force fields

Normally an atomistic simulation system is described by a pairwise interaction potential energy function $U_{pot}(r_{ij})$ involving all the atoms present in the system. Technically this function is defined as the physical model of the molecular system in consideration. At any

instance, two or more atoms may be involved in various types of motions like vibration including stretching, bond angle bending, and torsion of dihedral angle. These interactions are modeled using molecular mechanics methods (also known as force field) which consider only the motion of the nucleus of an atom and ignore the electronic motion. The separation of nuclear and electronic motions become the basis for the Born–Oppenheimer approximation, which simplify the construction of empirical force field (Ercolessi, 1997; Monticelli & Tieleman, 2013) and therefore enables one to write the energy of a system as a function of nuclear coordinates only (Leach, 2001). Additionally, two assumptions were considered in all common force fields, namely, additivity and transferability (Monticelli & Tieleman, 2013). The additivity designates that the (potential) energy of any system can be written as a sum of different potentials with a simple physical representatives like bond deformations, electrostatics, dispersion forces etc... And the transferability brings the meaning that the potential energy functions developed for a small set of molecules can be used to a much wider range of molecules with similar chemical groups.

In the bio-molecular environment the potential energy function can be grouped into two main parts: *bonded* and *non-bonded* potentials as shown in Equation (3.3a).

$$U_{pot}(\mathbf{r}^N) = V_{bonded} + V_{non-bonded} \tag{3.3a}$$

$$V_{bonded} = E_{bond} + E_{angle} + E_{tors} \tag{3.3b}$$

$$V_{non-bonded} = E_{LJ} + E_{elec} \tag{3.3c}$$

The $U_{pot}(\mathbf{r}^N)$ denotes the total potential energy which is a function of the positions ($\mathbf{r}$) of N particles (usually atoms). The *bonded* potential (V_{bonded}) consists energy terms for bond stretching (E_{bond}), bond bending (E_{angle}), and bond dihedral angle (E_{tors}) as shown in Equation (3.3b). Meanwhile, the *non-bonded* potential energy term ($V_{non-bonded}$) comprises Lennard-Jones potential function to describe the van der Waals interaction potential energy (E_{LJ}) and finally, the Coulombic term (E_{elec}) describes the electrostatic interactions between atoms, shown in Equation (3.3c).

The bond stretching and bond bending angles are principally described as harmonic oscillators (Leach, 2001; Lindahl, 2001) and their energy terms are given as:

$$E_{bond} = \sum \frac{1}{2} k_b (r_{ij} - r_{ij}^0)^2, \tag{3.4}$$

and

$$E_{bend} = \sum \frac{1}{2} k_\theta (\theta_{ijk} - \theta^0_{ijk})^2, \tag{3.5}$$

where r_{ij} is the distance between atoms i and j, θ_{ijk} is the angle between atoms i, j, and k, r^0_{ij} and θ^0_{ijk} are the equilibrium values; and k_b and k_θ are the force constants for bonds and angles, respectively. Meanwhile, the dihedral angle energy is represented as a cosine expansion (Leach, 2001)

$$E_{tors} = \sum k_\phi (1 + cos(n((\phi - \phi^0))), \tag{3.6}$$

where ϕ is the value of the dihderal angle, ϕ^0 is the equilibrium value and k_ϕ is the force constant affecting the barrier height and n is the multiplicity giving the number of minimum points in the function as the bond is rotated through 360°. The electrostatic interaction is described by the Coulombic term

$$E_{elec} = \sum \frac{q_i q_j}{4\pi\varepsilon_0 \varepsilon_r r_{ij}}, \tag{3.7}$$

where q_i and q_j are the partial charges of the atoms i and j, ε_0 is the vacuum permittivity between the atoms and ε_r is relative permittivity. The Lennard-Jones potential formula often given as

$$E_{LJ} = \sum \left(\frac{A_{ij}}{r^{12}_{rj}} - \frac{B_{ij}}{r^6_{ij}} \right), \tag{3.8}$$

where A_{ij} and B_{ij} are the strength parameters for repulsion and dispersion, respectively. The graphical representation of the potential energy landscape of molecular mechanics for the respective force fields are shown in Figure 3.1.

In many simulations, the general form of the total potential energy function contains the main five terms (Petrenko & Meller, 2010) as shown in the Equation (3.9) below:

$$U_{pot}(\mathbf{r}^N) = E_{bond} + E_{angle} + E_{tors} + E_{LJ} + E_{elec} \tag{3.9}$$

However, depending on the molecular system under study, the precise form of the potential function has numerous options, as the forms or the parameters of the energy terms may be varied (Monticelli & Tieleman, 2013; Petrenko & Meller, 2010).

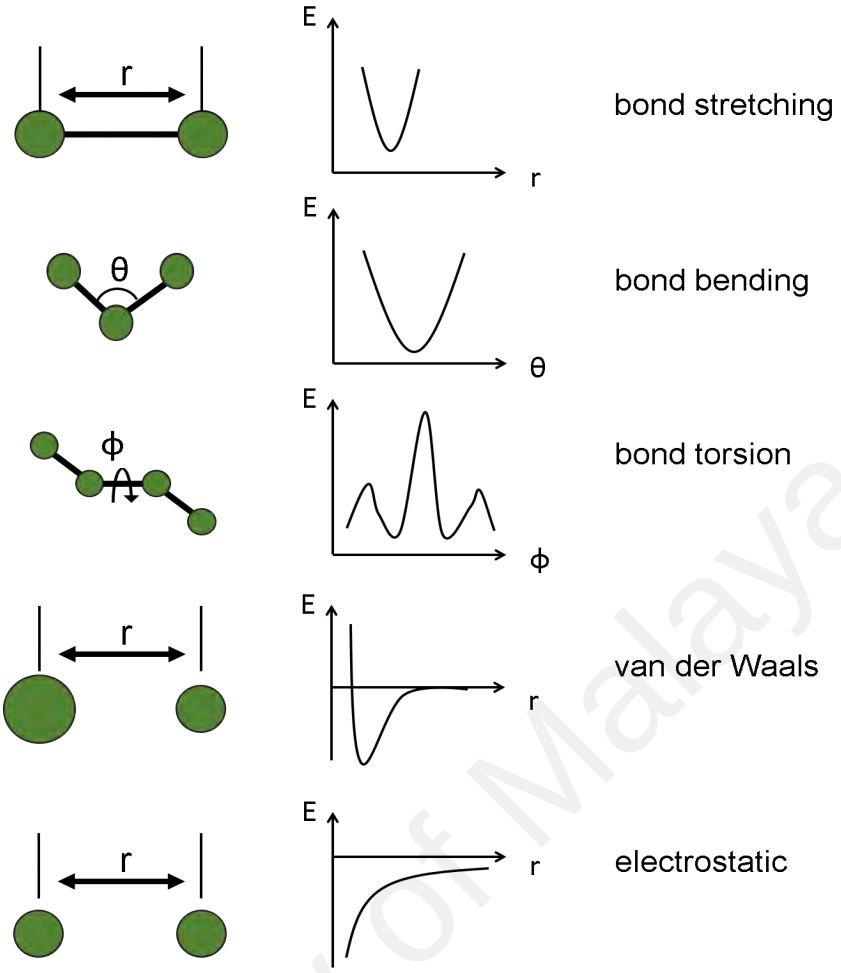

Figure 3.1: Inter- and intramolecular interactions described by molecular dynamics force fields. Redrawn from (McMullen Jr, 2005)

Usually, the potential energy function developed by considering bonded and non-bonded interactions, as in Equation (3.9) between the atoms, is differentiable with respect to the atomic co-ordinates. This gives the value and the direction of the force acting on an atom including the calculation of the acceleration which tells us how the velocity is changing. From the velocity variation, it is possible to determine approximate positions of the atoms at a very short time later. This process is called *integrating the equations of motion*, and repeating the calculation for a large number of small time-steps produces a time-evolving trajectory which contains the information of positions, velocities and forces of all atoms during the simulation. A good approximation of the potential function would provide an extremely detailed description of both dynamics and equilibrium properties of the system under study.

However, all the bonded interactions concern atoms which are closely bound to each other. This makes them very local in space, and mostly the number of interactions will

only increase linearly with the system size, meaning these are not very costly to calculate. In contrast, the non-bonded interactions between the atoms located in different molecules make the force calculation to account for roughly 90% of the total CPU processor usage, even if we assume all forces to be between pairs of particles and neglect contributions beyond some cut-off distance (Lindahl, 2001).

Integration algorithm

The time integration algorithms are based on finite difference methods, where the time is discretized on a finite grid, in which the time step Δt being the distance between two consecutive points on the grid. From the potential energy function of a system (like in Equation (3.9)), the forces acting on atoms can be determined for the configuration of atoms at the time t and the next new configuration of the atoms at time $(t + \Delta t)$ (Lindahl, 2001). By iterating the procedure, the time evolution of the system can be followed for a long times. Since these schemes are approximate, there are errors associated with them. Two, in particular, are:-

- *Truncation errors*, which are related to the accuracy of the finite difference method with respect to the true solution obtained. Principally, the finite difference methods are based on a Taylor expansion truncated at some term. These errors do not depend on the implementation, but they are intrinsic to the algorithm.

- *Round-off errors*, which are related to errors associated to a particular implementation of the algorithm. For instance, to the finite number of digits used in computer arithmetics. For instance, implementation of 64-bit precision (corresponding to "double precision") helps to keep round-off errors to a minimum.

Both types of errors can be reduced by decreasing the Δt (Frenkel & Smit, 2002). For large Δt, the truncation errors dominate, but they decrease quickly as Δt is decreased. Among various integration schemes, two popular integration methods for MD calculations are the "Verlet" and "Leap-Frog" algorithms.

The Verlet algorithm is one of the simplest of all integration algorithms where its simplicity and robustness made it the most popular algorithm for many years though it is now superseded by its derivatives. This algorithm was developed by Verlet (1967) and has since turned into an entire class of integrators. It is based on the idea of writing two

third-order Taylor expansions for the time dependence of the co-ordinates r_i at times $(t+\Delta t)$ (one forward in time) and $(t-\Delta t)$ (one backward in time),

$$r_i(t+\Delta t) = r_i(t) + \frac{dr_i(t)}{dt}\Delta t + \frac{d^2r_i(t)}{dt^2}\frac{(\Delta t)^2}{2} + \frac{d^3r_i(t)}{dt^3}\frac{(\Delta t)^3}{6} + O(\Delta t^4) \tag{3.10a}$$

$$r_i(t-\Delta t) = r_i(t) - \frac{dr_i(t)}{dt}\Delta t + \frac{d^2r_i(t)}{dt^2}\frac{(\Delta t)^2}{2} - \frac{d^3r_i(t)}{dt^3}\frac{(\Delta t)^3}{6} + O(\Delta t^4) \tag{3.10b}$$

Adding the two expressions (eq. (3.10a) and eq. (3.10b)) leads us to

$$r_i(t-\Delta t) = 2r_i(t) - r_i(t-\Delta t) + \frac{(\Delta t)^2}{m_i}F_i + O(\Delta t^4) \tag{3.11}$$

As one can see, the truncation error of the algorithm when evolving the system by t is of the order $(\Delta t)^4$, even if the third derivative does not appear explicitly (see Equation (3.11)). This algorithm is simple to implement, accurate and stable. However, a more practical problem with this approach is the velocity cannot be directly generated but requires the difference of two terms of the same magnitude, making this approach very sensitive to numerical precision and round-off errors. Nevertheless, one could compute velocities from the positions by using

$$v(t) = \frac{r_i(t+\Delta t) - r_i(t-\Delta t)}{2\Delta t} \tag{3.12}$$

A slightly modified, but theoretically equivalent, algorithm is the Leap-Frog algorithm see Hockney and Eastwood (1988), which handles velocities somewhat better.

$$r_i(t+\Delta t) \approx r_i(t) + \Delta t v_i(t+\frac{1}{2}\Delta t) \tag{3.13a}$$

$$v_i(t+\frac{1}{2}\Delta t) \approx v_i(t-\frac{1}{2}\Delta t) + \frac{\Delta t}{m_i}F_i \tag{3.13b}$$

This is a second order approximation of the equations of motion, but it avoids the difference between large terms when calculating the velocities. The only drawback is that the velocities are offset from the positions by half a step, but in the molecular dynamic software this drawback is circumvented by averaging the velocities at plus and minus

half a step to obtain the same value as the original Verlet algorithm would have produced without round-off errors (Lindahl, 2001).

Another algorithm is the velocity Verlet Algorithm. This uses a similar approach but explicitly incorporates velocity, solving the first-time step problem in the Basic Verlet algorithm:

$$r(t+\Delta t) \approx r(t) + v(t)\Delta t + \frac{1}{2}a(t)(\Delta t)^2 \tag{3.14a}$$

$$v(t+\Delta t) \approx v(t) + \frac{1}{2}[a(t) + a(t+\Delta t)]\Delta t \tag{3.14b}$$

The advantage of velocity algorithm is that it consumes less memory compared to Verlet algorithm.

Finally, the Beeman's Algorithm is closely related to Verlet Algorithm. It produces identical positions to Verlet, but is more accurate in velocities and gives better energy conservation.

$$r(t+\Delta t) \approx r(t) + v(t)\Delta t + \frac{2}{3}a(t)(\Delta t)^2 - \frac{1}{6}a(t-\Delta t)(\Delta t)^2 \tag{3.15a}$$

$$v(t+\Delta t) \approx v(t) + v(t)\Delta t + \frac{1}{3}a(t)\Delta t + \frac{5}{6}a(t)\Delta t - \frac{1}{6}a(t-\Delta t)(\Delta t) \tag{3.15b}$$

The disadvantage is that the more complex expressions make the calculation more expensive.

Constraint algorithms

Constraint algorithms are often applied to MD simulations where the simulations are carried out using internal coordinates that automatically satisfy the bond-length and bond-angle constraints. Extended simulations sometimes use a longer time step which upon successive application produce larger errors in the motions, and after a few steps the fluctuations will diverge, causing the whole simulation to crash. This problem is often overcome by employing the 'Constraint Dynamics' (Pinisetty, 2005). The applied constraint completely removes the bond and/or angle degrees of freedom from the system. Explicit constraint forces typically shorten the time-step significantly, making the

simulation less efficient computationally; that is, more computing power is required to compute a trajectory of a given length. In the simulation, most commonly used constraint algorithms are SHAKE and LINCS algorithm.

SHAKE *Algorithm*: The SHAKE algorithm was the first and most widespread algorithm developed to satisfy bond geometry constraint during molecular dynamics simulations (Ryckaert, Ciccotti, & Berendsen, 1977). It solves the system of non-linear constrained equations using the Gauss-Seidel method to approximate the solution to the system of linear equations. In this algorithm, the force necessary to restore each pair of atoms involved in a bond (or triplet in an angle) is calculated at the equilibrium value. Since a lot of bonds are connected in a macromolecular system, the algorithm has to be iterated continuously until convergence is achieved. This limits the applicability somewhat; for time steps greater than 2-3 fs it does not always converge, and the iteration makes it unsuitable for parallel computers since it incurs a lot of extra communication between processors.

LINCS *Algorithm*: This is an alternative constraint method, where the acronym LINCS stand for Linear Constraint Solver, which was developed in 1997 and based on EEM method (Edberg, Evans, & Morriss, 1986), and a modification thereof (Baranyai & Evans, 1990). This algorithm resets bonds to their correct lengths after an unconstrained update. Additionally, the non-iterative approach and its use of two steps, make it possible to extend the time steps at least to 3-4 fs and faster than SHAKE (Hess, Bekker, Berendsen, Fraaije, et al., 1997), but it can only be used with bond constraints and isolated angle constraints.

Besides the variation in the potential function, and the integration algorithm, there are other technical issues concerning the application of the MD simulation, some of which are briefly reviewed in the following sections.

3.2.3 Periodic boundary conditions

Periodic boundary conditions (PBC) enable a simulation to be performed using a relatively small number of atoms, in a such a way that the atoms experience forces as if they were in bulk fluid (Leach, 2001). If we try to simulate an isolated system, many of the atoms will experience a large and unnatural boundary surface as if they are in a vacuum environment and this may affect the calculation of the properties of the system. For instance, consider 1000 atoms arranged in a $10 \times 10 \times 10$ cube. Nearly half the atoms are on the outer faces, and these will have a large surface effect on the measured properties. Even for 10^6 atoms,

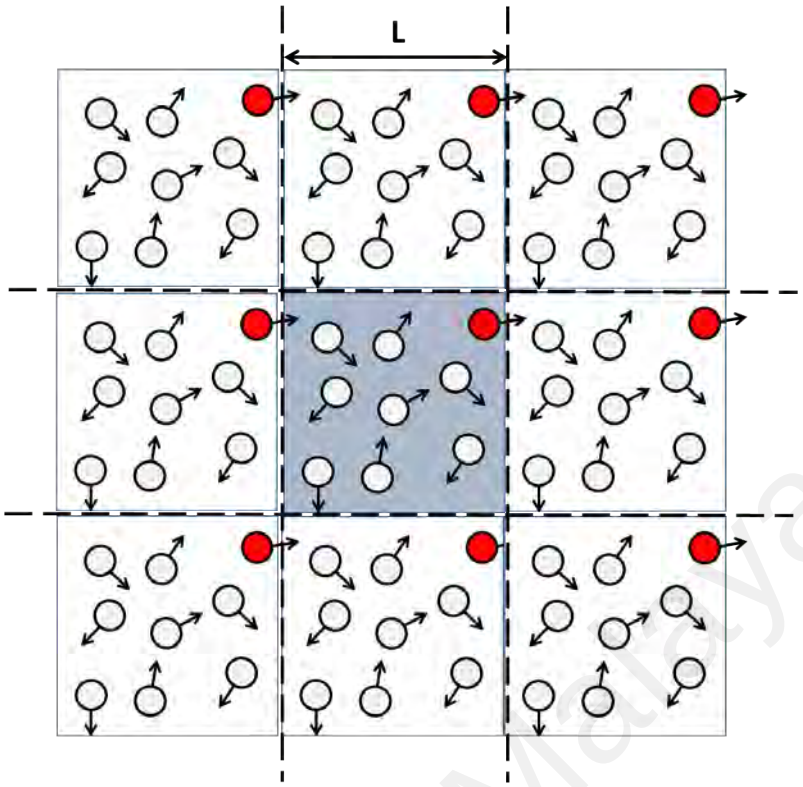

Figure 3.2: Periodic boundary conditions in two dimensions with the box dimension L. Redrawn from Leach (2001).

the surface atoms amount to 6% of the total, which is still nontrivial. This problem can be overcome by allowing a central 'box' (normally a cube) surrounded by its replicas in all directions (Allen, 2004), that is, the mirror images of the primary rectangular simulation cell are replicated at each side of the primary box – ending in an infinite system like a periodic crystal. In the course of the simulation, when an atom or molecule moves in the primary cell, its periodic image in every one of the other cells moves with exactly the same orientation in a similar fashion as shown in Figure 3.2. Provided the potential range is not too long, we can adopt the minimum image convention that each atom interacts with the nearest atom or image in the periodic array. Normally, calculations are performed only for the interactions within a spherical cut-off, where the atoms within this cut-off are kept in a so-called neighbor list, which is updated only every n time steps.

3.2.4 Spherical cut-offs

The non-bonded van der Waal's forces are fairly short-ranged due to the functional form of $\sim r^{-6}$, and, for this reason, the long-range forces are considered the least important. This motivates the use of cut-offs for Lennard-Jones interactions, which means that only

interactions between particles that lie within a certain cut-off distance, r, are included in the force calculations as shown in Figure 3.3. For electrostatic interactions, on the other hand, where the force scales as r^{-2}, cut-offs might seem a little abrupt (Wohlert, 2006). They may, however, be justified by the fact that for electrically neutral molecules the interactions will effectively be dipole-dipole interactions. Generally, the typical values for the cut-off distance are 10 to 20 Å, or at most half the distance to the nearest periodical image, i.e., half the simulation box side length, L, when using periodic boundary conditions.

The errors introduced by the truncation of the interactions may give unphysical correlations at the cut-off distance and this is treated by implementing Ewald summation method which is exact for the periodic systems or applying the computationally more effective Particle Mesh Ewald (PME) (Wohlert, 2006). With these methods, all electrostatic interactions in a periodic system can be included, out to the infinite range.

3.2.5 Time averages

Most of the features observed in experiments are attributed to the collective properties of a very large number of atoms under certain conditions, such as temperature, (T) and pressure (P). It is important to be able to control these conditions in MD simulations in order to reproduce the properties comparable to the experimental results. For this purpose, the MD simulations are usually carried out under certain ensembles, keeping constant values for some of the thermodynamic variables describing a system, such as the number

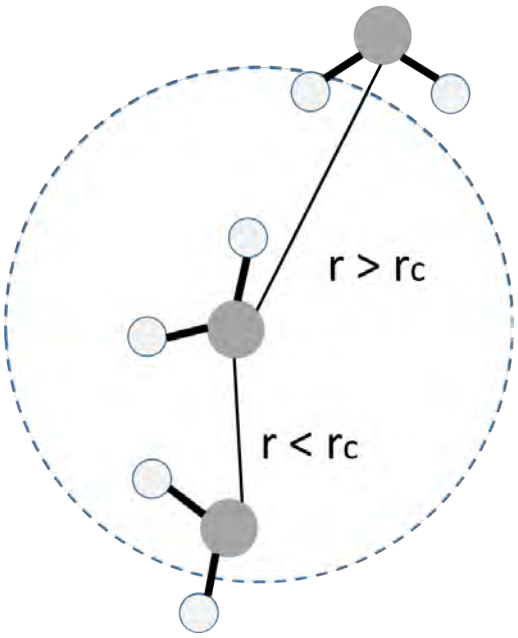

Figure 3.3: Cut-off. Redrawn from Wohlert (2006).

Table 3.1: Types of ensemble and constant parameters.

Ensemble type	Constant parameters
Microcanonical (NVE)	Fixed number of atoms, volume and energy
Canonical (NVT)	Fixed number of atoms, volume and temperature
Isobaric-Isothermal (NPT)	Fixed number of atoms, pressure and temperature
Grand canonical (μVT)	Fixed chemical potential, volume and temperature

of particles (N), the volume (V), the total energy (E), the temperature (T), the pressure (P) the chemical potential (μ) and heat capacity (C_V) (Allen & Tildesley, 1989).

In practice, the macroscopic thermodynamic state of a system is defined by a small set of these state variables, usually a combination of three variables as listed in table 3.1. Some of the most frequently used ensembles are: (a) Microcanonical ensemble, where the number of particles (N), the volume (V) and the total energy (E) are fixed, (b) Canonical ensemble, where the N, V and the temperature T are fixed, and (c) Isobaric-Isothermal ensemble, where the N, pressure P and temperature T are fixed. When the MD simulation is performed in the canonical (NVT) or in the isothermal-isobaric (NPT) ensemble, the system may be coupled to a thermostat, which ensures that the average temperature is maintained close to a certain value, or to a barostat, which adjusts the size and shape of the simulation cell in order to maintain the desired average pressure (Andersen, 1980; Hoover, 1985).

Besides this, the microscopic state of the system is defined by the atomic positions, r, and momenta, p. These are considered as coordinates in the multidimensional space called phase space. So for a system of N atoms this space has $6N$ dimensions (Haile, 1992). The single point in the phase space defines the microscopic state of the system and a collection of points is termed the ensemble averages of this particular macroscopic state. An MD simulation generates a sequence of points in the phase space as a function of time and despite these points belonging to the same ensemble, they correspond to the different conformations of the system and their respective momenta. Subsequently, the points obtained with respect to a particular thermodynamic ensemble is then used to get the time-averaged properties from the equation below:

$$\langle A \rangle_{MD} = \lim_{\tau \to \infty} \frac{1}{\tau} \int_{\tau=0}^{\tau} A(p^N(t), r^N(t)) dt \quad \approx \quad \frac{1}{M} \sum_{t=1}^{M} A(p^N, r^N), \tag{3.16}$$

where τ is the simulation time, M is the number of time steps in the simulation and $A(p^N, r^N)$ is the instantaneous value of the property of interest. The calculated time average is then considered to be equal to the experimental ensemble average by the most fundamental assumption, the *ergodic hypothesis*. This hypothesis states that the time averages calculated from the instantaneous time intervals in MD simulation eq. (3.16) is equal to the macroscopic ensemble average of a large number of conformations (Haile, 1992).

3.2.6 Limitations of MD Simulations

Although MD simulation is a powerful technique, it has several limitations. For example, it is well known that systems at atomistic levels obey quantum laws. But with reasonable approximations (like *Born-Oppenheimer* approximation) the law of Newton's equation of motion is applied to the particles to predict the system's behavior. Nonetheless, the use of classical mechanics is unable to describe chemical reactions such as bond formation and breaking between the particles in the system (Leach, 2001).

Another major criticism faced by a numerical simulation is the limited number of particles that make up the simulation system (N) – usually limited by the capacity of the computer (CPU power and memory storage). Even though the effect of small number of particles is taken care of by implementing PBC (as explained in section 3.2.3), it is well-known that the application of PBC also results in an unwanted periodical correlation for some measured properties, especially those which are dependent on the length scale. This correlation is minimized if a free surface is used. The periodic and free boundary conditions define the upper and lower limits of those affected properties and the difference between these two limits can be decreased as the number of particles increases.

The accuracy of the simulation is entirely dependent on the accuracy of the underlying force field which is regarded as the heart of almost every simulation technique. The force fields mainly contain several approximations and various fitted parameters for some selected residues which can usually be considered as a building block. For example, the building block of a protein is amino acids while for a membrane it is lipids. The realism of the simulation is entirely dependent on the ability of the chosen potential functions to reproduce the behavior of the system under the conditions in which the simulation is run.

Besides this, the truncation of non-bonded interactions also sets the limitation of a simulation. It is a common practice to truncate the non-bonded interactions to speed up the calculation of forces which is expensive in terms of computational time. For a Lennard-Jones interaction, it is reasonable to approximate the truncation distance to be 10-20 Å, but this might not always be applicable for electrostatic interactions if there are free charges in the system present.

One of the limitations is choosing the maximum time step for which the integration of the equations of motion is still stable. A typical value in practice is 2 fs ($10^{-15}s$). This means that 500,000 computationally expensive integration steps are necessary to calculate the dynamics of a system over 1 ns time period. If the simulation system is composed of a large number of atoms say a few tens of thousand atoms, this can take one to two weeks when run on, for example, in a single processor computer. This limits the length of the current simulation to nanoseconds time scale.

Despite all the limitations, if the approximations are kept in mind and the results are carefully checked, molecular dynamics simulation coupled with experiment can track the system's behavior across a vast spatiotemporal domains, especially for the motions present in biological macromolecules – length scales up to thousands of angstroms, with atomic precision, and timescales up to milliseconds, at femtosecond resolution.

3.2.7 Software packages for MD

In the beginning times of MD applications, various groups developed codes in FORTRAN and C languages and shared them among their members (Field, 1999). In some cases, the code used in one particular machine could not be used in another machine because of the machine dependent nature of the code. In later days, the MD codes were available in packages. The emergence of MD software packages has then widened the use of MD simulation method among computational scientists. Further, various kinds of support offered by the software developers, like tutorials and mailing lists, enable one to learn and understand quickly the usability of a particular software with excellence. Below, we give a brief account of several MD software packages which are being used reasonably among molecular dynamics simulators.

AMBER (Assisted Model Building using Energy Refinement): A suite of programs for molecular mechanics that allows users to carry out and analyze molecular dynamics

simulations, particularly for biomolecules like proteins, nucleic acids, and carbohydrates. The Amber software suite mainly contains three kinds of programs:

1. Preparation programs:

    - The main preparation programs are *Antechamber* and LEaP. The *Antechamber* is designed to be used with the GAFF force field (General Amber Force Field) and will automatically assign atom types and attempt to generate missing parameters for most organic molecules like proteins and nucleic acids. A range of input file formats are also supported – usually in PDB format and the output files are designed to be read into LEaP as part of the build procedure for proteins containing organic ligands. LEaP (xLEaP) is an X-windows-based program that provides for basic model building and Amber coordinate and parameter/topology input file generator. Also, it includes a molecular editor which allows for building residues and manipulating molecules.

2. Simulation programs:

    - The main simulation engine is the *sander*. This program simulates annealing with NMR-derived energy restraints and also allows for NMR refinement based on NOE-derived distance restraints, torsion angle restraints, and penalty functions based on chemical shifts and NOESY volumes. Besides, it is also used for replica-exchange, thermodynamic integration, and potential of mean force (PMF) calculations and the *sander* also includes QM/MM capability. The updated version of *sander* is known as *pmemd*. This code focuses on high and improved parallel scalability and supports the basic MD functions from *sander* to run them as efficiently as possible while still producing output statistically equivalent to that of *sander* (Salomon-Ferrer, Case, & Walker, 2013).

3. Analysis programs:

    - The *ptraj* & *cpptraj* programs are used to analyze MD trajectories (Roe & Cheatham III, 2013). They could compute a variety of properties, like RMS deviation from a reference structure, hydrogen bonding analysis, time-correlation functions, diffusional behavior, and etc... An overall view of

Amber's strength and weaknesses is highlighted by D. A. Case et al. (2005); Salomon-Ferrer, Case, and Walker (2013).

CHARMM (Chemistry at HARvard, Macromolecular Mechanics): This is a highly regarded and widely used simulation package. It has been developed over the last three decades with a primary focus on molecules of biological interest, including proteins, peptides, lipids, nucleic acids, carbohydrates, and small molecule ligands, as they occur in solution, crystals, and membrane environments (B. R. Brooks et al., 2009). CHARMM combines standard minimization and dynamics capabilities with expert features including free energy perturbation (FEP), correlation analysis and combined quantum, and molecular mechanics (QM/MM) methods. Simulations provide insight into molecular-level structure, interactions, and energetics. For the study of such systems, the program provides a large suite of computational tools that include numerous conformational and path sampling methods, free energy estimators, molecular minimization, dynamics, and analysis techniques, and model-building capabilities (B. R. Brooks et al., 2009).

GROMACS (GROningen MAchine for Chemical Simulations): GROMACS is a versatile package to perform molecular dynamics, i.e. simulate the Newtonian equations of motion for systems with hundreds to millions of particles. It is primarily designed for biochemical molecules like proteins and lipids that have a lot of complicated bonded interactions (Lindahl et al., 2001). GROMACS provides extremely high performance compared to all other programs and also can be run in parallel, using standard MPI communication (Van Der Spoel et al., 2005). Nevertheless, GROMACS follow a line of developments to meet the complexities of biomolecules. The latest release of GROMACS (Pronk et al., 2013) supports several implicit solvent models, as well as new free-energy algorithms, and the software now uses multithreading for efficient parallelization even on low-end systems, including windows-based workstations.

LAMMPS (Large-scale Atomic/Molecular Massively Parallel Simulator): LAMMPS is a classical molecular dynamics simulation code designed to run efficiently on parallel computers (Plimpton, 1995). One of its interesting features is the use of neighbor lists to keep track of nearby particles. The lists are then optimized for systems with particles that

are repulsive at short distances so that the local density of particles never becomes too large.

NAMD (NAnoscale Molecular Dynamics): This is a molecular dynamics simulation package written using the Charm++ parallel programming model, noted for its parallel efficiency and often used to simulate large systems (millions of atoms) (Phillips et al., 2005). NAMD uses the popular molecular graphics program VMD for simulation setup and trajectory analysis but is also file-compatible with AMBER, CHARMM, and X-PLOR. Recently, developers in NAMD produced a software called the "Force Field Toolkit" (ffTK), that greatly facilitates the development of parameters directly from first principles (Mayne, Saam, Schulten, Tajkhorshid, & Gumbart, 2013). ffTK, distributed as a plugin for the molecular modeling software VMD, addresses both theoretical and practical aspects of parameterization by automating tedious and error-prone steps, performing multidimensional optimizations, and providing quantitative assessment of parameter performance – all from within an easy-to-use graphical user interface.

3.3 Glycolipid bilayer simulation

As highlighted in Section 3.1.1, the MD method is being used widely in the context of lipid bilayer simulation. In literature numerous MD simulation works have been reported related on phospholipid bilayers (Abel, Dupradeau, Raman, MacKerell, & Marchi, 2011; H. J. Berendsen, 1996; Damodaran, Merz, & Gaber, 1992; Egberts, Marrink, & Berendsen, 1994; Heller, Schaefer, & Schulten, 1993; Kasson & Pande, 2004; Liu & Brady, 1997; Shinoda, DeVane, & Klein, 2010; Shinoda, Mikami, Baba, & Hato, 2003, 2004; Tieleman, Marrink, & Berendsen, 1997; Van der Ploeg & Berendsen, 1982, 1983) and most of them, nonetheless, emphasise the initial setup of simulation and dimensional analysis of simulation trajectories.

Meanwhile, there are a number of simulations on glycolipid bilayers (Chong, Hashim, & Bryce, 2006; Hall, Rog, Karttunen, & Vattulainen, 2010; Kapla et al., 2011; Konidala, He, & Niemeyer, 2006; H. Nguan et al., 2014; Róg et al., 2007), but comparatively low to phospholipid simulations. Possibly, the complexity of sugar group and the limited number of optimized force fields may be the reason for the low number of works reported in the literature. However, the glycolipid simulation studies that have been performed, explore both naturally occurring (Hall et al., 2010; Konidala et al., 2006; Lingwood et al., 2011;

Róg et al., 2007; Róg, Vattulainen, & Karttunen, 2005; Z. Zhang, Bhide, & Berkowitz, 2007) and synthetic glycolipid systems (Abel et al., 2011; Bogusz et al., 2000, 2001; Chong et al., 2006; Chong, Heidelberg, Hashim, & Gary, 2007).

3.3.1 GLYCAM force field

The modelling and simulation of carbohydrate-related compounds mainly depend on the force field type to reproduce comparable experimental results. In the AMBER simulation package environment, the *ff99SB* force field (especially for nucleic acids and proteins) augmented with the more specific force field, called Glycoprotein and Carbohydrate Parameters for AMBER (GLYCAM) to model glycosides. GLYCAM was developed to determine the structures of oligosaccharides and also to study oligosaccharide-protein interactions (Woods, Dwek, Edge, & Fraser-Reid, 1995).

Technically, the *ff99SB* parameter set for carbohydrates is inaccurate in torsional energy profiles, therefore, the new parameter set in GLYCAM emphasizes the fine tuning the calculations on the torsional energy term which were derived from *ab-initio* at the Hartree-Fock level with the split valence 6-31G* basis set. Beginning in the late 2011, a new versioning system was implemented for GLYCAM parameters. In the new system, all files containing parameters are versioned where the parameters employ letters and numbers. If a parameter set contains new functionality (e.g., the addition of new parameters) or fundamental changes (e.g., atom type name reassignments), a letter will be appended to its name. If the new version contains corrections (e.g., for typographical errors), its name will be appended with a number, like GLYCAM_06a or GLYCAM_06d and so on. All the works reported in this thesis use the parameter set version GLYCAM_06d together with simulation package Amber9 and Amber12 (D. Case et al., 2012) together with analysis package of AmberTools14 (D. Case et al., 2015). The work reported in Section 4.1 was performed using Amber9, meanwhile the works in Section 4.2 and Section 4.3 used Amber12.

In GLYCAM_06, the torsion terms have now been entirely developed by fitting to quantum mechanical data (B3LYP/6-31++G(2d,2p)/HF/6-31G(d)) for small-molecules (Kirschner et al., 2008). This made the GLYCAM_06 into an additive force field that is extensible to diverse molecular classes including lipids and glycolipids. The parameters are self-contained, such that it is not necessary to load any AMBER parameter files when

modeling carbohydrates or lipids. Further, GLYCAM and AMBER may be combined for modeling carbohydrate-protein complexes and glycoproteins.

Because the GLYCAM_06 torsion terms were derived by fitting to data for small, often highly symmetric molecules, asymmetric phase shifts were not required in the parameters. This has the significant advantage that it allows one set of torsion terms to be used for both α- and β-carbohydrate anomers regardless of monosaccharide ring size or conformation. Further, the GLYCAM_06 force field has been validated against quantum mechanical and experimental properties, including gas-phase conformational energies, hydrogen bond energies, and vibrational frequencies; solution-phase rotamer populations (from NMR data); and solid-phase vibrational frequencies and crystallographic unit cell dimensions. Although AMBER is equipped with various water (solvent) models like TIP3P (Jorgensen, Chandrasekhar, Madura, Impey, & Klein, 1983), TIP3P/F (Price & Brooks III, 2004), TIP4P (Jorgensen et al., 1983; Jorgensen & Madura, 1985), TIP4P/Ew (Horn, Swope, & Pitera, 2005; Horn et al., 2004), TIP5P (Mahoney & Jorgensen, 2000), POL3 (Caldwell & Kollman, 1995), and SPC/E (H. J. C. Berendsen, Grigera, & Straatsma, 1987); these are called TP3, TPF, TP4, T4E, TP5, PL3 and SPC, respectively. By default, we used TIP3P water model in the hydrated bilayer system in Section 4.3.

Besides the GLYCAM force field for carbohydrates, other force fields also been developed for carbohydrates like MM2 (Allinger, 1977), MM3 (Allinger, Yuh, & Lii, 1989), CHARMM (B. R. Brooks et al., 1983; Ha, Giammona, Field, & Brady, 1988; Reiling, Schlenkrich, & Brickmann, 1996), AMBER (Cornell et al., 1995; Weiner et al., 1984), GROMOS (Hermans, Berendsen, Van Gunsteren, & Postma, 1984; Van Gunsteren & Berendsen, 1987), and TRIPOS (Clark, Cramer, & Van Opdenbosch, 1989).

3.3.2 Single lipid modelling and bilayer construction

As stated in Section 1.3 (Motivation and research objectives), we study the properties of glycolipid bilayers in anhydrous and hydrated conditions by selecting a number of glycolipid molecules. For the bilayers in anhydrous condition, we chose four glycosides namely, βMal-C_{12}, βCel-C_{12}, βIsoMal-C_{12}, and βMal-$C_{12}C_{10}$ (see Table 3.2 (a)-(d) respectively) and built four double-bilayer systems where each system contained single type glycolipid. The βMal-C_{12}, which comprises two glucose units and linked by an $\alpha(1\rightarrow4)$ at glycosidic linkage between two sugars, is widely studied by experimental

method, like x-ray diffraction (Auvray, Petipas, Anthore, Rico-Lattes, & Lattes, 1995; Auvray et al., 2001, 1997). Meanwhile, the βCel-C_{12}, which is similar to βMal-C_{12}, has a $\beta(1\rightarrow4)$ link at the glycosidic linkage and the βIsoMal-C_{12}, unlike βMal-C_{12} and βCel-C_{12}, has an $\alpha(1\rightarrow6)$ connection between the two glucose rings. Additionally, the βMal-$C_{12}C_{10}$ has the same disaccharide headgroup as in βMal-C_{12} but it has a branch of two alkyl chains along the hydrocarbon region (see Table 3.2(d)).

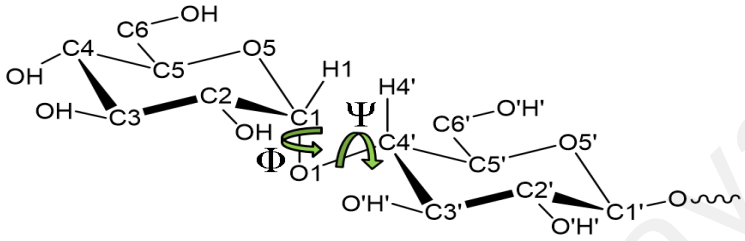

(a) Disaccharide maltoside with Φ and Ψ dihedral angles.

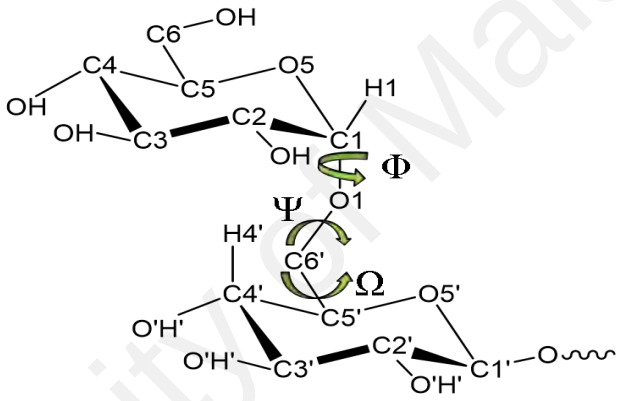

(b) Disaccharide isomaltoside with Φ, Ψ, and Ω dihedral angles.

Figure 3.4: (a) Maltoside and (b) Isomaltoside.

The initial coordinates of βMal-C_{12}, βMal-$C_{12}C_{10}$, βCel-C_{12}, and βIsoMal-C_{12} were modeled using the HyperChem package (Hyperchem(TM), 2003). The related protein data bank (PDB) file for each lipid is given in Appendix A. Following the IUPAC nomenclature, the glycosidic angles (Φ and Ψ) for maltose headgroup are defined as H1-C1-O1-C4' and C1-O1-C4'-H4' respectively (Comm., 1970; McNaught, 1996). Meanwhile, for an isomaltoside (βIsoMal-C_{12}), the dihedral angles Φ, Ψ, and Ω are defined as (O5-C1-O1-C6'), (C1-O1-C6'-C5') and (O1-C6'-C5'-C4') respectively. For a better understanding of the dihedral angles at the glycosidic linkage the Φ, Ψ, and Ω angles are illustrated in Figure 3.4. The initial values of Φ,Ψ, and Ω for βMal-C_{12}, βCel-C_{12}, and βIsoMal-C_{12} were obtained from the literature (Ham & Williams, 1970; Jeffrey & Huang, 1991; Ott & Meyer, 1996) (for details see Table 3.3).

Table 3.2: Glycolipids used in this study. (a) maltoside, (b) cellobioside, (c) isomaltoside, (e) branched chain maltoside, (e) Guerbet branched chain-(*R*-maltoside), (f) Guerbet branched chain-(*S*-maltoside).

	Name	Structure
(a)	βMal-C_{12}	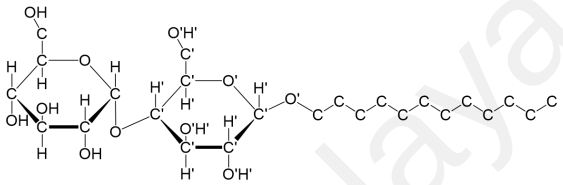
(b)	βCel-C_{12}	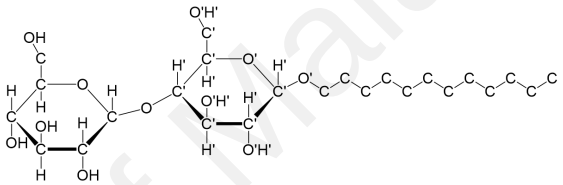
(c)	βIsoMal-C_{12}	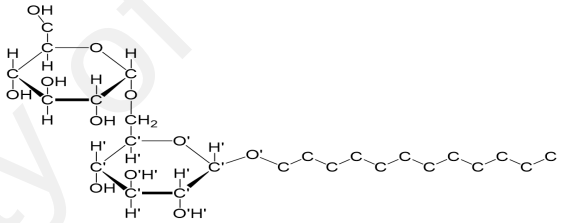
(d)	βMal-$C_{12}C_{10}$	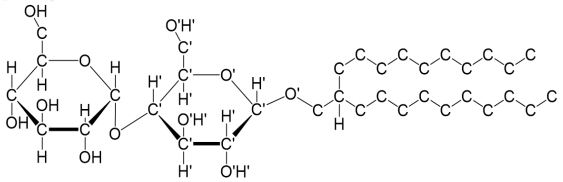
(e)	βMal-$C_{12}C_8$(*R*)	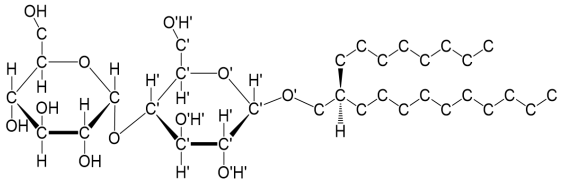
(f)	βMal-$C_{12}C_8$(*S*)	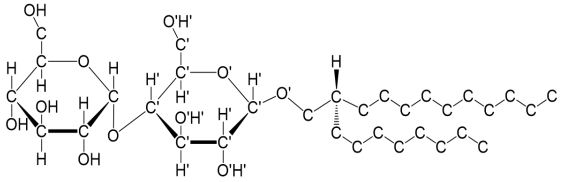

Table 3.3: Dihedral angles for the sugar units used in MD simulations.

Molecule	Φ	Ψ	Ω	Ref
βMal-C_{12}	-49.0	-36.0	–	Ott and Meyer (1996)
βCel-C_{12}	-25.0	48.0	–	Ham and Williams (1970)
βIsoMal-C_{12}	-49.2	167.3	-45.3	Jeffrey and Huang (1991)

The geometry of each structure was optimized within HyperChem and the crystal builder facility in HyperChem was then used to arrange the molecules in an 8×8 monolayer. This monolayer was geometry optimized and used to form a bilayer with the tail group of the lipids pointing towards each other and headgroups facing the opposite directions. Since there is no single crystal structure information available for βMal-C_{12} (Auvray et al., 2001), we have used a crystal builder option in HyperChem to build a single bilayer. Then, the bilayer was replicated to form a second bilayer to give a simulation cell with a total of 256 lipids. The double bilayer system was used to resemble closely the experimental (lamellar) conditions (Gentilcore, 2009).

In a previous bilayer simulation of alkyl monosaccharide glycolipids, (Chong et al., 2007) the chain region was found at the end of the simulation to be slightly tilted, which is consistent with the fact that at 27 °C, according to the phase diagram, (Auvray et al., 2001) the system exists in either the L_C (lamellar crystal) phase or L_β (gel) phase but not the L_α (fluid lamellar) phase; the latter phase comprises melted alkyl chains and corresponds to *smectic A* in thermotropic liquid crystal nomenclature (Vill, 2002). This phase occurs at much higher temperatures for the monoalkylated systems. Only the branched chain compounds give a thermotropic fluid lamellar phase at room temperature (Hashim et al., 2006). A study by Abe, Harata, Fujiwara, and Ohbu (1998) supports the assertion that the alkyl chains of glycolipid in L_C phase are not perpendicular to the bilayer normal but tilted slightly (Abe, Fujiwara, Ohbu, & Harata, 2000). Further, an x-ray studies on the L_C phase for both βMal-C_{14} and βMal-C_{16} have demonstrated these phases to be tilted and interdigitated (Ericsson, Ericsson, & Ulvenlund, 2005). Nonetheless, Abeygunaratne, Hashim, and Vill (2006) also provide information on the tilt glycolipid structure in the *smectic C* liquid crystals by using optical microscopic and the electric polarization experimental methods. Taking these observations into consideration, in our

model, we have pre-tilted the lipid chains at about 15 °C to the bilayer normal. At the same temperature, the branched chain glycolipids give an anhydrous fluid L_α phase (Hashim et al., 2006).

Meanwhile, for the bilayers in hydrated condition, we selected two glycosides namely, dodecyl maltoside, βMal-C_{12} and Guerbet branched chain maltoside, βMal-$C_{12}C_8$ (see Table 3.2 (e) and (f)) where both lipids form fluid lamellar L_α phase (Auvray et al., 2001; Hamid, Hashim, Seddon, & Brooks, 2014). Additionally, the Guerbet maltoside (βMal-$C_{12}C_8$) has a chiral center at the branching of asymmetric alkyl chains. This chiral center gives two possible additional chiral molecules with *R* & *S* isomers i.e. βMal-$C_{12}C_8$(*R*) and βMal-$C_{12}C_8$(*S*) as shown in Table 3.2 (e) and (f) respectively. Since the βMal-C_{12} and βMal-$C_{12}C_8$ have the same headgroup type – maltose and varying chains, the choice of these glycolipids gives an interesting platforms to investigate the bilayer properties that form in the lamellar fluid, L_α phase.

These three glycolipid molecules (βMal-C_{12}, βMal-$C_{12}C_8$(*R*), βMal-$C_{12}C_8$(*S*)) are then used to design a total of five simulation model systems in the L_α phase. Among these, two lamellar systems using monoalkylated lipid (βMal-C_{12}) are modelled with two hydration levels with weight fraction (12% and 23% w/w, H_2O:lipid) at temperature 80 °C referring to the phase diagram by Auvray et al. (2001) as shown in Figure 3.5. The red and green dots in the phase diagram represent hydration of lamellar phase with weight fraction at 12% and 23% of water respectively at temperature 80 °C. These systems were then named as βMal-C_{12}(12%wat) and βMal-C_{12}(23%wat).

Following that, another two lamellar systems were modelled with branched chain Guerbet glycosides (βMal-$C_{12}C_8$) – using *R* and *S* chiral conformations separately by referring to an experimental work by Hamid et al. (2014) at room temperature 27 °C and at 25% of hydration with weight fraction. The two bilayers were then named as βMal-$C_{12}C_8$(*R*)(25%wat) and βMal-$C_{12}C_8$(*S*)(25%wat) corresponding to *R* and *S* isomers respectively. Finally, a racemic mixture was modeled using *R* and *S* isomers, each with 50% contribution in weight fraction with the same hydration level compared to the bilayers with *R* and *S* isomers. This recemic system was named as βMal-$C_{12}C_8$(*RS*)(25%wat). Simulating these five systems in the fluid lamellar phase facilitates the investigation of bilayer properties related to the chiral effect, hydration levels, and temperature variation.

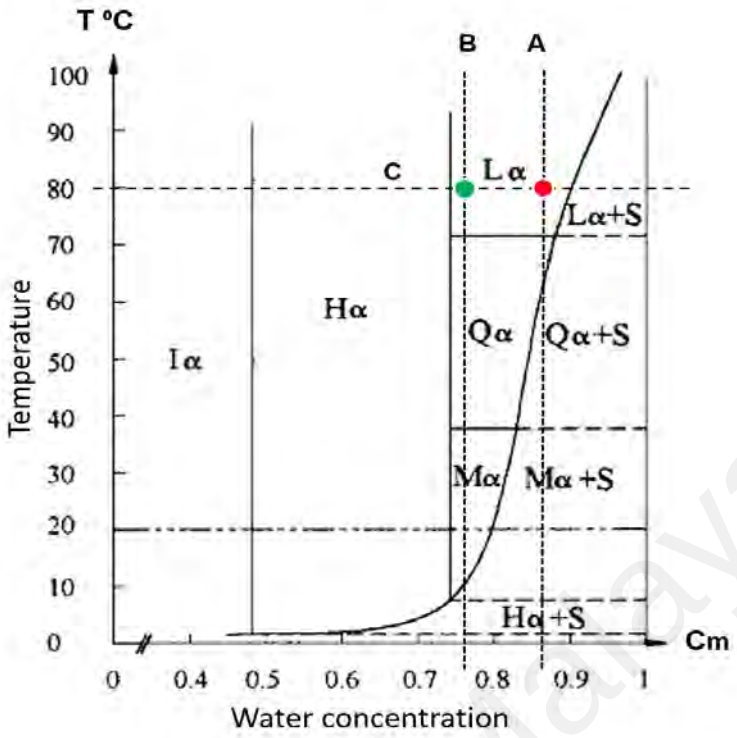

Figure 3.5: Lyotropic phase diagram of βMal-C_{12} obtained from Auvray et al. (2001). The labels I_α, H_α, M_α, S, Q_α, and L_α orderly represent phases such micelle, hexagonal, ordered micelle, solid, cubic, and fluid lamellar. The red and green points on the phase diagram represent coordinates for 12% and 23% water concentrations respectively at 80 °C.

We obtained the initial structure of single molecule βMal-C_{12} from previous work (bilayer in anhydrous condition). For the Guerbet branched chain maltoside βMal-$C_{12}C_8$, we used Gaussview09 (Frisch et al., 2009) to model the *R* and its chiral counter *S* isomers. All the three molecules were then geometry optimized using the steepest descent (SD) and conjugate gradient (CG) algorithms in Avogadro (Hanwell et al., 2012) prior to

Table 3.4: Lipid bilayer system description based on water concentration and temperature. Each system contains 128 glycolipids.

Lipids	Number of water molecules	Temperature
βMal-C_{12}(12%wat)	496	80 °C
βMal-C_{12}(23%wat)	1086	80 °C
βMal-$C_{12}C_8$(*R*)(25%wat)	1556	27 °C
βMal-$C_{12}C_8$(*S*)(25%wat)	1556	27 °C
βMal-$C_{12}C_8$(*RS*)(25%wat)	1556	27 °C

bilayer building. Next, the PACKMOL package (Martínez, Andrade, Birgin, & Martínez, 2009) was used to build all the five bilayer systems in the hydrated condition. In each bilayer, the hydrophobic chains were arranged inward pointing to the center of the bilayer while the hydrophilic sugar group pointed outward. The hydrophilic region was hydrated with explicit water molecules with a tolerance of about 2Å between the lipids and water molecules (Martínez et al., 2009). A summary for the bilayer systems and number of constituent molecules is given in Table 3.4.

3.3.3 Energy minimization and equilibration

For the bilayers in anhydrous condition, (especially the simulation work discussed in Section 4.1) the four glycoside lamellar systems were equilibrated using AMBER9, (D. Case et al., 2006) together with force field parameters *ff99*, (Hornak, Abel, Okur, Strockbine, & A., 2006) and GLYCAM_06d, (Kirschner et al., 2008) to model the tails and headgroups respectively. The charges for the atoms in the sugar and chain atoms are given in PREPIN file (see Appendix B). A non-bond cut-off of 9 Å was applied in calculating non-electrostatic interactions and long-range electrostatic interactions were treated using the particle mesh Ewald method (Darden, York, & Pedersen, 1993; Essmann et al., 1995). The SHAKE algorithm, (Miyamoto & Kollman, 1992) was used to constrain covalent bonds involving hydrogen. An equilibration procedure was applied, involving restrained energy minimizations on tail and headgroup moieties separately. The systems were heated gradually over 2 ns from 0 to 27 °C in the *NVT* ensemble, using the Andersen thermostat ($\tau_P = 0.5$ ps), (Andrea, Swope, & Andersen, 1983) and a 1 fs time step. Upon reaching 27 °C, the restraints were reduced on the lipids stepwise in the *NPT* ensemble using isotropic scaling of box dimensions (50 ns) followed by anisotropic scaling (100 ns) (Kapla et al., 2011). The Berendsen algorithm was used to achieve pressure coupling, with a coupling constant of 1 ps and for anisotropic coupling, a compressibility of 4.5×10^{-5}/bar. It is known from the literature that gentiobioside, which has $\beta(1\rightarrow6)$ connetion between sugars at the glycosidic linkage, showed a very slow rotational motion (Carrier, Giziewicz, Moir, Smith, & Jarrell, 1989). Since the βIsoMal-C_{12} (which has $\alpha(1\rightarrow6)$) is similar to gentiobioside, we extend our simulation in isotropic pressure coupling for about 80 ns, then followed by 100 ns in anisotropic pressure coupling to allow the sugars in βIsoMal-C_{12} to

sample sufficiently. The final 40 ns of the 150 or 180 ns glycolipid trajectories are used for analysis.

The βIsoMal-C_{12} appeared to compact more than the other three systems; therefore a more extensive isotropic simulation was performed for 80 ns, then followed by 100 ns of anisotropic simulation. As discussed below, the final 40 ns of the 150 or 180 ns glycolipid trajectories were used for analysis.

Meanwhile, for the simulation work discussed in Section 4.2, we follow a similar minimization and equilibration procedure. In fact, we reprised our earlier 150–180 ns simulations of those systems reported in Section 4.1, performing replicate simulations of 200 ns within the *NPT* ensemble at 27 °C, but permitting fully anisotropic pressure scaling (allow the box to adjust to the desired pressure in all three directions, *x,y*, and *z*), as opposed to the isotropic conditions used previously. The trajectory coordinates were archived every 5 ps. As bilayers need at least 20 ns run to equilibrate (Anézo, de Vries, Höltje, Tieleman, & Marrink, 2003), the last 160 ns of each 200 ns simulation was used for analysis. These simulations were performed with the GPU-accelerated version of the *pmemd* module.

But for the work discussed in Section 4.3, (five hydrated bilayers of single and branched chains) we followed slightly different minimization and equilibration procedures. We used the AMBER12 (D. Case et al., 2012; Götz et al., 2012; Grand, Götz, & Walker, 2013; Salomon-Ferrer, Götz, Poole, Le Grand, & Walker, 2013) software package to run the MD simulations. The force field parameter GLYCAM_06d (Kirschner et al., 2008) was used to assign the atom types, bond length, bond angle, dihedral angle and partial charges for the carbohydrate headgroup, while the *ff99SB* (Hornak et al., 2006) force field was used for the alkyl chain and water molecules. Prior to the production run, all the five systems were energy minimized in two stages. In the first stage, the Steepest descent (SD) and the adopted basis Newton-Raphson method were used to minimize each system to eliminate any unfavorable contacts and overlapping of atoms resulting from the model building procedure on the pre-constructed bilayer (D. Case et al., 2012). Initially, the headgroup moieties and water molecules were fixed by applying 5kcal/mol$Å^2$ of restraint and the chains were energy minimized. Then the headgroups were fixed with the same restraint value but the chain moieties and water molecules were energy minimized. In the following step, the chains were fixed but the headgroups and water molecules were energy

minimized. Finally, each bilayer was energy minimized before a short dynamic run at the final part. In all minimization cycles, the first 5000 steps were energy minimized using SD method followed by 2500 steps of conjugate gradient algorithm.

In the second stage, the energy for the minimized structures was equilibrated in canonical ensemble (*NVT*–constant number of particles *N*, volume, *V* and temperature, *T*) over 2 ns by increasing the temperature from 0 to 80 °C for monoalkylated systems (βMal-C_{12}(12%wat) and βMal-C_{12}(23%wat)) and from 0 to 27 °C for the branched chain Guerbet glycoside systems (βMal-$C_{12}C_8$(*R*)(25%wat), βMal-$C_{12}C_8$(*S*)(25%wat), and βMal-$C_{12}C_8$(*RS*)(25%wat)) using the Andersen thermostat (τ_P = 0.5 ps) (Andrea et al., 1983) with 1 fs time step. When the systems reached their desired temperatures, the equilibration was continued by reducing the restraints stepwise in an *NPT* ensemble (constant number of particles *N*, pressure *P*, and temperature *T*) using the weak semi-anisotropic pressure coupling with a 2 ps coupling constant to allow the simulation box to expand independently in the *x*-*y*, and *z* directions. Subsequently, the production was carried out in *NPT* ensemble by applying the periodic boundary conditions to the simulation box in all three coordinate directions (with *x*, *y* in the bilayer plane and z normal to the bilayer) in cubic lattice geometry. The Berendsen algorithm was used to achieve pressure coupling, with a coupling constant 1ps and for anisotropic coupling, a compressibility of 4.5×10^{-5}/bar. Non-bonded interactions were truncated with a cut-off range of 9.0Å and long-range electrostatic interactions were treated using the particle mesh Ewald summation method (Darden et al., 1993; Essmann et al., 1995). The SHAKE algorithm was used to constrain covalent bonds involving hydrogen atoms (Miyamoto & Kollman, 1992). The time step 1 fs was used and the simulation's trajectories were saved once every 5 ps. An example of topology file for a single molecule of βMal-C_{12} is given in Appendix C for a view.

This simulation was performed for a total duration of 300 ns dynamics where the first 75 ns was considered as pre-equilibration stage and the bilayer properties were calculated using the last 225 ns. The errors were estimated by block-wise averages with every block comprising 25 ns of production. These simulations were performed using the GPGPU-accelerated version of the simulation engine on NVIDIA Tesla graphic cards. A typical simulation performance for these systems on a GPGPU is 12ns/day, which is more than an order of magnitude higher than that of a typical CPU-based SMP (Symmetric

multiprocessing) machine simulation (Abou-Zied, Al-Lawatia, Elstner, & Steinbrecher, 2013). Post processing of trajectory was conducted using the *ptraj* and *cpptraj* modules from AMBER as well as in-house custom analysis tools.

3.4 Analysis on glycolipid bilayer

In this section, we list all the analysis performed on anhydrous and hydrated glycolipid bilayers. Some analysis were performed using *ptraj* or *cpptraj* which is a part of AMBER program. Otherwise, we used in-house scripts to complete the analysis.

3.4.1 Local density profiles, LDP

The local density profiles were calculated along the bilayer normal, taking the center of the bilayer as the origin and the distribution function $g(z)$ is calculated from the number density, $\rho(x,y,z)$, given as:

$$N_d = \iiint \rho(x,y,z)dxdydz \tag{3.17}$$

where N_d is the total number of atoms. Along the z-direction, we define the $g(z)$ as:

$$g(z) = \frac{\rho(z)}{\rho} = \frac{N(z)V_b}{A_b(\Delta z)N} \tag{3.18}$$

where A_b is bilayer area, Δz is the bin size along the z-axis and V_b is the bilayer volume. The distribution is normalized by dividing every bin box with total atoms present in the simulation box.

3.4.2 Dimensional analysis of bilayer

Area per lipid

The area per lipid at the interface of a bilayer was calculated by dividing the surface area of *xy* dimension with the total number of lipids present in a monolayer.

Bilayer thickness

The thickness of a bilayer (also called as Luzzati thickness – for further information please see Figure 4.25) was calculated by measuring the distance between two highest peaks from the LDP.

Bilayer repeat distance (d-spacing)

The bilayer repeat distance was calculated by taking the box dimension along the z-direction.

3.4.3 Ramachandran plot

The two-dimensional Ramachandran plot for the distribution of the dihedral angles at the glycosidic oxygen between the two sugar units in maltose disaccharide was done by writing in-house FORTRAN program.

3.4.4 Hydrogen bonding, HB

The hydrogen bond analysis was performed using the *ptraj* and *cpptraj* modules from AMBER9 and AmberTools14 respectively. For the HB in an anhydrous system we used *ptraj* while for the hydrated system we used *cpptraj*. In each module, the definitions for the donor and acceptor are slightly different. In *cpptraj* the hydrogen bond donors are defined as molecules that have a hydrogen attached to an electronegative atom (for example, hydroxyls or amines) and the acceptors are defined as molecules that have a lone pair of electrons located on an electronegative atom (for example, oxygen, nitrogen, or fluorine). Meanwhile, in *ptraj* the donor and the acceptor are defined vice versa.

In all glycolipid bilayer systems, we determined the HB interactions at the hydrophilic region only since in this region the sugars contain hydroxyl group as donors and hydrogen attached to oxygen as acceptors. We calculated two types of HBs – i) HB between lipid to lipid and ii) between lipid and water. In the anhydrous system, we calculated only the lipid to lipid HBs while in the hydrated system we calculated lipid to lipid and lipid to water HBs. Since hydrogen bond interaction is distance and directional dependence, we defined the O−O distance to be 4 Å and an angle cut-off of 120° from linearity as done by Chong et al. (2007) to do comparison with previous work.

3.4.5 Headgroup and chain tilt angle distributions

The chain tilt vector $\vec{T}$ is calculated together with the corresponding average tilt angle θ using procedure described by Van der Ploeg and Berendsen (1982). Thus $\vec{T}$ is defined as:

$$\vec{T} = \frac{1}{M} \times \sum_{i=1}^{\infty} \vec{R}_i, \tag{3.19}$$

where $\vec{R}_i$ is a normalized vector and the summation is done over the M hydrocarbon chains in the simulation system. Various definitions of $\vec{R}_i$ have been proposed by (Essex, Hann, & Richards, 1994; Van der Ploeg & Berendsen, 1982). Here, we calculated tilt angle and tilt vector via four methods:

Method A: The $\vec{R}_i$ vector for the single chain lipid is defined from the mid-point of C71-C72 to that of C80-C81 (see Figure 4.1). For the *sn*-1 chain of βMal-$C_{12}C_{10}$, $\vec{R}_i$ connects the mid-point of C72-C73 and C80-C81, while for *sn*-2, it links C72-C83 to C90-C91 (see Figure 4.1). $\vec{T}$ is averaged over the four layers indiscriminately.

Method B : The $\vec{R}_i$ is defined as in *Method A*. $\vec{T}$ is averaged over the first layer only.

Method C: As in *Method B*, the average $\vec{T}$ is defined over first layer only. But unlike *Methods A* and *B*, $\vec{R}_i$ is defined for single chain lipids from the mid-point of C74-C75 to that of C80-C81. For the *sn*-1 chain of βMal-$C_{12}C_{10}$, $\vec{R}_i$ connects the mid-point of C74-C75 and C80-C81, while for *sn*-2, this is taken from the mid-point of C84-C85 to that of C90-C91.

Method D: As in *Method B*, but the tail vector is defined from C73-C74 and C79-C80 for single alkyl chain. For the *sn*-1 chain of βMal-$C_{12}C_{10}$, $\vec{R}_i$ connects the mid-point of C73-C74 and C79-C80, while for *sn*-2, this is taken from the mid-point of C83-C84 to that of C89-C90

3.4.6 Chain order parameter

The degree of ordering in the chain region may be estimated from order parameter, S. This is derived from a 3×3 Saupe ordering tensor S, whose ij^{th} element is given as,

$$S_{ij} = \frac{1}{2}(\overline{3cos\theta_i cos\theta_j} - \delta_{ij}), \tag{3.20}$$

where θ_i is the angle between the i^{th} molecular axis and the bilayer normal, and the bar denotes time averaging (Saupe, 1964). For definition of an alkyl chain order parameter, we followed Van der Ploeg and Berendsen (1982) and the molecular axes for the n^{th} methylene group are defined by the H−H vector (x), the bisectrix of H−C_n−H angle (y) and vector C_{n-1} to C_{n+1} (z). From symmetry arguments, the tensor S is diagonal and S_{zz} represents the chain order parameter. The S_{zz} takes a value of unity if the average orientation is parallel to the bilayer normal (i.e. fully ordered); $-\frac{1}{2}$ if it is perpendicular to the normal; and zero

if the system is completely disordered. Related to deuterium NMR experiments, another informative order parameter is given as:

$$S_{CD} = \frac{2}{3}S_{xx} + \frac{1}{3}S_{yy}, \tag{3.21}$$

where $S_{xx}$and S_{yy} are the order parameters in x and y direction respectively.

3.4.7 *Gauche* and *trans* population distribution

Alkyl chains of several methylene groups with some degree of *gauche* and *trans* conformations (Mizushima, Morino, & Nozri, 1936) possibly determine the detailed phase behavior (Jeffrey & Wingert, 1992) especially of the lamellar assembly. These conformations were analyzed by calculating the probability, $P(\theta)$ of the *gauche*/*trans* conformers, defined as,

$$P(\theta) = \begin{cases} 1(\theta \geq \frac{2}{3}\pi), & \textit{trans} \text{ state} \\ -1(\theta < \frac{2}{3}\pi), & \textit{gauche} \text{ state} , \end{cases} \tag{3.22}$$

where θ is the dihedral angle formed by four consecutive carbons along the alkyl chain (Shinoda et al., 2004). The *ptraj* module in AMBER was used to evaluate this probability function together with Fortran code.

3.4.8 Distance between selected atoms

The radial distribution function (RDF) provides information on the probability of finding a particle at a certain radius away from another particle. From RDF, one could determine the distance between selected atoms (Leach, 2001; Róg et al., 2004). The RDF $g(r)$ is defined as below:

$$g(r) = \frac{N(r)}{4\pi\rho\,\delta r}, \tag{3.23}$$

where, $N(r)$ is the number of selected atoms between distance r and $r+dr$ from the reference atom. r is the number density (Damodaran et al., 1992).

In our simulation work, we measure the closeness or packing of the chains and headgroups in the bilayer systems. We also calculate the RDF between water and $-$OH group in the sugar moiety to understand the degree of hydration by water molecules.

Additionally, we calculate the RDFs using the *ptraj* module in AMBER and the details of those calculations are given in the respective sections.

3.4.9 Dynamic properties

To understand the dynamics of glycolipids in the bilayer system we calculate the rotational diffusion of the alkyl chains and sugar groups separately using autocorrelation function as in Equation (3.24). For the headgroup, we select three vectors for dynamics analysis namely, the reducing sugar (*ring1*), non-reducing sugar (*ring2*) and the combined sugar rings (*ring12*), represented by the appropriate unit vectors, $\overrightarrow{\mu}_{ring2}$ from C1 to C4, $\overrightarrow{\mu}_{ring1}$ from C1' to C4', and $\overrightarrow{\mu}_{ring12}$ from C1' to C4 respectively (see Figure 3.6(a)). Meanwhile, for the rotational diffusion of the chain region, we choose the C−H vectors along the alkyl chain.

Using these vectors in *ptraj* module from AMBER, the correlation times for the various motions were estimated using the second rank reorientational autocorrelation functions, $C_2(t)$ defined as:-

$$\begin{aligned} C_2(t) &= \frac{1}{2}\left\langle 3[\vec{\mu}(t).\vec{\mu}(0)]^2\right\rangle - \frac{1}{2}, \\ &= \frac{3}{2}\left\langle [\vec{\mu}(t).\vec{\mu}(0)]^2\right\rangle - \frac{1}{2}, \end{aligned} \tag{3.24}$$

where $\vec{\mu}(t)$ is a unit vector of the chosen rotational mode (Allen & Tildesley, 1989; Leach, 2001; P. Niemelä et al., 2004). The $C_2(t)$, which is based on the second rank Legendre polynomial $P_2(cos(\theta))$, was evaluated for each lipid over the production trajectory and averaged over the number of lipids within the system. In the isotropic condition the orientation of constituent particles are random and the corresponding average value of the term $\left\langle [\vec{\mu}(t).\vec{\mu}(0)]^2\right\rangle$ gives $1/3$. In order the function gives zero value for the isotropic condition the factor 3 is introduced in the Equation (3.24). The average $C_2(t)$ then fitted to a single-exponential function; from which the correlation time was obtained by integration using the trapezoidal rule. The use of single-exponential function to estimate the correlation time was referred from Shinoda et al. (2003). Their slow dynamics results of the highly branched chain agree well with the NMR experimental results. On the other hand, Róg et al. (2004), obtained a similar correlation profile like in Figure 4.16, and reported that the use of multiexponential fitting was not satisfactory. Thus, we used the single-exponential

function to do a rough estimation of the dynamics of lipid segments. The standard deviation of $C_2(t)$ was also determined to be within the range of ± 0.5 ns.

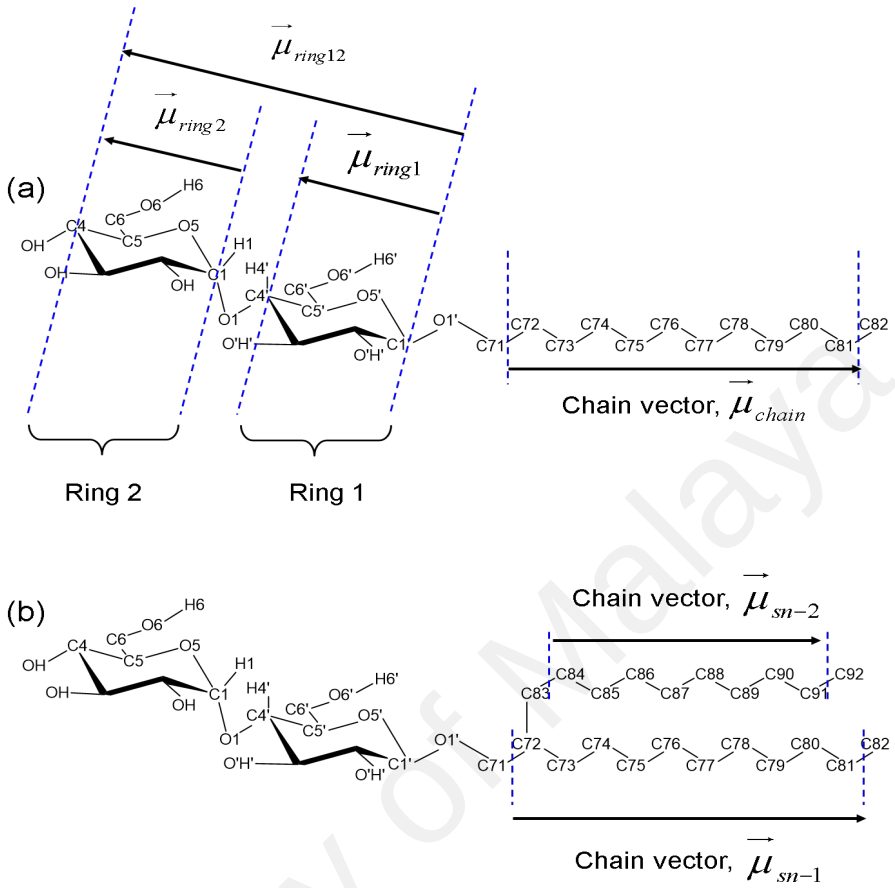

Figure 3.6: Diagram shows the vectors defined along reducing, non-reducing and chain segments for calculating the autocorrelation function to determine the dynamic properties.

The Equation (3.24) is also used to determine the rotational correlation time for the exocyclic group from each sugar unit. The respective vectors are defined along C6–OH and C6'–O'H' for non-reducing and reducing sugars.

3.4.10 Hydrogen bonding lifetime

We used *cpptraj* from AmberTools14 (Roe & Cheatham III, 2013) to determine the hydrogen bond lifetime at the hydrophilic regions of every bilayer system.

The lifetime analysis has been done by calculating the averages over windows for specified datasets. 'Lifetime' in this sense means 'whenever HB present' – the data is considered present when above or below a certain cut-off (the default is greater than 0.5, useful for hydrogen bond lifetime analysis). For example, in the case of a hydrogen bond 'series' dataset, if a hydrogen bond is present the set is 1, otherwise it is 0. For example, given the dataset {0 1 1 0 1 0 0 0 1 1}, the overall average is 0.5. However, there are 3

lifetimes of lengths 2, 1, and 2 (1 1, 1, and 1 1). The max lifetime is 2 and the average lifetime is 1.67, i.e. (2 + 1 + 2) / 3 lifetimes = 1.67. We operated on the raw data with in-house scripts to obtain the HB-lifetime values for the bilayer systems (D. Case et al., 2012).

CHAPTER 4

RESULTS AND DISCUSSIONS

The opposite of a correct statement is a false statement. But the opposite of a profound truth may well be another profound truth.
Niels Bohr (1885-1962)

4.1 Molecular dynamics study of anhydrous lamellar structures of synthetic glycolipids: effects of chain branching and disaccharide headgroup

In this section we report the results of a molecular dynamics simulation of anhydrous bilayers, namely dodecyl β-maltoside, dodecyl β-cellobioside, dodecyl β-isomaltoside and a $C_{12}C_{10}$ branched β-maltoside. We performed a systematic analysis on the bilayer structure, chain structure, and sugar headgroup conformation. We emphasized on calculating some bilayer properties like area per lipid, density profile, order parameter and chain tilting angle. This chapter ends with a discussion section relating to the analysis been done. (This work has been published at: *J. Phys. Chem. B* 2012, 116, 11626−11634)

4.1.1 Bilayer structure

We performed MD simulation of four glycolipid assemblies, βMal-C_{12}, βMal-$C_{12}C_{10}$, βCel-C_{12} and βIsoMal-C_{12}. The structure of each lipid is given in Figure 4.1. Based on the local density profiles (LDPs) of 20 ns block averages over the final 100 ns, it can be seen the lamellar structures for each glycolipid system has converged (4.2) (Anézo et al., 2003). We took the last 40 ns of these trajectories for performing subsequent structural and dynamic analyses. Based on these equilibrated trajectories, the average surface area per headgroup was calculated. The computed areas for βMal-C_{12} and βCel-C_{12} are very similar with the values of 38.8 and 38.7Å^2 respectively (Table 4.1). This is in reasonable agreement with the value of 43 Å^2 for βMal-C_{12} based on x-ray crystallographic layer spacing (H. S. Nguan, Heidelberg, Hashim, & Tiddy, 2010). Interestingly, the calculated headgroup surface area for βIsoMal-C_{12}, the third of the single chain glycosides studied here, is some 10Å^2 larger, at 48.6 Å^2 (Table 4.1); this is an increase of 26 % from its regioisomer, βMal-C_{12}. The area value is similar to that of the branched chain lipid βMal-

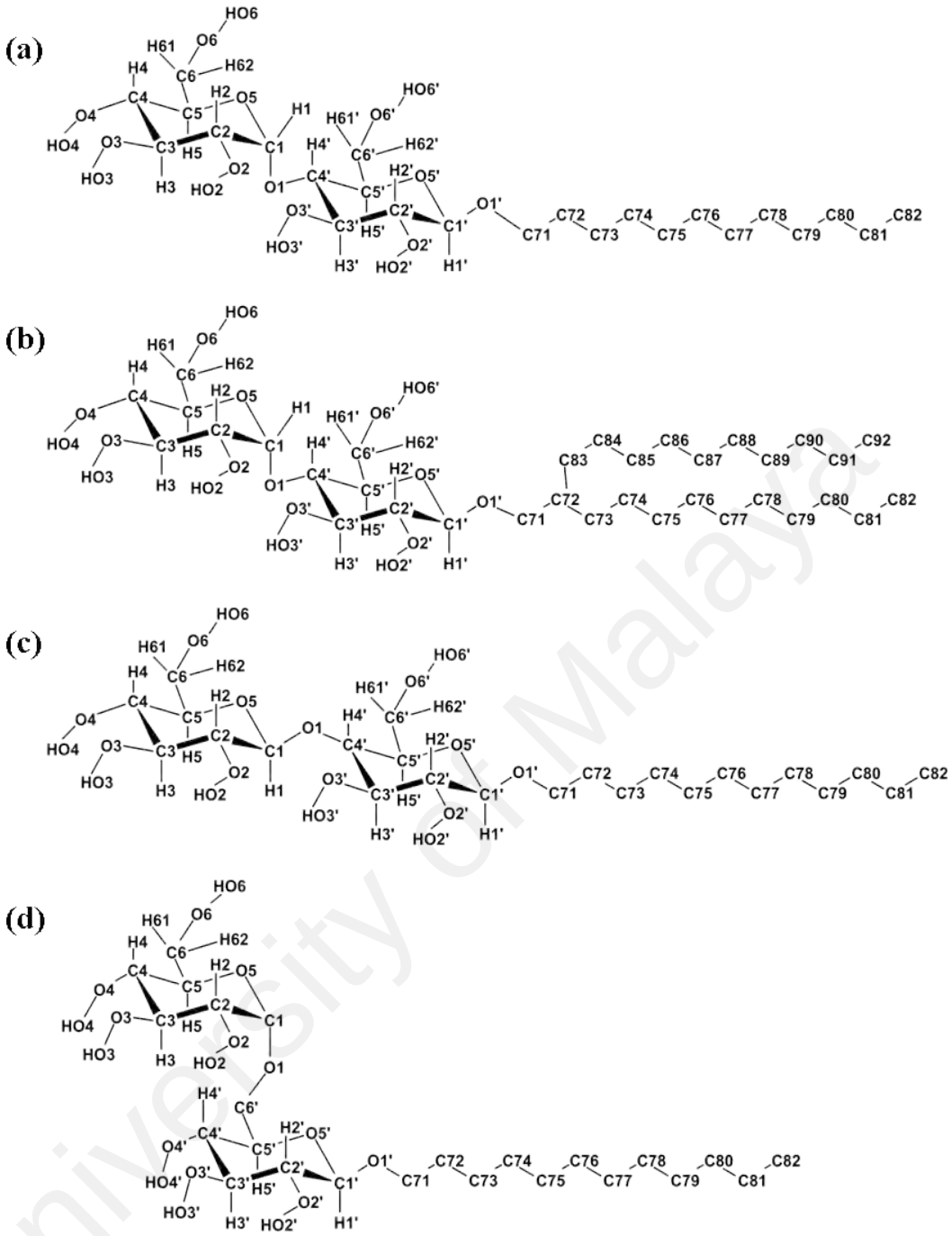

Figure 4.1: Glycosides simulated: (a) βMal-C_{12} (b) βMal-$C_{12}C_{10}$ (c) βCel-C_{12} (d) βIsoMal-C_{12}. Note: In part (d), H61' and H62' atoms were omitted for clarity; also, to avoid conflict with sugar atom labeling, each glycolipid's main alkyl chain is labeled from C71 to C82, starting from glycosidic oxygen, and the branched chain from C83 to C92.

$C_{12}C_{10}$, where the headgroup surface area increases further to 51.9 Å^2, (Table 4.1), 34 % larger than βMal-C_{12}. This is, presumably to accommodate strain introduced by the larger splay of the chain region.

In addition to the highest predicted surface area of the three single chain glycolipid systems, βIsoMal-C_{12} bilayer exhibits the largest degree of compaction, as can be seen

from the overlap of hydrophilic and hydrophobic domains in the local density profile (Figure 4.2d). The isomaltoside d spacing is 26.6 Å, some 19 and 18 % less than the d values observed for βMal-C_{12} and βCel-C_{12} respectively (Table 4.1).

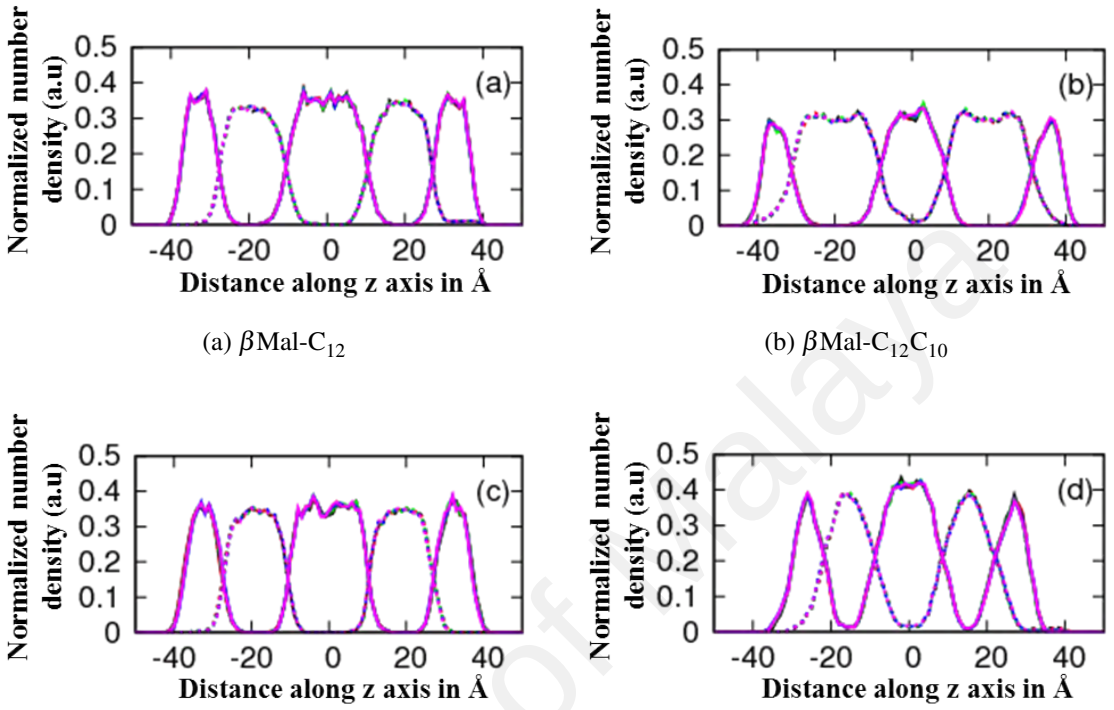

(a) βMal-C_{12} (b) βMal-$C_{12}C_{10}$

(c) βCel-C_{12} (d) βIsoMal-C_{12}

Figure 4.2: Local density profiles over 100 ns for (a) βMal-C_{12}, (b) βMal-$C_{12}C_{10}$, (c) βCel-C_{12}, and (d) βIsoMal-C_{12} for headgroup (solid line) and tail (dotted line). LDPs are computed for 1−20 ns (red), 21−40 ns (black), 41−60 ns (green), 61−80 ns (blue), and 81−100 ns (magenta).

From visual inspection of MD configurations (Figure 4.3), the compression of d spacing in the βIsoMal-C_{12} system is evident (Figure 4.3d). As before for headgroup surface area, the calculated bilayer distances are similar for βMal-C_{12} (33±1 Å) and βCel-C_{12} (32±1 Å); the spacing for βMal-C_{12} agrees to within the error when compared to that 33±1 Å at 20 °C from the small angle x-ray diffraction (Auvray et al., 2001). Interestingly, the average volumes of the simulation box $\langle V \rangle$ are similar for the three monoalkylated lipids, βMal-, βCel- and βIsoMal-C_{12} (Table 4.1). For βIsoMal-C_{12}, this observation results from a 19 % reduction in the z-direction of the bilayer normal (Figure 4.3), compensated by an increase in the xy area of the bilayer to result in an overall volume comparable to the other two isomers.

Table 4.1: Headgroup urface area per lipid (A), bilayer spacing (d), and average volume of simulation box ($\langle V \rangle$).

Glycolipid	A (Å^2)	d (Å)	$\langle V \rangle \times 10^3$ (Å^3)
	Calculated		
βMal-C_{12}	38.8 ± 0.2	32.9 ± 0.5	183.2 ± 0.6
βMal-$C_{12}C_{10}$	51.9 ± 0.2	36.1 ± 0.2	258.2 ± 0.8
βCel-C_{12}	38.4 ± 0.1	32.3 ± 0.2	181.9 ± 0.5
βIsoMal-C_{12}	48.6 ± 0.2	26.6 ± 0.6	185.3 ± 0.6
	Experiment		Ref
βMal-C_{12}(L_α)	43 (20°)	33.5 (20°)	Auvray et al. (2001)
		41.5 (80°)	H. S. Nguan et al. (2010)
βMal-$C_{12}C_8$ (L_α)	53 (25°)	36.2 (25°)	H. S. Nguan et al. (2010)
βMal-$C_{14}C_{10}$ (L_α)	58 (25°)	36.9 (25°)	H. S. Nguan et al. (2010)
βMal-C_{14} (L_C)		38.2 (25°)	Ericsson, Ericsson, and Ulvenlund (2005)
βMal-C_{16} (L_C)		41.2 (25°)	Ericsson, Ericsson, and Ulvenlund (2005)

We note that the simulated average d-spacing value for βMal-$C_{12}C_{10}$ is 36.1 Å. This is larger than the values of the single chain glycolipids here, and is similar to the experimental values of Guerbet maltosides with $C_{12}C_8$ and $C_{14}C_{10}$ branches, which have d-spacings of 36.2 Å and 36.9 Å respectively at 25 °C (Table 4.1) (H. S. Nguan et al., 2010). As a consequence of this branching, βMal-$C_{12}C_{10}$ packs least well of the four glycolipid simulations, with the largest average volume, of 258.2 Å^3 (Table 4.1).

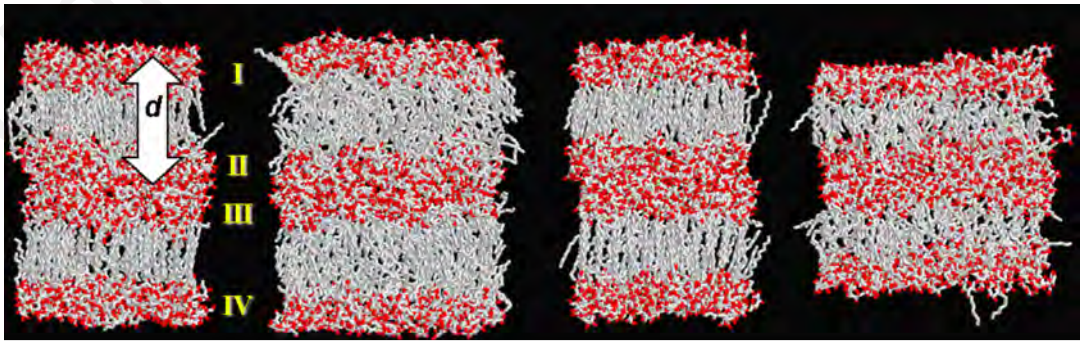

Figure 4.3: Molecular dynamics configuration at t=40 ns of lamellar assemblies and average interlayer spacing d of (a) βMal-C_{12} (b) βMal-$C_{12}C_{10}$ (c) βCel-C_{12} and (d) βIsoMal-C_{12}. Layers labeled I−IV.

4.1.2 Chain structure

We now characterize the simulated alkyl chain behavior of the four glycolipid assemblies. The C−D bond order parameter, $-\langle S_{CD}\rangle$ is given as a function of methylene carbon position in Figure 4.4. Here, we observe the overall trend is comparable for βMal-C_{12} and βCel-C_{12}, i.e.$-\langle S_{CD}\rangle$ profiles display a maximum at the 8^{th} methylene of the chain (ie. position C78 as defined in Figure 4.1. This parabolic chain ordering profile mirrors those obtained from previous simulations of chains of decanoate, DPPC and DMPC bilayers (Essex et al., 1994; Van der Ploeg & Berendsen, 1982, 1983). Here, $-\langle S_{CD}\rangle$ indicates that the alkyl chains of βCel-C_{12} are on average more aligned (more ordered) with the bilayer than those of the maltoside, with peak values (corresponding to the 8^{th} methylene unit) of 0.25 for βMal-C_{12} and 0.34 for βCel-C_{12} (Figure 4.4a).

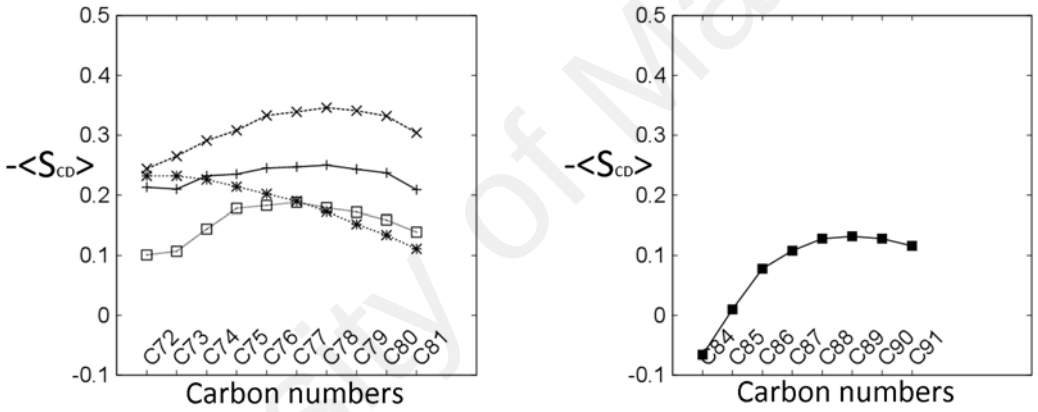

(a) The average order parameters, $-\langle S_{CD}\rangle$, for all the single chain lipids, βMal-C_{12} (+), βCel-C_{12} (×), and βIsoMal-C_{12} (∗) and (*sn*-1) chain in βMal-$C_{12}C_{10}$ (□).

(b) The average order parameters, $-\langle S_{CD}\rangle$, for (*sn*-2) chain in βMal-$C_{12}C_{10}$ system. (■).

Figure 4.4: Order parameter for (a) single chain lipids (βMal-C_{12}, βCel-C_{12}, βIsoMal-C_{12}) and (b) branched chain lipids βMal-$C_{12}C_{10}$. Connecting lines drawn only as a guide.

A cross-section through a typical MD snapshot for each of the four assemblies exemplifies this chain tilting behavior (Figure 4.6). However, for βIsoMal-C_{12}, $-\langle S_{CD}\rangle$ decreases monotonically across the chain order, to a more disordered state at the tail end (Figure 4.4a). For βMal-$C_{12}C_{10}$, from the values of $-\langle S_{CD}\rangle$ across chain length, the shorter *sn*-2 (C_{10}) chain is less ordered than the *sn*-1 (C_{12}) chain (Figure 4.4a). The maxima for the two chains are found at the 7^{th} and 9^{th} methlyenes for *sn*-1 and *sn*-2 respectively (Figure 4.4b). Interestingly, in contrast to the other chains, the *sn*-2 chain possesses an $-\langle S_{CD}\rangle$ with a small negative value, closer to the headgroup, indicating that the C−D bond is ordered to some degree parallel with respect to the bilayer normal.

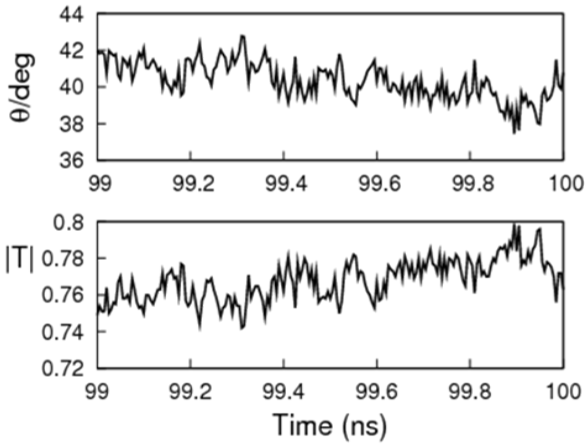

Figure 4.5: Short dynamic behavior for tilt vector and tilt angle θ for βMal-C_{12}

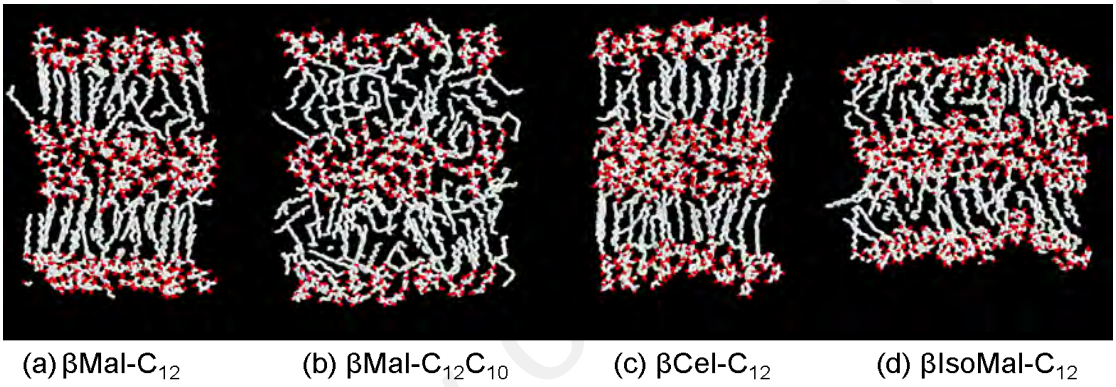

Figure 4.6: Representative MD configurations (*xy* slice)

These results are in qualitatively agreement to those measured for other lipid systems, for examples; 1-13-methylpentadecanoyl– 2-palmitoyl-phosphatidylcholine (13-MpPPC) and dimyristoylphosphatidylcholine (DMPC) by MD simulations (Lim & Klauda, 2011; Moore, Lopez, & Klein, 2001) and experiments (Nevzorov, Trouard, & Brown, 1999; Trouard et al., 1999). Obviously, these results differ quantitatively because of differing lipid structure, and environment (anhydrous *vs* aqueous conditions).

In order to quantitatively evaluate the degree of tilting in the bilayer assemblies, we calculate an ensemble-averaged tilt angle θ and tilt vector $\vec{T}$ for the four lamellar systems as described in Section 3.4.5. Here we use four different methods, labeled A−D (see Section 3.4.5); these approaches vary in their definitions of chain vector and degree of averaging (see Section 3.4.5).

Table 4.2: Average chain tilt angles and vectors by Methods A−D.

Lipid	***average tilt angle θ by method***				***average tilt vector $\lvert\vec{T}\rvert$ by method***			
	A	B	C	D	A	B	C	D
βMal-C_{12}	89.0 ± 0.4	38 ± 1	41 ± 2	38 ± 2	0.05 ± 0.02	0.79 ± 0.02	0.76 ± 0.03	0.91 ± 0.01
βMal-$C_{12}C_{10}$(*sn*-1)	91.0 ± 0.4	45 ± 2	54 ± 2	54 ± 1	0.17 ± 0.02	0.73 ± 0.02	0.60 ± 0.03	0.62 ± 0.01
βMal-$C_{12}C_{10}$(*sn*-2)	89.0 ± 0.9	70 ± 1	63 ± 1	66 ± 1	0.42 ± 0.02	0.49 ± 0.03	0.50 ± 0.01	0.50 ± 0.01
βCel-C_{12}	90.7 ± 0.3	36 ± 2	38 ± 2	32 ± 2	0.04 ± 0.01	0.83 ± 0.01	0.81 ± 0.02	0.87 ± 0.01
βIsoMal-C_{12}	89.3 ± 0.4	35 ± 2	39 ± 2	37 ± 2	0.05 ± 0.01	0.82 ± 0.02	0.78 ± 0.02	0.79 ± 0.02

Table 4.3: Layer and overall tilt angles θ (in deg), estimated from maxima of tilt angle distributions (Corrected Values in Parentheses), via *Method C*.

Layer	I	II	IV	V	Average
βMal-C_{12}	17	161(19)	18	162(18)	18
βMal-$C_{12}C_{10}$(*sn*-1)	20	160(20)	38	152(28)	27
βMal-$C_{12}C_{10}$(*sn*-2)	23	138(42)	31	155(25)	30
βCel-C_{12}	11	167(16)	12	(167(13)	13
βIsoMal-C_{12}	30	156(24)	25	157(23)	26

Method A, which indiscriminately averages tilt over the four layers of each system, yields average tilt angles close to 90° and tilt vectors close to zero, for each of the four glycolipid systems (Table 4.2). This indicates no net tilt over the four layers. The exception is the *sn*-2 chain of βMal-$C_{12}C_{10}$ which has a of 0.42. The surprisingly high non-zero value of the tilt modulus is due to the $x-y$ components of the tilt vector being non-zero on average, suggesting that while the z-component is not correlated on average across the four layers, the $x-y$ component is fairly correlated.

Methods B−D define tilt orientation of a single lipid leaflet. Here, for the monoalkylated systems of βMal-C_{12}, βCel-C_{12} and βIsoMal-C_{12}, we observe broad consensus of a 32−41° in tilt angle θ (or an average of 37°), with a corresponding tilt vector modulus in the range of ∼0.8−0.9 (Table 4.2). Interestingly, the value does not seem to vary strongly with headgroup identity. However, the actual value of θ seems rather high when compared to the recently reported value of 12° from x-ray studies on the L_C phase of a branched chain Guerbet glucoside (Hashim et al., 2010). For βMal-$C_{12}C_{10}$, the longer *sn*-1 chain is more tilted than the chains of the monoalkylated lipids, with an average tilt angle of 51°. However, the *sn*-2 chain appears to tilt yet more heavily, with a θ of ∼60−70° and of ∼0.5 (Table 4.2). We also note a level of negative correlation between the instantaneous values of θ and $\vec{T}$. This behavior is illustrated for βMal-C_{12} using *Method B* (Figure 4.5), although the observation appears to hold across method and lipid system; the complete set of angular correlation plots between normalized molecular vector and average tilt are given in Figure 4.7. This behavior is reasonable, given that, as angular tilt increases, the correlation between tilt directions must decrease for the monoalkylated

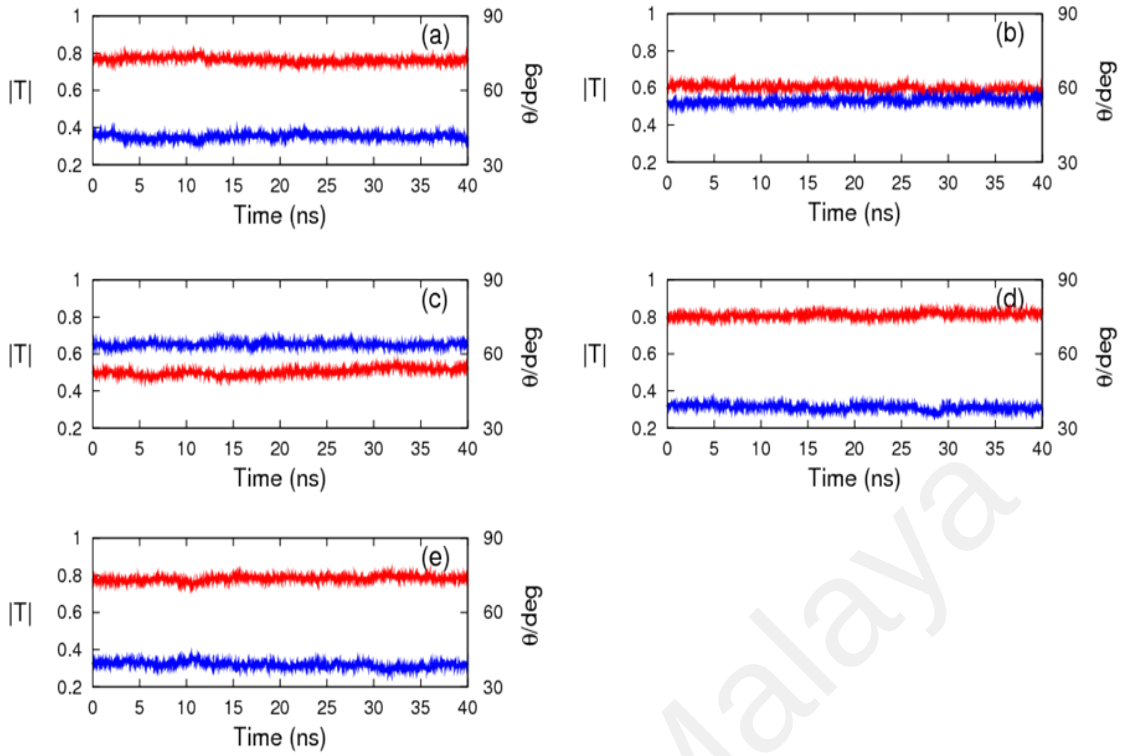

Figure 4.7: Angular correlation between normalized molecular vectors $\vec{S}_i$ expressed as the length $|\vec{T}|$ of the total vector, $\vec{T} = \frac{1}{N}\sum_{i=1}^{N}\vec{R}_i$ (plotted as red lines, on the left scale) and the angle θ of the average tilt (blue line and right scale). These quantities are plotted against time for the full 40 ns dynamics run for (a) βMal-C_{12}, (b) *sn*-1 for (c) *sn*-2 for βMal-$C_{12}C_{10}$ (d) βCel-C_{12}, (e) βIsoMal-C_{12}.

lipids. Finally, based on *Method C*, we consider the distribution of tilt angle, layer-by-layer, for the four glycolipid systems (Figure 4.8). It is evident that these distributions are skewed rather than Gaussian. The maxima of these distributions provide one further estimate of tilt angle (Table 4.3).

According to this measure, the tilt angles for layers I−IV of βMal-C_{12} are 17°, 161°, 18°, and 162°, respectively (Table 4.3). This provides a corrected average tilt angle of ∼18°, in rather closer agreement with the observed 12° tilt by the branched chain glucoside than the high Gaussian-based estimates of average tilt angle from methods A and B (Table 4.2). However, we note the approximate nature of this estimate given the uneven profile of the distributions in some cases (most particularly, the *sn*-2 chain of βMal-$C_{12}C_{10}$).

4.1.3 Headgroup structure

In each of the four simulated systems, the glycolipid headgroups are disaccharide moieties: β-maltose, β-cellobiose, and β-isomaltose. We first consider their flexibility. The $\Phi\Psi$ distributions resulting from the MD simulations indicate that, for all four systems, the

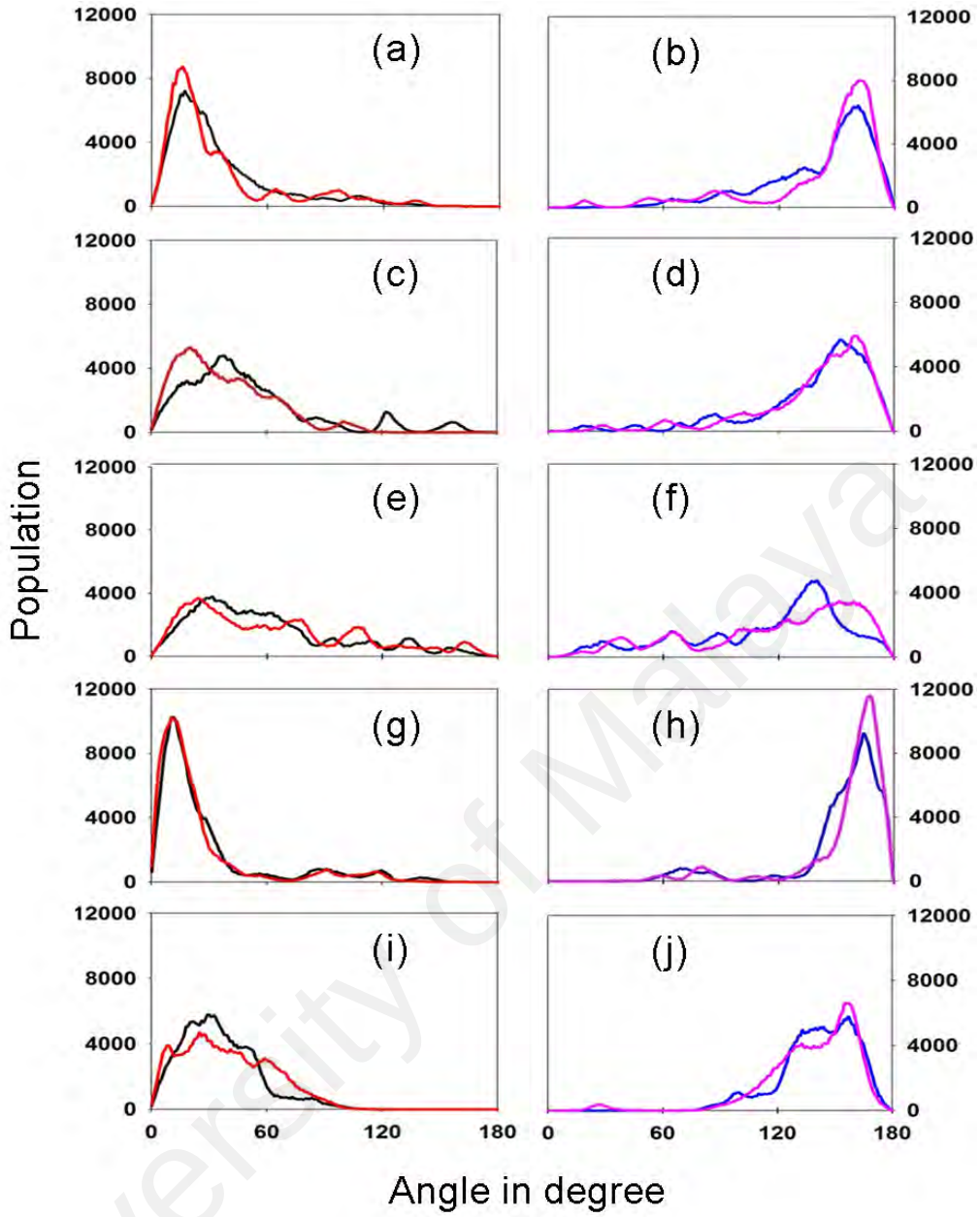

Figure 4.8: Distribution of alkyl chain tilt angle θ as a function of glycolipid layer using *Method C*. Label (a,b) for βMal-C_{12}, (c,d) for βMal-$C_{12}C_{10}$ (*sn*-1), (e,f) for βMal-$C_{12}C_{10}$ (*sn*-2), (g,h) for βCel-C_{12} and (i,j) for βIsoMal-C_{12}. Layer 1 is solid black line, Layer 3 is solid red line, Layer 2 is solid blue line and Layer 4 is pink color line.

glycosidic angles explore only one low energy $\Phi\Psi$ basin (see Figure 4.9). The distributions for βMal-C_{12}, βMal-$C_{12}C_{10}$, and βCel-C_{12} are similar in location and remain close to their crystallographic values. However, βIsoMal-C_{12} shifts from ($-49°$,$167°$) to a $\Phi\Psi$ minimum at around ($-130°$,$-55°$). Due to its α-(1$\rightarrow$6) linkage, βIsoMal possesses a third glycosidic torsion angle, Ω, which describes rotation around the C5'–C6' bond. In our simulation, this angle proved flexible, with its average value of $50°$ bounded by a standard deviation of $\sim 91°$. The higher value of standard deviation compared to it average

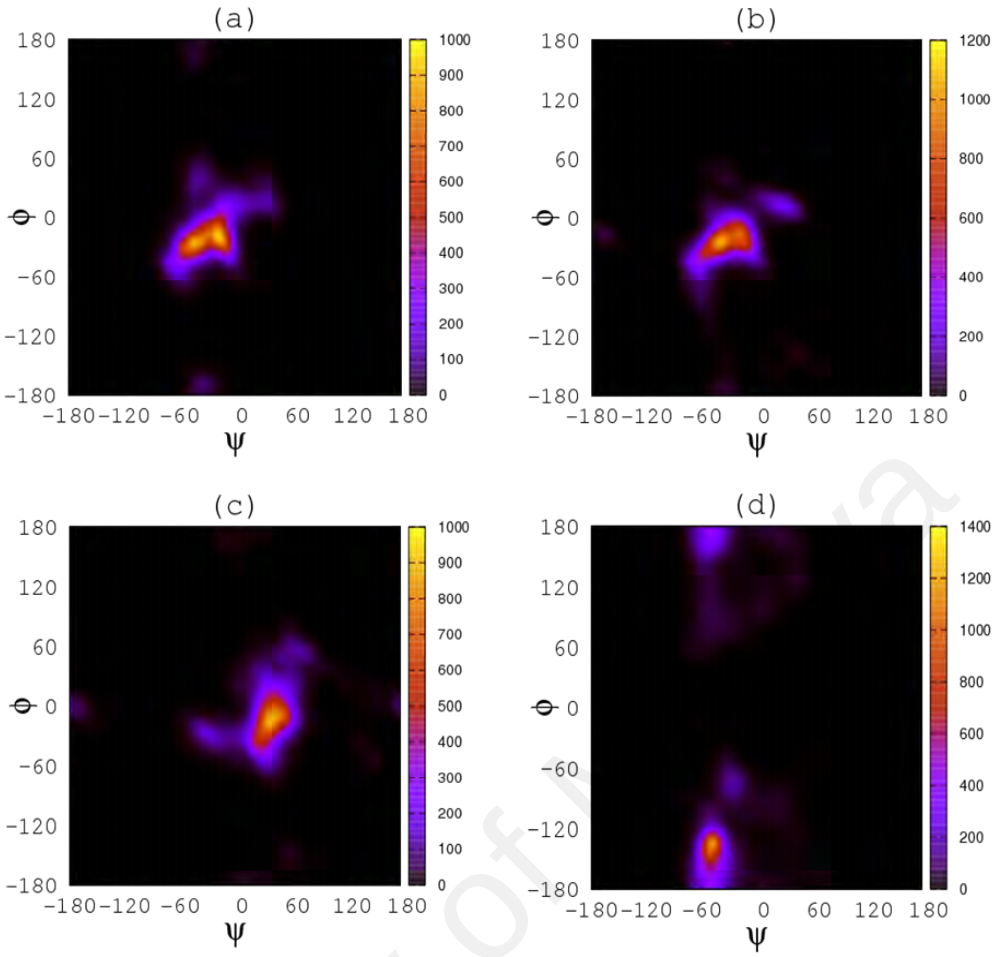

Figure 4.9: Ramachandran plots of Φ (H1-C1-O1-C4'), and Ψ (C1-O1-C4'-H4') for (a) βMal-C_{12}, (b) βMal-$C_{12}C_{10}$, (c) βCel-C_{12}, (d) βIsoMal-C_{12}.

statistically indicate the huge differences between the torsion angle values. We note that MD simulations have found the α-(1→6) linkage of isomaltose in aqueous solution to be more flexible than the α-(1→4) linkage of maltose (Best, Jackson, & Naidoo, 2001).

We next consider the polar interactions of the disaccharide headgroups. In theory, with each disaccharide possessing seven polar hydrogens are able to donate a hydrogen bond and 11 oxygens are able to accept 2 hydrogen bonds, where the maximum possible number of hydrogen bonds a headgroup can make is 29. Unsurprisingly, simulations of 7 disaccharides in aqueous solution, including maltose, have observed far less than this idealized theoretical value, with 12–13 hydrogen bonds to water typically formed by the solute (Cheetham & Dasgupta, 2006). Here, given the significant orientational constraints of a thermotropic bilayer, besides the restriction of the steric bulk and covalent structure of the lipids themselves, the hydrogen bonding interactions between headgroups are fewer still. Indeed, we find that the total number of intermolecular hydrogen bonds formed between

Table 4.4: Fractional Population of Hydrogen Bonds between Headgroups within a Layer (n_{intra}) and Both within and Across a Layer (n_{total})[a].

Lipid	n_{intra}	n_{total}	T^*/°C	Ref
βMal-C_{12}	3.9	7.2	245	(Marcus, 1986)
βMal-$C_{12}C_{10}$	3.8	6.7	n/a	
βCel-C_{12}	3.8	7.2	208	(Koeltzow & Urfer, 1984)
βIsoMal-C_{12}	3.5	7.2	154,157	(Koeltzow & Urfer, 1984)
βGlc-C_8	2.7	3.5	107	(Vill et al., 1989)

[a]Standard deviation varies between 0.10 and 0.15 hydrogen bonds. Literature values of clearing temperature (T^*) also reported, in °C.

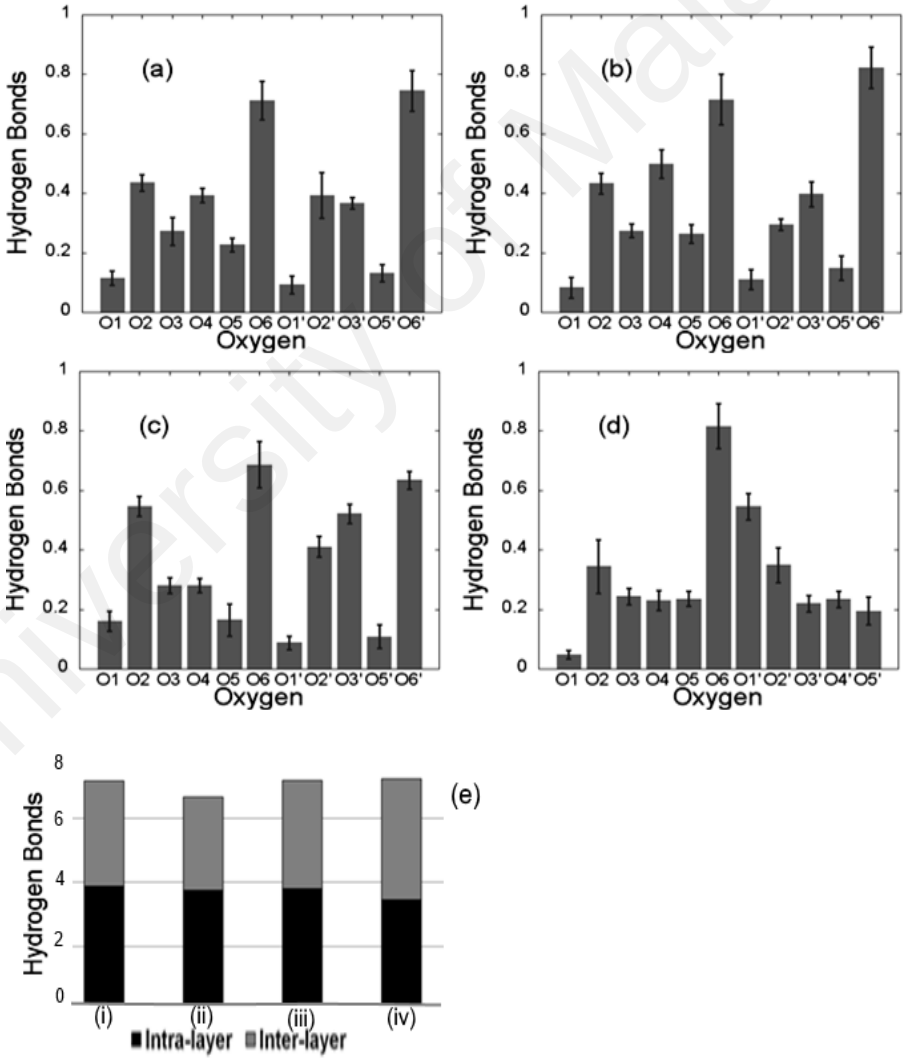

Figure 4.10: Intralayer hydrogen bond distribution over different oxygen locations (see 4.1) for (a) βMal-C_{12}, (b) βMal-$C_{12}C_{10}$, (c) βCel-C_{12}, and (d) βIsoMal-C_{12}. (e) Total number of hydrogen bonds for (i) βMal-C_{12}, (ii) βMal-$C_{12}C_{10}$, (iii)βCel-C_{12} and (iv)βIsoMal-C_{12}, comprised of interlayer (gray) and intralayer hydrogen bonds (black).

headgroups (i.e., both intra- and interlayer) range from 6.7 to 7.2 (Table 4.4). This value is approximately double that observed from thermotropic bilayer simulations of βGlc-C_8 , where an average of only 3.5 total hydrogen bonds were formed per headgroup (Chong et al., 2007). Interestingly, we observe that $\sim$55% of intermolecular hydrogen bonds formed are intralayer, except for the alkyl isomaltoside, where intra- and interlayer hydrogen bonds are formed in approximately equal proportions (see Table 4.4, Figure 4.10e).

It is also instructive to consider the distribution of intralayer hydrogen bonds as a function of oxygen sites around the sugar ring (Figure 4.10a–d). The distribution profiles for βMal-C_{12} and βMal-$C_{12}C_{10}$ are similar, both qualitatively and quantitatively (Figure 4.10a,b). In both cases, the greatest hydrogen bonding is predicted at O6 and O6' of $\sim$0.8 bonds (see Figure 4.1 for atom labeling); there is also significant hydrogen bonding at O2' and O3' of the reducing sugar and O2 and O4 of the nonreducing sugar. Overall, however, the branched chain glycolipid makes half a hydrogen bond less on average, relative to its single chain counterpart (n total, Table 4.4). The profile for βCel-C_{12} is broadly similar to βMal-C_{12}; the hydrogen bonding at O6 and O6', although slightly less at $\sim$0.7 interactions, lies within a standard deviation of the βMal-C_{12} values (Figure 4.10c). Greater hydrogen bonding for βCel-C_{12} is seen at O2 and O3' (Figure 4.10c) such that n total remains $\sim$7 hydrogen bonds (Table 4.4). Interestingly, the β-(1$\rightarrow$4) linkage of βCel-C_{12} appears to make these two proximal OH's (O2 and O3') more available for interaction with the OH's of neighboring glycolipids. However, the distribution for βIsoMal-C_{12} is quite distinct from the other three systems (Figure 4.10d). Relative to βMal-C_{12}, βMal-$C_{12}C_{10}$, and βCel-C_{12}, the O6 of βIsoMal-C_{12} also makes $\sim$0.8 hydrogen bonds but now O1 (bonded to C6') is largely unavailable for interaction due to its involvement in the α-(1$\rightarrow$6) linkage (Figure 4.10d).

4.1.4 Discussion

We have examined lamellar simulation models of four glycolipid systems, βMal-C_{12}, βMal-$C_{12}C_{10}$, βCel-C_{12}, and βIsoMal-C_{12}, exploring the effect on assemblage structure and dynamics of chain branching and different disaccharide headgroups. Considering first the effect of introducing a second, C_{10} alkyl chain into βMal-C_{12}, we observe an increased surface area per lipid (A) and an increased interlayer distance (d) (Table 4.1). Its bilayer spacing is comparable to Guerbet maltosides with $C_{12}C_8$ and $C_{14}C_{10}$ branched chains,

where both have been confirmed by optical polarizing microscopy and x-ray studies to exhibit an L_α phase at room temperature (Hashim et al., 2010, 2006). This increase in *A* and *d* arises from the increased volume occupied by the additional chain, which is on average 75 $Å^3$ larger than for βMal-C_{12} (Table 4.1). The *sn*-1 and in particular *sn*-2 chains of βMal-$C_{12}C_{10}$ are less ordered than the chain of dodecyl maltoside molecules. The average degree of tilt of the *sn*-1 chain is larger compared to that of βMal-C_{12} (Table 4.2 and 4.3). However, the *sn*-2 chain is more highly tilted than both, also occupying a wide range of tilt angles (Figure 4.8). The pattern of hydrogen bonding between headgroups is very similar for single and branched chain analogues; however, branching reduces the number of these hydrogen bonding interactions; this is possibly due to the greater packing constraints of increased steric congestion.

We also consider the effect of variation in disaccharide headgroup. βMal-C_{12} possesses an α-(1→4) linkage between its two glucosyl residues, whereas βCel-C_{12} is the β-(1→4) isomer. This configuration leads to subtly different predicted patterns in hydrogen bonding (Figure 4.10a,c) but approximately similar numbers of interactions between headgroups (Figure 4.10e, Table 4.4). Their chain regions appear comparable in structural and dynamic properties: for both, the chains are ordered (Figure 4.4a). This observation supports numerous experimental observations that these glycolipids exist in an ordered lamellar phase (L_C) or gel phase (L_β) at room temperature (Koeltzow & Urfer, 1984; Ryohei, 1958; Vill et al., 1989) Both chains also exhibit a maximum in order at their eighth carbon, a profile similar to that witnessed in simulations of other lipid bilayer systems (Essex et al., 1994; Van der Ploeg & Berendsen, 1982, 1983). For monosaccharide glycolipids, it has been suggested that the relative orientations of the C4 epimer and anomeric linkage influence the value of intralayer hydrogen bonding (Hashim et al., 2011). Thus, when these features are "*cis*" with respect to each other, as in the case of the alkyl β-galactoside and α-glucoside, the systems have higher clearing transitions, compared to those with a "*trans*" orientation, for example, alkyl α-galactoside and β-glucoside. Extending this idea to disaccharide lipids, we expect higher hydrogen bonding interactions for βCel-C_{12}, reflecting the *trans*−*trans* configurations, compared to βMal-C_{12} which has a *cis*−*trans* configuration. Our present investigation is unable to confirm this, but we note that, experimentally, the corresponding αMal-C_{12} (*cis,cis*) (Vill, Bocker, Thiem, &

Fischer, 2006) and αCel-C_{12} (*cis,trans*) have clearing transition temperatures of 205 °C and 224 °C, respectively, indicating that the above hypothesis is not unreasonable.

In this work, we find the most prominent difference in simulated properties by comparing βMal-C_{12} (or indeed βCel-C_{12}) with βIsoMal-C_{12}. The α-(1→6) linkage in the latter leads to significant changes in predicted bilayer properties: the surface area per headgroup is 10 $Å^2$ larger than for βMal-C_{12} or βCel-C_{12}, and the spacing d between layers is 18−19% less (Table 4.1). The ordering of the βIsoMal-C_{12} alkyl chain decreases monotonically toward its tip, as opposed to displaying a maximum around the eighth methylene (Figure 4.4a). Indeed, the chain order parameter for βIsoMal-C_{12} is small, suggesting its hydrophobic region may not be in an ordered lamellar phase, as implied by the experimental studies reported previously (Koeltzow & Urfer, 1984). The overall average tilt (Table 4.3) and its distribution (Figure 4.8) are different for the regioisomers (1→6 vs 1→4 glycosidic bond), with a broader distribution seen for βIsoMal-C_{12}.

Due to the presence of an additional covalent bond in the glycosidic linkage of βIsoMal-C_{12}, significant differences in the hydrogen bonding pattern for regioisomers are also observed (Figure 4.10a,d). Indeed, a slight increase in interlayer hydrogen bonding of headgroups occurs (Table 4.4). This appears to arise from greater exposure of the disaccharide group due to the extended structure of the 1→6 glycosidic linkage, and hence, its larger surface area (Table 4.1). This C5'−C6' bond is conformationally variable but also physically projects the nonreducing residue of the disaccharide headgroup further out from the chain region, making the headgroups more available for interaction. The alkyl chain is less ordered than in the corresponding (1→4)-linked malto- and cellobioside, and the interface region appears significantly undulated. Coiling of chain and undulation are consequences of increased surface area (Figure 4.6), which places constraints on the packing of the alkyl chains. These rather large differences in simulated structure between βMal-C_{12} and βIsoMal-C_{12} are reflected in a marked difference in observed clearing temperature, on the order of 100 °C (Table 4.4). This much lower clearing temperature for βIsoMal-C_{12} is also reflected by the lower number of predicted intralayer hydrogen bonds formed by its bilayer assembly (Table 4.4) (Chong et al., 2007).

For the two different β-(1→4) linked glycolipids, we find that cellobioside has a higher chain order parameter of about 0.34 (Figure 4.4a) compared to the corresponding α-(1→4)-linked maltoside (∼0.25). This is a reflection of cellobiose's more linear ribbon-

like structure compared to the bent shape of maltose, which gives rise to the helical turning in higher oligomers, (Hato, 2001; Hato et al., 1999) and thus influences chain order. This would suggest that the sugar groups pack more compactly in the cellobioside assembly compared to that of the maltoside. However, experimentally, the clearing transition temperature for maltoside (245 °C) is higher than that for the cellobioside (208 °C); (see Table 4.4) (Koeltzow & Urfer, 1984; Marcus, 1986). These observations suggest that extrapolation from tertiary homopolysaccharide structures is insufficient to account for the different clearing transitions of the glycosides.

Finally, we comment on the issue of chain orientation in the hydrophobic region. Previously, shorter chain monoalkyl glucopyranoside crystals have been reported as having head-to-head bilayer interdigitated chains or head-to-tail monolayers with no interdigitation (Jeffrey, 1990a; Jeffrey & Rosenstein, 1964; Jeffrey, Ruble, & Sepehrnia, 1985; Jeffrey, Yeon, & Abola, 1987). Alternatively, many natural glycolipids are found to pack in a tilted and not interdigitated form (Abrahamsson, Dahlen, & Pascher, 1977). Recent x-ray studies for longer chain length monoalkylated glycolipids (Ericsson, Ericsson, & Ulvenlund, 2005) found the L_C phase to be both interdigitated as well as tilted. In addition, the Guerbet glycoside C_8 was also found to be in a tilted L_C phase, with an estimated tilt angle of $\sim$12° from x-ray analysis (N. J. Brooks et al., 2011; Hashim et al., 2010). The present glycolipid simulations also observe stable tilted chain orientations, ranging from 13 to 26° depending on headgroup. The tilt observed here is also comparable to that estimated from earlier bilayer simulations of decanoate (10°), (Van der Ploeg & Berendsen, 1982) DPPC ($\sim$22°), and DPPE (19°) (Róg et al., 2007). This is also a similar finding to simulations of glycoglycerolipids containing glucosyl or galactosyl headgroups with phosphatidylcholine tails; there, tilt angles on the order of 19–20° were observed (Róg et al., 2007).

It is interesting to consider the estimate of net chain tilt using *method A*. This method averages tilt over layers without correcting for leaflet orientation. For all the glycolipids considered, the values of tilt via this method are around 90° (Table 4.2). Thus, each layer is tilting but there is no effective averaged tilt over a larger length scale, albeit here we only consider a four-layer glycolipid system. This may support previous claims of uncorrelated tilting in the hydrophobic region of glycolipids due to the hydrophilic region acting as a barrier to transmission of tilt information; (Abeygunaratne et al., 2006; Vill et al., 2006) this in turn could point to a possible low frequency relaxation process, found previously,

for example, in the Goldstone mode in tilted smectic C monophilic liquid crystals. Larger simulation cells however are warranted to explore this aspect further.

4.2 Conformational dynamics of dry lamellar crystals of sugar based lipids: an atomistic simulation study

Nothing in life is to be feared, it is only to be understood. Now is the time to understand more, so that we may fear less.
Marie Curie (1867-1934)

Although this section is related to the previous one in terms of condition and material (dodecyl β-maltoside, dodecyl β-cellobioside, dodecyl β-isomaltoside and a $C_{12}C_{10}$ branched β-maltoside), but the current simulation work was temporally extended to 200 ns. This extension helped to determine the dynamical behavior of the lipids, especially segments like reducing, non-reducing and chain in the bilayers. We also made an attempt to understand the dynamics between the branched alkyl chains and the sugar groups at the hydrophilic region. Finally, this section ends with the Discussion. (This work has been published in 2014 at: PLoS ONE 9(6): e101110)

4.2.1 Stability and structural properties of bilayers

In order to evaluate the equilibration of the four glycolipid bilayer systems, the time evolution of the surface area per lipid at the interface (A) and the local density profiles (LDP) were assessed over the 200 ns simulation (Figure 4.11 and 4.12 respectively). The four bilayer assemblies, βMal-C_{12}, βCel-C_{12}, βIsoMal-C_{12} , and βMal-$C_{12}C_{10}$ remained intact over the simulations and achieved equilibrium with respect to A and LDP by 40 ns. In the subsequent analyses, we, therefore, take the last 160 ns of each trajectory. The average area per lipid (A) and the d-spacing from the LDPs during the production stage are given in Table 4.5. Compared to the reported values in Section 4.1 in our replicate simulations here, A for the four glycolipid systems are similar to within the error; the d-spacing differ by about 3–16%. These variations could be attributed in part to the slight difference in simulation methodology: as opposed to the isotropic pressure scaling used in our previous study, here we apply fully anisotropic pressure scaling throughout the simulation, following the work of Doxastakis, Sakai, Ohtake, Maranas, and De Pablo (2007) on simulating the melting of phospholipid membranes under anhydrous conditions.

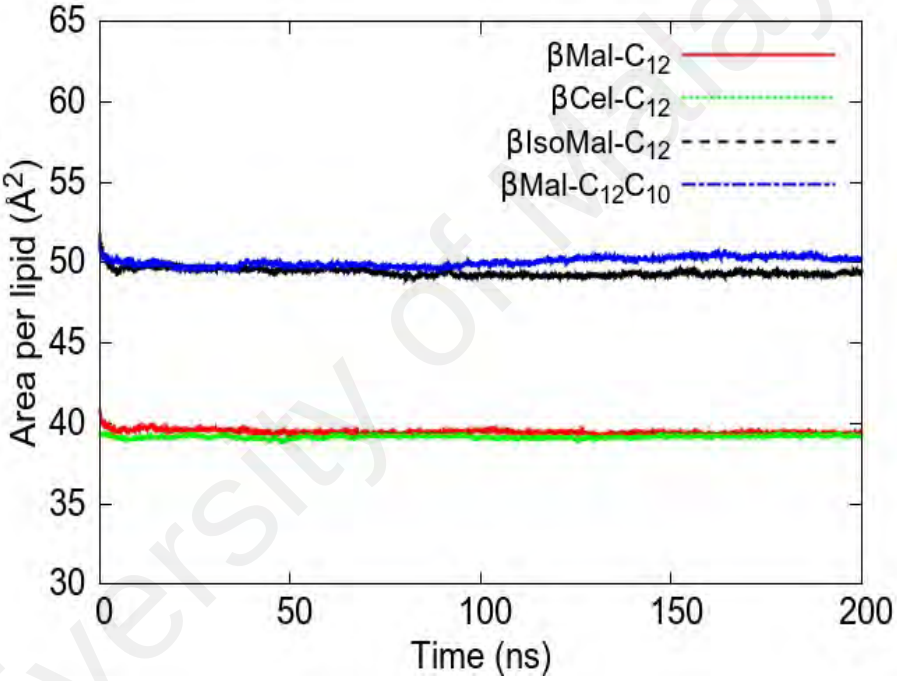

Figure 4.11: Area per lipid of βMal-C_{12}, βCel-C_{12}, βIsoMal-C_{12}, and βMal-$C_{12}C_{10}$.

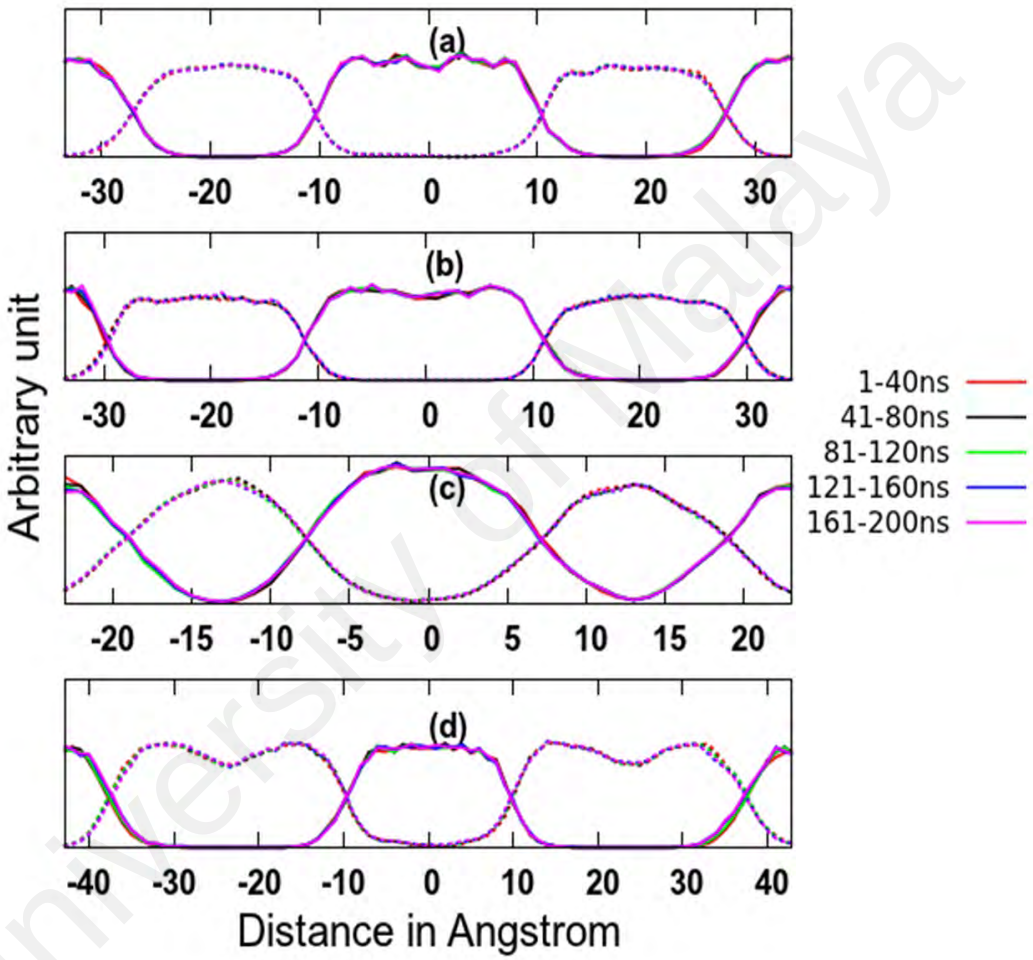

Figure 4.12: Local density profile. Each plot comprises 40 ns blocks of averages.(a) βMal-C_{12}, (b) βCel-C_{12}, (c) βIsoMal-C_{12}, and (d) βMal-$C_{12}C_{10}$.

Table 4.5: Average values at 27 °C of the simulated area per lipid, A and the bilayer spacing, d.

Lipids	Area per lipid, A/Å^2	Bilayer spacing, d/Å	Peak value of - Chain tilt angle, $\theta°$
βMal-C_{12}	39.4 ± 0.2 (38.8 ± 0.2)	32.2 ± 0.1 (32.9 ± 0.5)	18 ± 1 (18)
Experiment (Auvray et al., 2001)			
	43(20 °C)	33.5 (20 °C)	
		45.5 Å (at 80 °C)	
βCel-C_{12}	39.2 ± 0.2 (38.7 ± 0.1)	34.1 ± 0.1 (32.3 ± 0.2)	15 ± 1 (13)
βIsoMal-C_{12}	49.1 ± 0.3 (48.6 ± 0.2)	22.9 ± 0.2 (26.6 ± 0.6)	42, 59 ± 3 (26)
βMal-$C_{12}C_{10}$(*sn*-1)	50.1 ± 0.3 (51.9 ± 0.2)	41.9 ± 0.2 (36.1 ± 0.2)	24, 156 ± 3 (*sn*-1) (27)
βMal-$C_{12}C_{10}$(*sn*-2)			24, 156 ± 3 (*sn*-2) (30)
Experiment (Hamid et al., 2014)			
βMal-$C_{12}C_8$	53 (25 °C)	36.2 (25 °C)	
βMal-$C_{14}C_{10}$	58 (25 °C)	36.9 (25 °C)	

(Values in parenthesis are from Section 4.1)

4.2.2 Alkyl chain packing

The packing within the chain region for the βMal-C_{12}, βCel-C_{12}, and βIsoMal-C_{12} was assessed by computing the radial distribution function, giving the particle density variation as a function of distance from a reference particle, selected to be the carbon atoms C72, C76, and C81 along the hydrophobic chain. For all the three monoalkylated systems, the principal peaks in the RDF are around 5.1 Å, with the errors for βMal-C_{12} and βCel-C_{12} within $\pm$ 0.2 Å while for βIsoMal-C_{12} $\pm$ 0.5 Å, (Figure 4.13). The errors were estimated using 20 ns block averages. The RDF of βIsoMal-C_{12} shows a broader first maximum peak for all the three carbons along the alkyl chain (Figure 4.13c) compared to βMal-C_{12} and βCel-C_{12} (Figure 4.13a, b). While the peak locations are nearly the same for all systems, the broadening around the peak in the isomaltoside RDF is considerably larger than for the others, suggesting that the βIsoMal-C_{12} chains are less ordered compared to the other two monoalkylated lipids, despite being in the same phase. Furthermore, for isomaltoside, the second last carbon, C81, is more structured, while in the maltoside and cellobioside, it is the carbon closest to the headgroup, C72, which is more structured. To examine this observation visually, we have superimposed a vector (in yellow) for every chain in a given configuration snapshot (Figure 4.14). This figure points to a tighter packing in βCel-C_{12} compared to βMal-C_{12}, while for βIsoMal-C_{12} the chain vectors are more randomly orientated due to an increase in lateral area related to the α(1–6) glycosidic linkage. It also appears that some of the *sn*-2 chain vectors of the branched chain maltoside appear to protrude into the sugar region (Figure 4.14), while such protrusions are less obvious for its *sn*-1 vectors. The protrusion of the branched chain maltoside will be discussed in detail later.

4.2.3 *Gauche-trans* population for alkyl chain

The *gauche* populations were computed (as described in Section 3.4.7) for the lipid chains for βMal-C_{12}, βCel-C_{12} and βIsoMal-C_{12} in their L_C phase (Figure 4.15a–c) and for βMal-$C_{12}C_{10}$ in the L_α phase (Figure 4.15d–e). We find the monoalkylated glycolipids possess a low proportion of *gauche* conformations relative to *trans* conformations; for example, the average *gauche* populations for βCel-C_{12} and for βMal-C_{12} are 14 $\pm$ 3% and 16 $\pm$ 3%, respectively (Figure 4.15a & b).

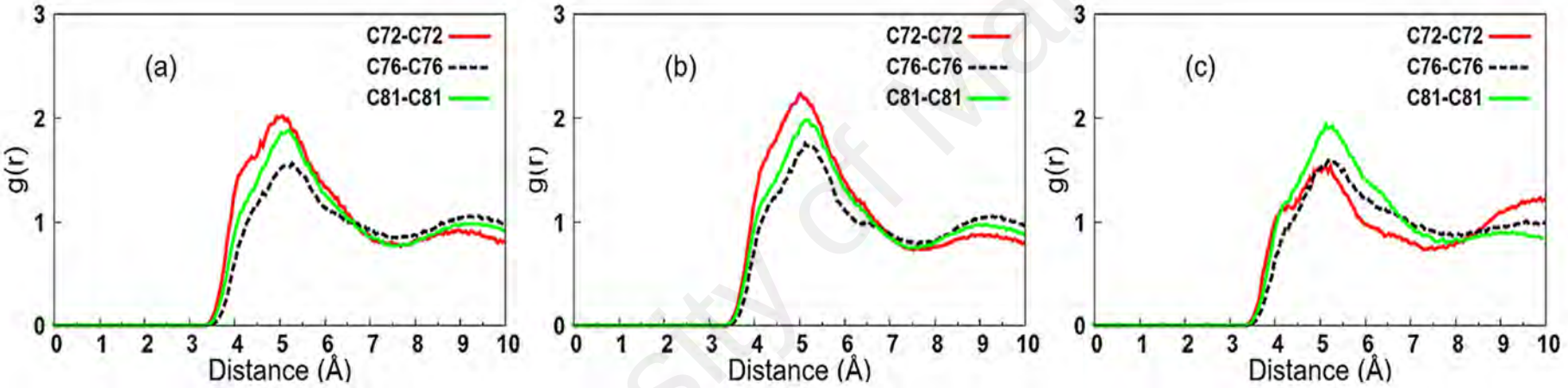

Figure 4.13: Radial distribution function for three carbon atoms along the alkyl chain for monoalkylated lipids: (a) βMal-C_{12}, (b) βCel-C_{12}, and (c) βIsoMal-C_{12}.

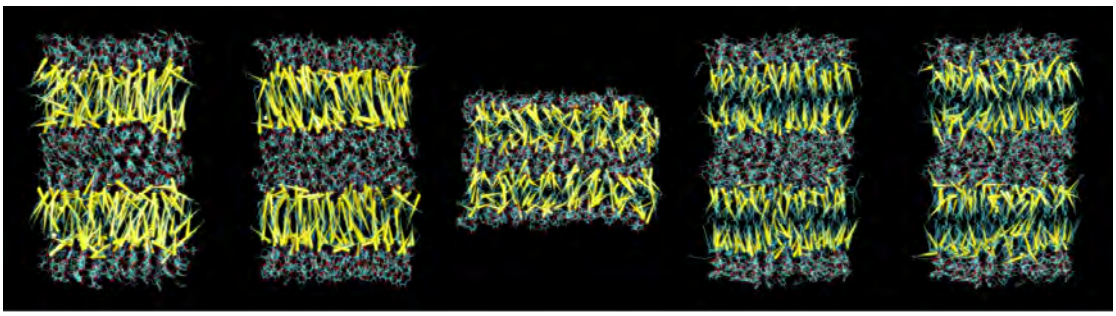

Figure 4.14: Snapshot of chain vectors between midpoints of C71–C72 and C80–C81 for monoalkylated lipids and chain *sn*-1. For chain *sn*-2, the vector is defined between midpoints of C71–C72 and C90-C91.

To within error, these results show that both βCel-C_{12} and βMal-C_{12} have similar *gauche* populations despite the fact that the former has two glucose units equatorially connected at the C1-O1 bond, while in the latter, the two units are axially connected (see Figure 4.1). The closely packed headgroups possibly induce the chains to align closer to each other, restricting isomeric rotation, and leading to fewer kinks or bending along the chain. βIsoMal-C_{12} has a higher predicted gauche population ($20 \pm 4\%$); its larger volume and area per lipid, as reported in Section 4.1 correlates with more freely rotating and flexible chains. For the branched glycolipid, βMal-$C_{12}C_{10}$ (in the L_α phase), although it has the same headgroup as βMal-C_{12} (in the L_C phase), the branching at C72 (Figure 4.1b) gives an overall increase in volume and headgroup area A. This corresponds to a significant increase in *gauche* population in the branched chain *sn*-1 (Figure 4.15d). Additionally, the *sn*-2 chain possesses a gauche population ranging from 40% (close to the sugar head) to 10% (at the tail end). The *gauche* profiles for *sn*-1 and *sn*-2 (Figure 4.15d and e) look similar in general. However, upon closer examination within each leaflet, close to the headgroup, the first four gauche fractions differ slightly with no definite pattern. This slight differentiation may cause unequal flexibility or mean curvature between leaflets leading to bilayer asymmetry (Domanov & Kinnunen, 2006; Lipowsky, 2013).

4.2.4 Rotation motions

Dynamics in the L_C phase is understandably limited compared to the L_α phase. Within this more restricted dynamical landscape, we seek to examine if there are dynamical features that differ as a function of stereochemical changes of glycolipid in the self-

assembled system. To this end, we examine the rotational modes of the alkyl chain and sugar headgroups.

Alkyl chain

Generally, rotational diffusion in the anhydrous glycolipid systems is slow (on the nanosecond timescale) for the alkyl chain C−H vectors in the chain region, unlike those reported for hydrated phospholipid bilayers in an L_α phase (P. Niemelä et al., 2004; P. S. Niemelä, Hyvönen, & Vattulainen, 2006). As a whole, the rotational autocorrelation functions $C_2(t)$ show a decreasing trend with time. However, upon closer scrutiny (Figure 4.17), the correlation times of the C−H vectors next to the sugar group are higher than those vectors further away from the sugar group. This observation agrees with a recent study on an anhydrous DPPC (dipalmitoylphosphatidylcholine) bilayer (Doxastakis et al., 2007) suggesting the tail region closer to the headgroup is mainly experiencing vibrations, with only a small number of conformation transitions.

When compared to the chains of βCel-C_{12} and βMal-C_{12}, the alkyl chain of βIsoMal-C_{12} shows slightly higher $C_2(t)$ values for carbons close to the headgroup (Figure 4.17). For example, C71 has a correlation time about 45 ns compared to 40 and 38 ns for βCel-C_{12} and βMal-C_{12} respectively (Figure 4.17). However, towards the end of the tail, the alkyl chain of βIsoMal-C_{12} has slightly lower correlation times compared to βCel-C_{12} and βMal-C_{12}. Thus, the alkyl chain carbons of βIsoMal-C_{12} appear to be more restricted in rotational motion involving carbons near the headgroup compared to the tail; the latter effect correlates with the chain disorder and partial interdigitation of βIsoMal-C_{12} compared to the other monoalkylated lipids (Figure 4.14). In the βMal-$C_{12}C_{10}$ system, the first two carbons in *sn*-1 chains show higher correlation time compared to those in the monoalkylated systems. On the other hand, the rest of the carbons behave similarly, as those in the single chain lipids, including *sn*-2.

Sugar head

A disaccharide unit contains two simple sugars connected via a flexible glycosidic bond, which allows each sugar moiety to rotate within its vicinity. We have determined the rotational diffusion of the sugars at the headgroup region using eq. (3.24).

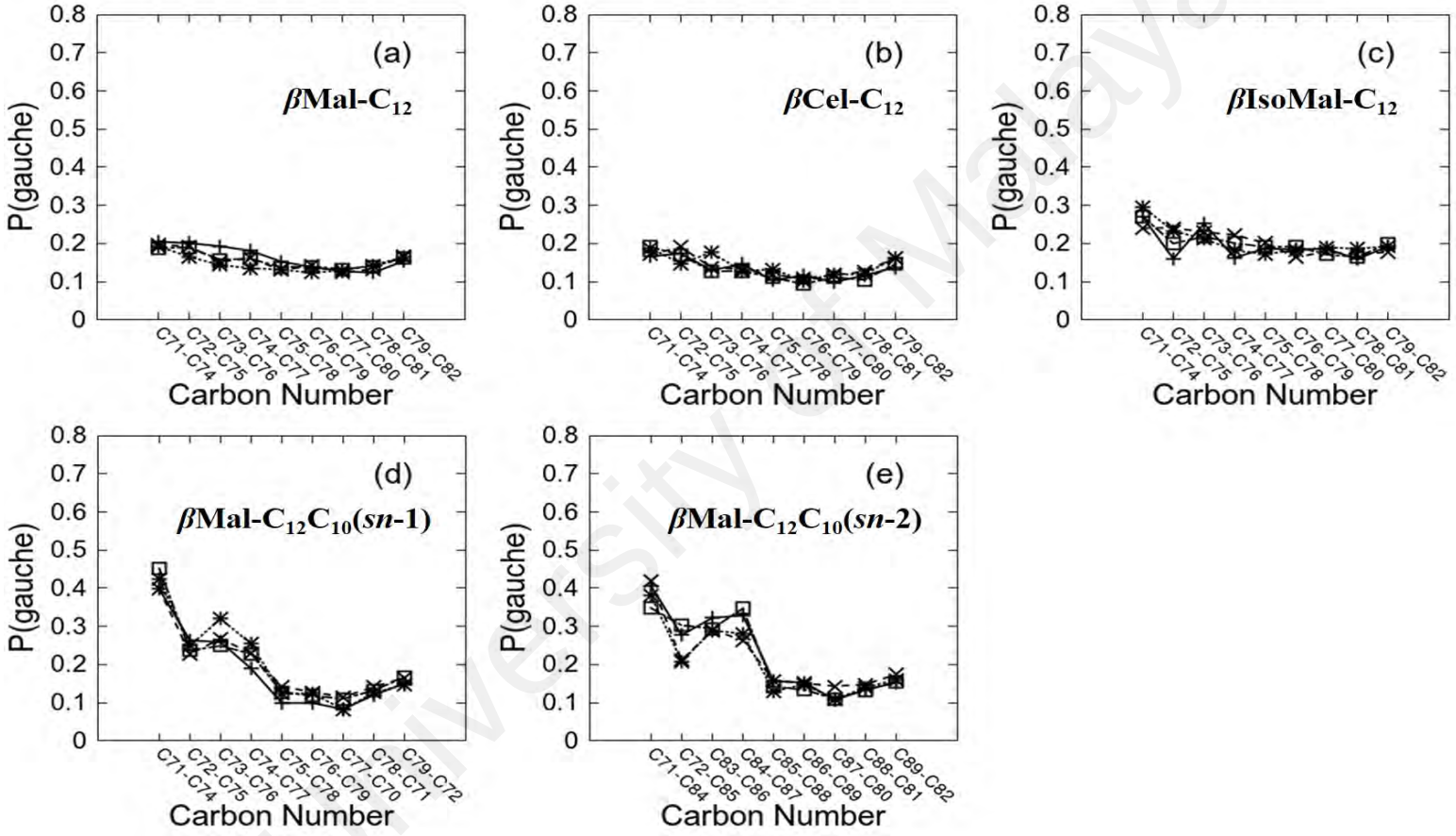

Figure 4.15: Fractional *gauche* polulation in, *P(gauche)*, dihedral angles between carbons in the alkyl chains. The dihedral angle label, for example C71–C74 represent C71–C72–C73–C4 following alkyl chain numbering in Figure 4.1. (a) βMal-C_{12}, (b) βCel-C_{12}, (c) βIsoMal-C_{12} , (d) βMal-$C_{12}C_{10}$. First lipid layer (□), second layer (×), third layer (+), and fourth layer (∗).

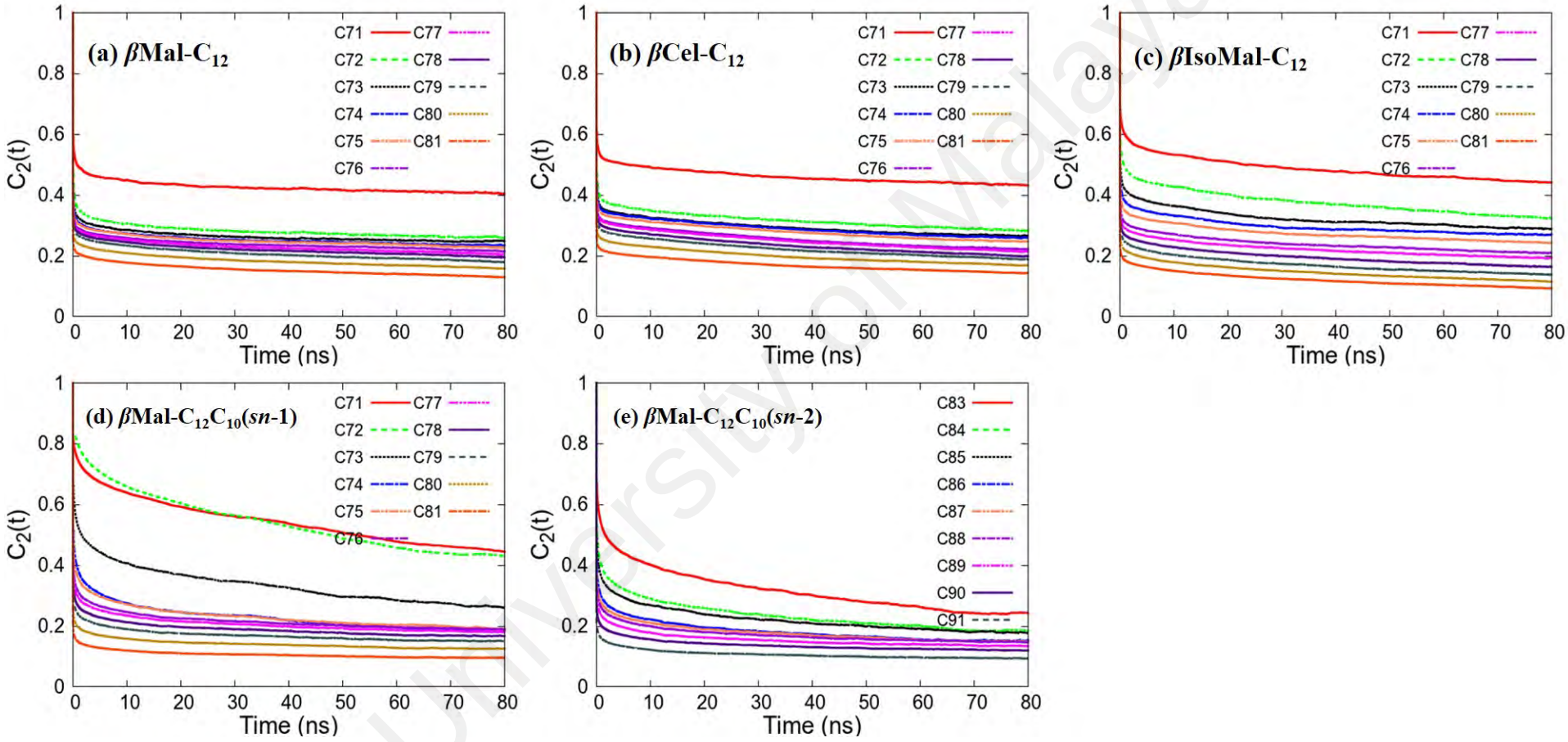

Figure 4.16: Correlation functions for each C−H vector along lipid alkyl chains are shown. The legend shows the carbon atoms following the numbering in Figure 4.1.

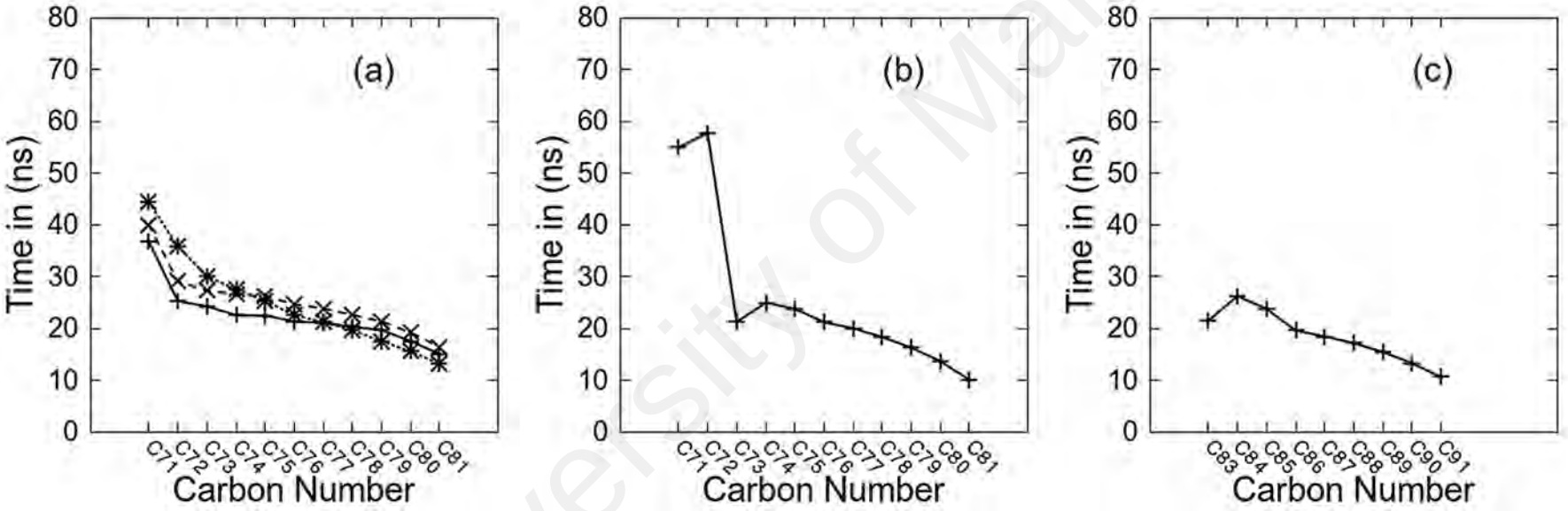

Figure 4.17: Correlation times as a function of each C−H vector along lipid alkyl chains are shown. The labeling of carbon atoms follows the naming convention as in Figure 4.1. (a) shows the correlation times for monoalkylated glycolipids, βMal-C_{12} (+), βCel-C_{12} ($\times$), and βIsoMal-C_{12} ($*$). (b) and (c) show correlation times for chains *sn*-1 and *sn*-2 respectively for βMal-$C_{12}C_{10}$.

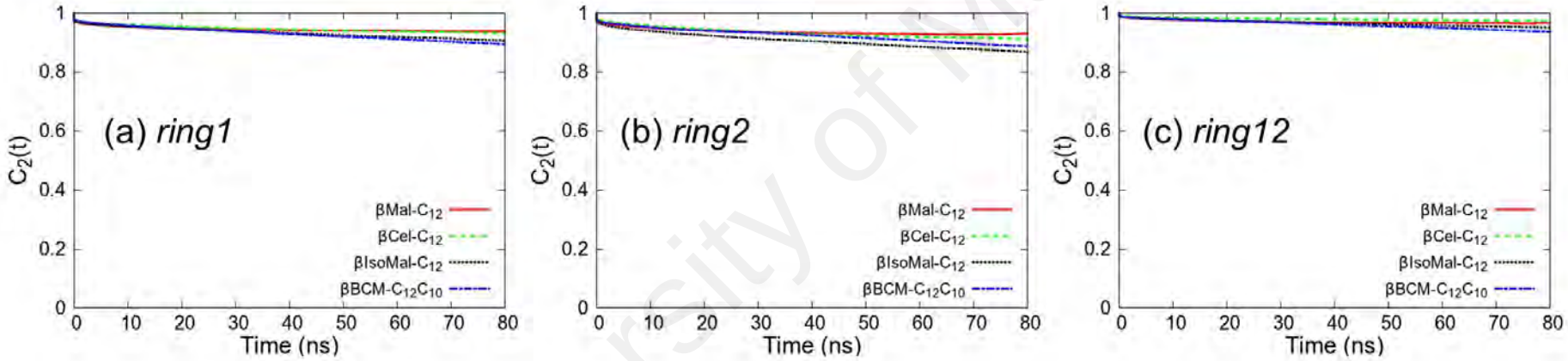

Figure 4.18: Second rank reorientational autocorrelation functions $C_2(t)$ for the sugars at the headgroup region for all the four glycosides, namely, βMal-C_{12}, βCel-C_{12}, βIsoMal-C_{12}, and βMal-$C_{12}C_{10}$ for (a) non-reducing sugar (*ring1*), (b) reducing sugar (*ring2*) and (c) both the sugars together (*ring12*).

Figure 4.18 shows the autocorrelation profiles for the non-reducing sugar (*ring1*), reducing sugar (*ring2*) and both sugars together (*ring12*), while Figure 4.19 gives the corresponding correlation times.

In general the non-reducing sugar (*ring2*) has slightly faster rotational diffusion than the reducing sugar (*ring1*) and the combined sugar headgroup (*ring12*). In particular for βIsoMal-C_{12} , the non-reducing sugar's correlation time ($\tau ring2$) on average is the smallest, which is consistent with the fact that this lipid has a smaller d-spacing and a larger A compared to the other glycolipid systems. Depending on the stereochemistry, the headgroup correlation time of the lipid headgroup differs only slightly such that, τ_{ring12} of βMal-C_{12} (with a α-(1→4)-linkage) and βCel-C_{12} (with an β-(1→4)-linkage) are 78 and 80 ns respectively. The τ_{ring12} values for βMal-C_{12} and βIsoMal-C_{12} are also similar despite the structural difference in the headgroup. The similarity in this dynamical behavior can be related to the distribution of hydrogen bonds in both βMal-C_{12} and βIsoMal-C_{12} . In both disaccharides, the major hydrogen bonding occurs at the hydroxymethyl group on the non-reducing sugar such that the O6 acts as an acceptor while the HO6 acts as a donor. However, the next most dominant hydrogen bond site is O6' in βMal-C_{12}, but O1' in βIsoMal-C_{12} (see Figure 4.20: (a) and (d) from Section 4.1 In βMal-C_{12} the O6'-HO6' group (see Figure 4.1) acts as donor and acceptor while in βIsoMal-C_{12} the O1' acts only as an acceptor. It was also found that the headgroup correlation time, τ_{ring12}, for the branched glycolipid is shorter (hence faster rotational diffusion) compared to the monoalkylated one, even though both βMal-C_{12} and βMal-$C_{12}C_{10}$ have the same sugar group. We note that the branched glycolipid exists in the L_α phase, where the constituent lipid chains tend to be more flexible, with many modes of motions, and the headgroup moiety is subjected to a greater motion due to the increased area per headgroup.

4.2.5 Chain tilting

The chain tilting behavior was analysed by choosing a vector from the midpoints of C71–C72 and C81–C82 for the monoalkylated and the *sn*-1 chains, while for the *sn*-2 chain, it is defined from the midpoints of C83–C84 and C91-C92 (see Figure 3.6(b)). We plotted the distributions of these tilt angles using the first leaflet for the four systems (Figure 4.20). The maximum tilt values for βCel-C_{12} and βMal-C_{12} do not differ from the previous simulations as in Section 4.1, with values of 18° and 15° respectively (Table 4.5).

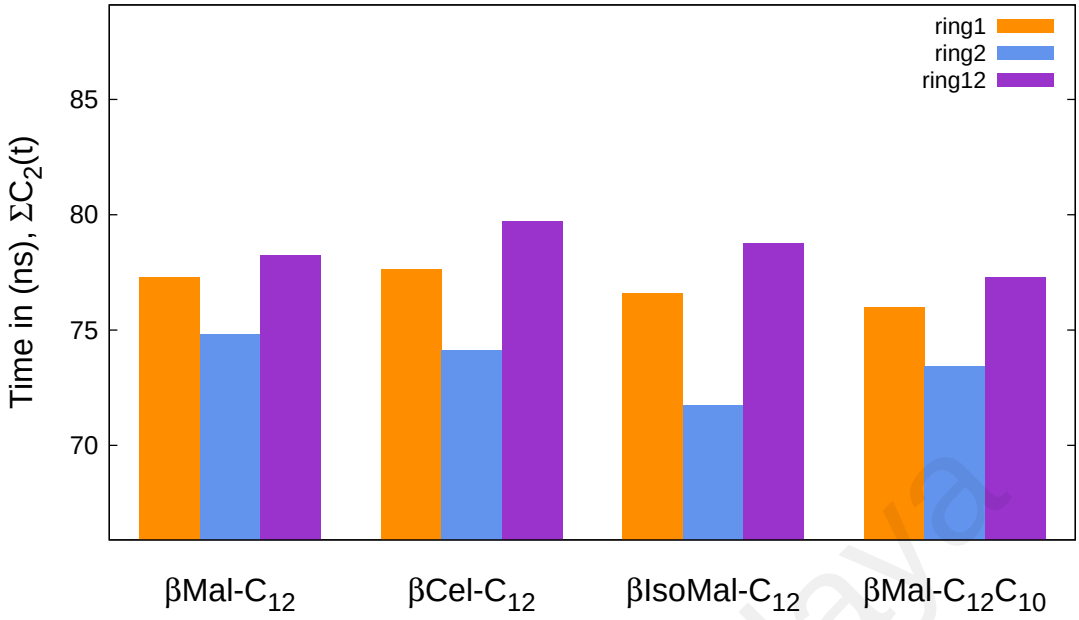

Figure 4.19: Correlation time of sugar headgroup of lipids: reducing sugar (*ring1*); non-reducing sugar (*ring2*); and combination of *ring1* and *ring2* (*ring12*)

Interestingly, for both the βIsoMal-C_{12} and βMal-$C_{12}C_{10}$, the maximum tilt values differ and the profiles display a more prominent bimodal distribution. In the case of isomaltoside, the two maxima are at 43° and 59° (Figure 4.20), which accounts for the significantly smaller *d*-spacing compared to the other two glycolipid systems considered here. A tilt angle θ of zero implies a perfect alignment of the chain vector with the layer normal, while a value of 180° implies the chain vector has "flipped" over. In the case of βIsoMal-C_{12} , the two peak values represent the most probable chain vector orientations possibly arising from the α(1–6) glycosidic linkage connecting the two glucose units. In the previous simulation, as in Section 4.1, these peaks were small, but are more populated in the current study; whilst this may arise simply from the additional sampling of this replicate, it may also be due to the greater freedom available to the system in using a fully anisotropic pressure scaling regime.

The branched chain glycoside is also bimodal in both the chain profiles. Firstly, the *sn*-1 and *sn*-2 chains have a non-zero population at the θ value of 90°, meaning some chains are parallel to the bilayer. In addition, there are double peaks symmetrical about the 90° angle for both the two branched chains, indicating there are two possible conformations equally populated at θ of 24° and 156°. To investigate this behavior and if it involves lipid

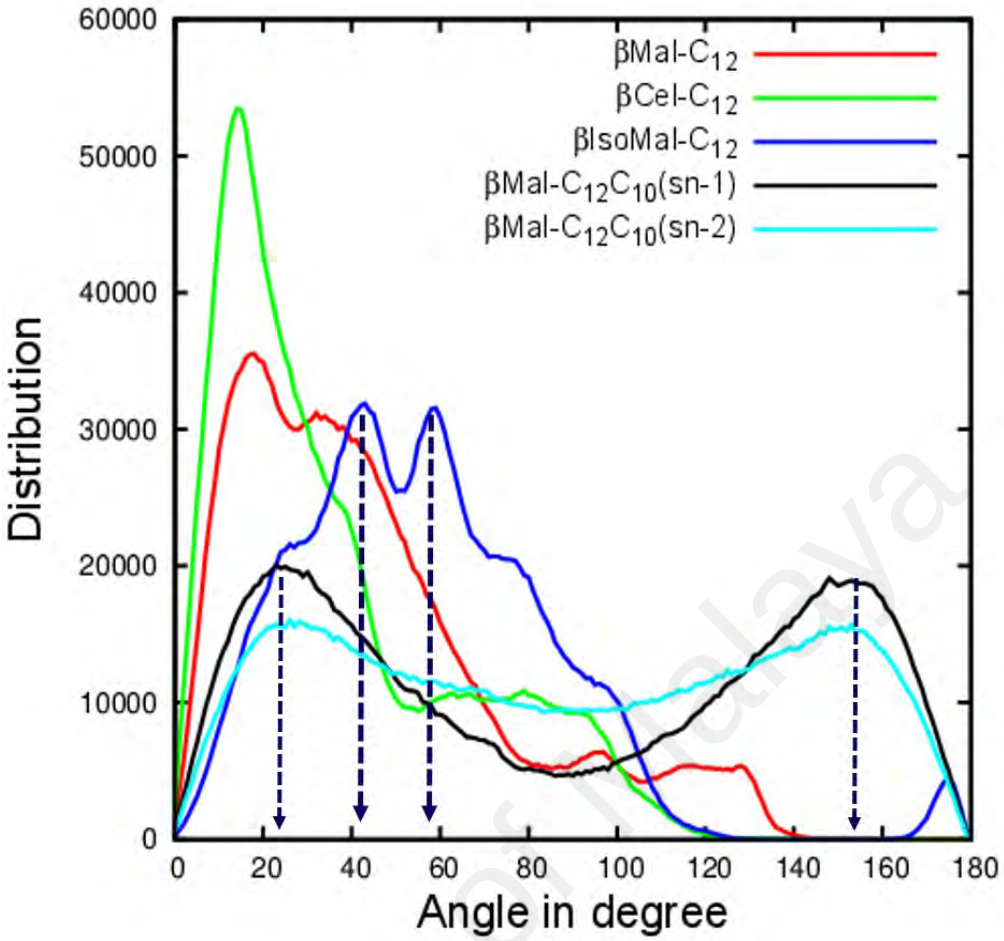

Figure 4.20: Distributions of alkyl chain tilt angle *theta* of various glycolipids forone layer. Plot shows the current results for 160 ns production runs for various glycoside systems in different colored lines, where medium violet red for βMal-C_{12}, black for βMal-$C_{12}C_{10}$-(*sn*-1), deep sky blue for βMal-$C_{12}C_{10}$-(*sn*-2), green for βCel-C_{12} and dark blue for βIsoMal-C_{12}.

flipping, we examined the glycolipid dynamics visually[1] and found evidence of chain penetration into the hydrophilic headgroup region. As an example of this behavior, we present a movie[2] of the last 160 ns production simulation, highlighting a lipid in the third leaflet (see Video S1 generated using VMD (Humphrey, Dalke, & Schulten, 1996)). It is apparent over the course of the simulation that its chain works its way into the sugar headgroup environment. Based on the tilt angle distribution in Figure 4.20, we estimate for every leaflet there are about 10% of such lipids, which can be verified by examining the chain layer. We also present a movie focusing on the dynamics of the lipid headgroup

[1]We enclosed a compact disk (CD) containing the simulation movies.

[2]The movies with the title Video S1 and Video S2 are also available at the supporting information section following the reference (Manickam Achari, Bryce, & Hashim, 2014).

region (Video S2); here we can see the emergence of the complementary hydrophobic cavity within the sugar region, which accommodates the lipid tail.

From these dynamics visualization studies, we also discount the possibility of lipid flip. Nevertheless, by observing the movie and the way the chain vectors *sn*-1 and *sn*-2 are defined, these two peak conformations (θ of 24° and 156°) are possible as shown in Figure 4.21a, a snapshot captured from the movie. These results imply the chains can readily protrude into the hydrophilic region due to the formation of a "cavity" or "hole" in the headgroup region by sugar cooperative motion (Figure 4.21c), which is large enough to accommodate the alkyl chain. Figure 4.21d shows the time evolution of a selected lipid, whose alkyl chain made an attempt to associate itself with the headgroup region (represented by the wire and VDW model).

4.2.6 Discussion

We report 160 ns simulations of four glycosides namely βMal-C_{12}, βCel-C_{12}, βIsoMal-C_{12} , and βMal-$C_{12}C_{10}$ in anhydrous bilayer assemblies to understand the relationship of structural and dynamical properties to the stereochemistry of these sugar based lipids. The stereochemistry of the sugar group is known to affect profoundly the assembly states and our work here has provided further evidence especially in the chain and headgroup orderings, structure and dynamics. For the three glycosides in the same L_C phase, the chains for βIsoMal-C_{12} are in a more disordered state compared to βCel-C_{12} and βMal-C_{12} (Figure 4.13 and 4.14). This is exemplified by the higher population of *gauche* chain dihedral conformations for βIsoMal-C_{12} compared to βCel-C_{12} and βMal-C_{12} (Figure 4.15). The lower ordering of the βIsoMal-C_{12} chains is most probably due to the increase in lateral area per lipid at the interface which is related to the α-(1→6) glycosidic linkage between two sugar moieties.

For the branched glycolipid, βMal-$C_{12}C_{10}$, which is in the L_α phase, a higher *gauche* population than for the monoalkylated lipid is observed although the systems are at the same temperature. Overall, this suggests the *gauche* population is influenced by chain branching and glycosidic linkage between two sugars, but less affected by the anomeric conformation or temperature. Consequently, the *gauche* populations affect some bilayer properties including the bilayer *d*-spacing, as have been demonstrated experimentally from the study of anhydrous octyl β-maltoside (βMal-C_8) and decyl β-maltoside (βMal-C_{10})

bilayers using differential scanning calorimetry (DSC) and small angle x-ray scattering (SAXS) at, ~25 °C in the L_C phase. In this study, the measured bilayer *d*-spacing was different before and after the glass transition T_g (Kocherbitov & Söderman, 2004). The *gauche* population in the L_α phase is higher compared to the glass phase by 3% and 7% for βMal-C_8 and βMal-C_8 respectively (Kocherbitov & Söderman, 2004). On cooling from the L_α phase into the glassy phase, both the systems retained their liquid crystalline chain ordering because a longer time was needed for the chains to regain the all-*trans* conformation (Kocherbitov & Söderman, 2004). In addition, long chain alkyl maltosides, such as tetradecyl β-maltoside (βMal-C_{14}) and hexadecyl β-maltoside (βMal-C_{16}) in the anhydrous state have been studied (Ericsson, Ericsson, Kocherbitov, et al., 2005); both systems have the same melting temperature of about 105 °C but phases below this temperature are complex and strongly driven by kinetics, causing them to be metastable. The lamellar structure in the anhydrous low temperature crystal has a *d*-spacing of about 37 Å but in the anhydrous high temperature crystal, the inter-lamellar distance is 43 Å. The difference of 6 Å (or 14%) could be attributed to the chain tilting together with the presence of an all-*trans* conformation in the anhydrous low temperature crystal (Figure 4.22). Meanwhile, the liquid crystalline state has a *d*-spacing about 40-41 Å (summary given in Table 4.6) where the value is closer to the *d*-spacing in the glass phase (Figure 4.22). But the ordered lamellar phase, which has the all-*trans* conformation for the chains, has about 7% less than the *d*-spacing (38 Å) compared to the L_α phase, which may be attributed to the tilted chain with respect to the bilayer normal. The presence of *gauche* conformations in the L_α phase reduces interdigitation, leading to a higher *d*-spacing relative to the other bilayer phases, except for the anhydrous high temperature crystal phase.

The sampling of chain conformations for the monoalkyl glycolipids in the lamellar crystalline phase, L_C, is further reflected by analysis of rotational diffusion (Figure 4.17). These lipid chains may interact non-specifically (Small, 1984), where the carbon atoms in the chains are able to rotate in a limited fashion within the lattice, leading to partial local rotations along the chain, as observed previously in the L_β or the gel phases for example (Tardieu et al., 1973). Although βMal-C_{12} and βMal-$C_{12}C_{10}$ have the same sugar headgroup, the carbons along the chain from both systems show different rotational behavior (Figure 4.17). This arises from the steric constraints of the two branching chains in βMal-$C_{12}C_{10}$; the resulting 'chain-overcrowding' in the hydrophobic region

leads to the dominance of a attractive van der Waals interaction. From our analysis of the autocorrelation function and visual inspection (Video S2), we note that the sugar headgroups also experience some partial "rotational motion", although much slower than the chain carbon partial rotation. Before leaving the subject on dynamics, we comment on one of the βIsoMal-C_{12} stereoisomers, namely the gentibioside, whose non-reducing sugar is attached to the reducing sugar by a β-(1→6) linkage. The bilayer L_α phase of this gentibioside was studied using a ^{2}H-NMR by Carrier et al. (1989), who found its headgroup dynamics is relatively slower compared to other glycolipids studied at that time. Qualitatively this finding perhaps could lend support for the observed difference in the dynamics of the isomaltose headgroup as compared to the other sugar lipids.

For phospholipid systems, there are extensive studies of headgroup dynamics focused specifically on the hydrophilic moiety's rotational diffusion, albeit mainly in aqueous solution (Essmann & Berkowitz, 1999; Moore et al., 2001; P. S. Niemelä et al., 2006). Many phospholipid headgroups act only as hydrogen bonding acceptors (Róg et al., 2007) but the sugar groups in glycolipids are both acceptors and donors of hydrogen bonding. This property of the headgroup grants glycolipids a strong coupling with its neighboring lipid headgroups in the self-assembly. Moreover, the covalent framework of the sugar, containing aligned C−H groups as well as polar groups leads to its amphoteric nature (Balasubramanian, Raman, & Sundari, 1993; Jimenez-Barbero et al., 1995; Lemieux, 1989). This important property of sugars increases the intra-layer hydrogen-bond interaction, self-assembly stability and makes the phase boundary temperature independent (Misran, Timimi, Heidelberg, Sugimura, & Hashim, 2013). So the headgroup motion is highly restricted by the extensive hydrogen bonds with the neighboring lipids. A comparison of the studies of phospholipid and glycolipid surfactants under thermotropic conditions by C. Huang and Li (1999) and Auvray et al. (2001) respectively, further illustrates the distinctive behavior of sugar lipids. In these studies, phosphatidylcholine lipids were reported to undergo a gel to liquid-crystalline transition at about 70 °C while, at nearly the same temperature, glycolipids such as βMal-C_{12} experienced a solid solid phase transition, followed by a gel to liquid-crystalline phase transition at, 103 °C.

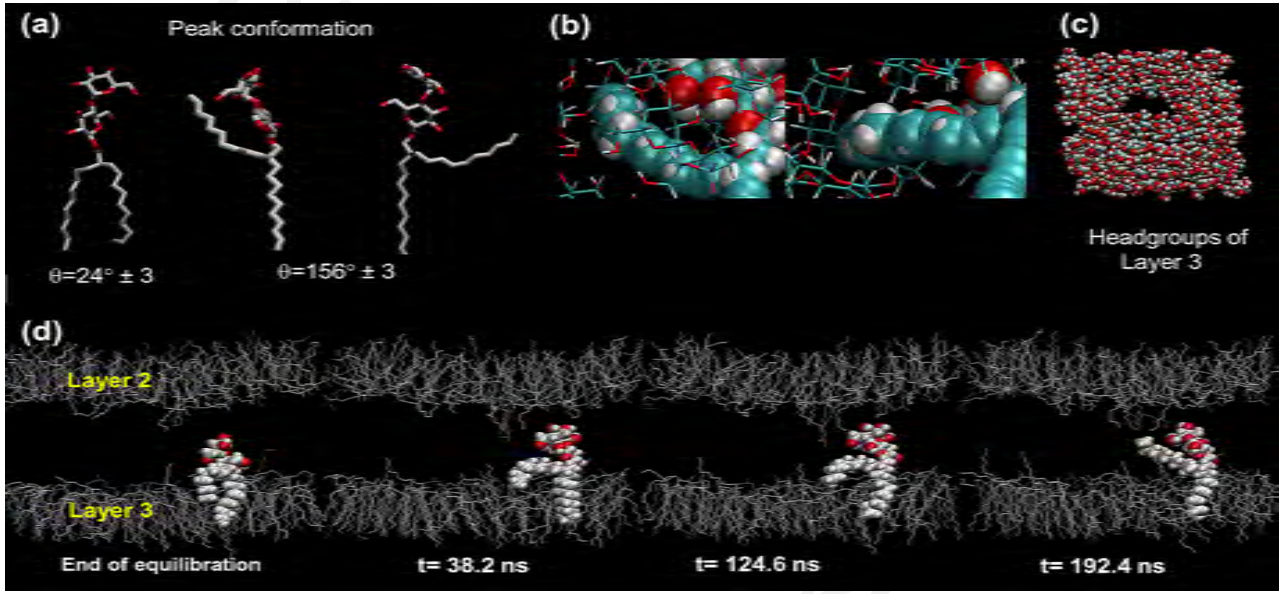

Figure 4.21: Some lipids' conformations and bilayer snapshots from the simulation. (a) Three possible lipid conformations with the chain tilt angle, θ°. (b) The dispersion interaction observed from two viewing angles, between the C−H from the sugar face and those of the alkyl chain by a representative lipid (enlarged) from the third layer. (c) A characteristic example of the sugar headgroup region (t=140 ns) from the third leaflet showing the hydrophobic cavity (top-view). (d) The time evolution of a typical side-view of the second and third leaflets. The lipid (drawn fully with VDW model) is seen to work itself into the hydrophilic region.

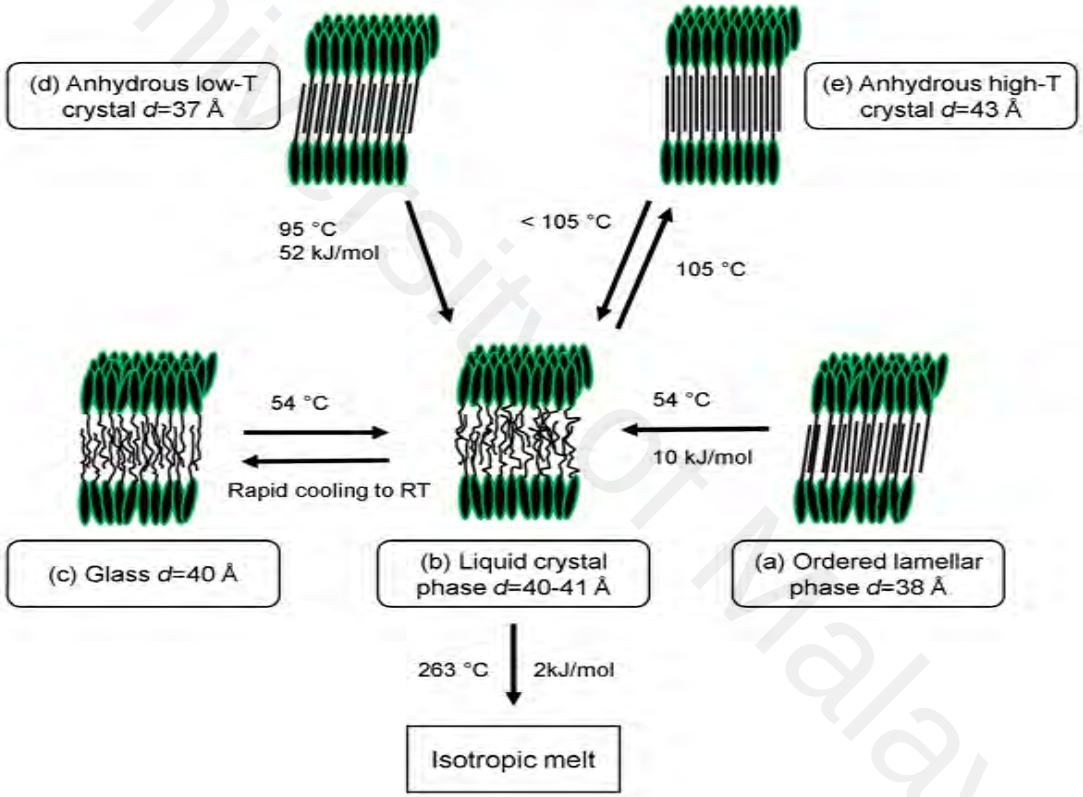

Figure 4.22: Schematic representations of the phase structures characterized for tetradecyl β-maltoside-($\beta C_{14}G_2$). Redrawn from Ericsson, Ericsson, Kocherbitov, et al. (2005).

Table 4.6: Phase transition temperatures for glycosides in an anhydrous condition from literatures. The lamellar distance of bilayers, d (in Å).

Lipid	Symbol	d-spacing/Å (at 20 °C)	Pre-transition temp (°C)	Solid-L_α transition temp. (°C) d-spacing	L_α-iso transition temp. (°C)	Reference
Octyl-β-glucoside	βC_8Glu			69.0	107.0	(Sakya, Seddon, & Vill, 1997)
Octyl-β-maltoside	βC_8Mal				122.7	(Kocherbitov & Söderman, 2004)
Decyl-β-maltoside	βC_{10}Mal		78.6[c]	96.5	203.0	(Kocherbitov & Söderman, 2004)
Decyl-β-maltoside	βC_{10}Mal			38.6	102.2	(Kocherbitov & Söderman, 2004)
Decyl-β-maltoside	βC_{10}Mal		25[a], 25[b]		208.0	(Kocherbitov & Söderman, 2004)
Dodecyl-β-maltoside	βC_{12}Mal	33.5	70[c]	103.0(41.5 Å)		(Auvray et al., 2001)
Dodecyl-β-maltoside	βC_{12}Mal	33.5	50[c]	128.0(32.4 Å)		(Auvray et al., 2001)
Tetradecyl-β-maltoside	βC_{14}Mal		95[d]	105.0 (40-41 Å)	263.0	(Ericsson, Ericsson, & Ulvenlund, 2005)
Hexadecyl-β-maltoside	βC_{16}Mal			105.0		(Ericsson, Ericsson, & Ulvenlund, 2005)

Note: (a) glassy state before heating (b) glassy state after heating (c) solid/solid transition (d) not solid/solid transition.

Ericsson, Ericsson, Kocherbitov, et al. (2005) has suggested that the melting of alkyl-maltosides (from lamellar crystal to a liquid crystal phase) is primarily governed by the nature of the headgroup rather than by the alkyl chain length, primarily due to the extensive inter-molecular hydrogen bonding within the headgroup.

Conventionally, the association of sugar headgroups with lipophilic alkyl tails is considered to be highly unfavourable. However, the amphoteric nature of the sugar headgroups here has made this possible: the lipid chain can associate itself with the hydrophobic face of the saccharide unit (Naidoo & Kuttel, 2001) (see Figure 4.21b). There are many examples of saccharide binding to aromatic groups, e.g. with the Tyr, Phe and Trp amino acid residues of proteins (Mitchell, Miles, Neres, Bichenkova, & Bryce, 2010; Vandenbussche et al., 2008). Our observation of chain-sugar association is not unreasonable, since other studies have appeared in recent years (e.g. Chen, Berns, and Berns (1981)). The formation of hydrophobic cavities may provide the seeding condition for lipid flip-flop, a rare event, which may possibly be observed in a much longer simulation even in an anhydrous bilayer system. A MD simulation, which demonstrated lipid flip, performed by Gurtovenko and Vattulainen (I. Yamashita, Kawabata, Kato, Hato, & Minamikawa, 2004), suggested that the formation of a water hole in the hydrophobic region is an enabling condition for the flip motion. Our results point to the effects of chain crowding in forcing some lipids to protrude into the hydrophilic region. It is interesting to consider the possibility that as these lipid tails vacate the hydrophobic cavity, the defects can permit seepage of water (if present) into these regions, potentially forming a pore for water. Therefore, our anhydrous branched chain glycolipid system, uncomplicated by the presence of solvent, may give insights into the formation of water defects in glycolipids (I. Yamashita et al., 2004).

4.3 Hydration and thermal effects on structure and dynamic properties of mono- and Guerbet branched-chain β-D-maltosides: an atomistic simulation study

A man who dares to waste one hour of time has not discovered the value of life.
Charles Darwin (1809-1882)

Unlike the previous sections on bilayers in dry condition, in this section we elaborate the results of five simulation systems (two single chain maltosides and three Guerbet branched chain maltosides) in hydrated conditions. The two single chain systems, namely βMal-C_{12}(12%wat) and βMal-C_{12}(23%wat), are simulated at 12% and 23% water concentration respectively at 80 °C. Meanwhile, the Guerbet branched chain systems, βMal-$C_{12}C_8$(*R*)(25%wat), βMal-$C_{12}C_8$(*S*)(25%wat), and βMal-$C_{12}C_8$(*RS*)(25%wat) were simulated at room temperature with 25% hydration level where the last system contains 50% of mass weight from *R* and *S* isomers. The glycolipids used are shown in Figure 4.23. In this study, we focus on the structure and dynamic properties of the bilayers with respect to the water concentration, temperature difference and effect of chain branching by allowing the hydrophilic moiety to be maltose in all the systems. We also address the chiral effect on the bilayers, especially for the branched chain systems.

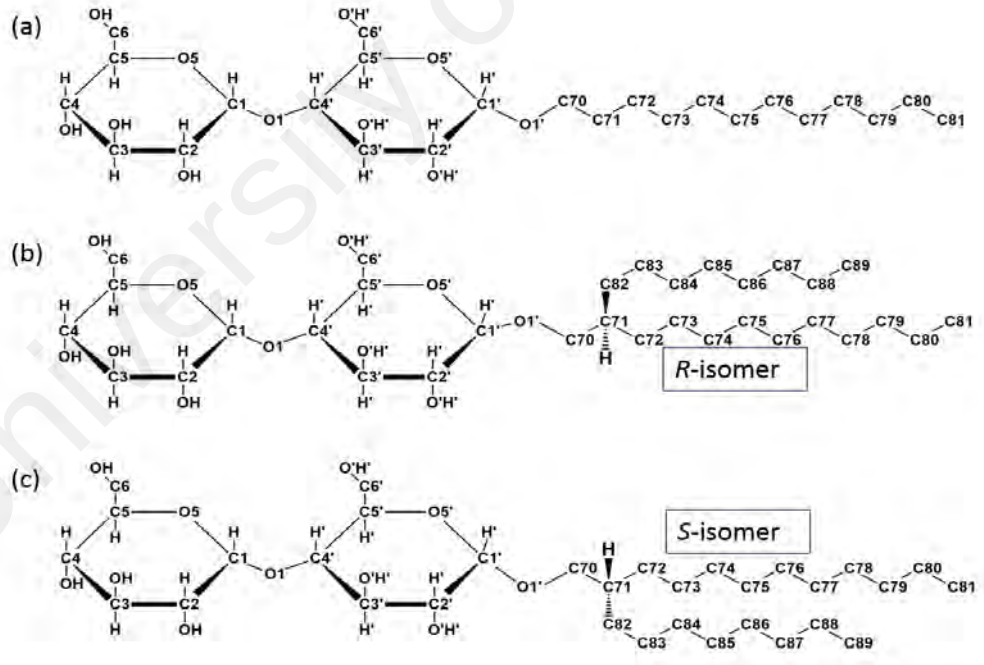

Figure 4.23: Mono- and branched glycosides used in the simulation: (a) βMal-C_{12} (b) βMal-$C_{12}C_8$(*R*) (*R*-isomer) and (c) βMal-$C_{12}C_8$(*S*) (*S*-isomer). The Φ and Ψ angle between the non-reducing and reducing sugar of maltoside is defined as H-C1-O1-C4' and C1-O1-C4'-H' respectively.

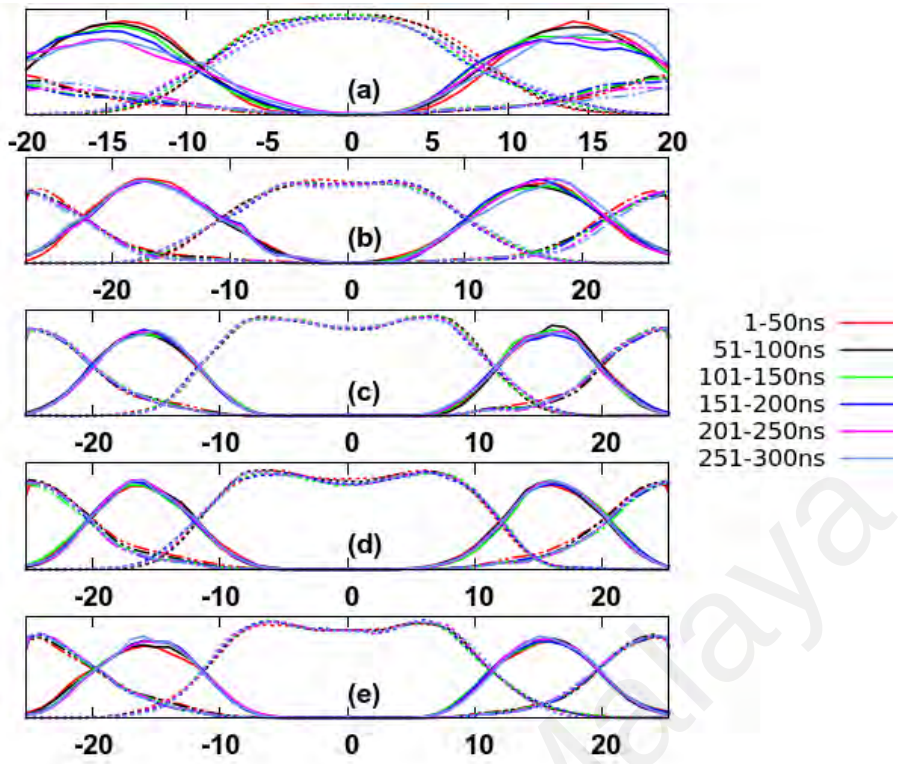

Figure 4.24: Local density profile (LDP) for the hydrated bilayer systems; (a)βMal-C_{12}(12%wat), (b)βMal-C_{12}(23%wat), (c)βMal-$C_{12}C_8$(*R*)(25%wat), (d)βMal-$C_{12}C_8$(*S*)(25%wat), and (e)βMal-$C_{12}C_8$(*RS*)(25%wat). Solid lines–sugar headgroup, short dash lines–tail groups, and long & short dash lines–water.

4.3.1 Stability of bilayer (LDP and area per lipid at bilayer interface)

Stable and equilibrated system is an essential requirement for calculating the structural and dynamical properties of a bilayer (Anézo et al., 2003). Local density profile (LDP) gives a way to determine the stability of the simulated bilayer system. Figure 4.24 shows the LDPs for all five simulated systems where each system contains six block averages of LDPs each with 50 ns production time length. The LDPs show the bilayers do not break or fluctuate far from the equilibrium and there are only small differences between different block averages during the simulations. The expected microphase separation of the hydrophilic, hydrophobic, and water regions is demonstrated by the maximum and minimum number density values along the bilayer normal. This implies that throughout the simulation the structures are intact and they are qualitatively similar in general. The LDP is also used to estimate the bilayer thickness by measuring the peak to peak distance. This estimation is followed by the description given by Nagle and Tristram-Nagle (2000a) where the peak

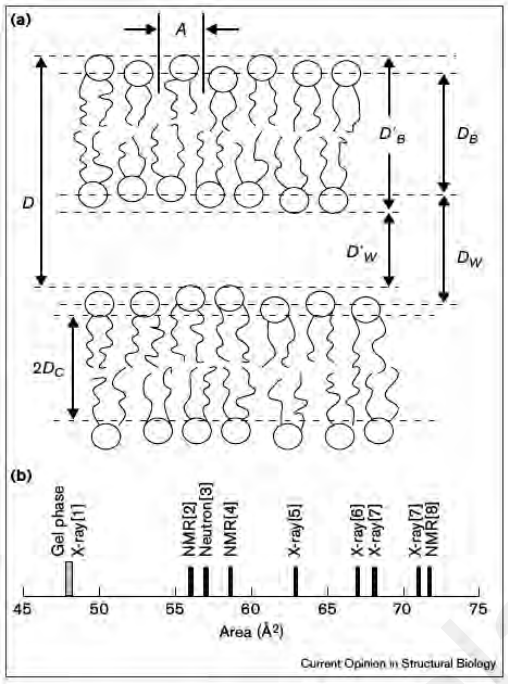

Figure 4.25: Lipid bilayer structural parameters. (a) A sketch of two bilayers, identifying the primary lamellar repeat spacing (D), the area (A) per molecule, the hydrophobic thickness ($2D_C$), the Luzzati thickness (D_B), the water thickness (D_W), the steric thickness (D'_B) and the steric water thickness (D'_W). (b) Prominent literature values of A for DPPC in the L_α phase (black) compared with the value of A in the gel phase (gray). Adopted from Nagle and Tristram-Nagle (2000a).

to peak distance corresponds to the Luzzati-thickness, D_B (please see Figure 4.25)[3]. The measured values of the bilayer thickness from LDPs are given in Table 4.7.

Additionally, the area per lipid at the interface along the bilayer plane (x-y direction) is also monitored to determine the stability of the simulation systems in NpT ensemble (Dickson et al., 2014). Figure 4.26(a), shows values for the area per lipid at the bilayer interface for all the simulated systems. The smooth function lines indicate the areas do not fluctuate significantly throughout the 300 ns production run. Meanwhile, Figure 4.26(b) shows the bilayer repeat distance (d-spacing) as a function of simulation time. A closer look at Figure 4.26(a and b) shows the function lines are almost smooth after around 65 ns of simulation run especially for βMal-C_{12}(12%wat) and βMal-C_{12}(23%wat). Thus, the first 75 ns of the simulation is considered as the time taken to reach the equilibrium state. Subsequently, the last 225 ns production run is used to calculate the structural and dynamical properties of all bilayers.

[3]For detailed information please see ref. (Nagle & Tristram-Nagle, 2000a)

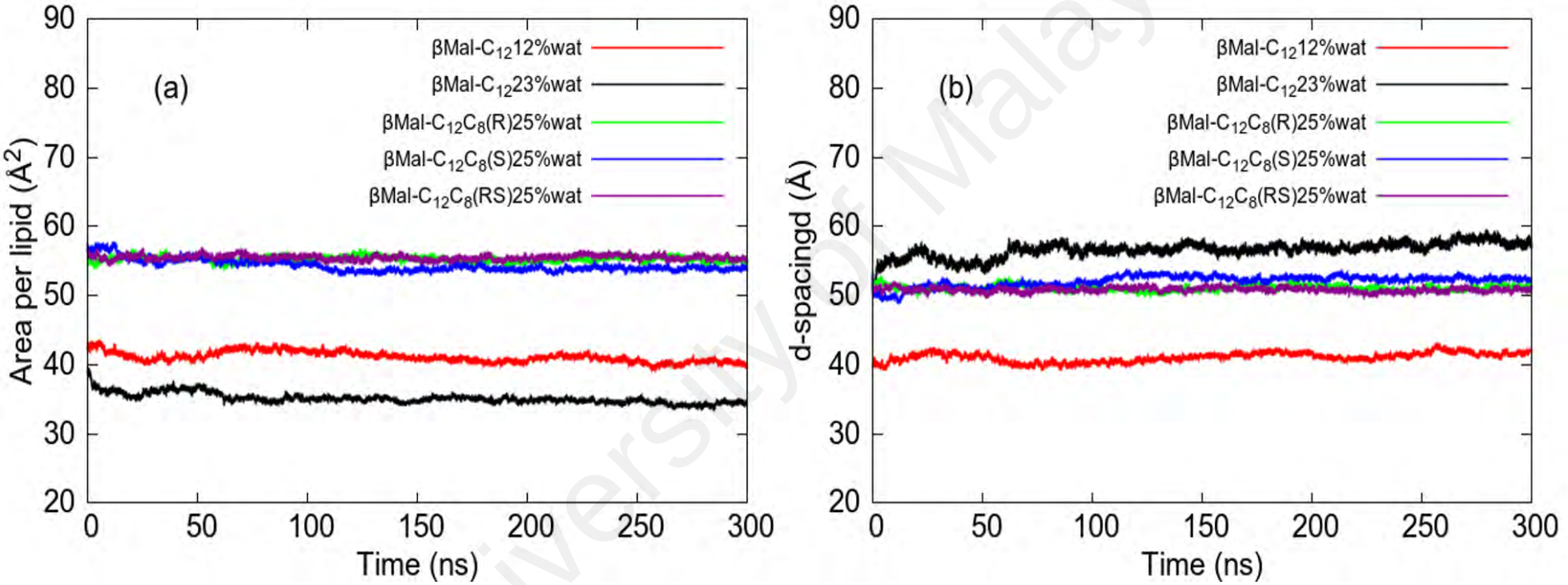

Figure 4.26: The time evolution of area per lipid at bilayer interface (a) and *d*-spacing (bilayer repeat distance) (b), are shown for the 300 ns simulation of βMal-C$_{12}$(12%wat) (red), βMal-C$_{12}$(23%wat) (black), βMal-C$_{12}$C$_8$(*R*)(25%wat) (green), βMal-C$_{12}$C$_8$(*S*)(25%wat) (blue), and βMal-C$_{12}$C$_8$(*RS*)(25%wat) (magenta). The area per lipids was obtained by dividing the area of *xy* plane of bilayer with the total number of lipid present while the *d*-pacing obtained from *z*-dimension of periodic box.

Table 4.7 shows the average values of the area per lipid at the bilayer interface, bilayer thickness, and bilayer repeat distance (*d*-spacing) of βMal-C_{12}(12%), βMal-C_{12}(23%), βMal-$C_{12}C_8$(*R*)(25%wat), βMal-$C_{12}C_8$(*S*)(25%wat), and βMal-$C_{12}C_8$(*RS*)(25%wat) for the last 225 ns production run. The βMal-C_{12}(12%wat) system has the average value of 41 $Å^2$ of area per lipid. This is about 5.7% higher than that of βMal-C_{12} (38.8 $Å^2$) in the anhydrous system in Section 4.1 Although it is expected that increasing the water content may increase the area per lipid at the bilayer interface (Mashl, Scott, Subramaniam, & Jakobsson, 2001), the current study shows an opposite trend, for βMal-C_{12}(23%wat) where the area is reduced by about 6 $Å^2$ compared to that βMal-C_{12}(12%wat). This difference may be due to the bilayer, βMal-C_{12}(23%wat), exist near to the phase boundary between lamellar and hexagonal assembly. Meanwhile, the branched chain systems have an average area per lipid value of about 55 $Å^2$. This is comparable to that obtained by Hamid et al. (2014) for the same system with same hydration, which was 64.1 $Å^2$. We also note here, that the value of area per lipid for anhydrous branched chain maltoside simulated previously was 51.9 $Å^2$ as reported in Section 4.1.

The Luzzati thickness of monoalkylated systems is 31.5 Å and for branched chain systems this is 32 Å. Both values agree closely to the experimental value, i.e 30 Å by Hamid et al. (2014), and this agreement possibly suggests that in the L_α phase, the chains area highly disordered and may not interdigitate even in the monoalkylated system.

The bilayer repeat distance (*d*-spacing) for monoalkylated, βMal-C_{12}(12%wat), is about 41 Å and this value is very close to the experimental value (39.2 Å) by Auvray et al. (1995, 2001) for the same compound. For βMal-C_{12}(23%wat), the bilayer repeat distance is 56.6 Å at higher water content which is about 38% higher than the βMal-C_{12}(12%wat). Additionally, at higher temperature (80 °C), the water molecules may also undergo high fluctuations and tumbling within the water layer due to their higher kinetic and vibrational energy. However, for the branched chain systems (βMal-$C_{12}C_8$(*R*)(25%wat), βMal-$C_{12}C_8$(*S*)(25%wat), and βMal-$C_{12}C_8$(*RS*)(25%wat)), the calculated average repeat distance is around 51.0 Å and this value is higher by about 10 Å compared to the reported experimental value by Hamid et al. (2014). These results show that the *d*-spacing is affected by the water content and also the chain branching but not the chirality.

Table 4.7: Area per lipid A, bilayer thickness, and bilayer repeat distance (d-spacing) for βMal-C_{12}(12%wat), βMal-C_{12}(23%wat), βMal-$C_{12}C_8$(R)(25%wat), βMal-$C_{12}C_8$(S)(25%wat), and βMal-$C_{12}C_8$(RS)(25%wat). The monoalkylated bilayers are at 80 °C and branched chain bilayers are at room temperature (27 °C). Temperatures different than these are specified explicitly.

Bilayer System	**Area per Lipid** A/Å^2	**Bilayer thickness (Luzzati's thickness)**		**Bilayer repeat distance (d-spacing)**	
		Simulation (this work)	Experimental	Simulation (this work)	Experimental
βMal-C_{12}(12%wat)	41.1 ± 0.7	29.0 ± 0.7		41.1 ± 0.6	39.2 (at 74 °C) [a]
βMal-C_{12}(23%wat)	35.1 ± 0.7	33.9 ± 0.8		56.6 ± 1.1	
βMal-$C_{12}C_8$(R)(25%wat)	55.3 ± 0.4	31.8 ± 0.4		51.1 ± 0.4	
βMal-$C_{12}C_8$(S)(25%wat)	54.3 ± 0.8	32.7 ± 0.3		52.1 ± 0.8	
βMal-$C_{12}C_8$(RS)(25%wat)	55.5 ± 0.3	31.4 ± 0.2		50.8 ± 0.3	
βMal-$C_{12}C_8$ (at 25 °C)	64.1 [b]		30 [b]		41 [b]
βMal-$C_{12}C_{10}$ (at 27 °C)	51.9 [c]	32.3 [c]			

[a] (Auvray et al., 2001), [b] (Hamid et al., 2014), [c] Section 4.1

Figure 4.27 shows the shaded area of local density profile for the last 50 ns simulation. The shaded regions vividly highlight the distribution of glycolipid segments (sugar headgroup & alkyl chain) and water molecules in the simulation periodic box. For clarity, the red, green, and blue color regions orderly represent sugar headgroup, alkyl chain, and water molecules. In βMal-C_{12}(12%wat) (see Figure 4.27 (a)) almost all waters are found between the sugar headgroups while in βMal-C_{12}(23%wat) and in all the branched chain systems (βMal-$C_{12}C_8$(*R*)(25%wat), βMal-$C_{12}C_8$(*S*)(25%wat), and βMal-$C_{12}C_8$(*RS*)(25%wat)) show a small amount of water molecules within sugar groups.

As a final check on the stability of simulated systems, the population of dihedral angles – Φ and Ψ of glycosidic angles between reducing and non-reducing sugar units of maltoside is plotted as shown in Figure 4.28 (Ramachandran plot). Throughout production period, the population of dihedral angles for βMal-C_{12}(12%wat) and βMal-C_{12}(23%wat) show a similar distribution where only one low energy of $\Phi\Psi$ minimum is found. In the same manner, the population of dihedral angles for branched chain maltosides, βMal-$C_{12}C_8$(*R*)(25%wat) and its chiral counter glycolipid, βMal-$C_{12}C_8$(*S*)(25%wat) and racemic mixture, βMal-$C_{12}C_8$(*RS*)(25%wat) also show single minimum energy location across the $\Phi\Psi$ distribution. The population trend indicates that the sugars keep intact with minimum rotation or twists along dihedral plane between the two sugar rings.

4.3.2 Hydrogen bonding network at the hydrophilic region

In general, sugar moiety in lipid contains multiple hydroxyl groups. For instance, a disaccharide glycoside, like a maltoside, possesses seven hydroxyl groups where each is able to donate a hydrogen bond (act as a donor) and eleven oxygen atoms, including the two glycosidic oxygen and two sugar ring oxygen to accept two hydrogen bonds (act as an acceptor). These altogether give a total of 29 hydrogen bonds. Surprisingly, a simulation study by Cheetham and Dasgupta (2006) on seven maltosides in aqueous solution have shown far less hydrogen bonds than this idealized theoretical value, with 12–13 hydrogen bonds, typically formed by the solute with water. Likewise, in our simulation studies, single and branched chain maltoside systems (βMal-C_{12}(12%wat), βMal-C_{12}(23%wat), βMal-$C_{12}C_8$(*R*)(25%wat), βMal-$C_{12}C_8$(*S*)(25%wat), and βMal-$C_{12}C_8$(*RS*)(25%wat)) in solution have around 9–13 total hydrogen bonds per lipid (n_{tot}) as shown in Table 4.8. Among these, the βMal-C_{12}(23%wat) shows higher intermolecular hydrogen bonds

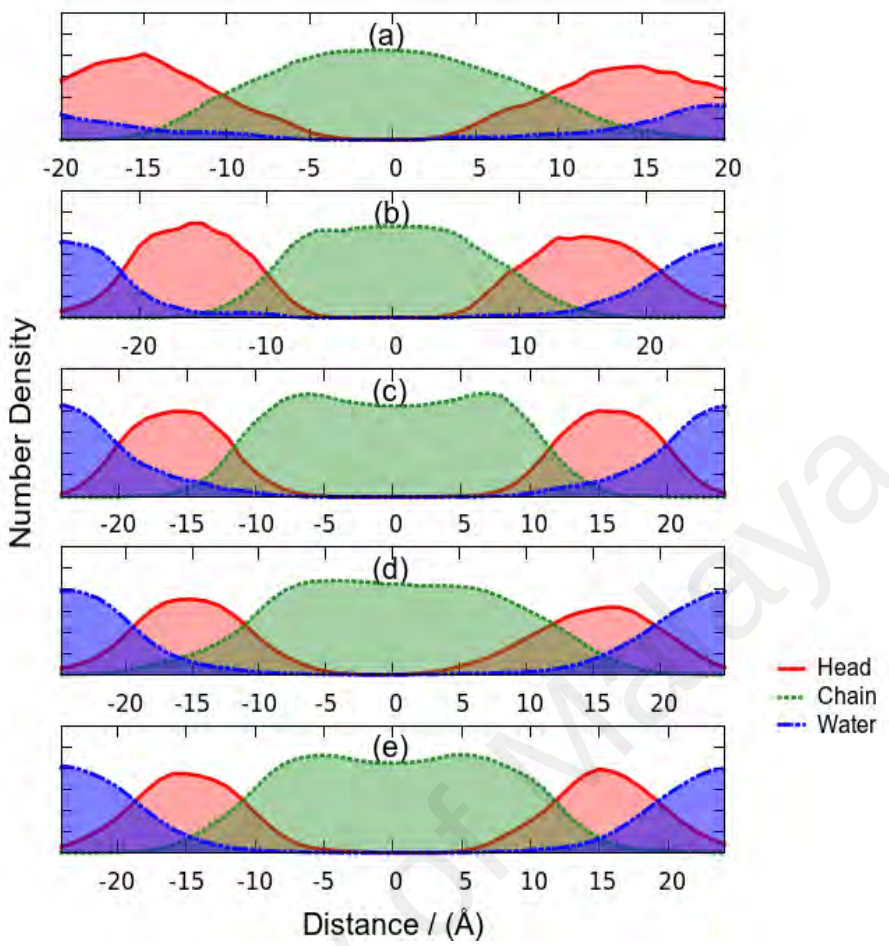

Figure 4.27: Shaded local density profile for the hydrated bilayer systems; (a)βMal-C_{12}(12%wat), (b)βMal-C_{12}(23%wat), (c)βMal-$C_{12}C_8$(*R*)(25%wat), (d)βMal-$C_{12}C_8$(*S*)(25%wat), and (e)βMal-$C_{12}C_8$(*RS*)(25%wat). Red color region – sugar headgroup, green color region – tail groups, and blue color region – water.

(hydrogen bonds between lipids), $n_{lipid-lipid}$ = 4.1, whereas the other systems studied here have an average of 3.35 intermolecular hydrogen bonds per lipid.

The hydrogen bonding interaction between water layer and lipid's sugar moieties ($n_{water-lipid}$) for all the branched chain systems has an average value about 9.60. Additionally, the HB between the chiral molecules (βMal-$C_{12}C_8$(*R*)(25%wat), βMal-$C_{12}C_8$(*S*)(25%wat)) and in the racemic bilayer system, βMal-$C_{12}C_8$(*RS*)(25%wat) have been tabulated in Table 4.9 by considering the like-isomers (*R*-*R* and *S*-*S* types) and their opposite counterparts (*R*-*S* and *S*-*R*). In the choice of an *R*-*S* pair, the *R* isomer is defined as a donor and the *S* isomer as an acceptor and in an *S*-*R* pair, the definition is vice-versa. The intermolecular HB values between the same type of isomers (*R*-*R* and *S*-*S* types) show almost similar value about ∼0.90 hydrogen bond per lipid whereas the average HB value between enantiomers (*R*-*S* and *S*-*R*) is about 0.69 that is ∼ 23% less

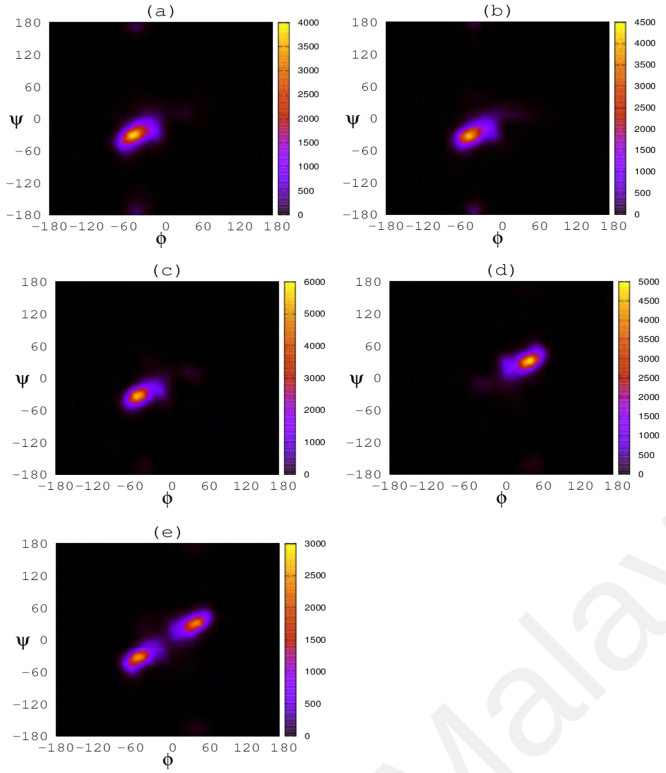

Figure 4.28: Dihedral angle (Φ and Ψ) population for the headgroup of the bilayer systems; (a)βMal-C_{12}(12%wat), (b)βMal-C_{12}(23%wat), (c)βMal-$C_{12}C_8$(*R*)(25%wat), (d)βMal-$C_{12}C_8$(*S*)(25%wat), and (e)βMal-$C_{12}C_8$(*RS*)(25%wat).

Table 4.8: Hydrogen bonding of lipid-lipid and water-lipid for the bilayer systems of βMal-C_{12}(12%wat), βMal-C_{12}(23%wat), βMal-$C_{12}C_8$(*R*)(25%wat), βMal-$C_{12}C_8$(*S*)(25%wat), and βMal-$C_{12}C_8$(*RS*)(25%wat). The average values are calculated for the last 225 ns trajectory of total 300 ns simulation run. The monoalkylated bilayers been simulated at 80 °C and branched chain bilayers are at room temperature (25 °C). (With error ±0.2).

	Lipid-Lipid, ($n_{lipid-lipid}$)	Water-Lipid, ($n_{water-lipid}$)	Total HB, n_{tot}
βMal-C_{12}(12%wat)	3.5	5.6	9.1
βMal-C_{12}(23%wat)	4.1	6.4	10.5
βMal-$C_{12}C_8$(*R*)(25%wat)	3.2	9.6	12.8
βMal-$C_{12}C_8$(*S*)(25%wat)	3.4	9.4	12.8
βMal-$C_{12}C_8$(*RS*)(25%wat)	3.3	9.7	13.0

than the former. This indicates that the intermolecular hydrogen bonding between the same isomer types is higher than their enantiomeric pairs. Meanwhile, the average water–lipid hydrogen bonding between the glycolipids *R* and *S* (as donors) and water (as acceptor) is about 2.8. Also, the opposite arrangement of the donors and acceptors, (*R* and

Table 4.9: Hydrogen bonding of lipid-lipid and water-lipid for the Guerbet branched system in recemic micture, βMal-$C_{12}C_8$(*RS*)(25%wat). The average values are calculated for the last 225 ns trajectory of total 300 ns simulation run. (All values are within error $\pm$0.2).

Acceptor	Donor	HB-value
Lipid-Lipid		
βMal-$C_{12}C_8$(*R*)(25%wat)	βMal-$C_{12}C_8$(*R*)(25%wat)	0.94
βMal-$C_{12}C_8$(*S*)(25%wat)	βMal-$C_{12}C_8$(*S*)(25%wat)	0.93
βMal-$C_{12}C_8$(*R*)(25%wat)	βMal-$C_{12}C_8$(*S*)(25%wat)	0.71
βMal-$C_{12}C_8$(*S*)(25%wat)	βMal-$C_{12}C_8$(*R*)(25%wat)	0.67
Water-Lipid		
βMal-$C_{12}C_8$(*R*)(25%wat)	Wat	2.84
βMal-$C_{12}C_8$(*S*)(25%wat)	Wat	2.85
Wat	βMal-$C_{12}C_8$(*R*)(25%wat)	2.03
Wat	βMal-$C_{12}C_8$(*S*)(25%wat)	1.95

S isomers–as acceptors) and water (as a donor), gives the average HB value about 2.0 (see Table 4.9). Besides, the single chain lipids (βMal-C_{12}(12%wat) and βMal-C_{12}(23%wat)) have lower HB values compared to the branched chains about 41% and 33% respectively.

It is also instructive to reflect the distribution of intermolecular hydrogen bonds as a function of oxygen sites around the sugar rings (Figure 4.29 a-e). This enable us to do a comparative study with the hydrogen bond results of the monolkylated maltoside from anhydrous bilayer system from Section 4.1. In general, the acceptor oxygen atoms at the glycosidic linkage (O1 and O1') and oxygen on the sugar rings (O5 and O5') show very low lipid-lipid and water-lipid hydrogen bonding values compared to other oxygen sites. Additionally, the patterns of the lipid-lipid HB distributions are almost the same with the single and branched chain maltosides where the O2, O4, O6, O2', O3', and O6' show stronger HB than the rest of the sites compared to the anhydrous bilayer from Section 4.1. Nevertheless, the water-lipid hydrogen bonding for the βMal-C_{12}(12%wat) is different compared to the other glycosides. The O3 site has the lowest HB value ($\sim$0.78) in βMal-C_{12}(12%wat) compared to about 1.4 in βMal-C_{12}(23%wat) and about 1.9 in

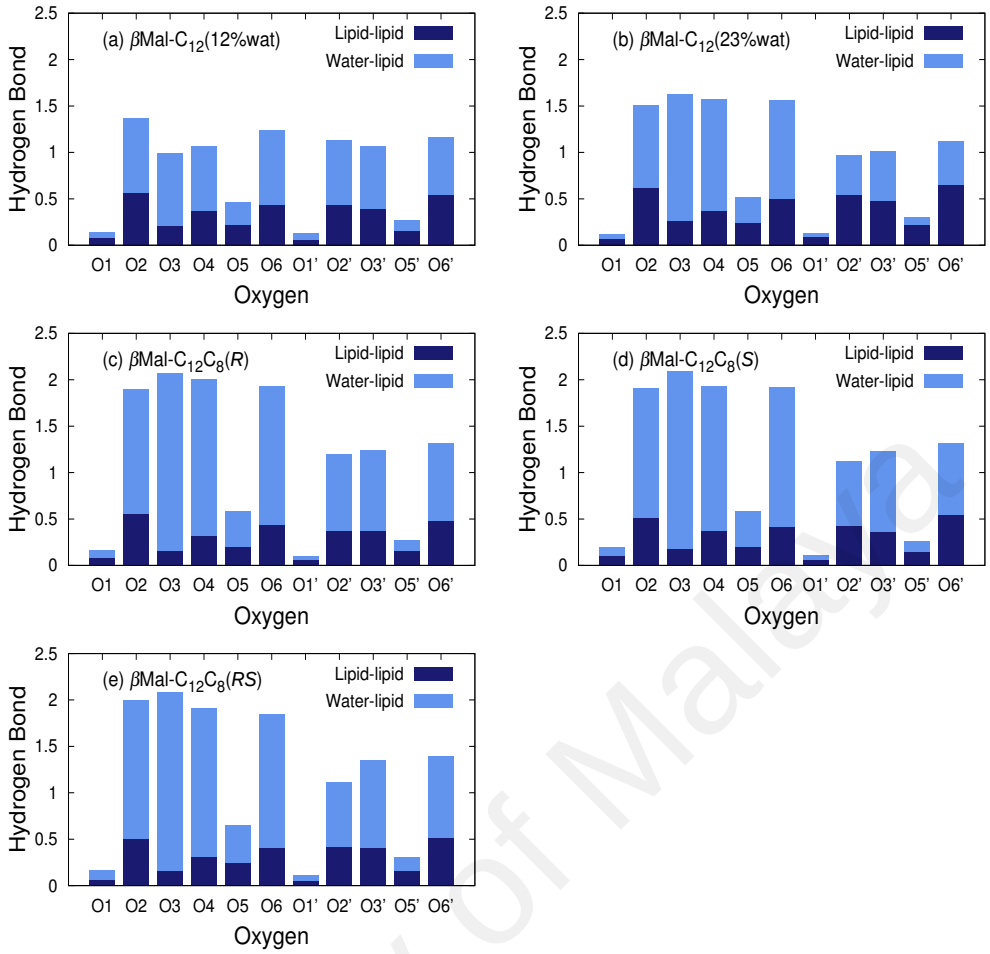

Figure 4.29: Hydrogen bonding of lipid-lipid and water-lipid for each oxygen site of hydroxyl group in the sugar. (a)βMal-C_{12}(12%wat), (b)βMal-C_{12}(23%wat), (c)βMal-$C_{12}C_8$(R)(25%wat), (d)βMal-$C_{12}C_8$(S)(25%wat), and (e)βMal-$C_{12}C_8$(RR)(25%wat), and (f)βMal-$C_{12}C_8$(SS)(25%wat). The βMal-$C_{12}C_8$(RR)(25%wat) and βMal-$C_{12}C_8$(SS)(25%wat) represent βMal-$C_{12}C_8$(R)(25%wat) and βMal-$C_{12}C_8$(S)(25%wat) respectively in the racemic mixture of βMal-$C_{12}C_8$(RS)(25%wat).

average from all three branched chain systems. However, the chiral (R& S), and racemic (RS) systems do not show any off trend profile for the water-lipid HBs.

4.3.3 Hydrogen bonding lifetime (HB-lifetime)

The hydrogen bonding lifetime (HB-lifetime) traditionally is considered as an important quantity to evaluate the strength of the HB interactions (Z. Zhang et al., 2007). But some relevant studies suggest that the HB-lifetime is an environment-dependent property and highly depends on the local structures of the residues and solvents (Chowdhary & Ladanyi, 2008; Tielrooij, Hunger, Buchner, Bonn, & Bakker, 2010). Nevertheless, carbohydrate amphiphilic molecules in self-assembled structures primarily influenced by HB interaction (Paleos & Tsiourvas, 2001), especially in the liquid crystalline phase. Thus, estimating

Table 4.10: Hydrogen bonding lifetime values (in ps) for βMal-C_{12}(12%wat), βMal-C_{12}(23%wat), βMal-$C_{12}C_8$(*R*)(25%wat), βMal-$C_{12}C_8$(*S*)(25%wat), and βMal-$C_{12}C_8$(*RS*)(25%wat). Group(I) represents the HB-lifetime between solute and solute. Group(II) represents the HB-lifetime between solute (acceptor) and solvent (donor). Group(III) represents the HB-lifetime between solute (donor) and solvent (acceptor).

Bilayer System	**Group(I): represent solute-solute HB-lifetime**										
Oxygen	O1'	O2'	O3'	O5'	O6'	O1	O2	O3	O4	O5	O6
βMal-C_{12}(12%wat)	7.5	23.0	21.3	14.7	23.4	8.1	24.3	14.0	21.0	18.9	17.8
βMal-C_{12}(23%wat)	7.5	26.9	23.1	16.4	23.1	8.1	23.4	14.4	19.3	19.8	16.2
βMal-$C_{12}C_8$(*R*)(25%wat)	8.6	34.8	34.1	21.2	37.5	10.1	34.0	16.2	29.4	21.8	24.6
βMal-$C_{12}C_8$(*S*)(25%wat)	8.7	36.7	30.2	19.8	34.7	11.7	30.7	17.8	32.0	23.1	23.9
βMal-$C_{12}C_8$(*RR*)(25%wat)	7.8	36.9	35.9	17.8	39.2	8.2	31.3	16.6	26.5	18.3	25.9
βMal-$C_{12}C_8$(*SS*)(25%wat)	8.1	33.7	35.6	18.7	28.2	12.4	29.0	17.3	31.6	21.0	24.6
	Group(II): solute(acceptor,A)-solvent(donor,D) HB-lifetime										
	O1'	O2'	O3'	O5'	O6'	O1	O2	O3	O4	O5	O6
βMal-C_{12}(12%wat)	6.7	19.1	16.1	9.7	19.1	7.3	17.5	16.4	16.3	13.1	18.2
βMal-C_{12}(23%wat)	6.7	17.2	15.2	9.8	17.3	7.1	16.7	21.3	17.3	12.8	21.0
βMal-$C_{12}C_8$(*R*)(25%wat)	6.7	30.0	21.2	10.5	30.5	7.7	25.9	35.0	27.0	16.6	33.5
βMal-$C_{12}C_8$(*S*)(25%wat)	7.1	28.9	23.2	11.2	28.9	7.7	25.9	34.9	25.9	15.8	32.9
βMal-$C_{12}C_8$(*RR*)(25%wat)	7.2	27.0	24.5	11.2	30.2	7.9	25.5	35.4	26.5	16.2	30.2
βMal-$C_{12}C_8$(*SS*)(25%wat)	7.5	30.2	22.6	11.6	30.5	7.9	28.3	32.0	27.2	16.0	31.8
	Group(III): solute(donor,D)-solvent(acceptor,A) HB-lifetime										
	O1'	O2'	O3'	O5'	O6'	O1	O2	O3	O4	O5	O6
βMal-C_{12}(12%wat)	-	33.9	22.4	-	20.5	-	22.4	19.7	21.9	-	17.2
βMal-C_{12}(23%wat)	-	32.4	21.4	-	19.5	-	23.5	22.2	26.7	-	17.8
βMal-$C_{12}C_8$(*R*)(25%wat)	-	61.5	40.6	-	35.4	-	44.8	38.3	44.2	-	32.3
βMal-$C_{12}C_8$(*S*)(25%wat)	-	57.4	38.7	-	34.9	-	45.0	39.5	44.1	-	33.3
βMal-$C_{12}C_8$(*RR*)(25%wat)	-	55.6	39.7	-	37.9	-	45.5	37.9	44.8	-	29.1
βMal-$C_{12}C_8$(*SS*)(25%wat)	-	51.2	40.7	-	33.6	-	42.8	42.7	47.0	-	30.3

the HB-lifetime may give a glimpse on the behavior of sugar residues in the conformation of lipids in the bilayer assembly. We calculate the HB-lifetime of mono- and branched chain Guerbet glycosides in three main categories: Group(I)–among lipid headgroups only; (solute-solute), Group(II)–solute as an acceptor and solvent as donor; (solute(as acceptor, A)-solvent(as donor, D), and Group(III)–solute as a donor and solvent as an acceptor; (solute(donor, D)-solvent(acceptor, A). The corresponding values of HB-lifetime are given in Table 4.10.

In general, we notice the HB-lifetime for monoalkylated glycolipids are shorter than branched chain glycolipids. In Group(I) and Group(II), all the glycosidic oxygen show very low HB-lifetime (average around 8.1 ps). This indicates that these oxygen are minimally involved with hydrogen bonding between solute-solute and solute-solvent. In Group(I), the hydroxyl oxygen (O2', O3', and O6') from the reducing sugar ring of the branched chain glycosides show longer HB-lifetime (above 30 ps) compared to oxygen from non-reducing sugars. The lifetimes for the other oxygen atoms (O2, O3, O4, O5, and O6) ranges from $\sim$16 to $\sim$34 ps.

The HB-lifetimes between solvent (water) and solute (lipid moiety), in Group(II), show that the reducing and non-reducing sugar ring oxygen atoms (O2', O3', O6', O2, O3, O4, and O6) are slightly lower compared to the same oxygen in Group(I). This indicates that the HB bond making and breaking between solute-solvent is much faster than those between solute-solute. However, in Group(III) oxygen atoms O2', O3', O6', O2, O3, O4, and O6, from Guerbet branched chain lipids, show higher HB-lifetimes while for single chain lipids the lifetimes are comparatively small.

4.3.4 Hydration at surrounding sugars

The water-lipid HB interaction of each oxygen site from the sugar moieties, is possibly related to the degree of water hydration surrounding each hydroxyl group from sugar. Qualitatively, this can be observed for every bilayer system from Figure 4.29. All the systems, except for βMal-C_{12}(12%wat), show a general trend in the HB values for each oxygen site where the oxygen O2, O3, O4, and O6 from the non-reducing sugar may be surrounded by higher water hydration than oxygen O2', O3', and O6' in the reducing sugar. However, for βMal-C_{12}(12%wat), the lower HB values surrounding each oxygen atom is due to the lower water concentration (12%wat) compared to the other systems.

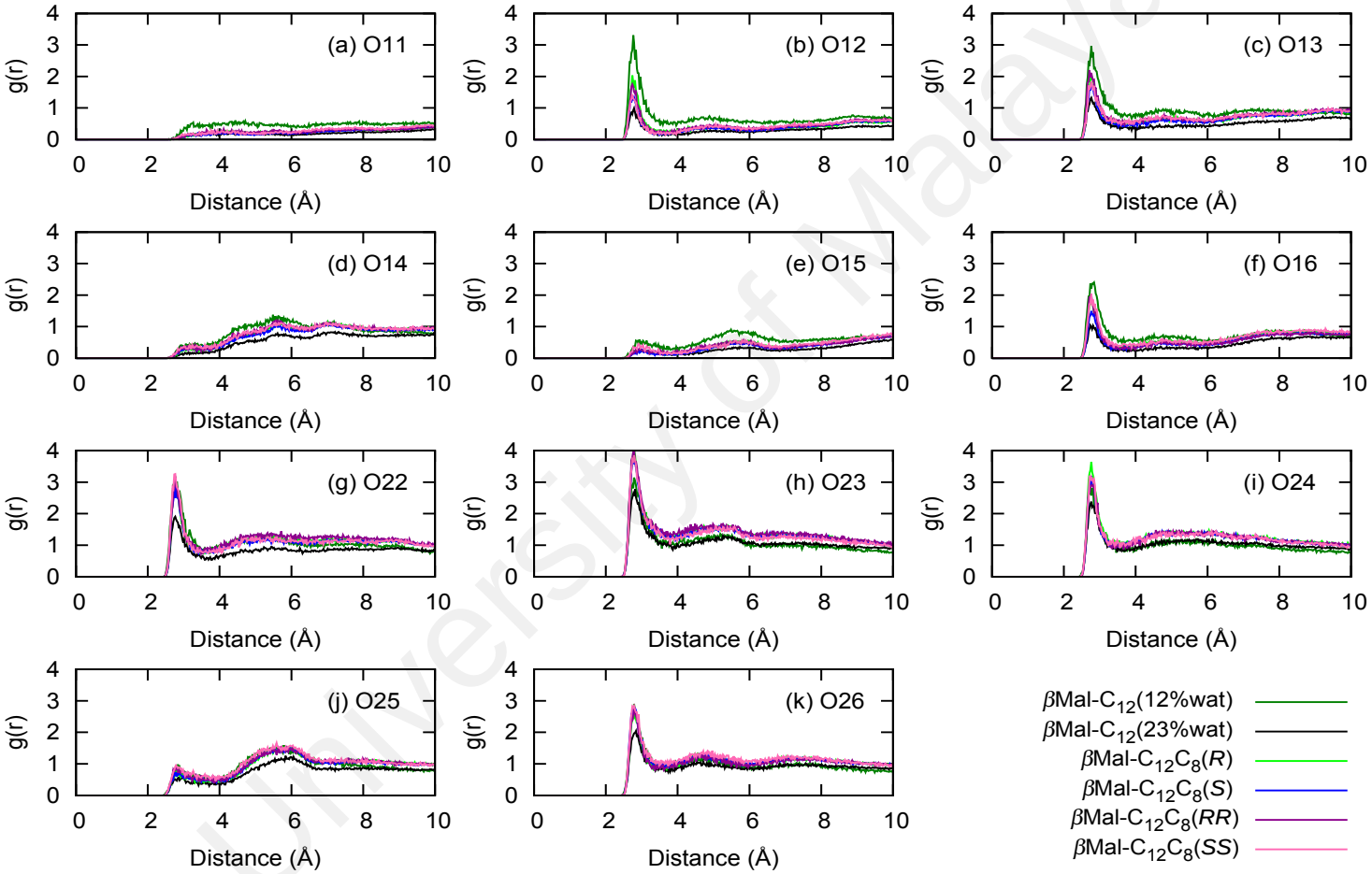

Figure 4.30: Radial distribution function (RDF) for the oxygen from sugar headgroup and oxygen from water molecules for single and branched chain maltosides.

The different hydration density at different location of the sugar headgroup is quantified by the radial distribution function (RDF) for the water oxygen atoms with respect to all the oxygen sites of the sugars. The peaks and valleys in this function (see Figure 4.30) reflect a non-uniform distribution of water density and the function's characteristic peaks represent the hydration shells formed by water molecules around the lipid oxygen atoms. The distances of the first and corresponding second shell at each oxygen atom in the reducing and non-reducing sugar oxygen are given in Table 4.11. The average first peak value for oxygen (O2, O3, O4, O6, O2', O3', and O6') from every bilayer system is around 2.78 $\pm$ 0.02 Å, indicating that the corresponding oxygen from hydroxyl groups are covered by the first shell of water layer. Meanwhile, oxygen O2, O3, and O4 from non-reducing sugars have second peaks at an average distance of 5.16 $\pm$ 0.16 Å. Likewise, the second peaks of oxygen O2', O3', and O6' from reducing ring gives an average distance of about 4.83 $\pm$ 0.12 Å for all the lamellar systems. But oxygen O2, O4, O2', O3', and O6' from βMal-C_{12}(23%wat) do not show the presence of a second peak which indicate these oxygen sites do not have structured water molecules after the first shell.

It is evident from Figure 4.30 that the glycosidic oxygen O1' and O1 and sugar ring oxygen O5' and O5, respectively from reducing and non-reducing sugars, have no first peak; indicating that those oxygen have a reduced ability to compete for the hydrogen bond partners due to their lower charge (Liu & Brady, 1997). Meanwhile, oxygen O2', O3', and O6' from βMal-C_{12}(12%wat) show higher peak values which indicate the water surrounding these oxygen have a higher order. This may be due to the low water concentration (12%wat) where the waters may get trapped between adjacent lipid molecules at the headgroup interface region and eventually orient to have maximum HB interaction.

Table 4.11: Radial distribution function values for hydroxyl oxygen with oxygen of the water molecules. The values are corresponding to the distance (in Å) of first peak (P1) and second peak (P2) is given below. (With error ±0.02).

	Non-reducing ring								**Reducing ring**					
Hydroxyl Oxygen	O2		O3		O4		O6		O2'		O3'		O6'	
Peak	P1	P2	P1	P2	P1	P2	P1	P2	P1	P2	P1	P2	P1	P2
βMal-C_{12}(12%wat)	2.78	5.2	2.81	5.38	2.79	5.21	2.8	4.57	2.77	4.87	2.75	4.84	2.8	4.75
βMal-C_{12}(23%wat)	2.8	-	2.81	5.27	2.78	-	2.83	4.61	2.79	-	2.76	-	2.76	-
βMal-$C_{12}C_8$(*R*)(25%wat)	2.79	5.26	2.79	5.27	2.78	4.97	2.81	4.57	2.74	4.95	2.76	5.04	2.76	4.81
βMal-$C_{12}C_8$(*S*)(25%wat)	2.8	5.06	2.78	5.2	2.78	4.9	2.8	4.77	2.75	4.75	2.78	4.87	2.76	4.63
βMal-$C_{12}C_8$(*RR*)(25%wat)	2.78	5.35	2.8	4.99	2.79	5.22	2.81	4.63	2.75	4.89	2.72	4.78	2.75	4.79
βMal-$C_{12}C_8$(*SS*)(25%wat)	2.76	5	2.8	5.31	2.72	-	2.77	4.84	2.75	5.08	2.77	4.75	2.76	4.71

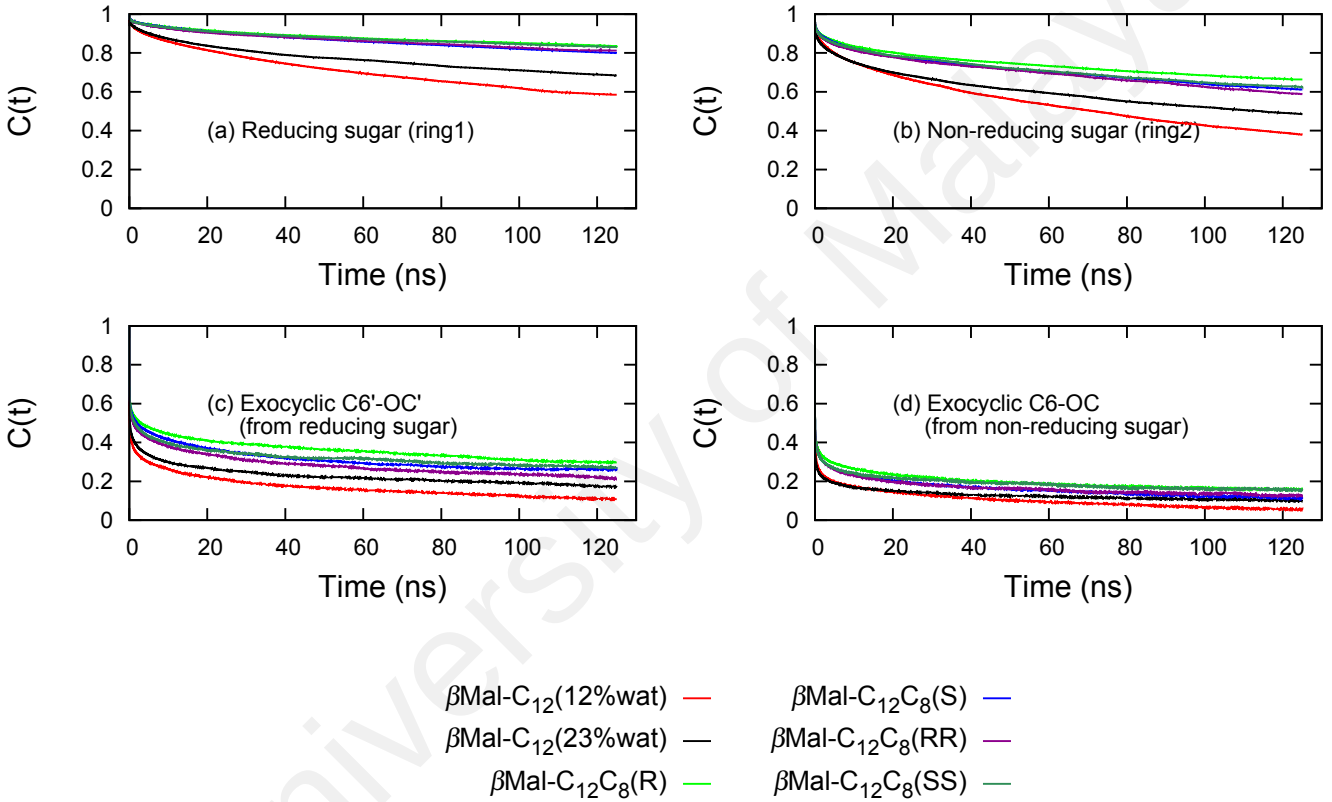

Figure 4.31: Rotational autocorrelation function (RACF) of all bilayer systems. (a) reducing sugar (*ring1*), (b) non-reducing sugar (*ring2*), (c) exocyclic residue from *ring1*, and (d) exocyclic residue from *ring2*.

4.3.5 Dynamics of sugars and exocyclic groups

We probe the dynamics of the maltose headgroup by calculating the rotational autocorrelation function (RACF) for each sugar units (reducing(*ring1*) and non-reducing(*ring2*)) separately along the vectors defined from CO1'—CO4' and CO1—CO4 in order for each sugar moiety. Additionally, we also calculated the RACF for the exocyclic group of the two sugars along the vector defined at the bond C6—O(hydroxyl) and C6'—O'(hydroxyl) for both the *ring1* and *ring2*. The RACF plot for the sugars are shown in Figure 4.31(a) and (b) and for the exocyclic group in Figure 4.31 (c) and (d).

The extracted correlation times from the plots are tabulated in Table 4.12 and we notice the dynamics of reducing sugars are slower than the non-reducing sugars. On average, the correlation time for the reducing sugars of branched chain glycosides is $\sim$71 ps while for non-reducing sugars the correlation time is reduced by $\sim$10% (61 ps). However, the monoalkylated bilayers show a much shorter correlation time compared to the branched ones. Both the reducing and non-reducing sugar units from βMal-C_{12}(12%wat) rotates approximately 5-6% faster than the same sugar unit from βMal-C_{12}(23%wat).

In general, the correlation times for the exocyclic residues from a reducing ring is longer than non-reducing sugars. For the branched system, the exocyclic group rotates four times faster than their non-reducing sugar units ($\sim$15 ps) where for monoalkylated systems, the same exocyclic group comparatively rotates five times faster ($\sim$10ps). Meanwhile, for the exocyclic groups from the reducing sugar of the branched system rotate about two times faster ($\sim$25 ps) than their sugar rings ($\sim$70 ps). Lastly, the same group from monoalkylated lipids of reducing ring rotates about three times faster ($\sim$20 ps) than the sugar ($\sim$65 ps).

Table 4.12: Correlation times for reducing and non-reducing sugars and the exocyclic residue from each sugar rings in (ns). All the correlation times are obtained by calculating the area under the RACF (see Figure 4.31) of every bilayer system.

	Reducing sugar (*ring1*)	Non-reducing sugar (*ring2*)	Exocyclic group of reducing sugar (exo-*ring1*)	Exocyclic group of non-reducing sugar (exo-*ring2*)
βMal-C_{12}(12%wat)	61.1	49.7	16.1	10.3
βMal-C_{12}(23%wat)	64.6	52.7	20.3	11.5
βMal-$C_{12}C_8$(*R*)(25%wat)	72	62	31.4	17.7
βMal-$C_{12}C_8$(*S*)(25%wat)	71.1	60.1	27.8	15
βMal-$C_{12}C_8$(*RR*)(25%wat)	71	59.5	25.4	15.1
βMal-$C_{12}C_8$(*SS*)(25%wat)	71.7	60.4	28	16.8
βMal-$C_{12}C_{10}$[a]	76	73	-	-

[a]Section 4.2

4.3.6 Orientations of headgroup and alkyl chains

The headgroup orientation of the reducing (*ring1*) and non-reducing (*ring2*) sugars, is observed by calculating the angular distribution separately with respect to the *z*-axis of the bilayer. The vectors representing each sugar ring are defined as the line connecting the carbons C1'—C4'(for *ring1*) and C1—C4(for *ring2*) respectively Figure 4.32(a and b) shows the distribution plots for both the sugars respectively for all the bilayer systems. Additionally, the angular values corresponding to the maximum population of each orientation and the values of full width at half maximum (FWHM) are given in Table 4.13. We also measured the angular orientations for *R* & *S* isomers in racemic mixture where the βMal-$C_{12}C_8$(*RR*)(25%wat) and βMal-$C_{12}C_8$(*SS*)(25%wat) represent the single isomer Guerbet glycosides, βMal-$C_{12}C_8$(*R*)(25%wat) and βMal-$C_{12}C_8$(*S*)(25%wat) in order.

Table 4.13: Maximum peak values of sugar headgroups for single and branched chain glycolipids and corresponding full width half maximum (FWHM), $\triangle$x values for the reducing sugar (*ring1*). The βMal-$C_{12}C_8$(*RR*)(25%wat) and βMal-$C_{12}C_8$(*SS*)(25%wat) represent βMal-$C_{12}C_8$(*R*)(25%wat) and βMal-$C_{12}C_8$(*S*)(25%wat) from racemic mixture βMal-$C_{12}C_8$(*RS*)(25%wat).

	Maximum peak values	$\triangle$x
βMal-C_{12}(12%wat)	19°, 98°	73°
βMal-C_{12}(23%wat)	23°, 159°	-
βMal-$C_{12}C_8$(*R*)(25%wat)	86°	54°
βMal-$C_{12}C_8$(*S*)(25%wat)	88°	65°
βMal-$C_{12}C_8$(*RR*)(25%wat)	86°	66°
βMal-$C_{12}C_8$(*SS*)(25%wat)	81°	65°

Headgroup angular orientation of *ring1* for all the branched chain glycosides shows a single maximum peak values above 80°. Among them, the headgroup of βMal-$C_{12}C_8$(*S*)(25%wat) shows an orientation of about 88° which indicates that its orientation slightly towards to the bilayer horizontal surface while βMal-$C_{12}C_8$(*SS*)(25%wat) from racemic mixture has an orientation of about 81°. Additionally, the βMal-$C_{12}C_8$(*R*)(25%wat) and βMal-$C_{12}C_8$(*RR*)(25%wat) show similar degree of orientations. The latter gives an impression that the *ring1* is about 8° below the bilayer surface while the former shows only a small amount of *ring1* align nearly parallel

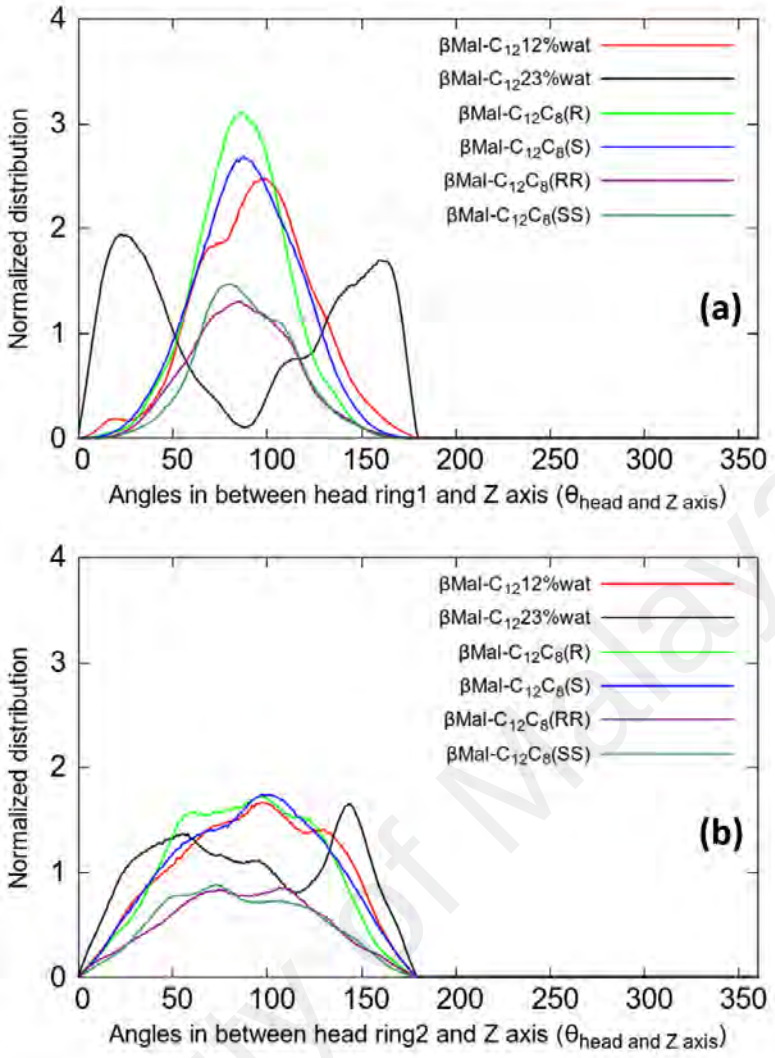

Figure 4.32: Distribution of headgroup angle measured with respect to the z-axis of the bilayer surface. (a) distribution of reducing sugar and (b) distribution of non-reducing sugar.

to the long axis of bilayer normal. However, the βMal-C_{12}(23%wat) shows two peaks – one at 23° and the other about 159°. The latter gives an impression that the *ring1* is about 70° below the bilayer surface while the former shows only a small amount of *ring1* align nearly parallel to the long axis of bilayer normal.

Beside, the non-reducing sugar (*ring2*) from all glycosides shows much broader peaks compared to *ring1* (see Figure 4.32(b)), which implies that the *ring2* is much flexible in nature and has more orientational possibilities. Among these distributions, *ring2* from βMal-C_{12}(23%wat) shows two peaks–one broader peak at around 55° and one sharp peak at 143° which suggests that some of *ring2* possibly burrow into *ring1* region.

The distribution of angles between the chains of the glycosides and the z-axis of the bilayer was calculated by defining vectors along the long chain (C71-C80)(*sn*-1) and the

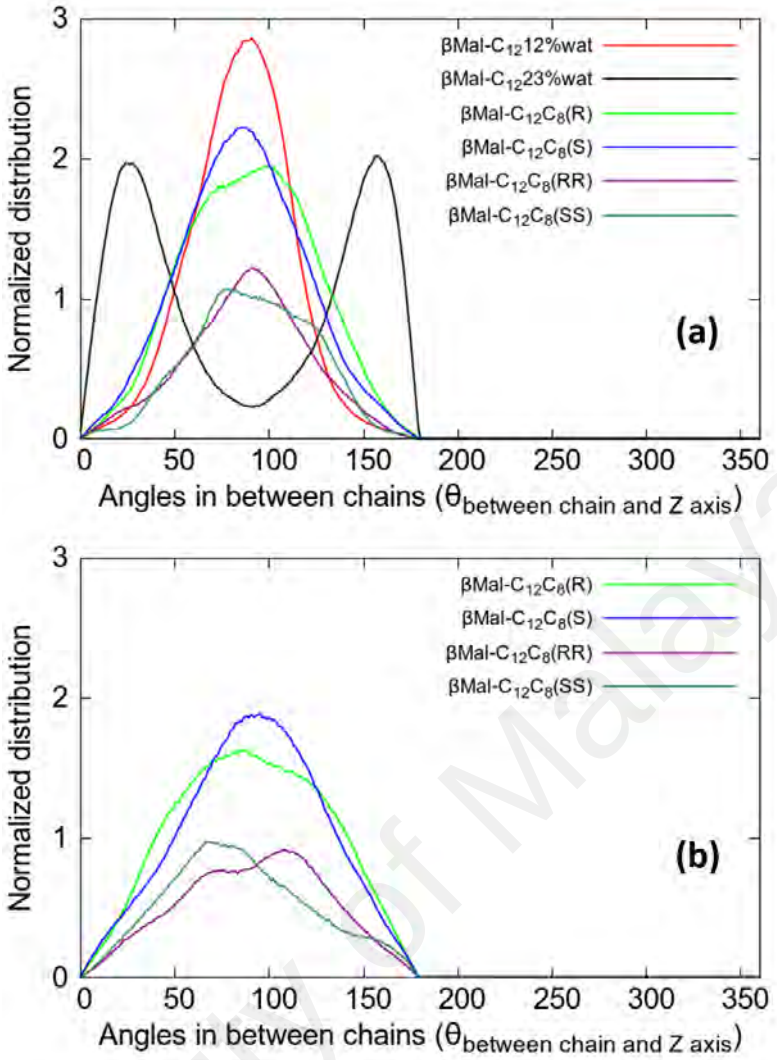

Figure 4.33: Angle distribution of chains with z-axis and (a) angle between long chain vector (connecting C71—C80), and (b) angle between short chain vector (connecting C83—C88).

short chain (C83-C88)(*sn*-2) (see Figure 4.23). The distribution of the angles is shown in Figure 4.33(a and b) and the corresponding maximum peak value of each distribution is tabulated in Table 4.14. The chain angular distributions for all the glycosides show unimodal distribution function except for βMal-C_{12}(23%wat) which shows a bimodal distribution with the maximum peaks at around 25° and 160°.

Table 4.14: Maximum peak values of angles (in degrees/θ°) from the distribution of angles between z-axis and the vector representing alkyl chain from each glycoside system.

Bilayer System	Angle between chain and z-axis	
	long chain	short chain
βMal-C_{12}(12%wat)	89.1°	-
βMal-C_{12}(23%wat)	25.3°, 158.6°	-
βMal-$C_{12}C_8$(R)(25%wat)	94.5°	107.6°
βMal-$C_{12}C_8$(S)(25%wat)	86.1°	93.4°
βMal-$C_{12}C_8$(RR)(25%wat)	91.3°	86.6°
βMal-$C_{12}C_8$(SS)(25%wat)	78.2°	64.4°

4.3.7 Hydrocarbon chain order parameter

An order parameter (OP), -S_{CD} calculation quantifies the bond ordering along the hydrocarbon chain such that the lower -S_{CD} indicates more disorder and bending (indication of fluid like) and for high -S_{CD} this denotes more ordering. The order parameters of the monoalkylated and branched chain glycoside bilayers in liquid crystalline state are shown in Figure 4.34. We notice the OP for βMal-C_{12}(12%wat) is higher than βMal-C_{12}(23%wat) indicating the alkyl chain for the former is more ordered ($\sim$0.28) than the latter. In particular, the OP of the carbons at the middle (C74-C76) of the long chain is higher than the carbons near to the headgroup and methyl groups at the lower half of the chain. Meanwhile, the hydrocarbons in βMal-C_{12}(23%wat), especially upper half and middle (C71-C75) show almost the same OP values ($\sim$0.20).

Meanwhile, the OP for both chains in branched glycosides shows lower ordering compared to the single chain lipids (see Figure 4.34 (c) and (d)). It is noticeable that the order parameters of all the longer chains (*sn*-1) are higher than the shorter ones. A closer look at the longer chain OP profile in Figure 4.34 (c) reveals that the corresponding OP profiles are distinguishable; βMal-$C_{12}C_8$(S)(25%wat) and βMal-$C_{12}C_8$(SS)(25%wat) have higher order compared to βMal-$C_{12}C_8$(R)(25%wat) and βMal-$C_{12}C_8$(RR)(25%wat). Also it is noticeable that the middle carbons in the long chains (C76 and C77) show higher OP values. However, the shorter chains show no distinct separation in the OP profiles (Figure 4.34(d)) and the order parameters for the upper half carbons show lower OP values

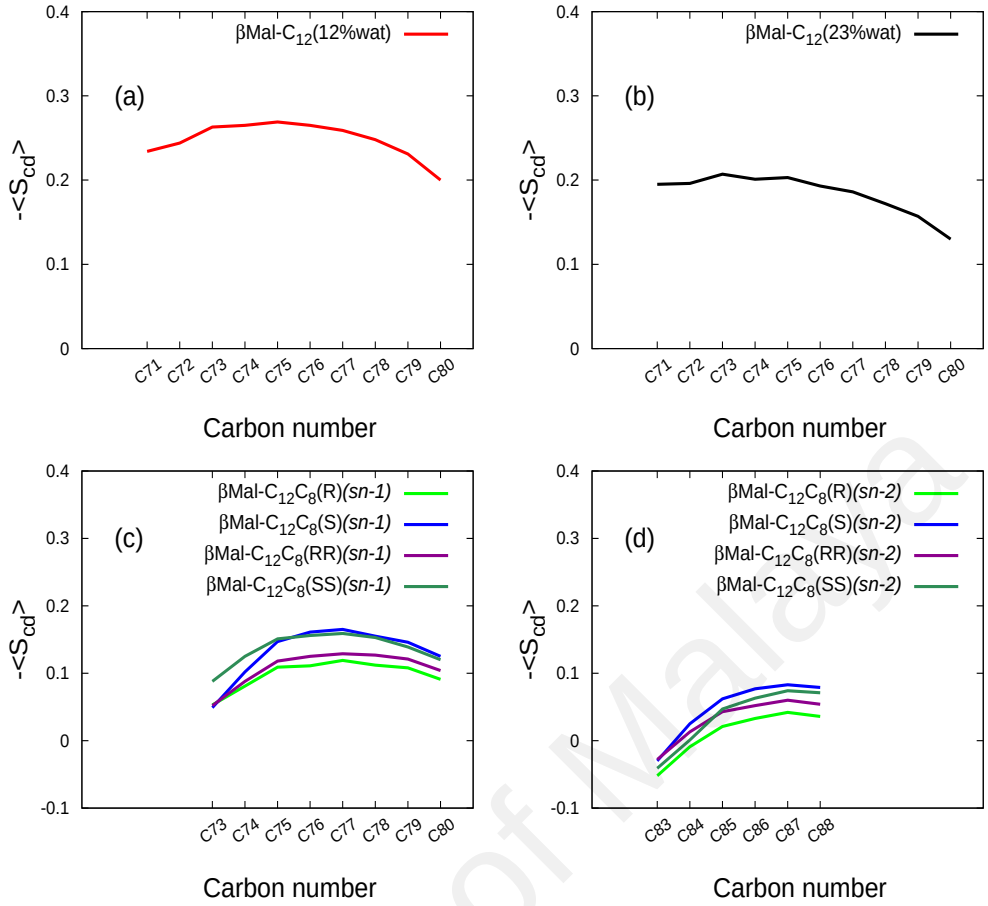

Figure 4.34: Chain order parameter of the hydrocarbons in each bilayer system; (a) for βMal-C_{12}(12%wat), (b) for βMal-C_{12}(23%wat), (c) & (d) shows the OP profiles for the long and short chains respectively in βMal-$C_{12}C_8$(*R*)(25%wat), βMal-$C_{12}C_8$(*S*)(25%wat), and lipids in the racemic mixture of βMal-$C_{12}C_8$(*RS*)(25%wat). The βMal-$C_{12}C_8$(*RR*)(25%wat) and βMal-$C_{12}C_8$(*SS*)(25%wat) represent lipids βMal-$C_{12}C_8$(*R*)(25%wat) and βMal-$C_{12}C_8$(*S*)(25%wat) from racemic mixture βMal-$C_{12}C_8$(*RS*)(25%wat).

than the terminal carbons. This is possibly due to the arrangement of lipids in bilayers where the bulky disaccharides with water molecules filling the sugar interface, allow the glycosidic region (region between sugar and alkyl chain) to have more space. This space enable the carbons C83, C84, and C85 to have low order than the rest of carbons along shorter chain. Order parameter calculations on phospholipid systems do not show similar OP profile (Essex et al., 1994; Róg et al., 2004). They show the carbons near the headgroup have high order and carbons near methyl group have lower order. However, our OP trend give an impression that the OP profile is dependent on the bulkiness of hydrophilic sugar moiety. Meanwhile, the higher OP for carbons near the methyl group is high may be due to the intercalation among neighboring long chains.

4.3.8 Discussion

We report a simulation study on glycolipid bilayers of maltosides with single chain (βMal-C_{12}(12%wat), βMal-C_{12}(23%wat)) and Guerbet branched chain. The Guerbet maltoside has a chiral center at the chain branching and this gives *R* and *S* chiral isomers with which a total of three bilayer systems were built, namely βMal-$C_{12}C_8$(*R*)(25%wat), βMal-$C_{12}C_8$(*S*)(25%wat), and βMal-$C_{12}C_8$(*RS*)(25%wat), where the latter is the racemic mixture with 50% mass weight from each *R* & *S* isomers. All the bilayer systems were simulated in liquid crystalline (L_α) phase for 300 ns, mainly to understand their structural and dynamical behaviors subjected to the variation in temperature, water concentration, and chain branching.

The stability of all the five simulated bilayers were monitored by observing the local density profile (LDP), area per lipid at the surface of bilayer interface, and contour plot of the dihedral angle between reducing and non-reducing sugars. The plots of LDP, area per lipid, and *d*-spacing show that all the bilayer systems are intact throughout the simulation time scale without a significant change in the plateau. Since sugar moieties have complex configuration, disaccharide containing molecules like maltoside need a longer simulation time to attain stable conformation as reported in Section 4.1. Referring to Figure 4.26 ((a) and (b)) the first 75 ns was allowed as a phase for the system to reach optimum stability and the last 225 ns production trajectory was taken for the analysis of bilayer properties.

The average area per lipid at interface for branched chain Guerbet maltosides in hydrated condition increases about 6% compared to the anhydrous branched chain glycolipid βMal-$C_{12}C_{10}$ (which is 51.9 Å^2) in Section 4.1. This increment suggests that the presence of water molecules possibly penetrate the hydrophilic sugar region and expand the surface area. The penetration of water molecules into the headgroup region can be seen clearly in Figure 4.27 (c, b, d), where hybrids of blue and red colour shaded regions indicate the headgroup region which had been hydrated. However, Hamid et al. (2014) reported the experimental value of area per lipid for the Guerbet glycoside as 64.1 Å^2, which is higher by about 14% more than the value from the current simulation. Also, from the x-ray experiment, there is no indication if the area per lipid value corresponds to the isomeric conformation of constituent glycosides; if the bilayers contain only the *R* or *S* or contain the mixture of the two chiral isomers with specific proportion. On the other hand, the three Guerbet branched chain bilayer models (βMal-$C_{12}C_8$(*R*)(25%wat),

βMal-$C_{12}C_8$(*S*)(25%wat), and βMal-$C_{12}C_8$(*RS*)(25%wat)) used in this simulation give almost similar area per lipid values ($\sim$55 Å^2) suggesting that the conformation of the lipids (*R* or *S*) is insignificant to the area per lipid. With this in mind, we ought to consider the experimental value (64.1 Å^2) for the area per lipid of branched chain Guerbet glycosides (βMal-$C_{12}C_8$) most probably due to presence of some impurity in the sample, although it is reported that the purity was confirmed within 98% (Hamid et al., 2014). It is also possible the difference observed here is due to the generalized force fields used in the simulation.

Meanwhile, the single chain glycosides show a different trend in the area per lipid values as the hydration level changes. The area per lipid of βMal-C_{12}(23%wat) shows a decrease of about 15% compared to βMal-C_{12}(12%wat) despite the water concentration being higher than βMal-C_{12}(12%wat). The area per lipid of the same compound (βMal-C_{12}) in dry condition was reported as 38.8 Å^2 in Section 4.1. Although, the area per lipid of βMal-C_{12}(12%wat) increases by 2.3 Å^2 compared to βMal-C_{12} in dry condition but the area per lipid of βMal-C_{12}(23%wat) decrease much smaller to 35.1 Å^2. The phase diagram by Auvray et al. (2001) (see Figure 3.5), shows that the βMal-C_{12} system at 23% water weight is near to the hexagonal region and most probably the lipids tend to form a hexagonal phase at a little higher hydrated condition (at 25% of water weight the lipids form a hexagonal phase). This gives an impression that near to the phase boundary, the lamellar assembly may exhibit some pre-transition anomaly behavior compared to the lamellar structure which is far away from phase boundary. Additionally, the lipid-lipid hydrogen bond interaction is much stronger than lipid-water hydrogen bonds in βMal-C_{12}(23%wat) bilayer system. This suggests the sugar groups are being held tightly enough to enable the area per lipid to shrink compared to other monoalkylated lipid. The close packing of sugar groups also reduces the water-lipid hydrogen bonding interaction because some of hydroxyl groups (OH) from sugars are inaccessible to the water molecules, thus it reduces the number of water-lipid HB.

In order to rationalize the small area per lipid value for βMal-C_{12}(23%wat), we also investigated the closeness of sugar moieties within the headgroup region by calculating the radial distribution function (RDF) for the oxygen and carbon atoms in the *ring1* and *ring2* separately (see Figure 4.35(a) and (b)). The RDF for the atoms in reducing ring (C1', C2', C3', C4', C5', and O5') in Figure 4.35 (a) shows high peaks compared to atoms in

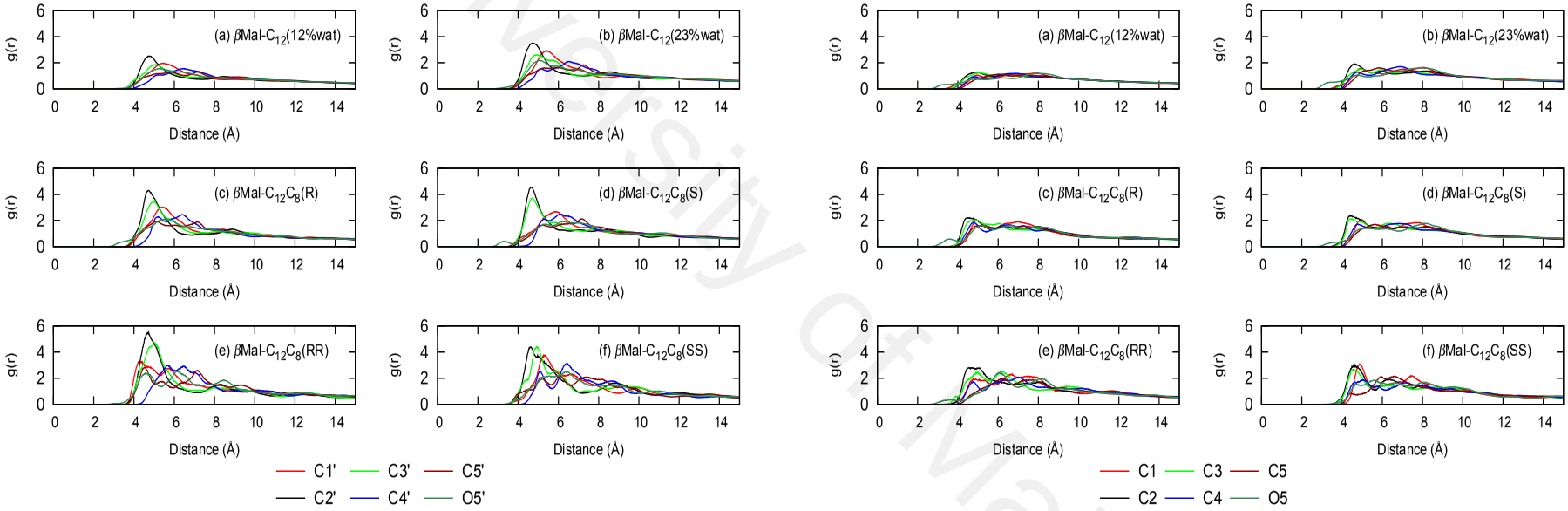

(a) Reducing sugar (*ring1*)

(b) Non-reducing sugar (*ring2*)

Figure 4.35: Radial distribution function (RDF) of the carbons and oxygen in the sugar rings of single- and branched chain glycosides.

non-reducing ring (C1, C2, C3, C4, C5, and O5) in Figure 4.35 (b). Qualitatively, the high peaks of *ring1* indicate it is closely packed at the hydrophilic region compared to *ring2*. In βMal-C_{12}(23%wat) system the *ring1* and *ring2* are arranged more closely than βMal-C_{12}(12%wat) and this supports the lower value of the area per lipid of βMal-C_{12}(23%wat). On the other hand, the increased water concentration of βMal-C_{12}(23%wat) does not increase its area per lipid but the repeat distance (*d*-spacing) of the bilayer increases.

Besides this, the angular distributions of sugar (*ring1*) and chain for βMal-C_{12}(23%wat) (see the bimodal distributions in Figure 4.32(a) and Figure 4.33(a)) show flipped orientations and these conformations possibly distort the bilayer arrangement of the lipids in the lamellar assembly. A similar kind of phenomena is observed in branched chain βMal-$C_{12}C_{10}$ in anhydrous condition as reported in Section 4.2, where the chains were trying to protrude into the headgroup region of sugar which was induced by the van der Waals' interaction between the hydrophobic tail and sugar ring face. But in the present case, the monoalkylated chain of βMal-C_{12}(23%wat), flips into the hydrophobic region. Similarly, *ring1* also flips into a more complex conformational arrangement. Comparing the distributions for the headgroup and chain of βMal-C_{12}(23%wat) with other systems, the former is probably undergoing fluctuations since this concentration is close to the phase boundary of lamellar and hexagonal (see Figure 3.5 (Auvray et al., 2001)).

The RDF calculations for oxygen at the hydration site (OH groups from sugars) show the presence of water shells around oxygen O2, O3, O4 and O6 (from *ring2*) for all glycosides, except for βMal-C_{12}(23%wat) where only O3 and O6 show the second peaks. This limited number of oxygen which are surrounded by a water shell indicate that other oxygen sites are unavailable for the water to form HB and this further support the notion that the sugars in βMal-C_{12}(23%wat) are closely packed. Meanwhile, the peaks in Figure 4.30, show the oxygen O2', O3', and O6' in βMal-C_{12}(12%wat) are surrounded by waters with a higher order.

The intermolecular hydrogen bonding (HB) analysis for all the oxygen sites (see Figure 4.29) from both the sugar rings in maltose headgroup is almost similar compared to the pattern for monoalkylated maltoside in anhydrous bilayer as reported in Section 4.1. This indicates the intermolecular HB strength is not affected much by the temperature difference. But the water-lipid HB is dependent to the hydration concentration. The increase of water concentration increases the number of HB value as can be seen in βMal-

C_{12}(12%wat) and βMal-C_{12}(23%wat) in Table 4.8. Meanwhile, the Guerbet glycosides' intermolecular HB values for all the oxygen sites show a slight reduction compared to the monoalkylated bilayers. This could be due to the presence of branched chain in the hydrophobic region. The higher density of hydrocarbons at the center of bilayer slightly increase the distance between sugar headgroups where the corresponding area per lipid at interface also increases. The slight increase in the area per lipid enables the water molecules to enter to the cavity in between the sugars, thus increases the number of water-lipid HB which can be seen in Figure 4.29. The HB analyses for the branched chain lamellar systems do not exhibit any significant indication that the presence of chirality affects the HB interactions. However, the chirality may influence the HB interactions at the headgroup minimally.

The bond order parameter of chain in βMal-C_{12}(12%wat) is lower than βMal-C_{12} in anhydrous condition from Section 4.1. This shows that at 80 °C βMal-C_{12}(12%wat) is more disordered than βMal-C_{12} in room temperature. Whereas the OP for the chain in βMal-C_{12}(23%wat) is much lower than βMal-C_{12}(12%wat) indicating the lipids near the phase boundary lower the bond ordering to give way to the lipids to involve in rearrangements. Meanwhile, the OP for the long chain from βMal-$C_{12}C_8$(*S*)(25%wat) and βMal-$C_{12}C_8$(*SS*)(25%wat), has slightly higher order than βMal-$C_{12}C_8$(*R*)(25%wat) and βMal-$C_{12}C_8$(*RR*)(25%wat). This might be possibly due to the chiral canter at the chain in the Guerbet glycosides of *R* and *S* isomers. This result implies the chirality affects the bond order parameter significantly.

The shorter HB-lifetime values for monoalkylated glycolipid compared to branched chain glycolipids indicate that temperature influences the HB-lifetime rate where the latter is at room temperature while the former is at 80 °C. Close investigation into the HB-lifetime reveals that the HB-lifetime around glycosidic and sugar oxygen are very low because these oxygen are weak in forming the HB interactions (Liu & Brady, 1997). It is noticeable from Table 4.10 that the HB-lifetime between lipid-lipid is slightly longer than the water-lipid for the Guerbet glycoside systems. This suggests a slow rate of hydrogen bond making and breaking happen between lipids compared between lipid and water, which is most probably due to the presence of water molecules between the sugar headgroups. Furthermore, the water facilitates effectively the hydrogen bond making and breaking at the headgroup. A recent simulation study by H. Nguan et al. (2014) on the Guerbet branched chain attached

to a single glucose sugar via glycosidic oxygen (βGlu-$C_{12}C_8$) in a reverse hexagonal phase in 14 and 22 % water concentration shows a trend in the HB-lifetime values. The lower water content system (14% water) reveals slightly higher HB-lifetime compared to higher water content system (22%). This trend is obviously vice-versa compared to the HB-lifetime values for the monoalkylated system studied here. The difference may be related to factors like the type of sugar. (mono- and di-saccharide), temperature, and the phase of assembly.

The correlation times from the rotational diffusion of the sugar units reveal that the non-reducing sugars from all systems rotate faster than the reducing sugar. This is due to the fact that the reducing sugar positioned in between the alkyl chain and the non-reducing sugar where it has been hydrated with water. This pattern of rotation is similar compared to the sugar rings' rotations in βMal-$C_{12}C_{10}$ as in Section 4.2. But the rotations of the Guerbet branched chain glycosides (βMal-$C_{12}C_8$) are much faster than that observed in the dry system because the presence of water reduces the intermolecular HB among the lipids. This helps to increase the rotational rate an order of magnitude faster especially in non-reducing sugar rings of Guerbet glycosides. Further, the correlation times of Guerbet glycosides suggest there is no chirality effect in the dynamics of sugars in branched systems. However, the rotation of sugar units from single chain lipids are much faster than branch chain lipids Table 4.12. This rotational speed increment mostly can be linked to the high temperature (80 degree Celsius) of the bilayer systems. Additionally, the number of water molecules are less compared to branched chain bilayers and at the high temperature, the sugars are prone to receive little higher kinetic energy. Therefore, the sugars in single chain possesses much shorter correlation time. A similar explanation can be attributed to the exocyclic groups in single chain lipids.

In general, the correlation times for the exocyclic groups from all glycosides show that their rotation is much faster than the corresponding sugar rings. Nonetheless, the correlation times between the exocyclic groups from *ring1* and *ring2* show time difference by a factor of two, where the exocyclic group from *ring2* rotates much faster than the exocyclic group from *ring1*. This can be seen in Table 4.12 where the correlation times for exocyclic groups from *ring1* and *ring2* are in the range of 16-31 ns and 10 to 17 ns respectively. This difference in the correlation time possibly related to the weaker HB interaction of OH group from *ring2* exocyclic group with neighbouring lipids compared to

the *ring1*'s exocyclic OH group (see Figure 4.29). Meanwhile, Lycknert and Widmalm (2004) determined the dynamics of exocyclic group of glucose from the O-antigen (part of the lipopolysaccharide from the Escherichia coli O91), using ^{13}C-NMR relaxation measurements. They reported the correlation time of the exocyclic group to be about 5.4 ns. Although this value indicates that the rotation of the exocyclic group in single glucose unit is much faster than the rotation rate of exocyclic groups from disaccharide unit, it reasonably supports the values obtained from current simulation despite other factors like temperature, solvent, and environment that play an important role in influencing the dynamics of exocyclic group (Soltesova, Kowalewski, & Widmalm, 2013).

CHAPTER 5

CONCLUSION AND FUTURE STUDIES

To invent, you need a good imagination and a pile of junk.
Thomas A. Edison (1847-1931)

This chapter concludes the molecular dynamics simulation studies on glycolipid bilayer systems in anhydrous and hydrated conditions. We summarize the simulation of anhydrous and hydrated systems by highlighting some of interesting results relating to the objectives outlined in Chapter 1. Following that, we also present some limitations in this work that might help for future refinement of this simulation. Finally, we give an outlook for the future expansion and development of this work.

5.1 Concluding remarks

Glycolipid is classified as an amphitropic liquid crystal which is able to self-assemble in dry or solvated environment through the separation of the extensively hydrogen bonded hydrophilic region from that of the repulsive hydrophobic alkyl chain. Among many self-assembly structures that a glycolipid could form, the lamellar is highly interesting since it resembles the closed structure of a vesicle (drug carrier) and the basic matrix of cellular membrane. The understanding of the complex organization within this glycolipid lamellar system is exceptionally important due to its versatility and applicability in many fields like pharmaceuticals, cosmetics and food industries. Therefore, a systematic examination of the structure and dynamics of the lipids as a function of sugar stereochemistry and hydrocarbon chain is necessary.

We choose glycolipids with disaccharide as the hydrophilic moiety which is linked to a single or branched alkyl chains, namely βMal-C_{12}, βMal-$C_{12}C_{10}$, βCel-C_{12}, βIsoMal-C_{12}, βMal-$C_{12}C_8$(*R*)(25%wat), βMal-$C_{12}C_8$(*S*)(25%wat), and βMal-$C_{12}C_8$(*RS*)(25%wat). We used the molecular dynamics simulation to probe the molecular level consequences of chain branching and headgroup identity on assemblage structure and dynamics of these lipids in lamellar assembly and to achieve the research objectives as outlined in Chapter 1. Our simulation results indicates that our research objectives were satisfactorily achieved.

The observations on the conformational behavior of sugars and chain moieties in the anhydrous condition for the four glycolipids, βMal-C_{12}, βMal-$C_{12}C_{10}$, βCel-C_{12}, and βIsoMal-C_{12} showed that the increased branching of the alkyl maltoside leads to a measurable differences in the dimensions and dynamics of the assembly and the effects are much less than the replacement of the maltosyl headgroup with an isomaltosyl moiety. Additionally, the headgroup appears to play a crucial role in determining the microscopic properties of the glycolipid assemblies examined here; indeed it is known that the headgroup is a key determinant of thermodynamic behavior, as reflected by the clearing temperature T* (Goodby et al., 2007). Also the chain packing is not influenced significantly by the anomeric configuration at the glycosidic linkage that connects two headgroups. Thus, the $\beta(1\rightarrow4)$ linked βCel-C_{12} has a similar packing to the $\alpha(1\rightarrow4)$ linked βMal-C_{12}. On the other hand, the RDF of the $\alpha(1\rightarrow6)$ link of βIsoMal-C_{12}, is a marked contrast to these two, implying it has a rather loosely packed structure. In the current study, where the lipids are at the room temperature, the chains do sample a small amount of *gauche* conformation. This suggests the L_C phase of these glycolipids is not entirely in a solid phase but to a certain extent possesses some chain disorder. Meanwhile, the chain packing showed that it is not influenced significantly by the anomeric configuration at the glycosidic linkage that connects the two headgroups. Thus, the $\beta(1\rightarrow4)$ linked βCel-C_{12} has a similar packing to the $\alpha(1\rightarrow4)$ linked βMal-C_{12}. But, the RDF of the $\alpha(1\rightarrow6)$ link of βIsoMal-C_{12}, is in a marked contrast to these two, implying it has a more loosely packed structure.

The rationalization of the stability of the bilayer structures with respect to the hydrogen bonding within sugars in the hydrophilic region is observed for the anhydrous and hydrated systems separately. The intermolecular hydrogen bonding interactions among sugar moieties in the anhydrous systems is influenced by the chain branching where the increment of area per lipid slightly reduces the HB strength. For the single chain systems, the conformation of glycosidic linkage between the two sugars, especially in the $\beta(1\rightarrow4)$ (βCel-C_{12}) allows close packing and increases the HB interactions. Meanwhile in the hydrated systems the intermolecular hydrogen bonding (HB) for all the oxygen sites (Figure 4.29) of both the sugar rings in maltose headgroup do not change much although the bilayers are under the influence of water concentration and temperature change below the clearing point. But the water-lipid HB is dependent on the hydration concentration where the proportional increase in the hydration level increases the water-lipid HB. Further,

the HB-lifetime between lipid-lipid and water-lipid for the Guerbet glycoside systems reveals that temperature does affects the rate. Nonetheless, temperature also affects the order parameter of the chiral lipids, especially in the racemic mixture of bilayer.

Observing the dynamics of sugar moieties at the headgroup and the chain segment with regards to the dry condition reveals that the headgroup and tail exhibit different behavior where the headgroup rotates slower than the tail by a factor of at least two. Additionally, we also observed an unusual feature for the anhydrous bilayer system of the branched chain glycolipids; in this system with its overcrowded chain region, the alkyl chains work themselves into the headgroup region and appear to associate with the more hydrophobic face of the sugar. The dynamic behavior for the hydrated systems also reveals that non-reducing sugar from all systems rotates faster than the reducing sugars, because the reducing sugar placed in between the alkyl chain and the non-reducing sugar has been hydrated with water. Nonetheless, the presence of water molecules in between the sugar headgroups helps to increase the sugar rings' rotational diffusion by forming intermolecular HBs. Finally, the exocyclic groups from all glycosides rotates much faster than the sugar rings and we observed no chirality effect on the rotational diffusion.

Understanding the consequences of large or subtle changes in the covalent structure of the glycolipids on their ensembles is a key step towards structure-based design of new glycolipid-based systems, as thermotropic and lyotropic materials has been documented to be suitable for a wide range of surfactant and thin film applications (Wai Ling, Wee Chen, Wan Haliza Abd, Rauzah, & Thorsten, 2010). Further work is necessary to explore the generality of these alkyl chain saccharide headgroup interactions for a range of glycolipid systems. Nevertheless, together with the emerging concepts of lateral segregation, lipid flip and domain formation, these findings provide new insights into our understanding of glycolipid lamellar stability and integrity.

Although our simulation results indicate that our research objectives were competently achieved, there are a few aspects that needs reevaluation and careful interpretation. The estimation of slow dynamics for the headgroup and alkyl chains which were done using the single exponential function need to be re-investigated using a multi-exponential function. Determination of the decay constants and a sum of them possibly gives more appropriate scenario to the reorientation nature. In addition to this, it is found that the carbons in alkyl chain reorient itself with different decay rate along the chain (see Figure 4.16). Although

this behavior could be microscopically related to the individual carbons, macroscopically this might be influencing the flexibility of a bilayer. Further investigations into this behavior is possibly needed to gather a more in depth understanding.

The hydrated systems were simulated for 300 ns and the production time might be insufficient to provide a satisfactory measurement for the dynamical behaviors. Nowadays simulations up to few microseconds is achievable with suitable choice of force field and simulation methods. Therefore, to observe lipids' and sugars' behavior at the phase transition region, especially for βMal-C_{12}(12%wat), one can revisit the simulation using coarse grain models. Although the coarse grain models are followed by some toleration from accuracy, nevertheless, some macroscopic behaviors are possibly observable.

5.2 Future work

Carbohydrate liquid crystals (Glycolipids) and its self-assembly phenomenon offer a fascinating fields of research. Possibly there is a huge number of surfactant types which can be formed with varying sugar headgroup as well as lengths and branching of alkyl chains. The amphiphilic nature of the glycolipids which undergo a microphase sepration of two incompatible molecular parts of those surfactants, selectively gives various types of self-assembly structures like micelle, hexagonal, lipid bilayer and complex three dimensional cubic structures with and without the presence of water. But a satisfying and complete understanding of the fundamental rules governing their assembly structures and the individual lipids is yet to be available. This may be due to the complex stereochemical conformation of sugars. To fill this gap, we have performed a computer modelling and extensive molecular dynamics simulation to understand and explore the self-assembly behavior of glycolipid bilayers in a bulky condition.

In future, we can apply quantum mechanical (QM) methods to obtain the electronic properties of synthetic glycolipids, like Guerbet branched chains. This will allow us to improve the currently available force field (like GLYCAM for sugars) to be used specifically on these materials. Further, performing the QM calculation onto these materials (Guerbet branched chains) in dry and solvated conditions and applying those force fields to simulate assembly structures in their respective conditions is highly encouraged since it possibly increases the degree of reality in simulation work. Additionally, the hybrid QM/MM approach, which uses both QM (for improved accuracy) and MM (for higher

speed) calculations, can be used to study the chemical processes in solutions and in proteins. The development of the hybrid QM/MM approach is guided by the general idea that large chemical systems may be partitioned into an electronically important region which requires a quantum chemical treatment and a remainder which only acts in a perturbation fashion and, thus admits a classical description. Therefore, in future, the application of this method to study the complex self-assembly behavior is highly anticipated. Besides, developing a coarse-grained (CG) model, in which small groups of atoms are treated as single particles, like $-$OH, possibly enables simulations with extended timescales ($\sim \mu$s) to be achieved especially in the context of glycolipid materials. The bottom-up approach in which the information at smaller scales is used to build models at larger scales, may be suitable to develop a model with the pseudo-molecular characters. This pseudo-molecular nature is generally derived from atomistic classical models. We have towering interest in applying this approach since we can use the QM study on Guerbet glycosides as mentioned above to develop the CG models. These models then could help to simulate phenomena like the fusion of two bilayers to understand their molecular nature more vividly.

Appendices

APPENDIX A

PDB FILE FOR EVERY SINGLE GLYCOLIPID MOLECULE

PDB file for Maltoside (βMal-C_{12}):

\small
REMARK
ATOM 1 O25 DDM 1 41.799 30.649 -26.049
ATOM 2 C25 DDM 1 41.727 29.258 -25.898
ATOM 3 C24 DDM 1 42.793 28.745 -24.865
ATOM 4 C23 DDM 1 44.141 29.190 -25.292
ATOM 5 C22 DDM 1 44.161 30.728 -25.492
ATOM 6 C21 DDM 1 43.067 31.109 -26.501
ATOM 7 H45 DDM 1 41.975 28.880 -26.848
ATOM 8 H44 DDM 1 42.413 29.086 -23.905
ATOM 9 H43 DDM 1 44.389 28.745 -26.207
ATOM 10 H42 DDM 1 44.006 31.218 -24.523
ATOM 11 H41 DDM 1 43.073 32.210 -26.456
ATOM 12 C26 DDM 1 40.283 28.888 -25.517
ATOM 13 O24 DDM 1 42.740 27.348 -24.782
ATOM 14 O23 DDM 1 45.122 28.856 -24.313
ATOM 15 O22 DDM 1 45.412 31.117 -25.930
ATOM 16 O14 DDM 1 43.398 30.602 -27.789
ATOM 17 H46 DDM 1 40.178 27.796 -25.448
ATOM 18 O26 DDM 1 39.948 29.455 -24.267
ATOM 19 H47 DDM 1 39.519 29.286 -26.252
ATOM 20 H24 DDM 1 43.331 27.074 -24.096
ATOM 21 H23 DDM 1 45.959 29.172 -24.634
ATOM 22 H22 DDM 1 45.451 32.060 -26.146
ATOM 23 H26 DDM 1 39.040 29.225 -24.029
ATOM 24 O15 DDM 1 42.170 30.268 -31.206
ATOM 25 C15 DDM 1 42.967 30.089 -30.046
ATOM 26 C14 DDM 1 42.405 30.769 -28.800
ATOM 27 C13 DDM 1 42.095 32.270 -29.124
ATOM 28 C12 DDM 1 41.265 32.353 -30.382
ATOM 29 C11 DDM 1 42.026 31.643 -31.523
ATOM 30 H35 DDM 1 43.977 30.473 -30.214
ATOM 31 H34 DDM 1 41.481 30.254 -28.560
ATOM 32 H33 DDM 1 43.054 32.853 -29.251
ATOM 33 H32 DDM 1 40.295 31.851 -30.303
ATOM 34 O11 DDM 1 41.294 31.801 -32.717
ATOM 35 C16 DDM 1 43.109 28.589 -29.854
ATOM 36 O13 DDM 1 41.267 32.817 -28.063
ATOM 37 O12 DDM 1 41.045 33.668 -30.710
ATOM 38 H31 DDM 1 43.017 32.118 -31.628
ATOM 39 H36 DDM 1 43.797 28.346 -29.002

```
ATOM     40  O16 DDM     1      41.873  27.963 -29.579
ATOM     41  H37 DDM     1      43.518  28.153 -30.727
ATOM     42  H13 DDM     1      41.024  33.712 -28.366
ATOM     43  H12 DDM     1      40.579  33.685 -31.545
ATOM     44  H16 DDM     1      42.056  27.025 -29.461
ATOM     45  C71 DDM     1      42.008  31.394 -33.886
ATOM     46  C72 DDM     1      41.236  31.801 -35.100
ATOM     47  C73 DDM     1      42.064  31.413 -36.370
ATOM     48  C74 DDM     1      41.364  31.921 -37.637
ATOM     49  C75 DDM     1      42.192  31.548 -38.850
ATOM     50  C76 DDM     1      41.417  32.026 -40.146
ATOM     51  C77 DDM     1      42.282  31.677 -41.342
ATOM     52  C78 DDM     1      41.508  32.071 -42.654
ATOM     53  C79 DDM     1      42.311  31.691 -43.858
ATOM     54  C80 DDM     1      41.461  32.090 -45.116
ATOM     55  C81 DDM     1      42.228  31.712 -46.395
ATOM     56  C82 DDM     1      41.402  32.123 -47.639
ATOM     57  H71 DDM     1      43.046  31.748 -33.899
ATOM     58  H72 DDM     1      42.193  30.358 -33.884
ATOM     59  H73 DDM     1      40.253  31.251 -35.207
ATOM     60  H74 DDM     1      41.127  32.894 -35.176
ATOM     61  H75 DDM     1      43.029  31.929 -36.395
ATOM     62  H76 DDM     1      42.227  30.326 -36.467
ATOM     63  H77 DDM     1      40.441  31.426 -37.720
ATOM     64  H78 DDM     1      41.270  33.003 -37.589
ATOM     65  H79 DDM     1      43.080  32.160 -38.699
ATOM     66  H80 DDM     1      42.387  30.460 -38.908
ATOM     67  H81 DDM     1      40.378  31.643 -40.246
ATOM     68  H82 DDM     1      41.327  33.087 -40.161
ATOM     69  H83 DDM     1      43.217  32.222 -41.332
ATOM     70  H84 DDM     1      42.530  30.658 -41.457
ATOM     71  H85 DDM     1      40.502  31.678 -42.632
ATOM     72  H86 DDM     1      41.314  33.109 -42.597
ATOM     73  H87 DDM     1      43.266  32.253 -43.867
ATOM     74  H88 DDM     1      42.501  30.614 -43.831
ATOM     75  H89 DDM     1      40.497  31.554 -45.101
ATOM     76  H90 DDM     1      41.308  33.157 -45.085
ATOM     77  H91 DDM     1      43.198  32.243 -46.473
ATOM     78  H92 DDM     1      42.390  30.649 -46.477
ATOM     79  H93 DDM     1      41.944  31.914 -48.551
ATOM     80  H94 DDM     1      40.506  31.591 -47.591
ATOM     81  H95 DDM     1      41.185  33.218 -47.670
TER
END
```

PDB file for Cellobioside (βCel-C_{12}):

```
REMARK
ATOM      1  O25 DDC     1     152.531 -89.028 -14.748
ATOM      2  C25 DDC     1     153.193 -90.201 -14.306
ATOM      3  C24 DDC     1     152.303 -91.427 -14.553
ATOM      4  C23 DDC     1     150.997 -91.253 -13.777
ATOM      5  C22 DDC     1     150.359 -89.924 -14.185
ATOM      6  C21 DDC     1     151.340 -88.756 -14.029
ATOM      7  H45 DDC     1     153.403 -90.118 -13.239
ATOM      8  H44 DDC     1     152.080 -91.515 -15.617
ATOM      9  H43 DDC     1     151.205 -91.259 -12.707
ATOM     10  H42 DDC     1     150.068 -89.988 -15.234
ATOM     11  H41 DDC     1     151.577 -88.591 -12.977
ATOM     12  C26 DDC     1     154.533 -90.305 -15.043
ATOM     13  O24 DDC     1     152.951 -92.603 -14.117
ATOM     14  O23 DDC     1     150.114 -92.311 -14.086
ATOM     15  O22 DDC     1     149.209 -89.686 -13.402
ATOM     16  O14 DDC     1     150.676 -87.613 -14.545
ATOM     17  H46 DDC     1     155.086 -91.177 -14.692
ATOM     18  O26 DDC     1     154.332 -90.413 -16.436
ATOM     19  H47 DDC     1     155.125 -89.412 -14.838
ATOM     20  H24 DDC     1     152.363 -93.346 -14.273
ATOM     21  H23 DDC     1     149.279 -92.148 -13.641
ATOM     22  H22 DDC     1     148.847 -88.831 -13.649
ATOM     23  H26 DDC     1     155.190 -90.442 -16.866
ATOM     24  O15 DDC     1     151.296 -84.025 -14.447
ATOM     25  C15 DDC     1     150.776 -85.278 -14.046
ATOM     26  C14 DDC     1     151.475 -86.456 -14.746
ATOM     27  C13 DDC     1     151.543 -86.214 -16.261
ATOM     28  C12 DDC     1     152.064 -84.809 -16.565
ATOM     29  C11 DDC     1     151.176 -83.802 -15.837
ATOM     30  H35 DDC     1     149.710 -85.303 -14.279
ATOM     31  H34 DDC     1     152.486 -86.560 -14.350
ATOM     32  H33 DDC     1     150.541 -86.316 -16.683
ATOM     33  H32 DDC     1     153.096 -84.708 -16.225
ATOM     34  O11 DDC     1     151.601 -82.485 -16.136
ATOM     35  C16 DDC     1     150.935 -85.355 -12.526
ATOM     36  O13 DDC     1     152.393 -87.161 -16.872
ATOM     37  O12 DDC     1     151.998 -84.575 -17.956
ATOM     38  H31 DDC     1     150.141 -83.933 -16.160
ATOM     39  H36 DDC     1     150.507 -86.280 -12.142
ATOM     40  O16 DDC     1     152.292 -85.278 -12.160
ATOM     41  H37 DDC     1     150.428 -84.502 -12.084
ATOM     42  H13 DDC     1     152.435 -86.968 -17.811
ATOM     43  H12 DDC     1     152.270 -83.670 -18.122
ATOM     44  H16 DDC     1     152.340 -85.183 -11.206
ATOM     45  C71 DDC     1     150.720 -81.512 -15.602
ATOM     46  C72 DDC     1     151.210 -80.119 -15.990
ATOM     47  C73 DDC     1     150.253 -79.064 -15.434
ATOM     48  C74 DDC     1     150.729 -77.666 -15.831
```

```
ATOM     49  C75 DDC     1     149.763 -76.612 -15.288
ATOM     50  C76 DDC     1     150.230 -75.218 -15.709
ATOM     51  C77 DDC     1     149.262 -74.162 -15.175
ATOM     52  C78 DDC     1     149.712 -72.770 -15.621
ATOM     53  C79 DDC     1     148.734 -71.719 -15.096
ATOM     54  C80 DDC     1     149.162 -70.326 -15.558
ATOM     55  C81 DDC     1     148.165 -69.286 -15.047
ATOM     56  C82 DDC     1     148.588 -67.891 -15.499
ATOM     57  H71 DDC     1     149.716 -81.659 -16.004
ATOM     58  H72 DDC     1     150.685 -81.580 -14.513
ATOM     59  H73 DDC     1     152.209 -79.960 -15.581
ATOM     60  H74 DDC     1     151.251 -80.041 -17.077
ATOM     61  H75 DDC     1     149.253 -79.233 -15.838
ATOM     62  H76 DDC     1     150.216 -79.140 -14.347
ATOM     63  H77 DDC     1     151.725 -77.492 -15.421
ATOM     64  H78 DDC     1     150.770 -77.594 -16.918
ATOM     65  H79 DDC     1     148.764 -76.795 -15.686
ATOM     66  H80 DDC     1     149.731 -76.673 -14.199
ATOM     67  H81 DDC     1     151.227 -75.032 -15.309
ATOM     68  H82 DDC     1     150.263 -75.162 -16.797
ATOM     69  H83 DDC     1     148.261 -74.359 -15.563
ATOM     70  H84 DDC     1     149.239 -74.206 -14.086
ATOM     71  H85 DDC     1     150.711 -72.567 -15.231
ATOM     72  H86 DDC     1     149.738 -72.729 -16.711
ATOM     73  H87 DDC     1     147.734 -71.934 -15.475
ATOM     74  H88 DDC     1     148.718 -71.751 -14.006
ATOM     75  H89 DDC     1     150.156 -70.103 -15.167
ATOM     76  H90 DDC     1     149.191 -70.297 -16.648
ATOM     77  H91 DDC     1     147.171 -69.503 -15.440
ATOM     78  H92 DDC     1     148.134 -69.313 -13.957
ATOM     79  H93 DDC     1     147.868 -67.163 -15.126
ATOM     80  H94 DDC     1     149.576 -67.669 -15.097
ATOM     81  H95 DDC     1     148.620 -67.842 -16.588
TER
END
```

PDB file for IsoMaltoside (βIsoMal-C_{12}):

```
REMARK
ATOM      1  O22 ISM     1      10.060   5.038   7.758
ATOM      2 2H6  ISM     1      10.078   4.078   7.543
ATOM      3  C22 ISM     1      10.328   5.745   6.576
ATOM      4 2H4  ISM     1      11.364   5.567   6.319
ATOM      5  C23 ISM     1      10.094   7.280   6.807
ATOM      6 3H4  ISM     1       9.113   7.456   7.221
ATOM      7  O23 ISM     1      11.120   7.724   7.672
ATOM      8 3H6  ISM     1      11.057   7.254   8.521
ATOM      9  C24 ISM     1      10.265   8.033   5.476
ATOM     10  H44 ISM     1      11.283   8.069   5.218
ATOM     11  O24 ISM     1       9.747   9.334   5.682
ATOM     12  H64 ISM     1      10.357   9.787   6.249
ATOM     13  C25 ISM     1       9.479   7.402   4.379
ATOM     14  H45 ISM     1       8.422   7.580   4.601
ATOM     15  C26 ISM     1       9.790   8.008   2.998
ATOM     16  H46 ISM     1       9.619   9.089   2.989
ATOM     17  O26 ISM     1      11.154   7.889   2.673
ATOM     18  H66 ISM     1      11.324   8.443   1.888
ATOM     19  H47 ISM     1       9.184   7.599   2.193
ATOM     20  O25 ISM     1       9.732   6.014   4.274
ATOM     21  C21 ISM     1       9.462   5.201   5.388
ATOM     22 1H4  ISM     1       9.862   4.207   5.171
ATOM     23  O16 ISM     1       8.079   5.097   5.636
ATOM     24  C16 ISM     1       7.378   4.232   4.760
ATOM     25  H36 ISM     1       7.458   4.561   3.703
ATOM     26  H37 ISM     1       7.633   3.188   4.914
ATOM     27  C15 ISM     1       5.881   4.304   5.053
ATOM     28  C14 ISM     1       5.066   3.296   4.183
ATOM     29  C13 ISM     1       3.529   3.407   4.411
ATOM     30  C12 ISM     1       3.017   4.881   4.445
ATOM     31 2H3  ISM     1       2.867   5.227   3.408
ATOM     32  O12 ISM     1       1.795   4.929   5.151
ATOM     33 2H5  ISM     1       1.402   5.808   5.019
ATOM     34 3H3  ISM     1       3.320   2.953   5.351
ATOM     35  O13 ISM     1       2.827   2.727   3.402
ATOM     36 3H5  ISM     1       1.910   3.097   3.367
ATOM     37  H34 ISM     1       5.229   3.642   3.173
ATOM     38  O14 ISM     1       5.427   1.951   4.381
ATOM     39  H54 ISM     1       4.911   1.397   3.749
ATOM     40  H35 ISM     1       5.689   4.070   6.073
ATOM     41  O15 ISM     1       5.370   5.620   4.727
ATOM     42  C11 ISM     1       4.039   5.804   5.118
ATOM     43 1H3  ISM     1       3.932   5.634   6.208
ATOM     44  O11 ISM     1       3.728   7.178   4.803
ATOM     45  C71 ISM     1       4.282   8.078   5.716
ATOM     46 1H7  ISM     1       3.935   7.771   6.696
ATOM     47 2H7  ISM     1       5.378   7.991   5.755
ATOM     48  C72 ISM     1       3.748   9.453   5.379
```

```
ATOM     49 3H7  ISM     1       3.939   9.674   4.305
ATOM     50  H74 ISM     1       2.695   9.365   5.560
ATOM     51  C73 ISM     1       4.270  10.543   6.284
ATOM     52  H75 ISM     1       4.211  10.282   7.335
ATOM     53  H76 ISM     1       5.367  10.544   6.202
ATOM     54  C74 ISM     1       3.743  11.933   6.006
ATOM     55  H77 ISM     1       3.728  12.119   4.929
ATOM     56  H78 ISM     1       2.662  11.929   6.214
ATOM     57  C75 ISM     1       4.524  12.945   6.827
ATOM     58  H79 ISM     1       4.303  12.691   7.837
ATOM     59  H80 ISM     1       5.619  12.948   6.511
ATOM     60  C76 ISM     1       3.873  14.306   6.586
ATOM     61 1H8  ISM     1       4.068  14.595   5.552
ATOM     62 2H8  ISM     1       2.778  14.229   6.704
ATOM     63  C77 ISM     1       4.449  15.313   7.582
ATOM     64 3H8  ISM     1       4.252  15.018   8.617
ATOM     65  H84 ISM     1       5.526  15.335   7.408
ATOM     66  C78 ISM     1       3.905  16.727   7.237
ATOM     67  H85 ISM     1       4.175  16.884   6.214
ATOM     68  H86 ISM     1       2.808  16.770   7.422
ATOM     69  C79 ISM     1       4.631  17.837   7.993
ATOM     70  H87 ISM     1       4.499  17.666   9.071
ATOM     71  H88 ISM     1       5.703  17.832   7.830
ATOM     72  C80 ISM     1       4.022  19.227   7.693
ATOM     73  H89 ISM     1       4.306  19.524   6.685
ATOM     74  H90 ISM     1       2.940  19.176   7.908
ATOM     75  C81 ISM     1       4.605  20.267   8.652
ATOM     76 1H9  ISM     1       4.387  20.054   9.719
ATOM     77 2H9  ISM     1       5.678  20.275   8.558
ATOM     78  C82 ISM     1       4.103  21.663   8.297
ATOM     79 3H9  ISM     1       4.745  22.403   8.786
ATOM     80  H94 ISM     1       4.220  21.817   7.216
ATOM     81  H95 ISM     1       3.021  21.743   8.479
TER
END
```

PDB file for branched chain maltoside (βMal-$C_{12}C_{10}$):

```
REMARK
ATOM      1  O22 BCM     1       3.710  -0.284   1.879
ATOM      2  H23 BCM     1       4.287   0.444   1.634
ATOM      3  C22 BCM     1       2.545  -0.368   0.988
ATOM      4  H22 BCM     1       1.884  -1.137   1.390
ATOM      5  C23 BCM     1       2.978  -0.869  -0.404
ATOM      6  H24 BCM     1       3.822  -0.246  -0.701
ATOM      7  O23 BCM     1       3.457  -2.280  -0.270
ATOM      8  H25 BCM     1       3.930  -2.487  -1.079
ATOM      9  C24 BCM     1       1.845  -0.804  -1.462
ATOM     10  H26 BCM     1       1.096  -1.535  -1.158
ATOM     11  O24 BCM     1       2.399  -1.138  -2.705
ATOM     12  H27 BCM     1       2.549  -2.085  -2.674
ATOM     13  C25 BCM     1       1.195   0.605  -1.564
ATOM     14  H28 BCM     1       2.007   1.285  -1.819
ATOM     15  C26 BCM     1       0.037   0.744  -2.557
ATOM     16  H29 BCM     1       0.481   0.698  -3.552
ATOM     17  O26 BCM     1      -0.989  -0.299  -2.438
ATOM     18  H31 BCM     1      -1.419  -0.176  -1.588
ATOM     19  H30 BCM     1      -0.413   1.733  -2.479
ATOM     20  O25 BCM     1       0.683   1.013  -0.180
ATOM     21  C21 BCM     1       1.714   0.953   0.941
ATOM     22  H21 BCM     1       1.176   1.118   1.875
ATOM     23  O14 BCM     1       2.647   2.037   0.782
ATOM     24  C14 BCM     1       2.264   3.369   1.325
ATOM     25  C13 BCM     1       2.959   3.540   2.718
ATOM     26  C12 BCM     1       2.833   5.017   3.212
ATOM     27  H12 BCM     1       1.799   5.339   3.333
ATOM     28  O12 BCM     1       3.492   5.160   4.510
ATOM     29  H13 BCM     1       2.998   5.873   4.921
ATOM     30  H14 BCM     1       4.023   3.301   2.700
ATOM     31  O13 BCM     1       2.271   2.673   3.637
ATOM     32  H15 BCM     1       2.852   2.377   4.341
ATOM     33  H16 BCM     1       1.196   3.408   1.537
ATOM     34  C15 BCM     1       2.787   4.406   0.297
ATOM     35  H17 BCM     1       3.820   4.145   0.063
ATOM     36  C16 BCM     1       1.862   4.405  -0.957
ATOM     37  H18 BCM     1       0.888   4.809  -0.682
ATOM     38  O16 BCM     1       2.460   5.149  -2.048
ATOM     39  H20 BCM     1       1.819   5.136  -2.762
ATOM     40  H19 BCM     1       1.740   3.369  -1.272
ATOM     41  O15 BCM     1       2.807   5.800   0.881
ATOM     42  C11 BCM     1       3.489   5.943   2.181
ATOM     43  H11 BCM     1       4.541   5.676   2.077
ATOM     44  O11 BCM     1       3.353   7.309   2.712
ATOM     45  C31 BCM     1       4.222   8.272   2.005
ATOM     46  H51 BCM     1       5.238   7.876   2.005
ATOM     47  H52 BCM     1       3.883   8.392   0.976
ATOM     48  C32 BCM     1       4.300   9.645   2.706
```

```
ATOM     49  H53 BCM     1       5.030  10.247   2.165
ATOM     50  C43 BCM     1       4.818   9.476   4.123
ATOM     51  C44 BCM     1       5.356  10.732   4.830
ATOM     52  C45 BCM     1       6.244  10.413   6.072
ATOM     53  C46 BCM     1       6.436  11.666   6.915
ATOM     54  C47 BCM     1       7.537  11.455   8.017
ATOM     55  C48 BCM     1       7.582  12.562   9.104
ATOM     56  C49 BCM     1       8.360  13.827   8.701
ATOM     57  C50 BCM     1       8.224  14.998   9.755
ATOM     58  C51 BCM     1       9.104  16.210   9.476
ATOM     59  C52 BCM     1       9.122  17.255  10.610
ATOM     60  H93 BCM     1       9.825  18.053  10.373
ATOM     61  H94 BCM     1       8.168  17.778  10.674
ATOM     62  H95 BCM     1       9.364  16.860  11.597
ATOM     63  H91 BCM     1      10.117  15.889   9.232
ATOM     64  H92 BCM     1       8.737  16.786   8.627
ATOM     65  H89 BCM     1       7.171  15.255   9.875
ATOM     66  H90 BCM     1       8.494  14.603  10.735
ATOM     67  H87 BCM     1       9.431  13.627   8.683
ATOM     68  H88 BCM     1       8.022  14.159   7.719
ATOM     69  H85 BCM     1       6.561  12.795   9.404
ATOM     70  H86 BCM     1       8.009  12.110   9.999
ATOM     71  H83 BCM     1       7.401  10.492   8.509
ATOM     72  H84 BCM     1       8.510  11.466   7.526
ATOM     73  H81 BCM     1       6.720  12.528   6.311
ATOM     74  H82 BCM     1       5.506  11.963   7.401
ATOM     75  H79 BCM     1       5.716   9.664   6.664
ATOM     76  H80 BCM     1       7.185   9.936   5.798
ATOM     77  H77 BCM     1       5.929  11.330   4.122
ATOM     78  H78 BCM     1       4.521  11.342   5.174
ATOM     79  H75 BCM     1       5.581   8.702   4.040
ATOM     80  H76 BCM     1       4.118   9.028   4.828
ATOM     81  C33 BCM     1       2.941  10.391   2.778
ATOM     82  H54 BCM     1       2.181   9.672   3.084
ATOM     83  H55 BCM     1       2.944  11.172   3.539
ATOM     84  C34 BCM     1       2.587  10.986   1.337
ATOM     85  H56 BCM     1       3.401  11.591   0.939
ATOM     86  H57 BCM     1       2.299  10.142   0.710
ATOM     87  C35 BCM     1       1.376  11.842   1.406
ATOM     88  H58 BCM     1       0.581  11.181   1.750
ATOM     89  H59 BCM     1       1.528  12.594   2.179
ATOM     90  C36 BCM     1       1.001  12.435   0.029
ATOM     91  H60 BCM     1       1.720  13.201  -0.261
ATOM     92  H61 BCM     1       0.955  11.718  -0.791
ATOM     93  C37 BCM     1      -0.279  13.140   0.089
ATOM     94  H62 BCM     1      -1.055  12.522   0.541
ATOM     95  H63 BCM     1      -0.214  13.866   0.900
ATOM     96  C38 BCM     1      -0.783  13.891  -1.181
ATOM     97  H64 BCM     1      -0.252  14.842  -1.225
ATOM     98  H65 BCM     1      -0.449  13.337  -2.059
ATOM     99  C39 BCM     1      -2.304  14.116  -1.255
```

```
ATOM    100  H66 BCM     1      -2.609  14.332  -2.279
ATOM    101  H67 BCM     1      -2.824  13.202  -0.968
ATOM    102  C40 BCM     1      -2.790  15.224  -0.333
ATOM    103  H68 BCM     1      -3.785  14.960   0.026
ATOM    104  H69 BCM     1      -2.281  15.260   0.630
ATOM    105  C41 BCM     1      -2.754  16.601  -0.973
ATOM    106  H70 BCM     1      -1.743  16.913  -1.235
ATOM    107  H71 BCM     1      -3.407  16.577  -1.846
ATOM    108  C42 BCM     1      -3.299  17.567   0.076
ATOM    109  H72 BCM     1      -3.384  18.595  -0.276
ATOM    110  H73 BCM     1      -4.269  17.276   0.479
ATOM    111  H74 BCM     1      -2.661  17.623   0.958
TER
END
```

PDB file for Guerbet branched chain (R) (βMal-$C_{12}C_8$(*R*)):

```
REMARK
ATOM      1  O22 BMR     1       3.529  40.989  60.583
ATOM      2  H22 BMR     1       4.170  40.399  60.177
ATOM      3  C22 BMR     1       4.213  41.859  61.462
ATOM      4  H42 BMR     1       4.700  41.260  62.232
ATOM      5  C23 BMR     1       3.224  42.817  62.127
ATOM      6  H43 BMR     1       2.679  43.381  61.369
ATOM      7  O23 BMR     1       2.310  42.081  62.913
ATOM      8  H23 BMR     1       1.862  41.452  62.343
ATOM      9  C24 BMR     1       4.019  43.770  63.022
ATOM     10  H44 BMR     1       4.491  43.196  63.822
ATOM     11  O24 BMR     1       3.137  44.714  63.591
ATOM     12  H24 BMR     1       2.458  44.239  64.076
ATOM     13  C25 BMR     1       5.090  44.486  62.187
ATOM     14  H45 BMR     1       4.593  45.098  61.436
ATOM     15  C26 BMR     1       5.952  45.418  63.048
ATOM     16  H46 BMR     1       5.331  46.191  63.499
ATOM     17  O26 BMR     1       6.605  44.694  64.070
ATOM     18  H26 BMR     1       7.143  45.302  64.581
ATOM     19  H47 BMR     1       6.704  45.896  62.419
ATOM     20  O25 BMR     1       5.950  43.558  61.543
ATOM     21  C21 BMR     1       5.287  42.637  60.691
ATOM     22  H41 BMR     1       6.032  41.909  60.389
ATOM     23  O14 BMR     1       4.702  43.284  59.564
ATOM     24  C14 BMR     1       5.612  43.698  58.549
ATOM     25  C13 BMR     1       5.876  42.559  57.550
ATOM     26  C12 BMR     1       6.668  43.054  56.337
ATOM     27  H32 BMR     1       7.686  43.300  56.643
ATOM     28  O12 BMR     1       6.687  41.970  55.433
ATOM     29  H12 BMR     1       7.109  41.224  55.866
ATOM     30  H33 BMR     1       4.918  42.164  57.208
ATOM     31  O13 BMR     1       6.622  41.504  58.120
ATOM     32  H13 BMR     1       6.041  40.988  58.683
ATOM     33  H34 BMR     1       6.552  44.050  58.977
ATOM     34  C15 BMR     1       4.953  44.836  57.749
ATOM     35  H35 BMR     1       4.018  44.474  57.316
ATOM     36  C16 BMR     1       4.599  46.041  58.630
ATOM     37  H36 BMR     1       3.824  45.764  59.343
ATOM     38  O16 BMR     1       5.734  46.508  59.329
ATOM     39  H16 BMR     1       5.469  47.251  59.878
ATOM     40  H37 BMR     1       4.215  46.847  58.003
ATOM     41  O15 BMR     1       5.801  45.280  56.700
ATOM     42  C11 BMR     1       6.022  44.300  55.699
ATOM     43  H31 BMR     1       5.059  44.028  55.263
ATOM     44  O11 BMR     1       6.837  44.928  54.700
ATOM     45  C51 BMR     1       7.130  44.145  53.544
ATOM     46  H51 BMR     1       7.847  43.375  53.824
ATOM     47  H52 BMR     1       6.218  43.675  53.164
ATOM     48  C52 BMR     1       7.784  44.963  52.403
```

```
ATOM     49  C63 BMR     1       6.903  46.200  52.038
ATOM     50  C64 BMR     1       7.479  47.034  50.877
ATOM     51  C65 BMR     1       6.794  48.379  50.563
ATOM     52  C66 BMR     1       7.571  49.071  49.417
ATOM     53  C67 BMR     1       6.895  50.325  48.832
ATOM     54  C68 BMR     1       7.756  50.914  47.691
ATOM     55  C69 BMR     1       7.090  52.110  46.985
ATOM     56  C70 BMR     1       7.973  52.670  45.858
ATOM     57  H89 BMR     1       7.464  53.505  45.375
ATOM     58  H90 BMR     1       8.923  53.021  46.261
ATOM     59  H91 BMR     1       8.166  51.897  45.111
ATOM     60  H87 BMR     1       6.137  51.793  46.558
ATOM     61  H88 BMR     1       6.901  52.903  47.711
ATOM     62  H85 BMR     1       8.715  51.235  48.102
ATOM     63  H86 BMR     1       7.942  50.136  46.947
ATOM     64  H83 BMR     1       5.913  50.052  48.441
ATOM     65  H84 BMR     1       6.769  51.073  49.619
ATOM     66  H81 BMR     1       8.561  49.349  49.787
ATOM     67  H82 BMR     1       7.703  48.356  48.601
ATOM     68  H79 BMR     1       5.762  48.196  50.257
ATOM     69  H80 BMR     1       6.799  49.018  51.447
ATOM     70  H77 BMR     1       8.529  47.238  51.098
ATOM     71  H78 BMR     1       7.408  46.436  49.968
ATOM     72  H75 BMR     1       5.898  45.868  51.768
ATOM     73  H76 BMR     1       6.826  46.848  52.913
ATOM     74  H53 BMR     1       8.738  45.329  52.787
ATOM     75  C53 BMR     1       8.067  43.997  51.205
ATOM     76  H54 BMR     1       8.167  42.972  51.569
ATOM     77  H55 BMR     1       7.205  44.009  50.535
ATOM     78  C54 BMR     1       9.361  44.276  50.401
ATOM     79  H56 BMR     1       9.371  45.300  50.043
ATOM     80  H57 BMR     1      10.225  44.153  51.056
ATOM     81  C55 BMR     1       9.519  43.334  49.184
ATOM     82  H58 BMR     1       9.934  42.383  49.523
ATOM     83  H59 BMR     1       8.543  43.145  48.735
ATOM     84  C56 BMR     1      10.432  43.949  48.103
ATOM     85  H60 BMR     1       9.970  44.874  47.749
ATOM     86  H61 BMR     1      11.399  44.191  48.547
ATOM     87  C57 BMR     1      10.650  43.017  46.894
ATOM     88  H62 BMR     1      11.206  42.134  47.220
ATOM     89  H63 BMR     1       9.682  42.696  46.503
ATOM     90  C58 BMR     1      11.431  43.735  45.776
ATOM     91  H64 BMR     1      10.854  44.602  45.443
ATOM     92  H65 BMR     1      12.383  44.087  46.178
ATOM     93  C59 BMR     1      11.706  42.828  44.560
ATOM     94  H66 BMR     1      12.286  41.963  44.885
ATOM     95  H67 BMR     1      10.756  42.481  44.149
ATOM     96  C60 BMR     1      12.488  43.581  43.463
ATOM     97  H68 BMR     1      11.898  44.438  43.130
ATOM     98  H69 BMR     1      13.426  43.947  43.884
ATOM     99  C61 BMR     1      12.802  42.687  42.248
```

```
ATOM    100  H70 BMR     1      13.382  41.822  42.574
ATOM    101  H71 BMR     1      11.868  42.334  41.806
ATOM    102  C62 BMR     1      13.603  43.438  41.173
ATOM    103  H72 BMR     1      13.805  42.770  40.335
ATOM    104  H73 BMR     1      13.036  44.296  40.811
ATOM    105  H74 BMR     1      14.553  43.784  41.585
TER
END
```

PDB file for Guerbet branched chain (S) (βMal-$C_{12}C_8$(*S*)):

```
REMARK
ATOM      1  O22 BMS     1      28.037  42.023  63.152
ATOM      2  H22 BMS     1      27.406  41.481  62.653
ATOM      3  C22 BMS     1      27.493  43.342  63.220
ATOM      4  H42 BMS     1      26.652  43.348  63.920
ATOM      5  C23 BMS     1      28.578  44.318  63.714
ATOM      6  H43 BMS     1      29.423  44.296  63.020
ATOM      7  O23 BMS     1      29.029  43.923  65.013
ATOM      8  H23 BMS     1      29.308  42.991  64.939
ATOM      9  C24 BMS     1      27.995  45.741  63.758
ATOM     10  H44 BMS     1      27.161  45.766  64.466
ATOM     11  O24 BMS     1      29.009  46.644  64.200
ATOM     12  H24 BMS     1      29.291  46.324  65.077
ATOM     13  C25 BMS     1      27.490  46.139  62.352
ATOM     14  H45 BMS     1      28.334  46.175  61.662
ATOM     15  C26 BMS     1      26.782  47.507  62.358
ATOM     16  H46 BMS     1      27.473  48.276  62.712
ATOM     17  O26 BMS     1      25.636  47.462  63.214
ATOM     18  H26 BMS     1      25.292  48.365  63.294
ATOM     19  H47 BMS     1      26.469  47.759  61.341
ATOM     20  O25 BMS     1      26.540  45.146  61.875
ATOM     21  C21 BMS     1      26.978  43.767  61.824
ATOM     22  H41 BMS     1      26.109  43.160  61.538
ATOM     23  O14 BMS     1      28.033  43.586  60.845
ATOM     24  C14 BMS     1      27.668  43.701  59.444
ATOM     25  C13 BMS     1      27.259  42.311  58.897
ATOM     26  C12 BMS     1      27.012  42.371  57.376
ATOM     27  H32 BMS     1      26.145  43.007  57.170
ATOM     28  O12 BMS     1      26.739  41.036  56.942
ATOM     29  H12 BMS     1      26.119  40.657  57.596
ATOM     30  H33 BMS     1      28.078  41.612  59.089
ATOM     31  O13 BMS     1      26.074  41.819  59.532
ATOM     32  H13 BMS     1      26.293  41.616  60.457
ATOM     33  H34 BMS     1      26.850  44.418  59.327
ATOM     34  C15 BMS     1      28.910  44.196  58.661
ATOM     35  H35 BMS     1      29.738  43.496  58.812
ATOM     36  C16 BMS     1      29.378  45.606  59.085
ATOM     37  H36 BMS     1      29.750  45.570  60.112
ATOM     38  O16 BMS     1      28.314  46.560  58.994
ATOM     39  H16 BMS     1      28.664  47.437  59.234
ATOM     40  H37 BMS     1      30.199  45.920  58.435
ATOM     41  O15 BMS     1      28.596  44.221  57.248
ATOM     42  C11 BMS     1      28.250  42.951  56.646
ATOM     43  H31 BMS     1      29.124  42.287  56.726
ATOM     44  O11 BMS     1      27.959  43.186  55.249
ATOM     45  C51 BMS     1      28.191  42.088  54.336
ATOM     46  H51 BMS     1      27.474  41.292  54.551
ATOM     47  H52 BMS     1      29.208  41.709  54.474
ATOM     48  C52 BMS     1      28.002  42.581  52.881
```

```
ATOM     49  C63 BMS     1      29.069  43.666  52.556
ATOM     50  C64 BMS     1      28.922  44.293  51.152
ATOM     51  C65 BMS     1      29.906  45.467  50.960
ATOM     52  C66 BMS     1      29.775  46.081  49.551
ATOM     53  C67 BMS     1      30.762  47.251  49.357
ATOM     54  C68 BMS     1      30.634  47.862  47.946
ATOM     55  C69 BMS     1      31.623  49.031  47.751
ATOM     56  C70 BMS     1      31.498  49.642  46.344
ATOM     57  H89 BMS     1      32.205  50.467  46.226
ATOM     58  H90 BMS     1      30.490  50.028  46.179
ATOM     59  H91 BMS     1      31.714  48.894  45.578
ATOM     60  H87 BMS     1      32.646  48.678  47.901
ATOM     61  H88 BMS     1      31.428  49.806  48.498
ATOM     62  H85 BMS     1      29.612  48.220  47.794
ATOM     63  H86 BMS     1      30.829  47.092  47.195
ATOM     64  H83 BMS     1      31.783  46.895  49.509
ATOM     65  H84 BMS     1      30.565  48.021  50.107
ATOM     66  H81 BMS     1      28.752  46.437  49.402
ATOM     67  H82 BMS     1      29.970  45.312  48.799
ATOM     68  H79 BMS     1      30.929  45.113  51.111
ATOM     69  H80 BMS     1      29.708  46.235  51.712
ATOM     70  H77 BMS     1      27.899  44.651  51.016
ATOM     71  H78 BMS     1      29.122  43.539  50.387
ATOM     72  H75 BMS     1      30.070  43.239  52.658
ATOM     73  H76 BMS     1      28.992  44.470  53.294
ATOM     74  H53 BMS     1      27.008  43.031  52.818
ATOM     75  C53 BMS     1      28.073  41.364  51.913
ATOM     76  H54 BMS     1      27.879  40.441  52.464
ATOM     77  H55 BMS     1      29.082  41.270  51.500
ATOM     78  C54 BMS     1      27.034  41.447  50.771
ATOM     79  H56 BMS     1      27.154  42.374  50.208
ATOM     80  H57 BMS     1      26.028  41.458  51.200
ATOM     81  C55 BMS     1      27.167  40.249  49.808
ATOM     82  H58 BMS     1      27.029  39.318  50.363
ATOM     83  H59 BMS     1      28.173  40.235  49.382
ATOM     84  C56 BMS     1      26.128  40.329  48.670
ATOM     85  H60 BMS     1      26.265  41.261  48.116
ATOM     86  H61 BMS     1      25.121  40.342  49.096
ATOM     87  C57 BMS     1      26.264  39.133  47.704
ATOM     88  H62 BMS     1      26.125  38.200  48.258
ATOM     89  H63 BMS     1      27.270  39.118  47.280
ATOM     90  C58 BMS     1      25.226  39.214  46.565
ATOM     91  H64 BMS     1      25.365  40.146  46.012
ATOM     92  H65 BMS     1      24.219  39.228  46.989
ATOM     93  C59 BMS     1      25.362  38.017  45.600
ATOM     94  H66 BMS     1      25.223  37.085  46.152
ATOM     95  H67 BMS     1      26.370  38.004  45.176
ATOM     96  C60 BMS     1      24.326  38.100  44.459
ATOM     97  H68 BMS     1      24.465  39.032  43.905
ATOM     98  H69 BMS     1      23.319  38.113  44.882
ATOM     99  C61 BMS     1      24.462  36.904  43.493
```

```
ATOM    100  H70 BMS     1      24.320  35.969  44.041
ATOM    101  H71 BMS     1      25.467  36.887  43.065
ATOM    102  C62 BMS     1      23.429  36.984  42.353
ATOM    103  H72 BMS     1      23.541  36.129  41.682
ATOM    104  H73 BMS     1      23.566  37.898  41.773
ATOM    105  H74 BMS     1      22.412  36.974  42.754
TER
END
```

APPENDIX B

PREPIN FILE FOR EACH GLYCOLIPID SYSTEM

PREPIN file for βMal-C_{12}

```
0    0    2
This is a remark line
.dat
DDM   INT  0
CORRECT     OMIT DU   BEG
0.0000
 1  DUMM  DU   M   0  -1  -2  0.000      .0        .0      .000
 2  DUMM  DU   M   1   0  -1  1.449      .0        .0      .000
 3  DUMM  DU   M   2   1   0  1.522    111.1       .0      .000
 4  O22   Oh   M   3   2   1  1.540    111.208  -180.000 -0.7130
 5  H22   Ho   E   4   3   2  0.968     92.309   167.099  0.4370
 6  C22   Cg   M   4   3   2  1.381     25.092   -48.391  0.2460
 7  H42   H1   E   6   4   3  1.097    106.397  -106.323  0.0000
 8  C23   Cg   M   6   4   3  1.551    109.378   135.962  0.2860
 9  H43   H1   E   8   6   4  1.047    107.796   -58.206  0.0000
10  O23   Oh   S   8   6   4  1.426    108.179    60.380 -0.6990
11  H23   Ho   E  10   8   6  0.951    107.226   -58.293  0.4270
12  C24   Cg   M   8   6   4  1.482    110.275  -178.116  0.2540
13  H44   H1   E  12   8   6  1.087    118.553   -64.228  0.0000
14  O24   Oh   S  12   8   6  1.400    110.544   175.469 -0.7100
15  H24   Ho   E  14  12   8  0.946    107.954    64.718  0.4360
16  C25   Cg   M  12   8   6  1.571    109.251    54.506  0.2830
17  H45   H1   E  16  12   8  1.052    108.455    58.271  0.0000
18  C26   Cg   3  16  12   8  1.539    113.303  -178.006  0.2760
19  H46   H1   E  18  16  12  1.099    110.127   -59.546  0.0000
20  O26   Oh   S  18  16  12  1.413    110.188    60.351 -0.6820
21  H26   Ho   E  20  18  16  0.966    110.190   179.816  0.4180
22  H47   H1   E  18  16  12  1.132    112.827   178.426  0.0000
23  O25   Os   M  16  12   8  1.401    111.119   -55.831 -0.5740
24  C21   Cg   M  23  16  12  1.423    113.647    59.406  0.5090
25  H41   H2   E  24  23  16  1.102    108.358  -172.289  0.0000
26  O14   Os   M  24  23  16  1.423    112.312    62.106 -0.4680
27  C14   Cg   M  26  24  23  1.427    115.955    50.999  0.2760
28  C13   Cg   3  27  26  24  1.567    113.353    63.085  0.2840
29  C12   Cg   B  28  27  26  1.509    109.504   168.250  0.3100
30  H32   H1   E  29  28  27  1.095    113.688    61.415  0.0000
31  O12   Oh   S  29  28  27  1.373    109.869  -177.015 -0.7180
32  H12   Ho   E  31  29  28  0.956    107.678   175.544  0.4370
33  H33   H1   E  28  27  26  1.129    110.476    46.736  0.0000
34  O13   Oh   S  28  27  26  1.453    108.814   -76.383 -0.7090
35  H13   Ho   E  34  28  27  0.976    105.102  -173.754  0.4320
```

36	H34	H1	E	27	26	24	1.085	112.363	-61.581	0.0000
37	C15	Cg	M	27	26	24	1.527	105.662	-177.226	0.2250
38	H35	H1	E	37	27	26	1.094	107.998	-51.007	0.0000
39	C16	Cg	3	37	27	26	1.519	111.785	65.528	0.2820
40	H36	H1	E	39	37	27	1.122	111.548	-59.840	0.0000
41	O16	Oh	S	39	37	27	1.413	112.363	60.351	-0.6880
42	H16	Ho	E	41	39	37	0.963	106.814	-179.263	0.4240
43	H37	H1	E	39	37	27	1.058	109.803	-178.878	0.0000
44	O15	Os	M	37	27	26	1.419	113.848	-174.015	-0.4710
45	C11	Cg	M	44	37	27	1.418	111.227	59.466	0.3840
46	H31	H2	E	45	44	37	1.104	110.318	55.275	0.0000
47	O11	Os	M	45	44	37	1.409	110.532	176.801	-0.1940
48	C71	Cg	M	47	45	44	1.429	113.678	-70.601	0.0000
49	H71	H1	E	48	47	45	1.097	112.995	-44.414	0.0000
50	H72	H1	E	48	47	45	1.052	111.510	65.708	0.0000
51	C72	Cg	M	48	47	45	1.495	109.191	-171.116	0.0000
52	H73	Hc	E	51	48	47	1.131	113.144	-66.414	0.0000
53	H74	Hc	E	51	48	47	1.101	112.172	62.799	0.0000
54	C73	Cg	M	51	48	47	1.565	108.557	177.194	0.0000
55	H75	Hc	E	54	51	48	1.095	111.599	-61.136	0.0000
56	H76	Hc	E	54	51	48	1.103	113.188	62.797	0.0000
57	C74	Cg	M	54	51	48	1.534	110.287	-175.153	0.0000
58	H77	Hc	E	57	54	51	1.051	108.065	-63.964	0.0000
59	H78	Hc	E	57	54	51	1.087	109.425	59.898	0.0000
60	C75	Cg	M	57	54	51	1.515	109.287	179.332	0.0000
61	H79	Hc	E	60	57	54	1.089	101.317	-66.751	0.0000
62	H80	Hc	E	60	57	54	1.107	112.345	55.999	0.0000
63	C76	Cg	M	60	57	54	1.584	108.261	177.513	0.0000
64	H81	Hc	E	63	60	57	1.112	115.269	-55.404	0.0000
65	H82	Hc	E	63	60	57	1.065	110.705	63.890	0.0000
66	C77	Cg	M	63	60	57	1.517	107.261	178.447	0.0000
67	H83	Hc	E	66	63	60	1.082	111.687	-64.075	0.0000
68	H84	Hc	E	66	63	60	1.055	116.248	58.420	0.0000
69	C78	Cg	M	66	63	60	1.573	108.624	177.096	0.0000
70	H85	Hc	E	69	66	63	1.080	110.489	-49.608	0.0000
71	H86	Hc	E	69	66	63	1.058	106.923	59.073	0.0000
72	C79	Cg	M	69	66	63	1.496	110.083	-177.799	0.0000
73	H87	Hc	E	72	69	66	1.108	109.892	-62.558	0.0000
74	H88	Hc	E	72	69	66	1.094	108.867	58.559	0.0000
75	C80	Cg	M	72	69	66	1.570	106.840	178.917	0.0000
76	H89	Hc	E	75	72	69	1.103	109.803	-59.674	0.0000
77	H90	Hc	E	75	72	69	1.078	107.775	61.206	0.0000
78	C81	Cg	M	75	72	69	1.539	109.500	-179.469	0.0000
79	H91	Hc	E	78	75	72	1.109	112.149	-61.133	0.0000
80	H92	Hc	E	78	75	72	1.078	112.352	62.845	0.0000
81	C82	Cg	M	78	75	72	1.549	109.673	-179.170	0.0000
82	H93	Hc	E	81	78	75	1.081	111.029	177.043	0.0000
83	H94	Hc	E	81	78	75	1.043	106.606	-61.007	0.0000
84	H95	Hc	E	81	78	75	1.117	112.714	59.204	0.0000

LOOP

```
C21  C22
C11  C12

IMPROPER

DONE
STOP
```

PREPIN file for βCel-C_{12}

```
   0    0    2
This is a remark line
molecule.res
DDC    INT  0
CORRECT     OMIT DU   BEG
0.0000
 1  DUMM  DU   M   0  -1  -2  0.000      .0        .0      .0000
 2  DUMM  DU   M   1   0  -1  1.449      .0        .0      .0000
 3  DUMM  DU   M   2   1   0  1.522   111.1        .0      .0000
 4  O22   OH   M   3   2   1  1.540   111.208   180.000 -0.7180
 5  H22   HO   E   4   3   2  0.981    39.611   -82.284  0.4370
 6  C22   CG   M   4   3   2  1.438    77.350    55.098  0.3100
 7  H42   H1   E   6   4   3  1.118   109.241   -82.842  0.0000
 8  C23   CG   M   6   4   3  1.531   109.238   159.299  0.2840
 9  H43   H1   E   8   6   4  1.115   110.791   -51.463  0.0000
10  O23   OH   S   8   6   4  1.405   109.369    66.466 -0.7090
11  H23   HO   E  10   8   6  0.941   107.461   -58.085  0.4320
12  C24   CG   M   8   6   4  1.529   109.477  -174.256  0.2760
13  H44   H1   E  12   8   6  1.116   110.746   -69.553  0.0000
14  O24   OH   S  12   8   6  1.404   108.741   173.130 -0.7140
15  H24   HO   E  14  12   8  0.942   106.215    64.849  0.4400
16  C25   CG   M  12   8   6  1.533   109.986    53.105  0.2250
17  H45   H1   E  16  12   8  1.117   110.509    60.114  0.0000
18  C26   CG   3  16  12   8  1.534   112.962  -178.599  0.2820
19  H46   H1   E  18  16  12  1.115   111.623   -61.053  0.0000
20  O26   OH   S  18  16  12  1.403   110.006    57.505 -0.6880
21  H26   HO   E  20  18  16  0.941   107.157  -179.808  0.4240
22  H47   H1   E  18  16  12  1.115   111.561   176.277  0.0000
23  O25   OS   M  16  12   8  1.413   109.213   -58.271 -0.4710
24  C21   CG   M  23  16  12  1.408   112.998    64.273  0.3840
25  H41   H2   E  24  23  16  1.091   110.945    60.565  0.0000
26  O14   OS   M  24  23  16  1.409   109.486  -178.094 -0.4680
27  C14   CG   M  26  24  23  1.413   118.735   -34.479  0.2760
28  C13   CG   3  27  26  24  1.540   106.903    97.206  0.2840
29  C12   CG   B  28  27  26  1.528   112.231   156.472  0.3100
30  H32   H1   E  29  28  27  1.116   111.510    71.325  0.0000
31  O12   OH   S  29  28  27  1.404   108.945  -170.015 -0.7180
32  H12   HO   E  31  29  28  0.942   107.091  -174.483  0.4370
33  H33   H1   E  28  27  26  1.116   109.660    34.232  0.0000
34  O13   OH   S  28  27  26  1.404   110.444   -83.211 -0.7090
35  H13   HO   E  34  28  27  0.941   107.328   166.025  0.4320
36  H34   H1   E  27  26  24  1.116   111.383   -25.505  0.0000
37  C15   CG   M  27  26  24  1.545   104.867  -143.984  0.2250
38  H35   H1   E  37  27  26  1.117   109.911   -41.438  0.0000
39  C16   CG   3  37  27  26  1.535   112.924    78.716  0.2820
40  H36   H1   E  39  37  27  1.114   111.976   -55.366  0.0000
41  O16   OH   S  39  37  27  1.404   109.593    63.454 -0.6880
42  H16   HO   E  41  39  37  0.942   107.568   175.324  0.4240
43  H37   H1   E  39  37  27  1.116   111.486  -178.505  0.0000
```

```
44  O15   OS   M  37  27  26  1.412   112.229  -160.044 -0.4710
45  C11   CG   M  44  37  27  1.405   111.979    59.793  0.3840
46  H31   H2   E  45  44  37  1.116   111.898    54.881  0.0000
47  O11   OS   M  45  44  37  1.409   102.523   173.455 -0.1940
48  C71   CG   M  47  45  44  1.413   112.899   -76.788  0.0000
49  H71   H1   E  48  47  45  1.115   109.018   -59.047  0.0000
50  H72   H1   E  48  47  45  1.115   108.805    61.273  0.0000
51  C72   CG   M  48  47  45  1.533   108.584  -178.510  0.0000
52  H73   HC   E  51  48  47  1.116   109.550   -56.252  0.0000
53  H74   HC   E  51  48  47  1.117   109.389    61.375  0.0000
54  C73   CG   M  51  48  47  1.537   110.894  -177.456  0.0000
55  H75   HC   E  54  51  48  1.116   109.414   -56.806  0.0000
56  H76   HC   E  54  51  48  1.116   109.079    60.357  0.0000
57  C74   CG   M  54  51  48  1.536   112.268  -178.305  0.0000
58  H77   HC   E  57  54  51  1.115   109.442   -56.597  0.0000
59  H78   HC   E  57  54  51  1.116   109.308    60.875  0.0000
60  C75   CG   M  57  54  51  1.537   111.534  -177.850  0.0000
61  H79   HC   E  60  57  54  1.116   109.436   -57.554  0.0000
62  H80   HC   E  60  57  54  1.116   109.254    59.700  0.0000
63  C76   CG   M  60  57  54  1.536   111.971  -178.971  0.0000
64  H81   HC   E  63  60  57  1.116   109.412   -57.629  0.0000
65  H82   HC   E  63  60  57  1.116   109.323    59.724  0.0000
66  C77   CG   M  63  60  57  1.537   111.786  -178.941  0.0000
67  H83   HC   E  66  63  60  1.115   109.404   -58.048  0.0000
68  H84   HC   E  66  63  60  1.116   109.351    59.385  0.0000
69  C78   CG   M  66  63  60  1.538   111.852  -179.347  0.0000
70  H85   HC   E  69  66  63  1.116   109.351   -58.221  0.0000
71  H86   HC   E  69  66  63  1.116   109.291    59.053  0.0000
72  C79   CG   M  69  66  63  1.537   111.920  -179.618  0.0000
73  H87   HC   E  72  69  66  1.116   109.391   -58.329  0.0000
74  H88   HC   E  72  69  66  1.116   109.399    59.048  0.0000
75  C80   CG   M  72  69  66  1.538   111.833  -179.622  0.0000
76  H89   HC   E  75  72  69  1.116   109.387   -58.515  0.0000
77  H90   HC   E  75  72  69  1.115   109.330    58.820  0.0000
78  C81   CG   M  75  72  69  1.537   111.982  -179.874  0.0000
79  H91   HC   E  78  75  72  1.116   109.592   -58.590  0.0000
80  H92   HC   E  78  75  72  1.116   109.575    58.909  0.0000
81  C82   CG   M  78  75  72  1.534   111.770  -179.862  0.0000
82  H93   HC   E  81  78  75  1.115   111.040  -179.915  0.0000
83  H94   HC   E  81  78  75  1.115   111.134   -60.132  0.0000
84  H95   HC   E  81  78  75  1.115   111.161    60.177  0.0000

LOOP
 C21  C22
 C11  C12

IMPROPER

DONE
STOP
```

PREPIN file for βIsoMal-C_{12}

```
   0    0    2
This is a remark line
molecule.res
ISM    INT  0
CORRECT     OMIT DU   BEG
0.0000
 1  DUMM  DU   M   0  -1  -2  0.000      .0        .0      .0000
 2  DUMM  DU   M   1   0  -1  1.449      .0        .0      .0000
 3  DUMM  DU   M   2   1   0  1.522   111.1        .0      .0000
 4  O22   OH   M   3   2   1  1.540   111.208   180.000 -0.7130
 5  H62   HO   E   4   3   2  0.945   132.965  -152.620  0.4370
 6  C22   CG   M   4   3   2  1.428    95.467   -36.588  0.2460
 7  H42   H1   E   6   4   3  1.108   112.279   177.214  0.0000
 8  C23   CG   M   6   4   3  1.567   112.454    53.435  0.2860
 9  H43   H1   E   8   6   4  1.056   110.978   -55.234  0.0000
10  O23   OH   S   8   6   4  1.407   109.651    62.744 -0.6990
11  H63   HO   E  10   8   6  0.959   114.718   -61.585  0.4270
12  C24   CG   M   8   6   4  1.559   106.761  -173.299  0.2540
13  H44   H1   E  12   8   6  1.107   111.586   -69.004  0.0000
14  O24   OH   S  12   8   6  1.408   104.059   172.661 -0.7100
15  H64   HO   E  14  12   8  0.967   115.169    62.011  0.4360
16  C25   CG   M  12   8   6  1.588   111.189    54.042  0.2830
17  H45   H1   E  16  12   8  1.037   105.344    66.679  0.0000
18  C26   CG   3  16  12   8  1.562   112.246  -173.304  0.2760
19  H46   H1   E  18  16  12  1.085   103.730   -64.576  0.0000
20  O26   OH   S  18  16  12  1.395   109.799    52.870 -0.6820
21  H66   HO   E  20  18  16  0.964   103.285   168.944  0.4180
22  H47   H1   E  18  16  12  1.127   106.772   174.841  0.0000
23  O25   OS   M  16  12   8  1.380   113.236   -48.386 -0.5740
24  C21   CG   M  23  16  12  1.393   116.123    48.987  0.5090
25  H41   H2   E  24  23  16  1.084   112.275  -177.283  0.0000
26  O16   OS   M  24  23  16  1.447   108.545    64.333 -0.1940
27  C16   CG   M  26  24  23  1.416   116.900    70.310  0.2820
28  H36   H1   E  27  26  24  1.025   111.963   -27.396  0.0000
29  H37   H1   E  27  26  24  1.143   106.740    87.338  0.0000
30  C15   CG   M  27  26  24  1.535   106.225  -152.745  0.2250
31  C14   CG   3  30  27  26  1.546   112.024  -167.540  0.2760
32  C13   CG   3  31  30  27  1.522   110.383   176.526  0.2840
33  C12   CG   B  32  31  30  1.557   110.278    54.584  0.3100
34  H32   H1   E  33  32  31  1.111   112.206    77.315  0.0000
35  O12   OH   S  33  32  31  1.389   107.443  -162.677 -0.7180
36  H52   HO   E  35  33  32  0.967   113.140   174.618  0.4370
37  H33   H1   E  32  31  30  1.039   110.351   -69.579  0.0000
38  O13   OH   S  32  31  30  1.406   112.613   172.695 -0.7090
39  H53   HO   E  38  32  31  0.964   119.981  -158.617  0.4320
40  H34   H1   E  31  30  27  1.162   103.501   -65.771  0.0000
41  O14   OH   S  31  30  27  1.402   113.736    54.040 -0.7140
42  H54   HO   E  41  31  30  0.945   110.846   166.675  0.4400
43  H35   H1   E  30  27  26  1.112   111.885   -51.967  0.0000
```

```
44  O15   OS   M  30  27  26  1.423   110.437    70.706 -0.4710
45  C11   CG   M  44  30  27  1.419   111.033  -174.300  0.3840
46  H31   H2   E  45  44  30  1.086   108.443    56.803  0.0000
47  O11   OS   M  45  44  30  1.385   107.798   179.823 -0.4580
48  C71   CG   M  47  45  44  1.422   118.330   -78.507  0.0000
49  H71   H1   E  48  47  45  1.086   112.800   -30.987  0.0000
50  H72   H1   E  48  47  45  1.147   104.391    88.557  0.0000
51  C72   CG   M  48  47  45  1.517   110.221  -147.220  0.0000
52  H73   HC   E  51  48  47  1.088   110.908   -65.454  0.0000
53  H74   HC   E  51  48  47  1.108   110.304    57.905  0.0000
54  C73   CG   M  51  48  47  1.528   109.452   173.546  0.0000
55  H75   HC   E  54  51  48  1.085   108.290   -55.559  0.0000
56  H76   HC   E  54  51  48  1.126   105.852    70.279  0.0000
57  C74   CG   M  54  51  48  1.516   117.914  -175.084  0.0000
58  H77   HC   E  57  54  51  1.108   105.858   -53.533  0.0000
59  H78   HC   E  57  54  51  1.096   108.741    67.092  0.0000
60  C75   CG   M  57  54  51  1.527   109.717  -174.137  0.0000
61  H79   HC   E  60  57  54  1.149   110.777   -64.461  0.0000
62  H80   HC   E  60  57  54  1.042   108.802    61.257  0.0000
63  C76   CG   M  60  57  54  1.558   115.527   175.857  0.0000
64  H81   HC   E  63  60  57  1.111   111.607   -57.266  0.0000
65  H82   HC   E  63  60  57  1.109   108.379    60.337  0.0000
66  C77   CG   M  63  60  57  1.577   111.135  -177.380  0.0000
67  H83   HC   E  66  63  60  1.117   101.507   -68.244  0.0000
68  H84   HC   E  66  63  60  1.105   106.944    48.347  0.0000
69  C78   CG   M  66  63  60  1.540   116.812   174.810  0.0000
70  H85   HC   E  69  66  63  1.128   107.008   -58.273  0.0000
71  H86   HC   E  69  66  63  1.115   114.939    67.142  0.0000
72  C79   CG   M  69  66  63  1.544   106.829  -169.743  0.0000
73  H87   HC   E  72  69  66  1.065   110.965   -60.903  0.0000
74  H88   HC   E  72  69  66  1.115   106.478    58.481  0.0000
75  C80   CG   M  72  69  66  1.490   108.297   173.584  0.0000
76  H89   HC   E  75  72  69  1.033   110.293   -46.239  0.0000
77  H90   HC   E  75  72  69  1.116   108.778    67.972  0.0000
78  C81   CG   M  75  72  69  1.562   111.868  -169.388  0.0000
79  H91   HC   E  78  75  72  1.086   112.948   -63.043  0.0000
80  H92   HC   E  78  75  72  1.104   112.649    59.949  0.0000
81  C82   CG   M  78  75  72  1.552   102.097   177.505  0.0000
82  H93   HC   E  81  78  75  1.042   105.398   176.625  0.0000
83  H94   HC   E  81  78  75  1.085   118.360   -67.126  0.0000
84  H95   HC   E  81  78  75  1.094   114.044    62.597  0.0000

LOOP

 C21  C22
 C11  C12

IMPROPER

DONE
STOP
```

PREPIN file for βMal-$C_{12}C_{10}$

```
   0    0    2
This is a remark line
molecule.res
BCM    INT  0
CORRECG     OMIT DU   BEG
0.0000
 1  DUMM  DU  M   0  -1  -2  0.000      .0        .0      .0000
 2  DUMM  DU  M   1   0  -1  1.449      .0        .0      .0000
 3  DUMM  DU  M   2   1   0  1.522   111.1        .0      .0000
 4  O22   OH  M   3   2   1  1.540   111.208   180.000 -0.7130
 5  H23   HO  E   4   3   2  0.959    85.277  -149.519  0.4370
 6  C22   CG  M   4   3   2  1.413   113.703   -41.365  0.2460
 7  H22   H1  E   6   4   3  1.090   108.471  -149.795  0.0000
 8  C23   CG  M   6   4   3  1.537   110.802    90.894  0.2860
 9  H24   H1  E   8   6   4  1.091   109.602   -53.674  0.0000
10  O23   OH  S   8   6   4  1.415   109.086    66.360 -0.6990
11  H25   HO  E  10   8   6  0.960   108.504   -62.881  0.4270
12  C24   CG  M   8   6   4  1.538   109.924  -174.058  0.2540
13  H26   H1  E  12   8   6  1.091   108.965   -67.315  0.0000
14  O24   OH  S  12   8   6  1.414   109.294   173.424 -0.7100
15  H27   HO  E  14  12   8  0.959   108.462    63.647  0.4360
16  C25   CG  M  12   8   6  1.543   110.485    52.982  0.2830
17  H28   H1  E  16  12   8  1.089   108.110    65.749  0.0000
18  C26   CG  3  16  12   8  1.537   112.736  -175.662  0.2760
19  H29   H1  E  18  16  12  1.090   109.412   -63.030  0.0000
20  O26   OH  S  18  16  12  1.414   111.800    57.624 -0.6820
21  H31   HO  E  20  18  16  0.960   108.473  -179.815  0.4180
22  H30   H1  E  18  16  12  1.090   109.182   178.439  0.0000
23  O25   OS  M  16  12   8  1.428   111.556   -53.899 -0.5740
24  C21   CG  M  23  16  12  1.430   116.138    55.746  0.5090
25  H21   H1  E  24  23  16  1.089   110.097  -175.273  0.0000
26  O14   OS  M  24  23  16  1.432   104.016    66.579 -0.4680
27  C14   CG  M  26  24  23  1.433   119.421    57.944  0.2760
28  C13   CG  3  27  26  24  1.549   113.266    61.687  0.2840
29  C12   CG  B  28  27  26  1.542   112.594   162.890  0.3100
30  H12   H1  E  29  28  27  1.091   109.558    72.179  0.0000
31  O12   OH  S  29  28  27  1.413   109.604  -167.592 -0.7180
32  H13   HO  E  31  29  28  0.960   108.385  -175.738  0.4370
33  H14   H1  E  28  27  26  1.091   108.711    41.912  0.0000
34  O13   OH  S  28  27  26  1.415   110.056   -78.001 -0.7090
35  H15   HO  E  34  28  27  0.960   108.475   175.995  0.4320
36  H16   H1  E  27  26  24  1.091   110.481   -60.950  0.0000
37  C15   CG  M  27  26  24  1.545   105.408  -178.123  0.2250
38  H17   H1  E  37  27  26  1.092   108.050   -56.320  0.0000
39  C16   CG  3  37  27  26  1.538   113.353    62.009  0.2820
40  H18   H1  E  39  37  27  1.090   109.292   -63.873  0.0000
41  O16   OH  S  39  37  27  1.412   112.096    56.884 -0.6880
42  H20   HO  E  41  39  37  0.960   108.395  -179.094  0.4240
43  H19   H1  E  39  37  27  1.090   109.131   177.836  0.0000
```

44	O15	OS	M	37	27	26	1.420	111.553	-174.799	-0.4710
45	C11	CG	M	44	37	27	1.422	111.867	64.269	0.3840
46	H11	H1	E	45	44	37	1.092	110.652	56.510	0.0000
47	O11	OS	M	45	44	37	1.431	103.378	174.784	-0.1940
48	C31	CG	M	47	45	44	1.426	114.283	-58.232	0.0000
49	H51	H1	E	48	47	45	1.092	107.997	-44.705	0.0000
50	H52	H1	E	48	47	45	1.091	108.647	72.584	0.0000
51	C32	CG	M	48	47	45	1.548	115.195	-165.916	0.0000
52	H53	HC	E	51	48	47	1.091	108.017	63.633	0.0000
53	C43	CG	3	51	48	47	1.567	110.728	-55.135	0.0000
54	C44	CG	3	53	51	48	1.560	120.584	149.163	0.0000
55	C45	CG	3	54	53	51	1.531	112.888	76.166	0.0000
56	C46	CG	3	55	54	53	1.538	123.134	163.280	0.0000
57	C47	CG	3	56	55	54	1.547	103.794	-179.170	0.0000
58	C48	CG	3	57	56	55	1.535	118.466	-178.442	0.0000
59	C49	CG	3	58	57	56	1.542	106.740	178.503	0.0000
60	C50	CG	3	59	58	57	1.533	114.609	-179.792	0.0000
61	C51	CG	3	60	59	58	1.538	109.268	178.245	0.0000
62	C52	CG	3	61	60	59	1.530	112.315	179.723	0.0000
63	H93	HC	E	62	61	60	1.090	109.251	179.799	0.0000
64	H94	HC	E	62	61	60	1.091	109.898	-60.554	0.0000
65	H95	HC	E	62	61	60	1.090	109.903	60.078	0.0000
66	H91	HC	E	61	60	59	1.091	109.227	-59.804	0.0000
67	H92	HC	E	61	60	59	1.091	109.424	58.955	0.0000
68	H89	HC	E	60	59	58	1.092	109.473	-61.670	0.0000
69	H90	HC	E	60	59	58	1.090	109.522	58.233	0.0000
70	H87	HC	E	59	58	57	1.092	108.647	-58.593	0.0000
71	H88	HC	E	59	58	57	1.092	108.796	58.792	0.0000
72	H85	HC	E	58	57	56	1.090	109.994	-62.024	0.0000
73	H86	HC	E	58	57	56	1.090	109.964	59.202	0.0000
74	H83	HC	E	57	56	55	1.091	107.976	-56.574	0.0000
75	H84	HC	E	57	56	55	1.092	108.037	59.518	0.0000
76	H81	HC	E	56	55	54	1.091	110.614	-60.621	0.0000
77	H82	HC	E	56	55	54	1.090	110.529	62.298	0.0000
78	H79	HC	E	55	54	53	1.082	105.431	-77.076	0.0000
79	H80	HC	E	55	54	53	1.090	106.197	41.160	0.0000
80	H77	HC	E	54	53	51	1.090	108.014	-164.613	0.0000
81	H78	HC	E	54	53	51	1.091	109.995	-46.773	0.0000
82	H75	HC	E	53	51	48	1.089	107.664	30.297	0.0000
83	H76	HC	E	53	51	48	1.091	108.692	-83.613	0.0000
84	C33	CG	M	51	48	47	1.563	101.392	178.137	0.0000
85	H54	HC	E	84	51	48	1.092	108.596	-57.452	0.0000
86	H55	HC	E	84	51	48	1.092	109.198	59.885	0.0000
87	C34	CG	M	84	51	48	1.525	116.381	-178.104	0.0000
88	H56	HC	E	87	84	51	1.082	105.846	-69.737	0.0000
89	H57	HC	E	87	84	51	1.090	108.130	50.138	0.0000
90	C35	CG	M	87	84	51	1.532	118.399	172.921	0.0000
91	H58	HC	E	90	87	84	1.091	110.277	-67.192	0.0000
92	H59	HC	E	90	87	84	1.092	109.906	54.294	0.0000
93	C36	CG	M	90	87	84	1.540	106.147	173.164	0.0000
94	H60	HC	E	93	90	87	1.092	108.709	-56.704	0.0000

```
 95  H61   HC  E  93  90  87  1.091   108.804    60.728  0.0000
 96  C37   CG  M  93  90  87  1.533   114.707  -177.507  0.0000
 97  H62   HC  E  96  93  90  1.090   109.622   -62.878  0.0000
 98  H63   HC  E  96  93  90  1.091   109.580    57.411  0.0000
 99  C38   CG  M  96  93  90  1.538   108.653   177.066  0.0000
100  H64   HC  E  99  96  93  1.091   109.122   -59.928  0.0000
101  H65   HC  E  99  96  93  1.091   109.047    58.417  0.0000
102  C39   CG  M  99  96  93  1.533   112.331   179.214  0.0000
103  H66   HC  E 102  99  96  1.091   109.304   -59.629  0.0000
104  H67   HC  E 102  99  96  1.091   109.389    59.793  0.0000
105  C40   CG  M 102  99  96  1.535   110.151  -179.924  0.0000
106  H68   HC  E 105 102  99  1.091   109.159   -60.852  0.0000
107  H69   HC  E 105 102  99  1.091   109.185    58.015  0.0000
108  C41   CG  M 105 102  99  1.534   111.503   178.516  0.0000
109  H70   HC  E 108 105 102  1.090   109.440   -58.964  0.0000
110  H71   HC  E 108 105 102  1.091   109.465    60.318  0.0000
111  C42   CG  M 108 105 102  1.532   110.997  -179.287  0.0000
112  H72   HC  E 111 108 105  1.090   109.426   179.792  0.0000
113  H73   HC  E 111 108 105  1.091   109.918   -60.420  0.0000
114  H74   HC  E 111 108 105  1.090   109.895    60.046  0.0000

LOOP
 C21  C22
 C11  C12

IMPROPER

DONE
STOP
```

PREPIN file for βMal-$C_{12}C_8$(*R*)(25%wat) and βMal-$C_{12}C_8$(*S*)(25%wat)

```
   0    0    2

This is a remark line
molecule.res
BMR   INT  0
CORRECT     OMIT DU   BEG
  0.0000
  1  DUMM  DU   M    0  -1  -2  0.000      .0        .0      .0000
  2  DUMM  DU   M    1   0  -1  1.449      .0        .0      .0000
  3  DUMM  DU   M    2   1   0  1.523   111.21       .0      .0000
  4  O22   Oh   M    3   2   1  1.540   111.208  -180.000-0.71300
  5  H22   Ho   E    4   3   2  0.961    95.973   -11.956 0.43700
  6  C22   Cg   M    4   3   2  1.413    89.676  -120.595 0.24600
  7  H42   H1   E    6   4   3  1.091   108.461    35.351 0.00000
  8  C23   Cg   M    6   4   3  1.529   110.103   -83.842 0.28600
  9  H43   H1   E    8   6   4  1.091   110.181   -57.440 0.00000
 10  O23   Oh   S    8   6   4  1.412   109.503    62.929-0.69900
 11  H23   Ho   E   10   8   6  0.960   108.294   -58.185 0.42700
 12  C24   Cg   M    8   6   4  1.529   108.003  -177.793 0.25400
 13  H44   H1   E   12   8   6  1.091   109.048   -64.225 0.00000
 14  O24   Oh   S   12   8   6  1.412   109.142   176.721-0.71000
 15  H24   Ho   E   14  12   8  0.960   108.295    57.461 0.43600
 16  C25   Cg   M   12   8   6  1.536   109.555    56.176 0.28300
 17  H45   H1   E   16  12   8  1.089   108.555    63.576 0.00000
 18  C26   Cg   3   16  12   8  1.533   111.703  -177.909 0.27600
 19  H46   H1   E   18  16  12  1.090   110.084   -61.303 0.00000
 20  O26   Oh   S   18  16  12  1.413   110.789    59.474-0.68200
 21  H26   Ho   E   20  18  16  0.959   108.595   179.230 0.41800
 22  H47   H1   E   18  16  12  1.091   109.250   179.414 0.00000
 23  O25   Os   M   16  12   8  1.420   111.359   -56.864-0.57400
 24  C21   Cg   M   23  16  12  1.419   114.400    57.703 0.50900
 25  H41   H2   E   24  23  16  1.085   106.353  -171.824 0.00000
 26  O14   Os   M   24  23  16  1.425   111.849    66.259-0.46800
 27  C14   Cg   M   26  24  23  1.425   115.679    74.649 0.27600
 28  C13   Cg   3   27  26  24  1.537   110.892    86.766 0.28400
 29  C12   Cg   B   28  27  26  1.531   111.330   170.850 0.31000
 30  H32   H1   E   29  28  27  1.092   109.485    69.350 0.00000
 31  O12   Oh   S   29  28  27  1.412   105.415  -172.550-0.71800
 32  H12   Ho   E   31  29  28  0.960   108.324   -59.506 0.43700
 33  H33   H1   E   28  27  26  1.091   108.773    50.958 0.00000
 34  O13   Oh   S   28  27  26  1.412   112.481   -69.390-0.70900
 35  H13   Ho   E   34  28  27  0.960   108.595    76.215 0.43200
 36  H34   H1   E   27  26  24  1.091   111.378   -36.406 0.00000
 37  C15   Cg   M   27  26  24  1.539   108.184  -156.820 0.22500
 38  H35   H1   E   37  27  26  1.092   109.076   -58.919 0.00000
 39  C16   Cg   3   37  27  26  1.535   112.373    59.441 0.28200
 40  H36   H1   E   39  37  27  1.089   109.869   -66.039 0.00000
 41  O16   Oh   S   39  37  27  1.412   111.037    55.120-0.68800
 42  H16   Ho   E   41  39  37  0.961   108.473  -179.129 0.42400
```

43	H37	H1	E	39	37	27	1.091	109.331	175.293	0.00000
44	O15	Os	M	37	27	26	1.419	111.056	-178.872	-0.47100
45	C11	Cg	M	44	37	27	1.419	113.494	65.585	0.38400
46	H31	H2	E	45	44	37	1.092	108.453	59.921	0.00000
47	O11	Os	M	45	44	37	1.434	106.125	177.378	-0.19400
48	C51	Cg	M	47	45	44	1.427	116.146	-176.598	0.00000
49	H51	H1	E	48	47	45	1.089	108.343	-72.742	0.00000
50	H52	H1	E	48	47	45	1.093	110.293	47.165	0.00000
51	C52	Cg	M	48	47	45	1.549	113.195	169.351	0.00000
52	C63	Cg	3	51	48	47	1.562	110.634	-54.505	0.00000
53	C64	Cg	3	52	51	48	1.541	113.212	-178.258	0.00000
54	C65	Cg	3	53	52	51	1.542	117.397	-171.858	0.00000
55	C66	Cg	3	54	53	52	1.547	108.576	177.368	0.00000
56	C67	Cg	3	55	54	53	1.540	115.176	171.006	0.00000
57	C68	Cg	3	56	55	54	1.545	110.263	-179.422	0.00000
58	C69	Cg	3	57	56	55	1.541	113.173	175.578	0.00000
59	C70	Cg	3	58	57	56	1.537	111.742	-179.999	0.00000
60	H89	Hc	E	59	58	57	1.091	109.563	179.343	0.00000
61	H90	Hc	E	59	58	57	1.090	110.277	-60.856	0.00000
62	H91	Hc	E	59	58	57	1.092	110.192	59.682	0.00000
63	H87	Hc	E	58	57	56	1.092	109.346	-59.612	0.00000
64	H88	Hc	E	58	57	56	1.092	109.445	59.363	0.00000
65	H85	Hc	E	57	56	55	1.092	108.896	-63.113	0.00000
66	H86	Hc	E	57	56	55	1.093	109.053	54.983	0.00000
67	H83	Hc	E	56	55	54	1.092	109.088	-59.237	0.00000
68	H84	Hc	E	56	55	54	1.093	109.512	59.916	0.00000
69	H81	Hc	E	55	54	53	1.093	108.484	-67.055	0.00000
70	H82	Hc	E	55	54	53	1.093	108.731	50.223	0.00000
71	H79	Hc	E	54	53	52	1.092	109.296	-62.614	0.00000
72	H80	Hc	E	54	53	52	1.091	110.126	57.306	0.00000
73	H77	Hc	E	53	52	51	1.092	107.960	-49.959	0.00000
74	H78	Hc	E	53	52	51	1.090	107.872	68.252	0.00000
75	H75	Hc	E	52	51	48	1.092	109.663	-56.578	0.00000
76	H76	Hc	E	52	51	48	1.091	108.850	61.661	0.00000
77	H53	Hc	E	51	48	47	1.092	106.703	62.748	0.00000
78	C53	Cg	M	51	48	47	1.564	108.348	179.424	0.00000
79	H54	Hc	E	78	51	48	1.092	109.935	-24.876	0.00000
80	H55	Hc	E	78	51	48	1.092	108.639	91.500	0.00000
81	C54	Cg	M	78	51	48	1.549	115.979	-144.249	0.00000
82	H56	Hc	E	81	78	51	1.085	110.386	-55.201	0.00000
83	H57	Hc	E	81	78	51	1.091	109.223	62.592	0.00000
84	C55	Cg	M	81	78	51	1.547	112.585	-176.388	0.00000
85	H58	Hc	E	84	81	78	1.091	108.979	-81.739	0.00000
86	H59	Hc	E	84	81	78	1.092	109.765	36.922	0.00000
87	C56	Cg	M	84	81	78	1.543	111.653	156.703	0.00000
88	H60	Hc	E	87	84	81	1.093	108.333	-61.603	0.00000
89	H61	Hc	E	87	84	81	1.091	109.175	56.416	0.00000
90	C57	Cg	M	87	84	81	1.542	113.086	178.106	0.00000
91	H62	Hc	E	90	87	84	1.093	109.029	-65.722	0.00000
92	H63	Hc	E	90	87	84	1.092	109.447	53.077	0.00000
93	C58	Cg	M	90	87	84	1.542	111.006	173.491	0.00000

```
 94  H64   Hc  E  93  90  87  1.093   108.832   -60.815 0.00000
 95  H65   Hc  E  93  90  87  1.091   108.935    57.325 0.00000
 96  C59   Cg  M  93  90  87  1.542   112.842   178.451 0.00000
 97  H66   Hc  E  96  93  90  1.091   109.024   -59.452 0.00000
 98  H67   Hc  E  96  93  90  1.092   109.208    59.312 0.00000
 99  C60   Cg  M  96  93  90  1.543   111.338   179.990 0.00000
100  H68   Hc  E  99  96  93  1.092   109.007   -60.350 0.00000
101  H69   Hc  E  99  96  93  1.092   109.004    58.009 0.00000
102  C61   Cg  M  99  96  93  1.541   112.386   178.804 0.00000
103  H70   Hc  E 102  99  96  1.092   109.407   -58.450 0.00000
104  H71   Hc  E 102  99  96  1.092   109.441    60.398 0.00000
105  C62   Cg  M 102  99  96  1.537   111.990  -178.924 0.00000
106  H72   Hc  E 105 102  99  1.091   109.538   179.818 0.00000
107  H73   Hc  E 105 102  99  1.091   110.191   -60.445 0.00000
108  H74   Hc  E 105 102  99  1.091   110.182    60.139 0.00000

LOOP
 C21  C22
 C11  C12

IMPROPER

DONE
STOP
```

APPENDIX C

EXAMPLE OF TOPOLOGY FILE FOR SINGLE MOLECULE βMAL-C_{12}

```
%VERSION  VERSION_STAMP = V0001.000  DATE = 08/25/15  09:54:54
%FLAG TITLE
%FORMAT(20a4)
default_name
%FLAG POINTERS
%FORMAT(10I8)
     81       7      46      36     108      47     177      83       0       0
    467       1      36      47      83       7      14      21       7       0
      0       0       0       0       0       0       0       0      81       0
      0
%FLAG ATOM_NAME
%FORMAT(20a4)
O22 H22 C22 H42 C23 H43 O23 H23 C24 H44 O24 H24 C25 H45 C26 H46 O26 H26 H47 O25
C21 H41 O14 C14 C13 C12 H32 O12 H12 H33 O13 H13 H34 C15 H35 C16 H36 O16 H16 H37
O15 C11 H31 O11 C71 H71 H72 C72 H73 H74 C73 H75 H76 C74 H77 H78 C75 H79 H80 C76
H81 H82 C77 H83 H84 C78 H85 H86 C79 H87 H88 C80 H89 H90 C81 H91 H92 C82 H93 H94
H95
%FLAG CHARGE
%FORMAT(5E16.8)
-1.29924999E+01 7.96314510E+00 4.48268580E+00 0.00000000E+00 5.21157780E+00
 0.00000000E+00-1.27373877E+01 7.78092210E+00 4.62846420E+00 0.00000000E+00
-1.29378330E+01 7.94492280E+00 5.15691090E+00 0.00000000E+00 5.02935480E+00
 0.00000000E+00-1.24276086E+01 7.61692140E+00 0.00000000E+00-1.04596002E+01
 9.27515070E+00 0.00000000E+00-8.52803640E+00 5.02935480E+00 5.17513320E+00
 5.64891300E+00 0.00000000E+00-1.30836114E+01 7.96314510E+00 0.00000000E+00
-1.29196107E+01 7.87203360E+00 0.00000000E+00 4.10001750E+00 0.00000000E+00
 5.13868860E+00 0.00000000E+00-1.25369424E+01 7.72625520E+00 0.00000000E+00
-8.58270330E+00 6.99736320E+00 0.00000000E+00-3.53512620E+00 0.00000000E+00
 0.00000000E+00 0.00000000E+00 0.00000000E+00 0.00000000E+00 0.00000000E+00
 0.00000000E+00 0.00000000E+00 0.00000000E+00 0.00000000E+00 0.00000000E+00
 0.00000000E+00 0.00000000E+00 0.00000000E+00 0.00000000E+00 0.00000000E+00
 0.00000000E+00 0.00000000E+00 0.00000000E+00 0.00000000E+00 0.00000000E+00
 0.00000000E+00 0.00000000E+00 0.00000000E+00 0.00000000E+00 0.00000000E+00
 0.00000000E+00 0.00000000E+00 0.00000000E+00 0.00000000E+00 0.00000000E+00
 0.00000000E+00
%FLAG ATOMIC_NUMBER
%FORMAT(10I8)
     8     1     6     1     6     1     8     1     6     1
     8     1     6     1     6     1     8     1     1     8
     6     1     8     6     6     6     1     8     1     1
     8     1     1     6     1     6     1     8     1     1
     8     6     1     8     6     1     1     6     1     1
     6     1     1     6     1     1     6     1     1     6
     1     1     6     1     1     6     1     1     6     1
```

```
     1      6      1      1      6      1      1      6      1      1
     1
%FLAG MASS
%FORMAT(5E16.8)
 1.60000000E+01 1.00800000E+00 1.20100000E+01 1.00800000E+00 1.20100000E+01
 1.00800000E+00 1.60000000E+01 1.00800000E+00 1.20100000E+01 1.00800000E+00
 1.60000000E+01 1.00800000E+00 1.20100000E+01 1.00800000E+00 1.20100000E+01
 1.00800000E+00 1.60000000E+01 1.00800000E+00 1.00800000E+00 1.60000000E+01
 1.20100000E+01 1.00800000E+00 1.60000000E+01 1.20100000E+01 1.20100000E+01
 1.20100000E+01 1.00800000E+00 1.60000000E+01 1.00800000E+00 1.00800000E+00
 1.60000000E+01 1.00800000E+00 1.00800000E+00 1.20100000E+01 1.00800000E+00
 1.20100000E+01 1.00800000E+00 1.60000000E+01 1.00800000E+00 1.00800000E+00
 1.60000000E+01 1.20100000E+01 1.00800000E+00 1.60000000E+01 1.20100000E+01
 1.00800000E+00 1.00800000E+00 1.20100000E+01 1.00800000E+00 1.00800000E+00
 1.20100000E+01 1.00800000E+00 1.00800000E+00 1.20100000E+01 1.00800000E+00
 1.00800000E+00 1.20100000E+01 1.00800000E+00 1.00800000E+00 1.20100000E+01
 1.00800000E+00 1.00800000E+00 1.20100000E+01 1.00800000E+00 1.00800000E+00
 1.20100000E+01 1.00800000E+00 1.00800000E+00 1.20100000E+01 1.00800000E+00
 1.00800000E+00 1.20100000E+01 1.00800000E+00 1.00800000E+00 1.20100000E+01
 1.00800000E+00 1.00800000E+00 1.20100000E+01 1.00800000E+00 1.00800000E+00
  1.00800000E+00
%FLAG ATOM_TYPE_INDEX
%FORMAT(10I8)
     1      2      3      4      3      4      1      2      3      4
     1      2      3      4      3      4      1      2      4      5
     3      6      5      3      3      3      4      1      2      4
     1      2      4      3      4      3      4      1      2      4
     5      3      6      5      3      4      4      3      7      7
     3      7      7      3      7      7      3      7      7      3
     7      7      3      7      7      3      7      7      3      7
     7      3      7      7      3      7      7      3      7      7
     7
%FLAG NUMBER_EXCLUDED_ATOMS
%FORMAT(10I8)
    11      4     14      8     14      7      6      1     11      6
     5      1     10      6      6      4      3      1      1      4
     6      2     10     16     15     13      8      7      1      5
     4      1      4     10      6      6      4      3      1      1
     4      6      2      7      9      5      4      9      5      4
     9      5      4      9      5      4      9      5      4      9
     5      4      9      5      4      9      5      4      9      5
     4      9      5      4      6      5      4      3      2      1
     1
%FLAG NONBONDED_PARM_INDEX
%FORMAT(10I8)
     1      2      4      7     11     16     22      2      3      5
     8     12     17     23      4      5      6      9     13     18
    24      7      8      9     10     14     19     25     11     12
    13     14     15     20     26     16     17     18     19     20
    21     27     22     23     24     25     26     27     28
%FLAG RESIDUE_LABEL
%FORMAT(20a4)
DDM
%FLAG RESIDUE_POINTER
```

```
%FORMAT(10I8)
     1
%FLAG BOND_FORCE_CONSTANT
%FORMAT(5E16.8)
 3.40000000E+02 3.10000000E+02 3.40000000E+02 2.85000000E+02 3.40000000E+02
  5.53000000E+02  3.20000000E+02
%FLAG BOND_EQUIL_VALUE
%FORMAT(5E16.8)
 1.09000000E+00 1.52000000E+00 1.09000000E+00 1.46000000E+00 1.09000000E+00
  9.60000000E-01  1.43000000E+00
%FLAG ANGLE_FORCE_CONSTANT
%FORMAT(5E16.8)
 4.00000000E+01 4.50000000E+01 4.50000000E+01 4.50000000E+01 4.50000000E+01
 6.00000000E+01 7.00000000E+01 6.00000000E+01 5.00000000E+01 1.00000000E+02
  6.00000000E+01  5.50000000E+01  7.00000000E+01  4.50000000E+01
  %FLAG ANGLE_EQUIL_VALUE
%FORMAT(5E16.8)
 1.91113635E+00 1.96524158E+00 1.98094955E+00 1.93731630E+00 1.91113635E+00
 1.91986300E+00 1.89368305E+00 1.91986300E+00 1.94778828E+00 1.95476960E+00
  1.91986300E+00  1.91113635E+00  1.87622975E+00  1.93731630E+00
%FLAG DIHEDRAL_FORCE_CONSTANT
%FORMAT(5E16.8)
  1.30000000E-01  1.00000000E-01  4.50000000E-01  1.70000000E-01  1.50000000E-01
  5.00000000E-02 -2.70000000E-01  6.00000000E-01  2.70000000E-01  1.60000000E-01
 3.00000000E-01  1.27000000E+00 3.70000000E-01 1.80000000E-01 -1.10000000E+00
  2.50000000E-01  1.00000000E-01 -1.00000000E-01  9.50000000E-01
  5.50000000E-01
  8.20000000E-01
%FLAG DIHEDRAL_PERIODICITY
%FORMAT(5E16.8)
 3.00000000E+00 3.00000000E+00 1.00000000E+00 3.00000000E+00 3.00000000E+00
 3.00000000E+00 1.00000000E+00 2.00000000E+00 3.00000000E+00 3.00000000E+00
 1.00000000E+00 2.00000000E+00 3.00000000E+00 3.00000000E+00 1.00000000E+00
 2.00000000E+00 3.00000000E+00 1.00000000E+00 2.00000000E+00 3.00000000E+00
  2.00000000E+00
%FLAG DIHEDRAL_PHASE
%FORMAT(5E16.8)
 0.00000000E+00 0.00000000E+00 0.00000000E+00 0.00000000E+00 0.00000000E+00
 0.00000000E+00 0.00000000E+00 0.00000000E+00 0.00000000E+00 0.00000000E+00
 0.00000000E+00 0.00000000E+00 0.00000000E+00 0.00000000E+00 0.00000000E+00
 0.00000000E+00 0.00000000E+00 0.00000000E+00 0.00000000E+00 0.00000000E+00
  0.00000000E+00
%FLAG SCEE_SCALE_FACTOR
%FORMAT(5E16.8)
 1.20000000E+00 1.20000000E+00 1.20000000E+00 1.20000000E+00 2.00000000E+00
 1.20000000E+00 1.00000000E+00 1.20000000E+00 1.20000000E+00 1.20000000E+00
 2.00000000E+00 2.00000000E+00 2.00000000E+00 1.20000000E+00 1.20000000E+00
 1.20000000E+00 2.00000000E+00 2.00000000E+00 2.00000000E+00 2.00000000E+00
  1.20000000E+00
%FLAG SCNB_SCALE_FACTOR
%FORMAT(5E16.8)
 2.00000000E+00 2.00000000E+00 2.00000000E+00 2.00000000E+00 2.00000000E+00
 2.00000000E+00 2.00000000E+00 2.00000000E+00 2.00000000E+00 2.00000000E+00
 2.00000000E+00 2.00000000E+00 2.00000000E+00 2.00000000E+00 2.00000000E+00
```

```
 2.00000000E+00 2.00000000E+00 2.00000000E+00 2.00000000E+00 2.00000000E+00
  2.00000000E+00
%FLAG SOLTY
%FORMAT(5E16.8)
 0.00000000E+00 0.00000000E+00 0.00000000E+00 0.00000000E+00 0.00000000E+00
  0.00000000E+00  0.00000000E+00
%FLAG LENNARD_JONES_ACOEF
%FORMAT(5E16.8)
 5.81803229E+05 0.00000000E+00 0.00000000E+00 7.91544157E+05 0.00000000E+00
 1.04308023E+06 4.66922514E+04 0.00000000E+00 6.78771368E+04 3.25969625E+03
 4.58874091E+05 0.00000000E+00 6.28541240E+05 3.63097246E+04 3.61397723E+05
 3.15360051E+04 0.00000000E+00 4.68930885E+04 2.09814978E+03 2.44050579E+04
 1.32801250E+03 6.82786631E+04 0.00000000E+00 9.71708117E+04 4.98586848E+03
  5.33379252E+04  3.25969625E+03  7.51607703E+03
%FLAG LENNARD_JONES_BCOEF
%FORMAT(5E16.8)
 6.99746810E+02 0.00000000E+00 0.00000000E+00 6.93079947E+02 0.00000000E+00
 6.75612247E+02 1.03606917E+02 0.00000000E+00 1.06076943E+02 1.43076527E+01
 5.89183300E+02 0.00000000E+00 5.85549272E+02 8.66220817E+01 4.95732238E+02
 8.51470647E+01 0.00000000E+00 8.81685417E+01 1.14788417E+01 7.10161395E+01
 9.13231543E+00 1.25287818E+02 0.00000000E+00 1.26919150E+02 1.76949863E+01
  1.04986921E+02  1.43076527E+01  2.17257828E+01
%FLAG BONDS_INC_HYDROGEN
%FORMAT(10I8)
    231     234       1     231     237       1     231     240     1     222
    225       1     222     228       1     213     216       1     213   219
      1     204     207       1     204     210       1     195     198     1
    195     201       1     186     189       1     186     192     1     177
    180       1     177     183       1     168     171       1     168   174
      1     159     162       1     159     165       1     150     153     1
    150     156       1     141     144       1     141     147     1     132
    135       3     132     138       3     123     126       5     111   114
      6     105     108       3     105     117       3      99     102     3
     90      93       6      81      84       6      75      78     3      72
     87       3      69      96       3      60      63       5     48     51
      6      42      45       3      42      54       3      36     39      3
     30      33       6      24      27       3      18      21      6     12
     15       3       6       9       3       0       3       6
%FLAG BONDS_WITHOUT_HYDROGEN
%FORMAT(10I8)
    222     231       2     213     222       2     204     213     2     195
    204       2     186     195       2     177     186       2   168     177
      2     159     168       2     150     159       2     141   150       2
    132     141       2     129     132       4     123     129     4     120
    123       4     105     111       7      99     105       2    99     120
      4      75      81       7      75     123       2      72    75       2
     72      90       7      69      72       2      69      99     2      66
     69       4      60      66       4      57      60       4    42      48
      7      36      42       2      36      57       4      24    30       7
     24      36       2      12      18       7      12      24     2       6
     12       2       6      60       2       0       6       7
%FLAG ANGLES_INC_HYDROGEN
%FORMAT(10I8)
    237     231     240       1     234     231     237       1   234     231
```

```
 240     1   228   222   231     2   225   222   228     1
 225   222   231     2   222   231   234     2   222   231
 237     2   222   231   240     2   219   213   222     2
 216   213   219     1   216   213   222     2   213   222
 225     2   213   222   228     2   210   204   213     2
 207   204   210     1   207   204   213     2   204   213
 216     2   204   213   219     2   201   195   204     2
 198   195   201     1   198   195   204     2   195   204
 207     2   195   204   210     2   192   186   195     2
 189   186   192     1   189   186   195     2   186   195
 198     2   186   195   201     2   183   177   186     2
 180   177   183     1   180   177   186     2   177   186
 189     2   177   186   192     2   174   168   177     2
 171   168   174     1   171   168   177     2   168   177
 180     2   168   177   183     2   165   159   168     2
 162   159   165     1   162   159   168     2   159   168
 171     2   159   168   174     2   156   150   159     2
 153   150   156     1   153   150   159     2   150   159
 162     2   150   159   165     2   147   141   150     2
 144   141   147     1   144   141   150     2   141   150
 153     2   141   150   156     2   138   132   141     4
 135   132   138     5   135   132   141     4   132   141
 144     2   132   141   147     2   129   132   135     6
 129   132   138     6   126   123   129     8   120   123
 126     8   111   105   117    11   108   105   111    11
 108   105   117     5   105   111   114    12   102    99
 105     4   102    99   120     6    99   105   108     4
  99   105   117     4    96    69    99     4    87    72
  90    11    78    75    81    11    78    75   123     4
  75    72    87     4    75    81    84    12    75   123
 126    14    72    69    96     4    72    75    78     4
  72    90    93    12    69    72    87     4    69    99
 102     4    66    69    96     6    63    60    66     8
  57    60    63     8    48    42    54    11    45    42
  48    11    45    42    54     5    42    48    51    12
  39    36    42     4    39    36    57     6    36    42
  45     4    36    42    54     4    27    24    30    11
  27    24    36     4    24    30    33    12    24    36
  39     4    15    12    18    11    15    12    24     4
  12    18    21    12    12    24    27     4     9     6
  12     4     9     6    60     4     6    12    15     4
   6    60    63    14     3     0     6    12     0     6
   9    11
%FLAG ANGLES_WITHOUT_HYDROGEN
%FORMAT(10I8)
 213   222   231     3   204   213   222     3   195   204
 213     3   186   195   204     3   177   186   195     3
 168   177   186     3   159   168   177     3   150   159
 168     3   141   150   159     3   132   141   150     3
 129   132   141     7   123   129   132     9   120   123
 129    10   105    99   120     7    99   105   111    13
  99   120   123     9    81    75   123    13    75    72
  90    13    75   123   120     7    75   123   129     7
  72    69    99     3    72    75    81    13    72    75
```

123 3 69 72 75 3 69 72 90 13
69 99 105 3 69 99 120 7 66 69
72 7 66 69 99 7 60 66 69 9
57 60 66 10 42 36 57 7 36 42
48 13 36 57 60 9 30 24 36 13
24 36 42 3 24 36 57 7 18 12
24 13 12 6 60 3 12 24 30 13
12 24 36 3 6 12 18 13 6 12
24 3 6 60 57 7 6 60 66 7
0 6 12 13 0 6 60 13

%FLAG DIHEDRALS_INC_HYDROGEN
%FORMAT(10I8)

228 222 231 234 1 228 222 231 237 1
228 222 231 240 1 225 222 231 234 1
225 222 231 237 1 225 222 231 240 1
219 213 222 225 1 219 213 222 228 1
219 213 222 231 2 216 213 222 225 1
216 213 222 228 1 216 213 222 231 2
213 222 231 234 2 213 222 231 237 2
213 222 231 240 2 210 204 213 216 1
210 204 213 219 1 210 204 213 222 2
207 204 213 216 1 207 204 213 219 1
207 204 213 222 2 204 213 222 225 2
204 213 222 228 2 201 195 204 207 1
201 195 204 210 1 201 195 204 213 2
198 195 204 207 1 198 195 204 210 1
198 195 204 213 2 195 204 213 216 2
195 204 213 219 2 192 186 195 198 1
192 186 195 201 1 192 186 195 204 2
189 186 195 198 1 189 186 195 201 1
189 186 195 204 2 186 195 204 207 2
186 195 204 210 2 183 177 186 189 1
183 177 186 192 1 183 177 186 195 2
180 177 186 189 1 180 177 186 192 1
180 177 186 195 2 177 186 195 198 2
177 186 195 201 2 174 168 177 180 1
174 168 177 183 1 174 168 177 186 2
171 168 177 180 1 171 168 177 183 1
171 168 177 186 2 168 177 186 189 2
168 177 186 192 2 165 159 168 171 1
165 159 168 174 1 165 159 168 177 2
162 159 168 171 1 162 159 168 174 1
162 159 168 177 2 159 168 177 180 2
159 168 177 183 2 156 150 159 162 1
156 150 159 165 1 156 150 159 168 2
153 150 159 162 1 153 150 159 165 1
153 150 159 168 2 150 159 168 171 2
150 159 168 174 2 147 141 150 153 1
147 141 150 156 1 147 141 150 159 2
144 141 150 153 1 144 141 150 156 1
144 141 150 159 2 141 150 159 162 2
141 150 159 165 2 138 132 141 144 4
138 132 141 147 4 138 132 141 150 5
135 132 141 144 4 135 132 141 147 4

135 132 141 150 5 132 141 150 153 2
132 141 150 156 2 129 132 141 144 6
129 132 141 147 6 126 123 129 132 8
126 123 -129 132 2 123 129 132 135 9
123 129 132 138 9 117 105 99 120 6
114 111 105 117 14 108 105 99 120 6
108 105 111 114 14 102 99 105 108 4
102 99 105 111 6 102 99 105 117 4
102 99 120 123 9 99 105 111 114 14
99 120 123 126 8 99 120 -123 126 2
96 69 99 102 4 96 69 99 105 5
96 69 99 120 6 90 72 69 96 6
87 72 69 96 4 87 72 69 99 5
87 72 75 123 5 87 72 90 93 14
84 81 75 123 14 81 75 72 87 6
81 75 123 126 6 78 75 72 87 4
78 75 72 90 6 78 75 81 84 14
78 75 123 120 6 78 75 123 126 4
78 75 123 129 6 75 72 69 96 5
75 72 90 93 14 72 69 99 102 5
72 75 81 84 14 72 75 123 126 5
69 72 75 78 5 69 72 90 93 14
69 99 105 108 5 69 99 105 117 5
66 69 72 87 6 66 69 99 102 6
63 60 66 69 8 63 60 -66 69 2
60 66 69 96 9 54 42 36 57 6
51 48 42 54 14 45 42 36 57 6
45 42 48 51 14 39 36 42 45 4
39 36 42 48 6 39 36 42 54 4
39 36 57 60 9 36 42 48 51 14
36 57 60 63 8 36 57 -60 63 2
33 30 24 36 14 30 24 36 39 6
27 24 30 33 14 27 24 36 39 4
27 24 36 42 5 27 24 36 57 6
24 36 42 45 5 24 36 42 54 5
21 18 12 24 14 18 12 24 27 6
15 12 6 60 5 15 12 18 21 14
15 12 24 27 4 15 12 24 30 6
15 12 24 36 5 12 6 60 63 5
12 24 30 33 14 12 24 36 39 5
9 6 12 15 4 9 6 12 18 6
9 6 12 24 5 9 6 60 57 6
9 6 60 63 4 9 6 60 66 6
6 12 18 21 14 6 12 24 27 5
3 0 6 9 14 3 0 6 12 14
3 0 6 60 14 0 6 12 15 6
0 6 60 63 6
%FLAG DIHEDRALS_WITHOUT_HYDROGEN
%FORMAT(10I8)
204 213 222 231 3 195 204 213 222 3
186 195 204 213 3 177 186 195 204 3
168 177 186 195 3 159 168 177 186 3
150 159 168 177 3 141 150 159 168 3
132 141 150 159 3 129 132 141 150 7

```
 123   129   132   141    10   120   123   129   132    11
 120   123  -129   132    12   120   123  -129   132    13
 111   105    99   120    15   111   105   -99   120    16
 105    99   120   123    10    99   120   123   129    11
  99   120  -123   129    12    99   120  -123   129    13
  90    72    69    99    17    90    72    75   123    17
  81    75    72    90    18    81    75   -72    90    19
  81    75   -72    90    20    81    75   123   120    15
  81    75  -123   120    16    81    75   123   129    15
  81    75  -123   129    16    75    72    69    99     3
  75   123  -120    99    10    75   123   129   132    10
  72    69    99   105     3    72    69    99   120     7
  72    75  -123   120     7    72    75   123   129     7
  69    72    75    81    17    69    72    75   123     3
  69    99   105   111    17    69    99  -120   123    10
  66    69    72    75     7    66    69    72    90    15
  66    69   -72    90    16    66    69    99   105     7
  66    69    99   120    21    60    66    69    72    10
  60    66    69    99    10    57    60    66    69    11
  57    60   -66    69    12    57    60   -66    69    13
  48    42    36    57    15    48    42   -36    57    16
  42    36    57    60    10    36    57    60    66    11
  36    57   -60    66    12    36    57   -60    66    13
  30    24    36    42    17    30    24    36    57    15
  30    24   -36    57    16    24    12     6    60     3
  24    36    42    48    17    24    36   -57    60    10
  18    12     6    60    17    18    12    24    30    18
  18    12   -24    30    19    18    12   -24    30    20
  18    12    24    36    17    12     6    60    57     7
  12     6    60    66     7    12    24    36    42     3
  12    24   -36    57     7     6    12    24    30    17
   6    12    24    36     3     6    60   -57    36    10
   6    60    66    69    10     0     6    12    18    18
   0     6   -12    18    19     0     6   -12    18    20
   0     6    12    24    17     0     6    60    57    15
   0     6   -60    57    16     0     6    60    66    15
   0     6   -60    66    16
%FLAG EXCLUDED_ATOMS_LIST
%FORMAT(10I8)
   2     3     4     5     6     7     9    20    21    22
  23     3     4     5    21     4     5     6     7     8
   9    10    11    13    20    21    22    23    24     5
   6     7     9    20    21    22    23     6     7     8
   9    10    11    12    13    14    15    20    21    22
  23     7     8     9    10    11    13    21     8     9
  10    11    13    21     9    10    11    12    13    14
  15    16    17    19    20    21    11    12    13    14
  15    20    12    13    14    15    20    13    14    15
  16    17    18    19    20    21    22    23    15    16
  17    19    20    21    16    17    18    19    20    21
  17    18    19    20    18    19    20    19    20    21
  22    23    24    22    23    24    25    33    34    23
  24    24    25    26    30    31    33    34    35    36
  41    25    26    27    28    30    31    32    33    34
```

```
   35    36    37    38    40    41    42    26    27    28
   29    30    31    32    33    34    35    36    41    42
   43    44    27    28    29    30    31    32    33    34
   41    42    43    44    45    28    29    30    31    41
   42    43    44    29    30    31    41    42    43    44
   42    31    32    33    34    42    32    33    34    42
    0    34    35    36    41    35    36    37    38    39
   40    41    42    43    44    36    37    38    40    41
   42    37    38    39    40    41    42    38    39    40
   41    39    40    41    40    41    42    43    44    45
   43    44    45    46    47    48    44    45    45    46
   47    48    49    50    51    46    47    48    49    50
   51    52    53    54    47    48    49    50    51    48
   49    50    51    49    50    51    52    53    54    55
   56    57    50    51    52    53    54    51    52    53
   54    52    53    54    55    56    57    58    59    60
   53    54    55    56    57    54    55    56    57    55
   56    57    58    59    60    61    62    63    56    57
   58    59    60    57    58    59    60    58    59    60
   61    62    63    64    65    66    59    60    61    62
   63    60    61    62    63    61    62    63    64    65
   66    67    68    69    62    63    64    65    66    63
   64    65    66    64    65    66    67    68    69    70
   71    72    65    66    67    68    69    66    67    68
   69    67    68    69    70    71    72    73    74    75
   68    69    70    71    72    69    70    71    72    70
   71    72    73    74    75    76    77    78    71    72
   73    74    75    72    73    74    75    73    74    75
   76    77    78    79    80    81    74    75    76    77
   78    75    76    77    78    76    77    78    79    80
   81    77    78    79    80    81    78    79    80    81
   79    80    81    80    81    81     0
%FLAG HBOND_ACOEF
%FORMAT(5E16.8)

%FLAG HBOND_BCOEF
%FORMAT(5E16.8)

%FLAG HBCUT
%FORMAT(5E16.8)

%FLAG AMBER_ATOM_TYPE
%FORMAT(20a4)
OH HO CG H1 CG H1 OH HO CG H1 OH HO CG H1 CG H1 OH HO H1 OS
CG H2 OS CG CG CG H1 OH HO H1 OH HO H1 CG H1 CG H1 OH HO H1
OS CG H2 OS CG H1 H1 CG HC HC CG HC HC CG HC HC CG HC HC CG
HC HC CG HC HC CG HC HC CG HC HC CG HC HC CG HC HC CG HC HC
HC
%FLAG TREE_CHAIN_CLASSIFICATION
%FORMAT(20a4)
M  E  M  E  3  E  S  E  3  E  S  E  3  E  3  E  S  E  E  E
M  E  M  M  M  M  E  S  E  E  S  E  E  3  E  3  E  S  E  E
E  M  E  M  M  E  E  M  E  E  M  E  E  M  E  E  M  E  E  M
E  E  M  E  E  M  E  E  M  E  E  M  E  E  M  E  E  M  E  E
```

```
E
%FLAG JOIN_ARRAY
%FORMAT(10I8)
     0     0     0     0     0     0     0     0     0     0
     0     0     0     0     0     0     0     0     0     0
     0     0     0     0     0     0     0     0     0     0
     0     0     0     0     0     0     0     0     0     0
     0     0     0     0     0     0     0     0     0     0
     0     0     0     0     0     0     0     0     0     0
     0     0     0     0     0     0     0     0     0     0
     0     0     0     0     0     0     0     0     0     0
     0
%FLAG IROTAT
%FORMAT(10I8)
     0     0     0     0     0     0     0     0     0     0
     0     0     0     0     0     0     0     0     0     0
     0     0     0     0     0     0     0     0     0     0
     0     0     0     0     0     0     0     0     0     0
     0     0     0     0     0     0     0     0     0     0
     0     0     0     0     0     0     0     0     0     0
     0     0     0     0     0     0     0     0     0     0
     0     0     0     0     0     0     0     0     0     0
     0
%FLAG RADIUS_SET
%FORMAT(1a80)
modified Bondi radii (mbondi)
%FLAG RADII
%FORMAT(5E16.8)
 1.50000000E+00 8.00000000E-01 1.70000000E+00 1.30000000E+00 1.70000000E+00
 1.30000000E+00 1.50000000E+00 8.00000000E-01 1.70000000E+00 1.30000000E+00
 1.50000000E+00 8.00000000E-01 1.70000000E+00 1.30000000E+00 1.70000000E+00
 1.30000000E+00 1.50000000E+00 8.00000000E-01 1.30000000E+00 1.50000000E+00
 1.70000000E+00 1.30000000E+00 1.50000000E+00 1.70000000E+00 1.70000000E+00
 1.70000000E+00 1.30000000E+00 1.50000000E+00 8.00000000E-01 1.30000000E+00
 1.50000000E+00 8.00000000E-01 1.30000000E+00 1.70000000E+00 1.30000000E+00
 1.70000000E+00 1.30000000E+00 1.50000000E+00 8.00000000E-01 1.30000000E+00
 1.50000000E+00 1.70000000E+00 1.30000000E+00 1.50000000E+00 1.70000000E+00
 1.30000000E+00 1.30000000E+00 1.70000000E+00 1.30000000E+00 1.30000000E+00
 1.70000000E+00 1.30000000E+00 1.30000000E+00 1.70000000E+00 1.30000000E+00
 1.30000000E+00 1.70000000E+00 1.30000000E+00 1.30000000E+00 1.70000000E+00
 1.30000000E+00 1.30000000E+00 1.70000000E+00 1.30000000E+00 1.30000000E+00
 1.70000000E+00 1.30000000E+00 1.30000000E+00 1.70000000E+00 1.30000000E+00
 1.30000000E+00 1.70000000E+00 1.30000000E+00 1.30000000E+00 1.70000000E+00
 1.30000000E+00 1.30000000E+00 1.70000000E+00 1.30000000E+00 1.30000000E+00
  1.30000000E+00
%FLAG SCREEN
%FORMAT(5E16.8)
  8.50000000E-01  8.50000000E-01  7.20000000E-01  8.50000000E-01  7.20000000E-01
  8.50000000E-01  8.50000000E-01  8.50000000E-01  7.20000000E-01  8.50000000E-01
  8.50000000E-01  8.50000000E-01  7.20000000E-01  8.50000000E-01  7.20000000E-01
  8.50000000E-01  8.50000000E-01  8.50000000E-01  8.50000000E-01  8.50000000E-01
  7.20000000E-01  8.50000000E-01  8.50000000E-01  7.20000000E-01  7.20000000E-01
  7.20000000E-01  8.50000000E-01  8.50000000E-01  8.50000000E-01  8.50000000E-01
  8.50000000E-01  8.50000000E-01  8.50000000E-01  7.20000000E-01  8.50000000E-01
```

```
 7.20000000E-01  8.50000000E-01  8.50000000E-01  8.50000000E-01  8.50000000E-01
 8.50000000E-01  7.20000000E-01  8.50000000E-01  8.50000000E-01  7.20000000E-01
 8.50000000E-01  8.50000000E-01  7.20000000E-01  8.50000000E-01  8.50000000E-01
 7.20000000E-01  8.50000000E-01  8.50000000E-01  7.20000000E-01  8.50000000E-01
 8.50000000E-01  7.20000000E-01  8.50000000E-01  8.50000000E-01  7.20000000E-01
 8.50000000E-01  8.50000000E-01  7.20000000E-01  8.50000000E-01  8.50000000E-01
 7.20000000E-01  8.50000000E-01  8.50000000E-01  7.20000000E-01  8.50000000E-01
 8.50000000E-01  7.20000000E-01  8.50000000E-01  8.50000000E-01  7.20000000E-01
 8.50000000E-01  8.50000000E-01  7.20000000E-01  8.50000000E-01  8.50000000E-01
 8.50000000E-01
%FLAG IPOL
%FORMAT(1I8)
     0
%
```

REFERENCES

Abe, Y., Fujiwara, M., Ohbu, K., & Harata, K. (2000). Crystal structures of glycolipids with odd and even numbered alkyl chains. *Journal of the Chemical Society, Perkin Transactions 2*(2), 341–351.

Abe, Y., Harata, K., Fujiwara, M., & Ohbu, K. (1998). Bilayer structure of glycolipid crystals. Thermal stability of the crystal and state of the alkyl chain. *Journal of the Chemical Society, Perkin Transactions 2*(1), 177–186.

Abel, S., Dupradeau, F. Y., Raman, E. P., MacKerell, J., A. D., & Marchi, M. (2011). Molecular simulations of dodecyl-β-maltoside micelles in water: influence of the headgroup conformation and force field parameters. *The Journal of Physical Chemistry B*, *115*(3), 487–99.

Abeygunaratne, S., Hashim, R., & Vill, V. (2006). Evidence for uncorrelated tilted layer structure and electrically polarized bilayers in amphiphilic glycolipids. *Physical Review E*, *73*(1), 011916.

Abeyrathne, A., Perera, A. C., & Karunaratne, D. N. (2013). Surfactant behaviour of five carbohydrate liquid crystals. *Journal of the National Science Foundation of Sri Lanka*, *41*(3), 185–194.

Abou-Zied, O. K., Al-Lawatia, N., Elstner, M., & Steinbrecher, T. B. (2013). Binding of hydroxyquinoline probes to human serum albumin: combining molecular modeling and förster's resonance energy transfer spectroscopy to understand flexible ligand binding. *The Journal of Physical Chemistry B*, *117*(4), 1062–1074.

Abrahamsson, S., Dahlen, B., & Pascher, I. (1977). Molecular arrangements in glycosphingolipids: the crystal structure of glucosylphytosphingosine hydrochloride. *Acta Crystallographica Section B: Structural Science*, *33*(7), 2008–2013.

Abriata, L. A., & Dal Peraro, M. (2015). Assessing the potential of atomistic molecular dynamics simulations to probe reversible protein-protein recognition and binding. *Scientific Reports*, *5*, 1–12.

Ahmad, M. U., Ali, S. M., Ahmad, A., Sheikh, S., Chen, P., & Ahmad, I. (2015). Carbohydrate mediated drug delivery: Synthesis and characterization of new lipid-conjugates. *Chemistry and physics of lipids*, *186*, 30–38.

Ahmad, N., Ramsch, R., Esquena, J., Solans, C., Tajuddin, H. A., & Hashim, R. (2012). Physicochemical characterization of natural-like branched-chain glycosides toward formation of hexosomes and vesicles. *Langmuir*, *28*(5), 2395–2403.

Ahmadi, S., Manickam Achari, V., Nguan, H., & Hashim, R. (2014). Atomistic simulation studies of the α/β-glucoside and galactoside in anhydrous bilayers: effect of the anomeric and epimeric configurations. *Journal of Molecular Modeling*, *20*(3), 1–12.

Akiyoshi, K. (2002). Hydrophobic effects. In N. Yui (Ed.), *Supramolecular design for biological applications* (pp. 13–24). Boca Raton: CRC Press.

Alder, B. J., & Wainwright, T. E. (1957). Phase transition for a hard sphere system. *The Journal of Chemical Physics*, *27*(5), 1208–1209.

Alder, B. J., & Wainwright, T. E. (1959). Studies in molecular dynamics. i. general method. *The Journal of Chemical Physics*, *31*(2), 459–466.

Allen, M. P. (2004). Introduction to molecular dynamics simulation. *Computational Soft Matter: From Synthetic Polymers to Proteins*, *23*, 1–28.

Allen, M. P., & Tildesley, D. J. (1989). *Computer simulation of liquids*. Oxford [England]: Oxford University Press.

Allinger, N. L. (1977). Conformational analysis. 130. MM2. A hydrocarbon force field utilizing V1 and V2 torsional terms. *Journal of the American Chemical Society*, *99*(25), 8127–8134.

Allinger, N. L., Yuh, Y. H., & Lii, J. H. (1989). Molecular mechanics. The MM3 force field for hydrocarbons. 1. *Journal of the American Chemical Society*, *111*(23), 8551–8566.

Andersen, H. C. (1980). Molecular dynamics simulations at constant pressure and/or temperature. *The Journal of Chemical Physics*, *72*(4), 2384–2393.

Andrea, T. A., Swope, W. C., & Andersen, H. C. (1983). The role of long ranged forces in determining the structure and properties of liquid water. *Journal of Chemical Physics*, *79*(9), 4576–4584.

Andrienko, D. (2006). Introduction to liquid crystals. *International Max Planck Research School, Bad Marienberg*.

Anézo, C., de Vries, A. H., Höltje, H.-D., Tieleman, D. P., & Marrink, S.-J. (2003). Methodological issues in lipid bilayer simulations. *The Journal of Physical Chemistry B*, *107*(35), 9424–9433.

Anishkin, A., & Sukharev, S. (2004). Water dynamics and dewetting transitions in the small mechanosensitive channel MscS. *Biophysical Journal*, *86*(5), 2883–2895.

Antonietti, M., & Förster, S. (2003). Vesicles and liposomes: a self-assembly principle beyond lipids. *Advanced Materials*, *15*(16), 1323–1333.

Arunan, E., Desiraju, G. R., Klein, R. A., Sadlej, J., Scheiner, S., Alkorta, I., Clary, D. C., Crabtree, R. H., Dannenberg, J. J., Hobza, P., et al. (2011). Definition of the hydrogen bond (IUPAC recommendations 2011). *Pure and Applied Chemistry*, *83*(8), 1637–1641.

Auvray, X., Petipas, C., Anthore, R., Rico-Lattes, I., & Lattes, A. (1995). X-ray diffraction study of the ordered lyotropic phases formed by sugar-based surfactants. *Langmuir*, *11*(2), 433–439.

Auvray, X., Petipas, C., Dupuy, C., Louvet, S., Anthore, R., Rico-Lattes, I., & Lattes, A. (2001). Small-angle x-ray diffraction study of the thermotropic and lyotropic phases of five alkyl cyclic and acyclic disaccharides: Influence of the linkage between the hydrophilic and hydrophobic moieties. *The European Physical Journal E: Soft Matter and Biological Physics*, *4*(4), 489–504.

Auvray, X., Petipas, C., Lattes, A., & Rico-Lattes, I. (1997). Role of solvent-head-group interaction on the formation of lyotropic liquid-crystals in structured non-aqueous solvents. *Colloids and Surfaces A: Physicochemical and Engineering Aspects*, *123*, 247–251.

Balasubramanian, D., Raman, B., & Sundari, C. S. (1993). Polysaccharides as amphiphiles. *Journal of the American Chemical Society*, *115*(1), 74–77.

Ball, D. W., Hill, J. W., & Scott, R. J. (2011). *Introduction to chemistry: general, organic, and biological (v.1.0).* Retrieved from `http://2012books.lardbucket.org/books/introduction-to-chemistry-general-organic-and-biological` ([Accessed: 2015-09-01])

Balzer, D. (2000). Introduction. In D. Balzer & H. Lüders (Eds.), *Nonionic surfactants: Alkyl polyglucosides* (pp. 1–5). New York: Marcel Dekker.

Balzer, D., & Lüders, H. (2000). *Nonionic surfactants: Alkyl polyglucosides*. New York: Marcel Dekker.

Baranyai, A., & Evans, D. J. (1990). New algorithm for constrained molecular-dynamics simulation of liquid benzene and naphthalene. *Molecular Physics*, *70*(1), 53–63.

Barón, M. (2001). Definitions of basic terms relating to low-molar-mass and polymer liquid crystals. *Pure and Applied Chemistry*, *73*(5), 845–895.

Ben-Naim, A. (1980). *Hydrophobic interactions*. New York: Plenum Press.

Berendsen, H. J. (1996). Bio-molecular dynamics comes of age. *Science*, *271*(5251), 954–955.

Berendsen, H. J. C., Grigera, J. R., & Straatsma, T. P. (1987). The missing term in effective pair potentials. *The Journal of Physical Chemistry*, *91*(24), 6269–6271.

Berger, O., Edholm, O., & Jähnig, F. (1997). Molecular dynamics simulations of a fluid bilayer of dipalmitoylphosphatidylcholine at full hydration, constant pressure, and constant temperature. *Biophysical journal*, *72*(5), 2002–2013.

Best, R. B., Jackson, G. E., & Naidoo, K. J. (2001). Molecular dynamics and NMR study of the $\alpha(1\rightarrow4)$ and $\alpha(1\rightarrow6)$ glycosidic linkages: maltose and isomaltose. *The Journal of Physical Chemistry B*, *105*(20), 4742–4751.

Bogusz, S., Venable, R. M., & Pastor, R. W. (2000). Molecular dynamics simulations of octyl glucoside micelles: structural properties. *The Journal of Physical Chemistry B*, *104*(23), 5462–5470.

Bogusz, S., Venable, R. M., & Pastor, R. W. (2001). Molecular dynamics simulations of octyl glucoside micelles: dynamic properties. *The Journal of Physical Chemistry B*, *105*(35), 8312–8321.

Borshchevskiy, V., Moiseeva, E., Kuklin, A., Büldt, G., Hato, M., & Gordeliy, V. (2010). Isoprenoid-chained lipid β-XylOC$_{16+4}$-A novel molecule for *in meso* membrane protein crystallization. *Journal of Crystal Growth*, *312*(22), 3326–3330.

Boyd, B. J., Drummond, C. J., Krodkiewska, I., & Grieser, F. (2000). How chain length, headgroup polymerization, and anomeric configuration govern the thermotropic and lyotropic liquid crystalline phase behavior and the air-water interfacial adsorption of glucose-based surfactants. *Langmuir*, *16*(19), 7359–7367.

Boyd, B. J., Krodkiewska, I., Drummond, C. J., & Grieser, F. (2002). Chiral glucose-derived surfactants: the effect of stereochemistry on thermotropic and lyotropic phase behavior. *Langmuir*, *18*(3), 597–601.

Boyd, B. J., Whittaker, D. V., Khoo, S.-M., & Davey, G. (2006). Lyotropic liquid crystalline phases formed from glycerate surfactants as sustained release drug delivery systems. *International Journal of Pharmaceutics*, *309*(1), 218–226.

Brooks, B. R., Brooks, C. L., MacKerell, A. D., Nilsson, L., Petrella, R. J., Roux, B., Won, Y., Archontis, G., Bartels, C., Boresch, S., et al. (2009). CHARMM: the biomolecular simulation program. *Journal of Computational Chemistry*, *30*(10), 1545–1614.

Brooks, B. R., Bruccoleri, R. E., Olafson, B. D., States, D. J., Swaminathan, S., & Karplus, M. (1983). CHARMM: a program for macromolecular energy, minimization, and dynamics calculations. *Journal of Computational Chemistry*, *4*(2), 187–217.

Brooks, N. J., Hamid, H. A., Hashim, R., Heidelberg, T., Seddon, J. M., Conn, C. E., Mirzadeh Husseini, S. M., Zahid, N. I., & Hussen, R. S. D. (2011). Thermotropic and lyotropic liquid crystalline phases of Guerbet branched-chain-D-glucosides. *Liquid Crystals*, *38*(11-12), 1725–1734.

Brown, D. A., & London, E. (1997). Structure of detergent-resistant membrane domains: does phase separation occur in biological membranes? *Biochemical and Biophysical Research Communications*, *240*(1), 1–7.

Brown, G., & Wolken, J. (1979). *Liquid crystals and biological structures*. New York: Academic Press.

Bujarski, J. J., Hardy, S. F., Miller, W. A., & Hall, T. C. (1982). Use of dodecyl-β-D-maltoside in the purification and stabilization of RNA polymerase from brome mosaic virus-infected barley. *Virology*, *119*(2), 465–473.

Burducea, G. (2004). Lyotropic liquid crystals I. Specific structures. *Romanian Reports in Physics*, *56*(1), 66–86.

Caldwell, J. W., & Kollman, P. A. (1995). Structure and properties of neat liquids using nonadditive molecular dynamics: water, methanol, and n-methylacetamide. *The Journal of Physical Chemistry*, *99*(16), 6208–6219.

Cambi, A., & Lidke, D. (2015). *Cell membrane nanodomains from biochemistry to nanoscopy*. Boca Raton: CRC Press/Taylor & Francis Group.

Carreño, L. J., Saavedra-Ávila, N. A., & Porcelli, S. A. (2016). Synthetic glycolipid activators of natural killer t cells as immunotherapeutic agents. *Clinical & Translational Immunology*, *5*(4), e69.

Carrier, D., Giziewicz, J., Moir, D., Smith, I. C., & Jarrell, H. C. (1989). Dynamics and orientation of glycolipid headgroups by 2H-NMR: Gentiobiose. *Biochimica Et Biophysica Acta (BBA)-Biomembranes*, *983*(1), 100–108.

Case, D., Berryman, J., Betz, R., Cerutti, D., Cheatham, T. I., Darden, T., Duke, R., Giese, T., Gohlke, H., Goetz, A., Homeyer, N., Izadi, S., Janowski, P., Kaus, J., Kovalenko, A., Lee, T., LeGrand, S., Li, P., Luchko, T., Luo, R., Madej, B., Merz, K., Monard, G., Needham, P., Nguyen, H., Nguyen, H., Omelyan, I., Onufriev, A., Roe, D., Roitberg, A., Salomon-Ferrer, R., Simmerling, C., Smith, W., Swails, J., Walker, R., Wang, J., Wolf, R., Wu, X., York, D., & Kollman, P. (2015). Amber 15. *University of California, San Francisco*.

Case, D., Darden, T., Cheatham, I., Simmerling, C., Wang, J., Duke, R., Luo, R., Merz, K., Pearlman, D., Crowley, M., Walker, R., Zhang, W., Wang, B., Hayik, S., Roitberg, A., Seabra, G., Wong, K., Paesani, F., Wu, X. L., Brozell, S., Tsui, V., Gohlke, H., Yang, L., Tan, C., Mongan, J., Hornak, V., Cui, G., Beroza, P., Mathews, D., Schafmeister, C., Ross, W., & Kollman, P. (2006). *Amber 9.* University of California.

Case, D., Darden, T., Cheatham, T. I., Simmerling, C., Wang, J., Duke, R., Luo, R., Walker, R., Zhang, W., Merz, K., Roberts, B., Wang, B., Hayik, S., Roitberg, A., Seabra, G., Kolossvai, I., Wong, K., Paesani, F., Vanicek, J., Liu, J., Wu, X., Brozell, S., Steinbrecher, T., Gohlke, H., Cai, Q., Ye, X., Wang, J., Hsieh, M.-J., Cui, G., Roe, D., Mathews, D., Seetin, M., Sagui, C., Babin, V., Luchko, T., Gusarov, S., Kovalenko, A., & Kollman, P. (2012). *Amber 12.* University of California.

Case, D. A., Cheatham, T. E., Darden, T., Gohlke, H., Luo, R., Merz, K. M., Onufriev, A., Simmerling, C., Wang, B., & Woods, R. J. (2005). The amber biomolecular simulation programs. *Journal of Computational Chemistry*, *26*(16), 1668–1688.

Chandrasekhar, S. (1992). *Liquid crystals* (2nd ed.). Cambridge: Cambridge University Press.

Cheetham, N. W. H., & Dasgupta, P. (2006). Studies of disaccharide solvation-molecular dynamics versus HPLC retention. *Australian Journal of Chemistry*, *58*(11), 803–809.

Chen, C. H., Berns, D. S., & Berns, A. S. (1981). Thermodynamics of carbohydrate-lipid interactions. *Biophysical Journal*, *36*(2), 359–367.

Chester, M. A. (1997). Nomenclature of glycolipids. *Pure and Applied Chemistry*, *69*(12), 2475–2487.

Chong, T. T., Hashim, R., & Bryce, R. A. (2006). Molecular dynamics simulation of monoalkyl glycoside micelles in aqueous solution: influence of carbohydrate headgroup stereochemistry. *The Journal of Physical Chemistry B*, *110*(10), 4978–4984.

Chong, T. T., Heidelberg, T., Hashim, R., & Gary, S. (2007). Computer modelling and simulation of thermotropic and lyotropic alkyl glycoside bilayers. *Liquid Crystals*, *34*(2), 251–265.

Chowdhary, J., & Ladanyi, B. M. (2008). Hydrogen bond dynamics at the water/hydrocarbon interface. *The Journal of Physical Chemistry B*, *113*(13), 4045–4053.

Cladis, P. E., Palffy-Muhoray, P., & Saupe, A. (1998). *Dynamics and defects in liquid crystals: a festschrift in honor of alfred saupe*. Amsterdam: Gordon and Breach Science Publishers.

Clark, M., Cramer, R. D., & Van Opdenbosch, N. (1989). Validation of the general purpose tripos 5.2 force field. *Journal of Computational Chemistry*, *10*(8), 982–1012.

Collings, P. J. (2002). *Liquid crystals: nature's delicate phase of matter*. Nwe Jersey: Princeton University Press.

Collings, P. J., & Hird, M. (1997). *Introduction to liquid crystals: chemistry and physics*. London: Tailor & Francis.

Collings, P. J., & Patel, J. S. (1997). *Handbook of liquid crystal research*. New York: Oxford University Press.

Comm., I.-I. (1970). IUPAC-IUB commission on biochemical nomenclature. Abbreviations and symbols for the description of the conformation of polypeptide chains. Tentative rules (1969). *Biochemistry*, *9*(18), 3471–3479.

Cook, A. G., Wardell, J. L., & Imrie, C. T. (2011). Carbohydrate liquid crystals: synthesis and characterisation of the methyl-6-o-(*n*-acyl)-α-D-glucopyranosides. *Chemistry and Physics of Lipids*, *164*(2), 118–124.

Cornell, W. D., Cieplak, P., Bayly, C. I., Gould, I. R., Merz, K. M., Ferguson, D. M., Spellmeyer, D. C., Fox, T., Caldwell, J. W., & Kollman, P. A. (1995). A second generation force field for the simulation of proteins, nucleic acids, and organic molecules. *Journal of the American Chemical Society*, *117*(19), 5179–5197.

Corti, M., Cantù, L., Brocca, P., & Del Favero, E. (2007). Self-assembly in glycolipids. *Current Opinion in Colloid & Interface Science*, *12*(3), 148–154.

Cullis, P. R., & De Kruijff, B. (1979). Lipid polymorphism and the functional roles of lipids in biological membranes. *Biochimica Et Biophysica Acta (BBA)-Reviews on Biomembranes*, *559*(4), 399–20.

Curatolo, W. (1987). The physical properties of glycolipids. *Biochimica et Biophysica Acta (BBA)-Reviews on Biomembranes*, *906*(2), 111–36.

Damasceno, F. R. C., Cammarota, M. C., & Freire, D. M. G. (2012). The combined use of a biosurfactant and an enzyme preparation to treat an effluent with a high fat content. *Colloids and Surfaces B: Biointerfaces*, *95*, 241–246.

Damodaran, K. V., Merz, K. M., & Gaber, B. P. (1992). Structure and dynamics of the dilauroylphosphatidylethanolamine lipid bilayer. *Biochemistry*, *31*(33), 7656–7664.

Danielli, J. F., & Davson, H. (1935). A contribution to the theory of permeability of thin films. *Journal of Cellular and Comparative Physiology*, *5*(4), 495–508.

Darden, T., York, D., & Pedersen, L. (1993). Particle mesh Ewald: an N·log (N) method for Ewald sums in large systems. *Journal of Chemical Physics*, *98*(12), 10089–10092.

de Gennes, P.-G., & Prost, J. (1993). *The physics of liquid crystals* (Vol. 23). Oxford: Oxford University Press.

Dembitsky, V. M. (2004a). Astonishing diversity of natural surfactants: 1. glycosides of fatty acids and alcohols. *Lipids*, *39*(10), 933–953.

Dembitsky, V. M. (2004b). Chemistry and biodiversity of the biologically active natural glycosides. *Chemistry & Biodiversity*, *1*(5), 673–781.

Demchenko, A. P. (2012). Modern views on the structure and dynamics of biological membranes. *Biopolymers and Cell*, *28*(1), 24–38.

de Vries, A. H., Yefimov, S., Mark, A. E., & Marrink, S. J. (2005). Molecular structure of the lecithin ripple phase. *Proceedings of the National Academy of Sciences of the United States of America*, *102*(15), 5392–5396.

Dickson, C. J., Madej, B. D., Skjevik, Å. A., Betz, R. M., Teigen, K., Gould, I. R., & Walker, R. C. (2014). Lipid14: the amber lipid force field. *Journal of Chemical Theory and Computation*, *10*(2), 865–879.

Dierking, I. (2003). *Textures of liquid crystals*. Verlag: John Wiley & Sons.

Domanov, Y. A., & Kinnunen, P. K. (2006). Antimicrobial peptides temporins B and L induce formation of tubular lipid protrusions from supported phospholipid bilayers. *Biophysical Journal*, *91*(12), 4427–4439.

Domanski, A. W., Wolinski, T. R., & Borys, W. (1990). Fiber-optic liquid crystalline high-sensitivity temperature sensor. In *Oe/fibers'89* (pp. 573–581).

dos Santos, S., Medronho, B., dos Santos, T., & Antunes, F. E. (2013). Amphiphilic molecules in drug delivery systems. In J. Coelho (Ed.), *Drug delivery systems: advanced technologies potentially applicable in personalised treatment* (pp. 35–85). Dordrecht: Springer.

Dowhan, W., Bogdanov, M., & Mileykovskaya, E. (2008). Functional roles of lipids in membranes. In D. E. Vance & J. E. Vance (Eds.), *Biochemistry of lipids, lipoproteins and membranes* (5th ed., pp. 1–38). Amsterdam ; Boston: Elsevier.

Doxastakis, M., Sakai, V. G., Ohtake, S., Maranas, J., & De Pablo, J. (2007). A molecular view of melting in anhydrous phospholipidic membranes. *Biophysical Journal*, *92*(1), 147–161.

Doyle, P. S., & Underhill, P. T. (2005). Brownian dynamics simulations of polymers and soft matter. In *Handbook of materials modeling* (pp. 2619–2630). Springer.

Drummond, C. J., & Fong, C. (1999). Surfactant self-assembly objects as novel drug delivery vehicles. *Current Opinion in Colloid & Interface Science*, *4*(6), 449–456.

Dunmur, D. (2011). *Soap, science, and flat-screen tvs : a history of liquid crystals*. New York: Oxford University Press.

Dunmur, D. A., & Palffy-Muhoray, P. (1988). Effect of electric and magnetic fields on orientational disorder in liquid crystals. *The Journal of Physical Chemistry*, *92*(6), 1406–1419.

Edberg, R., Evans, D. J., & Morriss, G. (1986). Constrained molecular dynamics: simulations of liquid alkanes with a new algorithm. *The Journal of Chemical Physics*, *84*(12), 6933–6939.

Eeman, M., & Deleu, M. (2010). From biological membranes to biomimetic model membranes. *Biotechnologie, Agronomie, Société et Environnement*.

Egberts, E., Marrink, S. J., & Berendsen, H. J. (1994). Molecular dynamics simulation of a phospholipid membrane. *European Biophysical Journal*, *22*(6), 423–436.

Ellens, H., Bentz, J., & Szoka, F. C. (1985). Proton-and calcium-induced fusion and destabilization of liposomes. *Biochemistry*, *24*(13), 3099–3106.

Engström, S., Nordén, T. P., & Nyquist, H. (1999). Cubic phases for studies of drug partition into lipid bilayers. *European Journal of Pharmaceutical Sciences*, *8*(4), 243–254.

Epand, R. M. (2015). Introduction to membrane lipids. In D. M. Owen (Ed.), *Methods in membrane lipids* (2nd ed., pp. 1–6). New York: Springer.

Ercolessi, F. (1997). A molecular dynamics primer. *Spring college in computational physics, ICTP, Trieste*, *19*.

Ericsson, C. A., Ericsson, L. C., Kocherbitov, V., Soderman, O., & Ulvenlund, S. (2005). Thermotropic phase behaviour of long-chain alkylmaltosides. *Physical Chemistry Chemical Physics*, *7*(15), 2970–2977.

Ericsson, C. A., Ericsson, L. C., & Ulvenlund, S. (2005). Solid-state phase behaviour of dodecylglycosides. *Carbohydrate Research*, *340*(8), 1529–1537.

Essex, J. W., Hann, M. M., & Richards, W. G. (1994). Molecular-dynamics simulation of a hydrated phospholipid-bilayer. *Philosophical Transactions of the Royal Society of London, Series B*, *344*(1309), 239–260.

Essmann, U., & Berkowitz, M. L. (1999). Dynamical properties of phospholipid bilayers from computer simulation. *Biophysical Journal*, *76*(4), 2081–2089.

Essmann, U., Perera, L., Berkowitz, M. L., Darden, T., Lee, H., & Pedersen, L. G. (1995). A smooth particle mesh Ewald method. *Journal of Chemical Physics*, *103*(19), 8577–8593.

Fahy, E., Subramaniam, S., Brown, H. A., Glass, C. K., Merrill, A. H., Murphy, R. C., Raetz, C. R., Russell, D. W., Seyama, Y., Shaw, W., et al. (2005). A comprehensive classification system for lipids. *Journal of Lipid Research*, *46*(5), 839–862.

Feller, S. E. (2000). Molecular dynamics simulations of lipid bilayers. *Current Opinion in Colloid & interface science*, *5*(3), 217–223.

Field, M. J. (1999). *A practical introduction to the simulation of molecular systems*. Cambridge University Press.

Fischer, E., & Helferich, B. (1911). About new synthetic glucosides. *Justus Liebigs Annalen der Chemie*, *383*, 68–91.

Frank, H. S., & Evans, M. W. (1945). Free volume and entropy in condensed systems iii. entropy in binary liquid mixtures; partial molal entropy in dilute solutions; structure and thermodynamics in aqueous electrolytes. *The Journal of Chemical Physics*, *13*(11), 507–532.

Frenkel, D., & Smit, B. (2002). Molecular dynamics simulations. In D. Frenkel & B. Smit (Eds.), *Understanding molecular simulation (second edition)* (Second Edition ed., pp. 63–107). San Diego: Academic Press.

Friedel, G. (1922). The mesomprphic states of matter. *The Journal of Physical Chemistry B*, *18*, 273–474.

Frisch, M. J., Trucks, G. W., Schlegel, H. B., Scuseria, G. E., Robb, M. A., Cheeseman, J. R., Scalmani, G., Barone, V., Mennucci, B., Petersson, G. A., Nakatsuji, H., Caricato, M., Li, X., Hratchian, H. P., Izmaylov, A. F., Bloino, J., Zheng, G., Sonnenberg, J. L., Hada, M., Ehara, M., Toyota, K., Fukuda, R., Hasegawa, J., Ishida, M., Nakajima, T., Honda, Y., Kitao, O., Nakai, H., Vreven, T., Montgomery Jr., J. A., Peralta, J. E., Ogliaro, F., Bearpark, M. J., Heyd, J., Brothers, E. N., Kudin, K. N., Staroverov, V. N., Kobayashi, R., Normand, J., Raghavachari, K., Rendell, A. P., Burant, J. C., Iyengar, S. S., Tomasi, J., Cossi, M., Rega, N., Millam, N. J., Klene, M., Knox, J. E., Cross, J. B., Bakken, V., Adamo, C., Jaramillo, J., Gomperts, R., Stratmann, R. E., Yazyev, O., Austin, A. J., Cammi, R., Pomelli, C., Ochterski, J. W., Martin, R. L., Morokuma, K., Zakrzewski, V. G., Voth, G. A., Salvador, P., Dannenberg, J. J., Dapprich, S., Daniels, A. D., Farkas, O., Foresman, J. B., Ortiz, J. V., Cioslowski, J., & Fox, D. J. (2009). *Gaussian 09*. Gaussian, Inc.

Garelli-Calvet, R., Brisset, F., Rico, I., & Lattes, A. (1993). *Bis*-gluconamides and *bis*-Lactobionamides ovel α,ω)-type (bolaform) surfactants with two sugar head groups. *Synthetic Communications*, *23*(1), 35–44.

Garidel, P. (2002). Calorimetric and spectroscopic investigations of phytosphingosine ceramide membrane organisation. *Physical Chemistry Chemical Physics*, *4*(10), 1934–1942.

Garidel, P. (2006). Structural organisation and phase behaviour of a stratum corneum lipid analogue: ceramide 3A. *Physical Chemistry Chemical Physics*, *8*(19), 2265–2275.

Garidel, P., Howe, J., Milkereit, G., Rössle, M., Linser, S., Gerber, S., Willumeit, R., Gutsmann, T., Vill, V., & Brandenburg, K. (2008). Structural polymorphism of hydrated ether-linked dimyristyl maltoside and melibioside. *Chemistry and Physics of Lipids*, *151*(1), 18–29.

Garstecki, P., & Hołyst, R. (2001). Scattering patterns of self-assembled gyroid cubic phases in amphiphilic systems. *The Journal of Chemical Physics*, *115*(2), 1095–1099.

Garstecki, P., & Holyst, R. (2002). Scattering patterns of self-assembled cubic phases. 1. the model. *Langmuir*, *18*(7), 2519–2528.

Gentilcore, A. (2009). *A multiscale computational investigation of forces between lipid bilayers* (Unpublished doctoral dissertation). The Johns Hopkins University.

Gerber, S., Wulf, M., Milkereit, G., Vill, V., Howe, J., Roessle, M., Garidel, P., Gutsmann, T., & Brandenburg, K. (2009). Phase diagrams of monoacylated amide-linked disaccharide glycolipids. *Chemistry and Physics of Lipids*, *158*(2), 118–130.

Goodby, J. W. (1998). Liquid crystals and life. *Liquid Crystals*, *24*(1), 25–38.

Goodby, J. W., Cowling, S., Davisa, E., & Queneaub, Y. (2014). Liquid crystal glycolipids. *Carbohydrate Chemistry: Chemical and Biological Approaches*, *40*, 312–340.

Goodby, J. W., Görtz, V., Cowling, S. J., Mackenzie, G., Martin, P., Plusquellec, D., Benvegnu, T., Boullanger, P., Lafont, D., Queneau, Y., et al. (2007). Thermotropic liquid crystalline glycolipids. *Chemical Society Reviews*, *36*(12), 1971–2032.

Goodby, J. W., Pfannemüller, B., Welte, W., Chin, E., & Goodby, J. (2006). Liquid-crystalline glycolipids: towards understanding the roles of liquid crystals in biological and life processes. *Liquid Crystals*, *33*(11-12), 1229–1245.

Gorter, E., & Grendel, F. (1925). On biomolecular layers of lipids on the chromocytes of the blood. *Journal of Experimental Medicine*, *41*, 439–443.

Götz, A. W., Williamson, M. J., Xu, D., Poole, D., Le Grand, S., & Walker, R. C. (2012). Routine microsecond molecular dynamics simulations with AMBER on GPUs. 1. Generalized Born. *Journal of Chemical Theory and Computation*, *8*(5), 1542–1555.

Grand, S. L., Götz, A. W., & Walker, R. C. (2013). SPFP: speed without compromise–a mixed precision model for GPU accelerated molecular dynamics simulations. *Computer Physics Communications*, *184*(2), 374–380.

Gumbart, J., Wang, Y., Aksimentiev, A., Tajkhorshid, E., & Schulten, K. (2005). Molecular dynamics simulations of proteins in lipid bilayers. *Current Opinion in Structural Biology*, *15*(4), 423–431.

Guo, C., Wang, J., Cao, F., Lee, R. J., & Zhai, G. (2010). Lyotropic liquid crystal systems in drug delivery. *Drug Discovery Today*, *15*(23), 1032–1040.

Ha, S. N., Giammona, A., Field, M., & Brady, J. W. (1988). A revised potential-energy surface for molecular mechanics studies of carbohydrates. *Carbohydrate Research*, *180*(2), 207–221.

Haile, J. M. (1992). *Molecular dynamics simulation: elementary methods*. Canada: John Wiley & Sons, Inc.

Hall, A., Rog, T., Karttunen, M., & Vattulainen, I. (2010). Role of glycolipids in lipid rafts: a view through atomistic molecular dynamics simulations with galactosylceramide. *The Journal of Physical Chemistry B*, *114*(23), 7797–807.

Ham, J. T., & Williams, D. G. (1970). The crystal and molecular structure of methyl β-cellobioside-methanol. *Acta Crystallographica Section B: Structural Science*, *26*(9), 1373–1383.

Hamid, H. A., Hashim, R., Seddon, J. M., & Brooks, N. J. (2014). Lyotropic phase behaviour and structural parameters of monosaccharide and disaccharide guerbet branched-chain β-D-glycosides. *Advanced Materials Research*, *895*, 111–115.

Hamley, I. W. (2000). *Introduction to soft matter: polymer, colloids, amphiphiles and liquid crystals*. Chichester: John Wiley & Sons.

Hanwell, M. D., Curtis, D. E., Lonie, D. C., Vandermeersch, T., Zurek, E., & Hutchison, G. R. (2012). Avogadro: an advanced semantic chemical editor, visualization, and analysis platform. *Journal of Cheminformatics*, *4*, 1–17.

Hashim, R., Hamid, H. A. A., Seddon, J. M., Brooks, N. J., Heidelberg, T., Zahid, N. M., & Mirzadeh, S. M. (2010). *Mesophase structure investigation of branched chain glycosides.*

Hashim, R., Hashim, H. H. A., Rodzi, N. Z. M., Hussen, R. S. D., & Heidelberg, T. (2006). Branched chain glycosides: enhanced diversity for phase behavior of easily accessible synthetic glycolipids. *Thin Solid Films*, *509*(1), 27–35.

Hashim, R., Mirzadeh, S. M., Heidelberg, T., Minamikawa, H., Yoshiaki, T., & Sugimura, A. (2011). A reevaluation of the epimeric and anomeric relationship of glucosides and galactosides in thermotropic liquid crystal self-assemblies. *Carbohydrate Research*, *346*(18), 2948–56.

Hashim, R., Sugimura, A., Minamikawa, H., & Heidelberg, T. (2012). Nature-like synthetic alkyl branched-chain glycolipids: a review on chemical structure and self-assembly properties. *Liquid Crystals*, *39*(1), 1–17.

Hato, M. (2001). Synthetic glycolipid/water systems. *Current Opinion in Colloid & Interface Science*, *6*(3), 268–276.

Hato, M., & Minamikawa, H. (1996). The effects of oligosaccharide stereochemistry on the physical properties of aqueous synthetic glycolipids. *Langmuir*, *12*(6), 1658–1665.

Hato, M., Minamikawa, H., Tamada, K., Baba, T., & Tanabe, Y. (1999). Self-assembly of synthetic glycolipid/water systems. *Advances in Colloid and Interface Science*, *80*(3), 233–270.

Hato, M., Yamashita, J., & Shiono, M. (2009). Aqueous phase behavior of lipids with isoprenoid type hydrophobic chains. *The Journal of Physical Chemistry B*, *113*(30), 10196–10209.

Heimburg, T. (2000). A model for the lipid pretransition: coupling of ripple formation with the chain-melting transition. *Biophysical Journal*, *78*(3), 1154–1165.

Heimburg, T. (2009). Physical properties of biological membranes. *arXiv preprint arXiv:0902.2454*.

Heller, H., Schaefer, M., & Schulten, K. (1993). Molecular dynamics simulation of a bilayer of 200 lipids in the gel and in the liquid crystal phase. *The Journal of Physical Chemistry*, *97*(31), 8343–8360.

Hermans, J., Berendsen, H. J., Van Gunsteren, W. F., & Postma, J. P. (1984). A consistent empirical potential for water-protein interactions. *Biopolymers*, *23*(8), 1513–1518.

Hess, B., Bekker, H., Berendsen, H. J., Fraaije, J. G., et al. (1997). LINCS: a linear constraint solver for molecular simulations. *Journal of Computational Chemistry*, *18*(12), 1463–1472.

Hiemenz, P. C., & Rajagopalan, R. (1997). *Principles of colloid and surface chemistry (revised and expanded)* (3rd ed.). New York: Marcel Dekker.

Hinz, H. J., Kuttenreich, H., Meyer, R., Renner, M., Fruend, R., Koynova, R., Boyanov, A., & Tenchov, B. (1991). Stereochemistry and size of sugar head groups determine structure and phase behavior of glycolipid membranes: densitometric, calorimetric, and x-ray studies. *Biochemistry*, *30*(21), 5125–5138.

Hockney, R. W., & Eastwood, J. W. (1988). *Computer simulation using particles*. CRC Press.

Hoffmann, B., & Platz, G. (2001). Phase and aggregation behaviour of alkylglycosides. *Current Opinion in Colloid & Interface Science*, *6*(2), 171–177.

Hofsäß, C., Lindahl, E., & Edholm, O. (2003). Molecular dynamics simulations of phospholipid bilayers with cholesterol. *Biophysical Journal*, *84*(4), 2192–2206.

Holmberg, K., Jönsson, B., Kronberg, B., & Lindman, B. (2003). *Surfactants and polymers in aqueous solution* (2nd ed.). England: John Wiley & Sons.

Hoogboom, J., Rasing, T., Rowan, A. E., & Nolte, R. J. M. (2006). LCD alignment layers. controlling nematic domain properties. *Journal of Materials Chemistry*, *16*(14), 1305–1314.

Hoover, W. G. (1985). Canonical dynamics: equilibrium phase-space distributions. *Physical Review A*, *31*(3), 1695–1697.

Horn, H. W., Swope, W. C., & Pitera, J. W. (2005). Characterization of the TIP4P-Ew water model: vapor pressure and boiling point. *The Journal of Chemical Physics*, *123*(19), 194504.

Horn, H. W., Swope, W. C., Pitera, J. W., Madura, J. D., Dick, T. J., Hura, G. L., & Head-Gordon, T. (2004). Development of an improved four-site water model for biomolecular simulations: TIP4P-Ew. *The Journal of Chemical Physics*, *120*(20), 9665–9678.

Hornak, V., Abel, R., Okur, A., Strockbine, B., & A., R. (2006). Comparison of multiple amber force fields and development of improved protein backbone parameters. *Proteins*, *65*, 712–725.

Howe, J., von Minden, M., Gutsmann, T., Koch, M. H., Wulf, M., Gerber, S., Milkereit, G., Vill, V., & Brandenburg, K. (2007). Structural preferences of dioleoyl glycolipids with mono-and disaccharide head groups. *Chemistry and Physics of Lipids*, *149*(1), 52–58.

Huang, C., & Li, S. (1999). Calorimetric and molecular mechanics studies of the thermotropic phase behavior of membrane phospholipids. *Biochimica Et Biophysica Acta (BBA)-Reviews on Biomembranes*, *1422*(3), 273–307.

Huang, N. M., Shahidan, R., Khiew, P. S., Peter, L., & Kan, C. S. (2004). In situ templating of PbS nanorods in reverse hexagonal liquid crystal. *Colloids and Surfaces A: Physicochemical and Engineering Aspects*, *247*(1), 55–60.

Humphrey, W., Dalke, A., & Schulten, K. (1996). VMD: visual molecular dynamics. *Journal of Molecular Graphics*, *14*(1), 33–38.

Hyperchem(TM). (2003). *Hypercube, Inc., 1115 NW 4th Street, Gainesville, Florida 32601 USA.*

Imura, T., Ohta, N., Inoue, K., Yagi, N., Negishi, H., Yanagishita, H., & Kitamoto, D. (2006). Naturally engineered glycolipid biosurfactants leading to distinctive self-assembled structures. *Chemistry-A European Journal*, *12*(9), 2434–2440.

Imura, T., Yanagishita, H., Ohira, J., Sakai, H., Abe, M., & Kitamoto, D. (2005). Thermodynamically stable vesicle formation from glycolipid biosurfactant sponge phase. *Colloids and Surfaces B: Biointerfaces*, *43*(2), 115–121.

Inès, M., & Dhouha, G. (2015). Glycolipid biosurfactants: Potential related biomedical and biotechnological applications. *Carbohydrate Research*, *416*, 59–69.

Ipsen, J. H., Karlström, G., Mourtisen, O., Wennerström, H., & Zuckermann, M. (1987). Phase equilibria in the phosphatidylcholine-cholesterol system. *Biochimica et Biophysica Acta (BBA)-Biomembranes*, *905*(1), 162–172.

Israelachvili, J. N. (2011). *Intermolecular and surface forces: Revised third edition* (3rd ed.). Burlington, MA: Academic Press.

Jain, M. K. (1979). Molecular motions in biomembranes. *Proceedings of the Indian National Science Academy*, *6*, 558–566.

Jákli, A., & Saupe, A. (2006). *One- and two-dimensional fluids: properties of smectic, lamellar and columnar liquid crystals*. Boca Raton: Taylor & Francis.

Janiak, M. J., Small, D. M., & Shipley, G. G. (1979). Temperature and compositional dependence of the structure of hydrated dimyristoyl lecithin. *Journal of Biological Chemistry*, *254*(13), 6068–6078.

Jayaraman, N., Singh, M. K., Rao, D. S. S., & Prasad, S. K. (2007). Studies of the mesomorphic behavior of bivalent carbohydrate amphiphiles. *Journal of Materials Chemistry*, *17*(21), 2228–2232.

Jeffrey, G. A. (1986). Carbohydrate liquid-crystals. *Accounts of Chemical Research*, *19*(6), 168–173.

Jeffrey, G. A. (1990a). Crystallographic studies of carbohydrates. *Acta Crystallographica Section B: Structural Science*, *46 (Pt 2)*, 89–103.

Jeffrey, G. A. (1990b). Molecular packing and hydrogen bonding in the crystal structures of the n-(n-alkyl)-D-gluconamide and the 1-deoxy-(n-methyl-alkanamido)-D-glucitol mesogens. *Molecular Crystals and Liquid Crystals*, *185*(1), 209–213.

Jeffrey, G. A., & Huang, D. B. (1991). Hydrogen bonding in the crystal structure of α, β-panose. *Carbohydrate Research*, *222*, 47–55.

Jeffrey, G. A., & Rosenstein, R. D. (1964). Crystal-structure analysis in carbohydrate chemistry. *Advances in Carbohydrate Chemistry and Biochemistry*, *19*, 7–22.

Jeffrey, G. A., Ruble, J. R., & Sepehrnia, B. (1985). The crystal structure of isobutyl 2,3,4-tri-o-acetyl-1-thio-β-D-xylopyranoside. *Carbohydrate Research*, *144*(2), 197–203.

Jeffrey, G. A., & Wingert, L. M. (1992). Carbohydrate liquid crystals. *Liquid Crystals*, *12*(2), 179–202.

Jeffrey, G. A., Yeon, Y., & Abola, J. (1987). The crystal structures of octyl alpha-D-glucopyranoside monohydrate and hemihydrate: mesogenic structures with interdigitizing alkyl chains. *Carbohydrate Research*, *169*, 1–11.

Jimenez-Barbero, J., Junquera, E., Martin-Pastor, M., Sharma, S., Vicent, C., & Penades, S. (1995). Molecular recognition of carbohydrates using a synthetic receptor. A model system to understand the stereoselectivity of a carbohydrate-carbohydrate interaction in water. *Journal of the American Chemical Society*, *117*(45), 11198–11204.

John, G., & Vemula, P. K. (2006). Design and development of soft nanomaterials from biobased amphiphiles. *Soft Matter*, *2*(11), 909 – 914.

Jorgensen, W. L., Chandrasekhar, J., Madura, J. D., Impey, R. W., & Klein, M. L. (1983). Comparison of simple potential functions for simulating liquid water. *The Journal of Chemical Physics*, *79*(2), 926–935.

Jorgensen, W. L., & Madura, J. D. (1985). Temperature and size dependence for Monte Carlo simulations of TIP4P water. *Molecular Physics*, *56*(6), 1381–1392.

Kapla, J., Stevensson, B., Dahlberg, M., & Maliniak, A. (2011). Molecular dynamics simulations of membranes composed of glycolipids and phospholipids. *The Journal of Physical Chemistry B*, *116*(1), 244–252.

Karukstis, K. K., Duim, W. C., Van Hecke, G. R., & Hara, N. (2012). Biologically relevant lyotropic liquid crystalline phases in mixtures of n-octyl-β-D-glucoside and water. Determination of the phase diagram by fluorescence spectroscopy. *The Journal of Physical Chemistry B*, *116*(12), 3816–3822.

Kasahara, K., & Sanai, Y. (1999). Possible roles of glycosphingolipids in lipid rafts. *Biophysical Chemistry*, *82*(2-3), 121–127.

Kasson, P. M., & Pande, V. S. (2004). Molecular dynamics simulation of lipid reorientation at bilayer edges. *Biophysical Journal*, *86*(6), 3744–3749.

Kauzmann, W. (1959). Some factors in the interpretation of protein denaturation. *Advances in Protein Chemistry*, *14*, 1–63.

Kelker, H. (1973). History of liquid crystals. *Molecular Crystals and Liquid Crystals*, *21*(1-2), 1–48.

King, M. (2014a). *Introduction to biological membranes.* ([Accessed: 2014-12-25])

King, M. (2014b). *Synthesis of sphingosine and the ceramides.* ([Accessed: 2014-12-25])

Kirsch, P., & Bremer, M. (2000). Nematic liquid crystals for active matrix displays: molecular design and synthesis. *Angewandte Chemie International Edition*, *39*(23), 4216–4235.

Kirschner, K. N., Yongye, A. B., Tschampel, S. M., Gonzalez-Outeirino, J., Daniels, C. R., Foley, B. L., & Woods, R. J. (2008). Glycam06: a generalizable biomolecular force field. carbohydrates. *Journal of Computational Chemistry*, *29*(4), 622–55.

Kitamoto, D., Isoda, H., & Nakahara, T. (2002). Functions and potential applications of glycolipid biosurfactants – from energy-saving materials to gene delivery carriers –. *Journal of Bioscience and Bioengineering*, *94*(3), 187 – 201.

Kitamoto, D., Morita, T., Fukuoka, T., Konishi, M., & Imura, T. (2009). Self-assembling properties of glycolipid biosurfactants and their potential applications. *Current Opinion in Colloid & Interface Science*, *14*(5), 315–328.

Klaus, G. (2005). The dynamics of membrane lipids. In P. L. Yeagle (Ed.), *The structure of biological membranes* (2nd ed., pp. 147–171). Boca Raton: CRC Press.

Klein, K. (2002). Liquid crystals and emulsions: a wonderful marriage. *Cosmetics and Toiletries*, *117*(5), 30–34.

Köberl, M., Schöppe, A., Hinz, H.-J., & Rapp, G. (1998). Cooperativity of glycolipid phase transitions: a critical comparison of results from equilibrium x-ray, density and microcalorimetric measurements. *Chemistry and Physics of Lipids*, *95*(1), 59–82.

Koch, R. (1884). Die aetiologie der tuberculose. *Mitt K. Gesundh*, *2*.

Kocherbitov, V., & Söderman, O. (2004). Glassy crystalline state and water sorption of alkyl maltosides. *Langmuir*, *20*(8), 3056–3061.

Koeltzow, D. E., & Urfer, A. D. (1984). Preparation and properties of pure alkyl glucosides, maltosides and maltotriosides. *Journal of the American Oil Chemists Society*, *61*(10), 1651–1655.

Konidala, P., He, L., & Niemeyer, B. (2006). Molecular dynamics characterization of n-octyl-β-D-glucopyranoside micelle structure in aqueous solution. *Journal of Molecular Graphics and Modelling*, *25*(1), 77–86.

Koynova, R., & Tenchov, B. (2013). Transitions between lamellar and non-lamellar phases in membrane lipids and their physiological roles. *OA Biochemistry*, *1*(1), 1–9.

Kučerka, N., Liu, Y., Chu, N., Petrache, H. I., Tristram-Nagle, S., & Nagle, J. F. (2005). Structure of fully hydrated fluid phase DMPC and DLPC lipid bilayers using x-ray scattering from oriented multilamellar arrays and from unilamellar vesicles. *Biophysical Journal*, *88*(4), 2626–2637.

Kulkarni, C. V. (2012). Lipid crystallization: from self-assembly to hierarchical and biological ordering. *Nanoscale*, *4*(19), 5779–5791.

Lambert, O., Levy, D., Ranck, J. L., Leblanc, G., & Rigaud, J. L. (1998). A new "gel-like" phase in dodecyl maltoside-lipid mixtures: implications in solubilization and reconstitution studies. *Biophysical Journal*, *74*(2 Pt 1), 918–30.

Larsson, K., & Dejmek, P. (1990). Crystals and liquid crystal structures of lipid. In K. Larsson & S. Friberg (Eds.), *Food emulsions* (2nd ed., pp. 97–127). New York: Marcel Dekker.

Leach, A. R. (2001). *Molecular modelling: principles and applications*. England: Prentice Hall.

Lemaur, V., da Silva Filho, D. A., Coropceanu, V., Lehmann, M., Geerts, Y., Piris, J., Debije, M. G., van de Craats, A. M., Senthilkumar, K., Siebbeles, L. D. A., et al.

(2004). Charge transport properties in discotic liquid crystals: a quantum-chemical insight into structure-property relationships. *Journal of the American Chemical Society*, *126*(10), 3271–3279.

Lemieux, R. U. (1989). Rhône-poulenc lecture. The origin of the specificity in the recognition of oligosaccharides by proteins. *Chemical Society Reviews*, *18*, 347–374.

Lewis, R. N. A. H., & McElhaney, R. N. (1992). The mesomorphic phase behavior of lipid bilayers. In P. Yeagle (Ed.), *The structure of biological membranes* (pp. 73–155). Boca Raton: CRC Press.

Lim, J. B., & Klauda, J. B. (2011). Lipid chain branching at the iso- and anteiso-positions in complex chlamydia membranes: A molecular dynamics study. *Biochimica et Biophysica Acta (BBA)-Biomembranes*, *1808*(1), 323–331.

Lindahl, E. (2001). *Computational modeling of biological membrane and interface dynamics* (Unpublished doctoral dissertation). Royal Institute of Technology,Stockholm.

Lindahl, E., Hess, B., & Van Der Spoel, D. (2001). Gromacs 3.0: a package for molecular simulation and trajectory analysis. *Journal of Molecular Modeling*, *7*(8), 306–317.

Lingwood, D., Binnington, B., Rog, T., Vattulainen, I., Grzybek, M., Coskun, U., Lingwood, C. A., & Simons, K. (2011). Cholesterol modulates glycolipid conformation and receptor activity. *Nature Chemical Biology*, *7*(5), 260–262.

Lipková, J., Zygalakis, K. C., Chapman, S. J., & Erban, R. (2011). Analysis of brownian dynamics simulations of reversible bimolecular reactions. *SIAM Journal on Applied Mathematics*, *71*(3), 714–730.

Lipowsky, R. (2013). Spontaneous tubulation of membranes and vesicles reveals membrane tension generated by spontaneous curvature. *Faraday Discussions*, *161*, 305–331.

Liu, Q., & Brady, J. W. (1997). Model dependence of the anisotropic structuring of solvent water around sugars in molecular dynamics simulations. *The Journal of Physical Chemistry B*, *101*(8), 1317–1321.

Loerbroks, C., Heimermann, A., & Thiel, W. (2015). Solvents effects on the mechanism of cellulose hydrolysis: a QM/MM study. *Journal of Computational Chemistry*, *36*(15), 1114–1123.

London, E. (2005). How principles of domain formation in model membranes may explain ambiguities concerning lipid raft formation in cells. *Biochimica et Biophysica Acta (BBA)-Molecular Cell Research*, *1746*(3), 203–220.

Luckhurst, G. R. (1993). Orientational order in liquid crystals: experiment and theory. *Berichte der Bunsengesellschaft für physikalische Chemie*, *97*(10), 1169–1187.

Lycknert, K., & Widmalm, G. (2004). Dynamics of the escherichia coli O91 O-Antigen polysaccharide in solution as studied by Carbon-13 NMR relaxation. *Biomacromolecules*, *5*(3), 1015–1020.

Mahoney, M. W., & Jorgensen, W. L. (2000). A five-site model for liquid water and the reproduction of the density anomaly by rigid, nonpolarizable potential functions. *The Journal of Chemical Physics*, *112*(20), 8910–8922.

Manickam Achari, V., Bryce, R. A., & Hashim, R. (2014). Conformational dynamics of dry lamellar crystals of sugar based lipids: an atomistic simulation study. *PloS One*, *9*(6), e101110.

Mannock, D. A., Lewis, R. N., McElhaney, R. N., Akiyama, M., Yamada, H., Turner, D. C., & Gruner, S. M. (1992). Effect of the chirality of the glycerol backbone on the bilayer and nonbilayer phase transitions in the diastereomers of di-dodecyl-β-D-glucopyranosyl glycerol. *Biophysical Journal*, *63*(5), 1355–1368.

Mannock, D. A., & McElhaney, R. N. (2004). Thermotropic and lyotropic phase properties of glycolipid diastereomers: role of headgroup and interfacial interactions in determining phase behaviour. *Current Opinion in Colloid & Interface Science*, *8*(6), 426–447.

Marcus, M. A. (1986). The mesophase of dodecyl maltoside. *Molecular Crystals and Liquid Crystals Science and Technology Section A*, *3*(3-4), 85–89.

Marcus, M. A., & Finn, P. L. (1985). The S_A phase of an alkylated sugar viewed as a lyotropic phase. *Molecular Crystals and Liquid Crystals Letters*, *2*(5), 159–166.

Martínez, L., Andrade, R., Birgin, E. G., & Martínez, J. M. (2009). Packmol: A package for building initial configurations for molecular dynamics simulations. *Journal of Computational Chemistry*, *30*(13), 2157–2164.

Martinez-Seara, H., & Rog, T. (2013). Molecular dynamics simulations of lipid bilayers: simple recipe of how to do it. In L. Monticelli & E. Salonen (Eds.), *Biomolecular simulations* (pp. 407–429). Springer.

Mashl, R. J., Scott, H. L., Subramaniam, S., & Jakobsson, E. (2001). Molecular simulation of dioleoylphosphatidylcholine lipid bilayers at differing levels of hydration. *Biophysical Journal*, *81*(6), 3005–3015.

Mayne, C. G., Saam, J., Schulten, K., Tajkhorshid, E., & Gumbart, J. C. (2013). Rapid parameterization of small molecules using the force field toolkit. *Journal of Computational Chemistry*, *34*(32), 2757–2770.

McCammon, J. A., Gelin, B. R., & Karplus, M. (1977). Dynamics of folded proteins. *Nature*, *267*, 585–590.

McCammon, J. A., & Karplus, M. (1980). Dynamics of tyrosine ring rotations in a globular protein. *Biopolymers*, *19*(7), 1375–1405.

McIntosh, T. J. (1980). Differences in hydrocarbon chain tilt between hydrated phosphatidylethanolamine and phosphatidylcholine bilayers. A molecular packing model. *Biophysical Journal*, *29*(2), 237–245.

McMullen Jr, R. L. (2005). *Molecular dynamics simulations of amphiphilic molecules* (Unpublished doctoral dissertation). Department of Chemistry and Biochemistry, Seton Hall University.

McNaught, A. D. (1996). International Union of Pure and Applied Chemistry and International Union of Biochemistry and Molecular Biology - Joint Commission on Biochemical Nomenclature - Nomenclature of carbohydrates - Recommendations 1996. *Pure and Applied Chemistry*, *68*(10), 1919–2008.

Meier, G., Sackmann, E., & Grabmaier, J. G. (1975). *Applications of liquid crystals*. Berlin: Springer-Verlag.

Merrill, A. H., Schmelz, E. M., Dillehay, D. L., Spiegel, S., Shayman, J. A., Schroeder, J. J., Riley, R. T., Voss, K. A., & Wang, E. (1997). Sphingolipids–the enigmatic lipid class: biochemistry, physiology, and pathophysiology. *Toxicology and Applied Pharmacology*, *142*(1), 208 – 225.

Merz, K. M. (1997). Molecular dynamics simulations of lipid bilayers. *Current Opinion in Structural biology*, *7*(4), 511–517.

Milkereit, G., Morr, M., Thiem, J., & Vill, V. (2004). Thermotropic and lyotropic properties of long chain alkyl glycopyranosides: Part III: pH-sensitive headgroups. *Chemistry and Physics of Lipids*, *127*(1), 47–63.

Minamikawa, H., & Hato, M. (2005). Headgroup effects on phase behavior and interfacial properties of β-3,7-dimethyloctylglycoside/water systems. *Chemistry and Physics of Lipids*, *134*(2), 151–160.

Misran, O., Timimi, B. A., Heidelberg, T., Sugimura, A., & Hashim, R. (2013). Deuterium NMR investigation of the lyotropic phases of alkyl β-glycoside/D_2O systems. *The Journal of Physical Chemistry B*, *117*(24), 7335–7344.

Mitchell, F. L., Miles, S. M., Neres, J., Bichenkova, E. V., & Bryce, R. A. (2010). Tryptophan as a molecular shovel in the glycosyl transfer activity of trypanosoma cruzi trans-sialidase. *Biophysical Journal*, *98*(9), L38–L40.

Miyamoto, S., & Kollman, P. A. (1992). SETTLE - an analytical version of the SHAKE and RATTLE algorithm for rigid water models. *Journal of Computational Chemistry*, *13*(8), 952–962.

Mizushima, S.-I., Morino, Y., & Nozri, S. (1936). Raman effect and free rotation. *Nature*, *137*, 945–945.

Monticelli, L., & Tieleman, D. P. (2013). Force fields for classical molecular dynamics. In L. Monticelli & E. Salonen (Eds.), *Biomolecular simulations* (pp. 197–213). Springer.

Moore, P. B., Lopez, C. F., & Klein, M. L. (2001). Dynamical properties of a hydrated lipid bilayer from a multinanosecond molecular dynamics simulation. *Biophysical Journal*, *81*(5), 2484–2494.

Moretti, S. (2011). In silico experiments in scientific papers on molecular biology. *Science Studies*, *24*(2), 23–42.

Muckom, R. J., Stanzione, F., Gandour, R. D., & Sum, A. K. (2013). Dendritic amphiphiles strongly affect the biophysical properties of dppc bilayer membranes. *The Journal of Physical Chemistry B*, *117*(6), 1810–1818.

Müller, P., & Herrmann, A. (2002). Rapid transbilayer movement of spin-labeled steroids in human erythrocytes and in liposomes. *Biophysical Journal*, *82*(3), 1418–1428.

Muñoz, J., & Alfaro, M. C. (2000). Rheological and phase behaviour of amphiphilic lipids. *Grasas y Aceites*, *51*(1-2), 6–25.

Muslim, A.-M., & Bryce, R. A. (2004). Carbohydrate conformation in aqueous solution: calculation of a QM/MM potential of mean force. *Chemical Physics Letters*, *388*(4), 473–478.

Nagarajan, R. (2002). Molecular packing parameter and surfactant self-assembly: the neglected role of the surfactant tail. *Langmuir*, *18*(1), 31–38.

Nagle, J. F., & Tristram-Nagle, S. (2000a). Lipid bilayer structure. *Current Opinion in Structural Biology*, *10*(4), 474–480.

Nagle, J. F., & Tristram-Nagle, S. (2000b). Structure of lipid bilayers. *Biochimica et Biophysica Acta (BBA)-Reviews on Biomembranes*, *1469*(3), 159–195.

Naidoo, K. J., & Kuttel, M. (2001). Water structure about the dimer and hexamer repeat units of amylose from molecular dynamics computer simulations. *Journal of Computational Chemistry*, *22*(4), 445–456.

Nevzorov, A. A., Trouard, T. P., & Brown, M. F. (1999). Lipid bilayer dynamics from orientation and frequency dependent deuterium NMR relaxation. *Biophysical Journal*, *76*(1), A441–A441.

Newton, M. D., Jeffrey, G. A., & Takagi, S. (1979). Application of *ab initio* molecular orbital calculations to the structural moieties of carbohydrates. 5. The geometry of the hydrogen bonds. *Journal of the American Chemical Society*, *101*(8), 1997–2002.

Nguan, H., Ahmadi, S., & Hashim, R. (2014). Molecular dynamics simulations of the lyotropic reverse hexagonal (H_{II}) of guerbet branched-chain β-D-glucoside. *Physical Chemistry Chemical Physics*, *16*(1), 324–334.

Nguan, H. S., Heidelberg, T., Hashim, R., & Tiddy, G. J. T. (2010). Quantitative analysis of the packing of alkyl glycosides: a comparison of linear and branched alkyl chains. *Liquid Crystals*, *37*(9), 1205–1213.

Niemelä, P., Hyvönen, M. T., & Vattulainen, I. (2004). Structure and dynamics of sphingomyelin bilayer: insight gained through systematic comparison to phosphatidylcholine. *Biophysical Journal*, *87*(5), 2976–2989.

Niemelä, P. S., Hyvönen, M. T., & Vattulainen, I. (2006). Influence of chain length and unsaturation on sphingomyelin bilayers. *Biophysical Journal*, *90*(3), 851–863.

Nilsson, F., Söderman, O., & Johansson, I. (1996). Physical-chemical properties of the n-octyl β-D-glucoside/water system. A phase diagram, self-diffusion NMR, and SAXS study. *Langmuir*, *12*(4), 902–908.

Nilsson, F., Söderman, O., & Johansson, I. (1998). Four different C_8G_1 alkylglucosides. Anomeric effects and the influence of straight vs branched hydrocarbon chains. *Journal of Colloid and Interface Science*, *203*(1), 131–139.

Nitschke, M., & Costa, S. (2007). Biosurfactants in food industry. *Trends in Food Science & Technology*, *18*(5), 252–259.

Ohya, Y. (2002). Hydrogen bonds. In N. Yui (Ed.), *Supramolecular design for biological applications* (pp. 25–64). Boca Raton: CRC Press.

Ott, K. H., & Meyer, B. (1996). Molecular dynamics simulations of maltose in water. *Carbohydrate Research*, *281*(1), 11–34.

Overbeek, J. T. G. (1977). Recent developments in the understanding of colloid stability. *Journal of Colloid and Interface Science*, *58*(2), 408–422.

Pabst, G., Kučerka, N., Nieh, M.-P., Rheinstädter, M., & Katsaras, J. (2010). Applications of neutron and x-ray scattering to the study of biologically relevant model membranes. *Chemistry and Physics of Lipids*, *163*(6), 460–479.

Paleos, C. M., & Tsiourvas, D. (2001). Liquid crystals from hydrogen-bonded amphiphiles. *Current Opinion in Colloid & Interface Science*, *6*(3), 257–267.

Palffy-Muhoray, P. (2007). Orientationally ordered soft matter: the diverse world of liquid crystals. *Electronic-Liquid Crystal Communications*.

Petrenko, R., & Meller, J. (2010). Molecular dynamics. In *els* (pp. 1–13). Chichester: John Wiley & Sons Ltd.

Phillips, J. C., Braun, R., Wang, W., Gumbart, J., Tajkhorshid, E., Villa, E., Chipot, C., Skeel, R. D., Kale, L., & Schulten, K. (2005). Scalable molecular dynamics with NAMD. *Journal of Computational Chemistry*, *26*(16), 1781–1802.

Pinisetty, D. (2005). *Molecular dynamics simulations of biological membranes in the presence of cryoprotectants* (Unpublished master's thesis). The Department of Mechanical Engineering, Louisiana State University and Agricultural and Mechanical College.

Plimpton, S. (1995). Fast parallel algorithms for short-range molecular dynamics. *Journal of Computational Physics*, *117*(1), 1–19.

Posse de Chaves, E., & Sipione, S. (2010). Sphingolipids and gangliosides of the nervous system in membrane function and dysfunction. *FEBS Letters*, *584*(9), 1748–1759.

Price, D. J., & Brooks III, C. L. (2004). A modified TIP3P water potential for simulation with Ewald summation. *The Journal of Chemical Physics*, *121*(20), 10096–10103.

Pronk, S., Páll, S., Schulz, R., Larsson, P., Bjelkmar, P., Apostolov, R., Shirts, M. R., Smith, J. C., Kasson, P. M., van der Spoel, D., et al. (2013). Gromacs 4.5: a high-throughput and highly parallel open source molecular simulation toolkit. *Bioinformatics*, btt055.

Rahman, A. (1964). Correlations in the motion of atoms in liquid argon. *Physical Review*, *136*(2A), A405–A411.

Rahman, A., & Stillinger, F. H. (1971). Molecular dynamics study of liquid water. *The Journal of Chemical Physics*, *55*(7), 3336–3359.

Ram, P., Kim, E., Thomson, D., Howard, K., & Prestegard, J. (1992). Computer modelling of glycolipids at membrane surfaces. *Biophysical journal*, *63*(6), 1530–1535.

Raychaudhuri, S. (2008). Introduction to Monte Carlo simulation. In *Simulation conference, 2008. wsc 2008. winter* (pp. 91–100).

Reiling, S., Schlenkrich, M., & Brickmann, J. (1996). Force field parameters for carbohydrates. *Journal of Computational Chemistry*, *17*(4), 450–468.

Reis, R., Pacheco, G., Pereira, A., & Freire, D. (2013). Biosurfactants: production and applications. *New York: InTech*.

Roe, D. R., & Cheatham III, T. E. (2013). Ptraj and cpptraj: software for processing and analysis of molecular dynamics trajectory data. *Journal of Chemical Theory and Computation*, *9*(7), 3084–3095.

Róg, T., Murzyn, K., Gurbiel, R., Takaoka, Y., Kusumi, A., & Pasenkiewicz-Gierula, M. (2004). Effects of phospholipid unsaturation on the bilayer nonpolar region a molecular simulation study. *Journal of Lipid Research*, *45*(2), 326–336.

Róg, T., Vattulainen, I., Bunker, A., & Karttunen, M. (2007). Glycolipid membranes through atomistic simulations: effect of glucose and galactose head groups on lipid bilayer properties. *The Journal of Physical Chemistry B*, *111*(34), 10146–10154.

Róg, T., Vattulainen, I., & Karttunen, M. (2005). Modeling glycolipids: taken one. *Cellular and Molecular Biology Letters*, *10*(4), 625–630.

Ryckaert, J.-P., Ciccotti, G., & Berendsen, H. J. C. (1977). Numerical integration of the cartesian equations of motion of a system with constraints: molecular dynamics of n-alkanes. *Journal of Computational Physics*, *23*(3), 327–341.

Ryohei, H. (1958). Studies on alkyl derivatives of carbohydrate. II Syntheses of alkyl-β-cellobiosides. *Yakugaku Zasshi*, *78*, 999–1002.

Sackmann, H. (1989). Plenary lecture. Smectic liquid crystals. A historical review. *Liquid Crystals*, *5*(1), 43–55.

Sagnella, S. M., Conn, C. E., Krodkiewska, I., & Drummond, C. J. (2009). Soft ordered mesoporous materials from nonionic isoprenoid-type monoethanolamide amphiphiles self-assembled in water. *Soft Matter*, *5*(23), 4823–4834.

Sakya, P., Seddon, J., Templer, R., Mirkin, R., & Tiddy, G. (1997). Micellar cubic phases and their structural relationships: the nonionic surfactant system c12eo12/water. *Langmuir*, *13*(14), 3706–3714.

Sakya, P., Seddon, J., & Vill, V. (1997). Thermotropic and lyotropic phase behaviour of monoalkyl glycosides. *Liquid Crystals*, *23*(3), 409–424.

Sakya, P., Seddon, J. M., & Templer, R. H. (1994). Lyotropic phase behaviour of n-octyl-1-o-β-D-glucopyranoside and its thio derivative n-octyl-1-s-β-D-glucopyranoside. *Journal de Physique II*, *4*, 1311–1331.

Salim, M., Minamikawa, H., Sugimura, A., & Hashim, R. (2014). Amphiphilic designer nano-carriers for controlled release: from drug delivery to diagnostics. *Medicinal Chemistry Communications*.

Salomon-Ferrer, R., Case, D. A., & Walker, R. C. (2013). An overview of the amber biomolecular simulation package. *Wiley Interdisciplinary Reviews: Computational Molecular Science*, *3*(2), 198–210.

Salomon-Ferrer, R., Götz, A. W., Poole, D., Le Grand, S., & Walker, R. C. (2013). Routine microsecond molecular dynamics simulations with AMBER on GPUs. 2. Explicit solvent particle mesh Ewald. *Journal of Chemical Theory and Computation*, *9*(9), 3878–3888.

Sankaram, M. B., & Thompson, T. E. (1990). Modulation of phospholipid acyl chain order by cholesterol. A solid-state deuterium nuclear magnetic resonance study. *Biochemistry*, *29*(47), 10676–10684.

Sasaki, T., Demura, M., Kato, N., & Mukai, Y. (2011). Sensitive detection of protein-lipid interaction change on bacteriorhodopsin using dodecyl β-D-maltoside. *Biochemistry*, *50*(12), 2283–90.

Satoh, A. (2011). *Introduction to practice of molecular simulation: molecular dynamics, monte carlo, brownian dynamics, lattice boltzmann and dissipative particle dynamics*. London: Elsevier.

Saupe, A. (1964). Kernresonanzen in kristallinen flüssigkeiten und in kristallinflüssigen lösungen. teil i. *Zeitschrift fur Naturforschung A: Journal of Physical Sciences*, *19*, 161–171.

Schlick, T. (2013). The 2013 nobel prize in chemistry celebrates computations in chemistry and biology. *SIAM News*, *46*(10).

Schmidt-Mende, L., Fechtenkötter, A., Müllen, K., Moons, E., Friend, R. H., & MacKenzie, J. (2001). Self-organized discotic liquid crystals for high-efficiency organic photovoltaics. *Science*, *293*(5532), 1119–1122.

Seddon, J. M. (1990). Structure of the inverted hexagonal (H_{II}) phase, and non-lamellar phase transitions of lipids. *Biochimica et Biophysica Acta (BBA)-Reviews on Biomembranes*, *1031*(1), 1–69.

Seddon, J. M. (2002). Liquid crystals (editorial). *Current Opinion in Colloid & Interface Science*, *7*, 296–297.

Seddon, J. M., Ces, O., Templer, R. H., Mannock, D. A., & McElhaney, R. N. (2003). Structure and phase behaviour of synthetic glycolipids. *Molecular Crystals and Liquid Crystals*, *402*(1), 77–84.

Seddon, J. M., Robins, J., Gulik-Krzywicki, T., & Delacroix, H. (2000). Inverse micellar phases of phospholipids and glycolipids. Invited lecture. *Physical Chemistry Chemical Physics*, *2*(20), 4485–4493.

Seddon, J. M., & Templer, R. H. (1995). Polymorphism of lipid-water systems. In R. Lipowsky & E. Sackmann (Eds.), *Structure and dynamics of membranes* (2nd ed., Vol. 1, pp. 99–149). Amsterdam: Elsevier SPC.

Sengupta, A. (2013). *Topological microfluidics*. Heidelberg, Germany: Springer International Publishing.

Shah, J. C., Sadhale, Y., & Chilukuri, D. M. (2001). Cubic phase gels as drug delivery systems. *Advanced Drug Delivery Reviews*, *47*(2-3), 229–250. (Lipid Assemblies for Drug Delivery)

Shaw, D. (1992). *Introduction to colloid and surface chemistry (colloid & surface engineering)* (4th ed.). Oxford: Butterworth-Heinemann.

Shinoda, W., DeVane, R., & Klein, M. L. (2010). Zwitterionic lipid assemblies: molecular dynamics studies of monolayers, bilayers, and vesicles using a new coarse grain force field. *The Journal of Physical Chemistry B*, *114*(20), 6836–6849.

Shinoda, W., Mikami, M., Baba, T., & Hato, M. (2003). Molecular dynamics study on the effect of chain branching on the physical properties of lipid bilayers: structural stability. *The Journal of Physical Chemistry B*, *107*(50), 14030–14035.

Shinoda, W., Mikami, M., Baba, T., & Hato, M. (2004). Molecular dynamics study on the effects of chain branching on the physical properties of lipid bilayers: 2. Permeability. *The Journal of Physical Chemistry B*, *108*(26), 9346–9356.

Simons, K., & Ikonen, E. (1997). Functional rafts in cell membranes. *Nature*, *387*(6633), 569–572.

Singer, S. J., & Nicolson, G. L. (1972). The fluid mosaic model of the structure of cell membranes. *Science*, *175*(4023), 720–731.

Singh, M. K., & Jayaraman, N. (2009). Carbohydrate-based liquid crystals. *Journal of the Indian Institute of Science*, *89*(2), 113–135.

Singh, M. K., Jayaraman, N., Rao, D., & Prasad, S. K. (2008). Effect of the C-2 hydroxyl group on the mesomorphism of alkyl glycosides: synthesis and thermotropic behavior of alkyl 2-deoxy-D-*arabino*-hexopyranosides. *Chemistry and Physics of Lipids*, *155*(2), 90–97.

Singh, S. (2000). Phase transitions in liquid crystals. *Physics Reports*, *324*(2), 107–269.

Singh, S., & Dunmur, D. A. (2002). *Liquid crystals: fundamentals*. New Jersey: World Scientific.

Sluckin, T. J., Dunmur, D. A., & Stegemeyer, H. (2004). Crystals that flow. *Liquid Crystals Series Taylor & Francis: London*.

Small, D. M. (1984). Lateral chain packing in lipids and membranes. *Journal of Lipid Research*, *25*(13), 1490–1500.

Soltesova, M., Kowalewski, J., & Widmalm, G. (2013). Dynamics of exocyclic groups in the Escherichia coli O91 O-antigen polysaccharide in solution studied by carbon-13 NMR relaxation. *Journal of Biomolecular NMR*, *57*(1), 37–45.

Sotomayor, M., & Schulten, K. (2004). Molecular dynamics study of gating in the mechanosensitive channel of small conductance mscs. *Biophysical Journal*, *87*(5), 3050–3065.

Srivastava, P. K. (2005). *Elementary biophysics: an introduction*. Harrow: Alpha Science International.

Stillinger, F. H., & Rahman, A. (1974). Improved simulation of liquid water by molecular dynamics. *Journal of Chemical Physics*, *60*, 1545–1557.

Stubenrauch, C. (2001). Sugar surfactants-aggregation, interfacial, and adsorption phenomena. *Current Opinion in Colloid & Interface Science*, *6*(2), 160–170.

Tanford, C. (1980). *The hydrophobic effect: formation of micelles and biological membranes*. New York: Wiley.

Tardieu, A., Luzzati, V., & Reman, F. C. (1973). Structure and polymorphism of the hydrocarbon chains of lipids: a study of lecithin-water phases. *Journal of Molecular Biology*, *75*(4), 711–733.

Tessier, M. B., DeMarco, M. L., Yongye, A. B., & Woods, R. J. (2008). Extension of the GLYCAM06 biomolecular force field to lipids, lipid bilayers and glycolipids. *Molecular Simulation*, *34*(4), 349–364.

Tiddy, G. J. T. (1980). Surfactant-water liquid crystal phases. *Physics Reports*, *57*(1), 1–46.

Tieleman, D. P., Marrink, S. J., & Berendsen, H. J. (1997). A computer perspective of membranes: molecular dynamics studies of lipid bilayer systems. *Biochimica et Biophysica Acta (BBA)-Reviews on Biomembranes*, *1331*(3), 235–70.

Tielrooij, K.-J., Hunger, J., Buchner, R., Bonn, M., & Bakker, H. J. (2010). Influence of concentration and temperature on the dynamics of water in the hydrophobic hydration shell of tetramethylurea. *Journal of the American Chemical Society*, *132*(44), 15671–15678.

Tolédano, V., P.and Dmitriev. (1996). *Reconstructive phase transitions: in crystals and quasicrystals*. Singapore: World Scientific.

Tresset, G. (2009). The multiple faces of self-assembled lipidic systems. *BMC Biophysics*, *2*(1), 1–25.

Trouard, T. P., Nevzorov, A. A., Alam, T. M., Job, C., Zajicek, J., & Brown, M. F. (1999). Influence of cholesterol on dynamics of dimyristoylphosphatidylcholine bilayers as studied by deuterium NMR relaxation. *Journal of Chemical Physics*, *110*(17), 8802–8818.

Tschierske, C. (2002). Amphotropic liquid crystals. *Current Opinion in Colloid & Interface Science*, *7*(5-6), 355–370.

Uchegbu, I. F., & Vyas, S. P. (1998). Non-ionic surfactant based vesicles (niosomes) in drug delivery. *International Journal of pharmaceutics*, *172*(1), 33–70.

Vandenbussche, S., Díaz, D., Fernández-Alonso, M. C., Pan, W., Vincent, S. P., Cuevas, G., Cañada, F. J., Jiménez-Barbero, J., & Bartik, K. (2008). Aromatic-carbohydrate interactions: an NMR and computational study of model systems. *Chemistry-A European Journal*, *14*(25), 7570–7578.

Van der Ploeg, P., & Berendsen, H. J. C. (1982). Molecular dynamics simulation of a bilayer membrane. *The Journal of Chemical Physics*, *76*(6), 3271–3276.

Van der Ploeg, P., & Berendsen, H. J. C. (1983). Molecular dynamics of a bilayer membrane. *Molecular Physics*, *49*(1), 233–248.

Van Der Spoel, D., Lindahl, E., Hess, B., A. R. van Buuren, A. R., Apol, E., Meulenhoff, P. J., Tieleman, D. P., Sijbers, A. L. T. M., Feenstra, K. A., van Drunen, R., & Berendsen, H. J. C. (2010). *Gromacs user manual version 4.6-beta1*.

Van Der Spoel, D., Lindahl, E., Hess, B., Groenhof, G., Mark, A. E., & Berendsen, H. J. (2005). Gromacs: fast, flexible, and free. *Journal of Computational Chemistry*, *26*(16), 1701–1718.

Van Gunsteren, W. F., & Berendsen, H. J. C. (1987). Gromos-87 manual. *BIOMOS bv Nijenborgh*, *4*, 9747.

Venable, R. M., Brooks, B. R., & Pastor, R. W. (2000). Molecular dynamics simulations of gel (L_β) phase lipid bilayers in constant pressure and constant surface area ensembles. *The Journal of Chemical Physics*, *112*, 4822.

Verlet, L. (1967). Computer "experiments" on classical fluids. I. Thermodynamical properties of lennard-jones molecules. *Physical Review*, *159*(1), 98–103.

Verwey, E. J. W., Overbeek, J. T. G., & Overbeek, J. T. G. (1999). *Theory of the stability of lyophobic colloids*. Courier Corporation.

Vill, V. (2002). *Liqcryst 4.2*. Fujitsu FQS, Fukuoka.

Vill, V., Bocker, T., Thiem, J., & Fischer, F. (1989). Studies on liquid-crystalline glycosides. *Liquid Crystals*, *6*(3), 349–356.

Vill, V., Bocker, T., Thiem, J., & Fischer, F. (2006). Studies on liquid-crystalline glycosides. *Liquid Crystals*, *33*(11-12), 1353–1358.

Vill, V., & Hashim, R. (2002). Carbohydrate liquid crystals: structure-property relationship of thermotropic and lyotropic glycolipids. *Current Opinion in Colloid & Interface Science*, *7*(5), 395–409.

Vill, V., Von Minden, H., Koch, M., Seydel, U., & Brandenburg, K. (2000). Thermotropic and lyotropic properties of long chain alkyl glycopyranosides: Part I: monosaccharide headgroups. *Chemistry and Physics of Lipids*, *104*(1), 75–91.

von Minden, H. M., Brandenburg, K., Seydel, U., Koch, M., Garamus, V., Willumeit, R., & Vill, V. (2000). Thermotropic and lyotropic properties of long chain alkyl glycopyranosides. Part II. Disaccharide headgroups. *Chemistry and Physics of Lipids*, *106*(2), 157–179.

von Minden, H. M., Morr, M., Milkereit, G., Heinz, E., & Vill, V. (2002). Synthesis and mesogenic properties of glycosyl diacylglycerols. *Chemistry and Physics of Lipids*, *114*(1), 55–80.

Wai Ling, K., Wee Chen, G., Wan Haliza Abd, M., Rauzah, H., & Thorsten, H. (2010). Pyroelectric detection in glycolipid thin film. *Thin Solid Films*, *518*(15), 4412–4416.

Wang, T.-Y., Leventis, R., & Silvius, J. R. (2000). Fluorescence-based evaluation of the partitioning of lipids and lipidated peptides into liquid-ordered lipid microdomains: a model for molecular partitioning into "lipid rafts". *Biophysical Journal*, *79*(2), 919–933.

Weiner, S. J., Kollman, P. A., Case, D. A., Singh, U. C., Ghio, C., Alagona, G., Profeta, S., & Weiner, P. (1984). A new force field for molecular mechanical simulation of nucleic acids and proteins. *Journal of the American Chemical Society*, *106*(3), 765–784.

Wohlert, J. (2006). *Atomistic computer simulations of lipid bilayers* (Unpublished doctoral dissertation). Royal Institute of Technology, Department of Physics-Theoretical Biological Physics.

Wojtowicz, P. J., Sheng, P., & Priestley, E. (1975). *Introduction to liquid crystals*. New York: Plenum Press.

Woods, R. J., Dwek, R. A., Edge, C. J., & Fraser-Reid, B. (1995). Molecular mechanical and molecular dynamic simulations of glycoproteins and oligosaccharides. 1. GLYCAM_93 parameter development. *The Journal of Physical Chemistry*, *99*(11), 3832–3846.

Xiao, S., Myers, M., Miao, Q., Sanaur, S., Pang, K., Steigerwald, M. L., & Nuckolls, C. (2005). Molecular wires from contorted aromatic compounds. *Angewandte Chemie International Edition*, *117*(45), 7556–7560.

Yamashita, I., Kawabata, Y., Kato, T., Hato, M., & Minamikawa, H. (2004). Small angle x-ray scattering from lamellar phase for β-3,7-dimethyloctylglucoside/water system: comparison with β-n-alkylglucosides. *Colloids and Surfaces A: Physicochemical and Engineering Aspects*, *250*(1), 485–490.

Yamashita, J., Shiono, M., & Hato, M. (2008). New lipid family that forms inverted cubic phases in equilibrium with excess water: molecular structure–aqueous phase structure relationship for lipids with 5, 9, 13, 17-Tetramethyloctadecyl and 5, 9, 13, 17-Tetramethyloctadecanoyl chains. *The Journal of Physical Chemistry B*, *112*(39), 12286–12296.

Zhang, J. Z., lin Wang, Z., Liu, J., Chen, S., & yu Liu, G. (2003). *Self-assembled nanostructures*. New York: Kluwer Academic/Plenum.

Zhang, Z., Bhide, S. Y., & Berkowitz, M. L. (2007). Molecular dynamics simulations of bilayers containing mixtures of sphingomyelin with cholesterol and phosphatidylcholine with cholesterol. *The Journal of Physical Chemistry B*, *111*(44), 12888–12897.

LIST OF SCIENTIFIC CONTRIBUTIONS

Academic Journal Publications

1. Manickam Achari, V., Nguan, H.S., Heidelberg, T., Bryce, R.A., and Hashim, R. (2012). Molecular dynamics study of anhydrous lamellar structures of synthetic glycolipids: effects of chain branching and disaccharide headgroup. *The Journal of Physical Chemistry B*, 116(38): 11626–11634.

2. Kotena, Z. M., Behjatmanesh-Ardakani, R., Hashim, R., & Achari, V. M. (2013). Hydrogen bonds in galactopyranoside and glucopyranoside: a density functional theory study. *Journal of molecular modeling*, 19(2), 589-599.

3. Manickam Achari, V., Bryce, R.A., and Hashim, R. (2014). Conformational dynamics of dry lamellar crystals of sugar based lipids: an atomistic simulation study. *PloS One*, 9(6): e101110.

4. Ahmadi, S., Achari, V. M., Nguan, H., & Hashim, R. (2014). Atomistic simulation studies of the α/β-glucoside and galactoside in anhydrous bilayers: effect of the anomeric and epimeric configurations. *Journal of molecular modeling*, 20(3), 1-12.

Oral presentations

1. "Molecular Dynamics Simulation of Bio-Related Glycolipid Membranes" at The Fifth Mathematics and Physical Sciences Graduate Congress (5th MPSGC), at Faculty of Science, Chulalongkorn University (CU), Bangkok, Thailand, from 7th until 9th December 2009.

2. "Simulation of Lyotropic Glycolipid Bilayers in Varying Water Concentration" at 3rd Penang ICYC 2010 Conference at USM: 23rd until 25th June 2010.

Poster presentations

1. "Simulation Study to Determine the Stability of Lamellar Phases of Aqueous Glycolipid Surfactants" at InForm (Integrating Nanomaterials in Formulations) Connect 2010 Seminar, University of Malaya, 13th until 15th January 2010.

2. "Self-Assembly of Glycolipids in Multi-Layer: A Simulation Study" at International Conference on Materials for Advanced Technologies" (ICMAT2011 – under simposium D: Nanoformulation 2011), SUNTEC, Singapore, 26th Jun hingga 1st Julai 2011.

3. "Molecular Dynamics Study of Anhydrous Lamellar Structures of Synthetic Glycolipids: Effect of Chain Branching and Disaccharide Headgroup", at Kavli 2012, Chinese Academy of Sciences Kavli China, 5th July 2012.

4. "Hydration and Thermal effects on Structure and Dynamic Properties of Mono- and Guerbet Branched-chain β-D-Maltosides: An Atomistic Simulation Study", at the ACCMS-8 conference at the National Taiwan University of Science and Technology (NTUST), Taipei, Taiwan (June 16-18, 2015).

Awards

1. "Pasca Biasiwazah Scholarship" was awarded from University of Malaya (December 2007 until December 2010".

2. Postgraduate Research Fund (PPP) grant from University of Malaya.

3. Travel grant awarded by InForm FP7 for participation in the NanoFormulation 2011 26th June until 1st July 2011 in Singapore.

4. Best poster award at the ACCMS-8 conference at the National Taiwan University of Science and Technology (NTUST), Taipei, Taiwan (June 16-18, 2015).

Workshops attended

1. "Growth of Hierarchical Functional Materials in Complex Fluids" at Kavli Institute for Theoretical Physics China (KITPC) at the Chinese Academy of Sciences Kavli from 5th July until 5th August 2011.

2. "Membrane Biophysics | Theory and Experiment" at Kavli Institute for Theoretical Physics China (KITPC) at the Chinese Academy of Sciences Kavli from 7th May until 1st June 2012.

3. “Workshop on Methods and Applications of Molecular Simulations Techniques; Monte Carlo & Coarse-Grained Molecular Dynamics (MCCGMD 2012)” at Information Counter, Level G, Malaysia Genome Institute, Bangi, Kajang, from 25th until 29th June 2012.

4. “Compute Unified Device Architecture (CUDA) for General-purpose computing on Graphics Processing Units (GPGPU) basic programming workshop.” At Multimedia Computing Lab (MMCL), Faculty of Engineering, Multimedia University, Cyberjaya Campus, Malaysia from 20th until 21st February 2013.